Thermodynamically Consistent Formulation of Induced Anisotropy in Polar Ice Accounting for Grain Rotation, Grain-size Evolution and Recrystallization

Vom Fachbereich Mechanik der
Technischen Universität Darmstadt
zur Erlangung des akademischen Grades eines
Doktors der Naturwissenschaften (Dr. rer. nat.)
Genehmigte Dissertation vorgelegt von

Luca Placidi, M. Sc. nat.

aus Roma, Italia

Referent:	Prof. K. Hutter, Ph. D.
Korreferent:	Prof. Dr. rer nat./Caltech USA B. Svendsen
Tag der Einreicung:	15. Juli 2004
Tag der mündlichen Prüfung:	17. November 2004

Darmstadt 2004
D 17

Acknowledgement

I am grateful to Prof. Kolumban Hutter for the time he wanted to spend in numerous discussions with me about the themes of the dissertation. His ideas and his suggestions form the basis of this work. I am grateful to him even to have given to me the possibility to take part of his group. He is able to create an atmosphere in which the scientific result takes the main role and I took advantage of this air in my work. He is able, in fact, to draw out the best of the scientific matter from his co-workers and I am proud to have been one of them. Of course, his capacity to enter in the details of the works of different types is an extraordinary characteristic of Prof. Hutter and is fundamental to lead a group in this manner.

I want to express my gratitude to doctor Sérgio H. Faria. He initiates me to the main subjects of the thesis: the theoretical glaciology and the thermodynamics. His contribution to this work is huge. Not only he showed to me the sea of the literature and gave me a secure guide to sail it properly but also he was a valid teacher able to be present and enlightening in each step of my course. His care on my scientific growth was noteworthy and extraordinary. It is impossible to mention here all the contributions belonging to him and present in the thesis. Such contributions, in fact, permeate every part of this work.

The role of Prof. Ralf Greve during my time in Darmstadt was very important. Every time I needed a link to the knowledge of the glaciological community, upon which he is one of the best representative, he was present, active and stimulating. Without his intuitions about the mechanical behaviour of ice samples, the anisotropic generalization of Glen flow law, that I consider the main result of the thesis, would have take much more time to come out.

Doctor Ing. Habil. Yongqi Wang was able to find a serious error in the expression of the evolution equation of the Orientation Distribution Function (ODF) in the three-dimensional and axi-symmetric case. On the basis of this formulation he taught me to write a simple numerical simulation with the finite difference method, that has not found the place in the thesis. However, this collaboration was very important because it gave me the feeling that the closure of the problem of the simulation of an anisotropic ice sheet was really possible. Among this contribution, I would like to acknowledge him especially for his availability to try to solve any problem I needed to subject to him.

I thank Angelika Humbert for her catching and stimulating enthusiasm in the work and in her life. I thank doctor Bernd Muegge, the computer administrator, for his patience of a saint to have taught me everything I needed and every time I asked. I express my gratitude to doctor Shiva Pudasaini, every time available for fruitful and interesting discussions. I would like also to thank sincerely the entire AG3 group, with which it was possible to establish good relations, sometimes even of friendships: Motasem Saidan, Mahmoud Reza Maneshkarimi, Ana Ursescu, Min-Ching Chiou and Chung Fang.

I am thankful to Prof. Bob Svendsen for acting as a co-referee in my Ph. D. examination. I want to underline his care in the comprehension of my work and his availability for interactions and discussions during the last IUTAM conference in Warsaw.

Luca Placidi Roma, February, 25, 2005

Zusammenfassung

In dieser Arbeit wird eine Theorie vorgestellt, welche Phänomene in Verbindung mit der Dynamik polykristalliner Materialien, erklärt wie zum Beispiel das thermomechanische Verhalten von Eis in Inlandeisschilden. Basierend auf der Mischungstheorie mit Kontinuierlcher Diversität werden mit Hilfe des zweiten Hauptsatzes der Thermodynamik Einschränkungen der möglichen konstitutiven Gleichungen hergeleitet uns so ein theoretisches Verfahren entwickelt, das in der Lage ist, den Einflußder Mikrostruktur auf die mechanischen Eigenschaften polykristallinen Materials zu untersuchen. Es wird ein anisotropes Konstitutivgesetz des Streckungstensors eines inkompressiblen, polykristallinen Materials in Abhänigkeit des deviatorischen Spannungstensors und der Gitterorientierungen (mit Hilfe des Orientierungsverteilungsfunktion (ODF) der Kristallite) des Polykristalls vorgestellt. Mittels eines solchen Gesetzes ist es möglich mechanische Reaktionen für jeden Deformationszustand zu verstehen. Das gesetz ist objektiv, seine Gültigkeit wird durch einige Beispiele belegt. Die Entwicklung der Anisotropie wird durch den Verlauf der ODF modelliert, also nicht *ab initio* vorgegeben. Die Massenbilanz der Mischung (mit Kontinuierlches Diversität) ergibt eine Funktion mit zwei Konstitutivegleichungen, die Rotation der Körner und die Korngrenzen Migration (GBM) bzw. den Rekristallationsvorgang beschreiben. Es wird eine explizit Formulierung der Gleichungen vorgeschlagen. Aus der Massenbilanz erhält man außerdem eine allgemeine Evolutionsgleichung für die Korn größe. Hieraus ergeben sich zwei weitere Konstitutivgleichangen, die den Effekt des Korn wachstums bzw. der Polygonisation auf die Entwicklung der Korn größenverteilung beschreiben. Auch für diese Gleichungen werden explizite Formulierungen vorgeschlagen. Desweiteren werden Ergebnisse für die Entwicklung der Versetzungschichte vorgestellt.

Abstract

In this thesis we present a general theory able to comprehend important phenomena related to the dynamics of a polycrystalline material such as the ice of an ice sheet. The theoretical framework is founded upon the Theory of Mixtures with Continuous Diversity, for which the second law of thermodynamics is exploited to get a complete set of restrictions on the constitutive equations. The main goal of such an exploitation is to provide a theoretical tool to investigate the effects of the micostructure on the mechanical behaviour of polycrystalline materials. An explicit anisotropic constitutive law is given for the stretching tensor of an incompressible polycrystalline material in terms of its deviatoric stress tensor and of the distribution (Orientation Distribution Function or ODF) of the lattice orientations of the crystallites belonging to the polycrystal. Such a law is able to comprehend the mechanical response for any state of deformation, it is objective and its validity is checked by some remarkable examples. The evolution of the anisotropy is modelled with the aid of the evolution of the ODF, and it is not postulated *ab initio*. The balance of mass, as it is given in the form of the presented mixture with continuous diversity, provides such an evolution equation, that contains two constitutive functions. They are able to model the grain rotation and the Grain Boundary Migation (GBM) and recrystallization, respectively. We provide also a proposal for the explicit form of these two functions. From the balance of mass in the form of the presented mixture with continuous diversity, we have also derived a general evolution equation of the distribution

of grain sizes. Two constitutive functions are present in this new equation. They are able to model the effects of grain growth and polygonization, respectively, on the evolution of the distribution of grain sizes. Even in this case, we give our proposal for the explicit form of these two functions. Results about the evolution of the dislocation density is also given.

Riassunto

In questa tesi é presentata una teoria generale capace di comprendere importanti fenomeni fisici relativi alla dinamica di un generico materiale policristallino, come il ghiaccio di un ice sheet. Il fondamento teorico é preso dalla Teoria delle Miscele con Continua Diversitá, attraverso la quale é stato possibile investigare il secondo principio della termodinamica, al fine di ottenere un insieme completo di restrizioni sulle equazioni costitutive. L'obiettivo principale di questo lavoro é quello di fornire alla comunitá scientifica uno strumento teorico capace di comprendere gli effetti della microstruttura sul comportamento meccanico dei materiali policristallini. Nella tesi si fornisce inoltre una esplicita equazione costitutiva per il tensore della velocitá di deformazione di un materiale policristallino e incompressibile in termini della parte deviatorica del tensore degli stress e della distribuzione (ODF) delle orientazioni del reticolo dei cristalli appartenenti al policristallo. Tale legge é in grado di prevedere la risposta meccanica per un qualsiasi stato di deformazione, essa é oggettiva e la sua validitá é dimostrata per mezzo di esempi notevoli. Si pretende inoltre di modellizzare l'evoluzione dell'anisotropia attraverso la sola equazione di evoluzione della distribuzione ODF delle orientazioni dei cristalli nel policristallo. Tale equazione non é postulata *ab initio* ma é derivata dal bilancio della massa relativo alla presente formulazione della teoria delle miscele con continua diversitá, in cui sono presenti due funzioni costitutive. Esse sono in grado di modellizzare i fenomeni della rotazione di grano e della migrazione della frontiera (GBM) fra grani, detta recristallizzazione. Nella tesi viene anche illustrata una proposta per l'esplicitazione di tali funzioni. Dalla stessa equazione del bilancio di massa é inoltre possibile derivare un'equazione di evoluzione per la distribuzione della taglia dei grani, in cui sono presenti ulteriori due funzioni costitutive, capaci di modellizzare ulteriori fenomeni della microstruttura in grado di avere un effetto su tale distribuzione: la crescita di grano e la poligonizzazione. Anche in questo caso si é voluto fornire una proposta per l'esplicitazione di tali funzioni. Nella tesi sono anche presenti alcuni risultati sull'evoluzione della funzione di densitá di dislocazione.

Contents

Chapter 1

A Brief Introduction, Notation

One of the most important difficulties in the analysis of polycrystalline ice under the conditions that occur in an ice sheet, such as Greenland or Antarctica, should cause major concerns in any scientist exposed to it: different samples with the same shape and size can have the unpleasent property to yield different results in a laboratory experiment aimed at a relationship between the deviatoric stress and the stretching (or strain rate) tensors. Generally, this difficulty is explained by the statement that the mechanical response depends upon the history of deformation. However, one can not control the entire history of a given sample; moreover, such a justification does not point out the road to the solution of the problem: knowledge of the mechanical response, in a general situation, before the performance of the experiment.

An alternative explanation has been used in the literature. This is based on the consideration that knowledge of the microstructure can completely characterize the mechanical response of a polycrystalline material. Experimental analyses of the microstructure provide a wealth of information. The duty of a theoretical work is, therefore, to understand which ones can usefully be applied.

Besides the length of linear defects per unit volume (the dislocation density ρ_d), two other parameters are also considered to be important: grain sizes and lattice orientations. The main topic of this thesis is to analyse the role of the distributions of grain sizes and lattice orientations in the mechanics of polycrystalline materials, taking special care to the case of incompressible ice.

If the crystallites in a polycrystal exhibit an anisotropic mechanical response, then the behaviour of the polycrystal likely depends on the distribution of the lattice orientations. This is also the case of ice. Thus, in Chapter 2, we review many theories on the mechanics of polycrystalline ice that take the problem of anisotropy, and in general of microstructure, into acount.

Besides a brief introduction into the legacy of isotropic ice, we discuss the influence of grain size on the mechanical response. The compatibility between grain-size and lattice orientation dependent deformation mechanisms is also discussed in Chapter 2. Whereas some authors have expressed doubts regarding the influence of the grain size on the mechanical response of polycrystalline ice, all scientists agree on the importance of the influence of lattice orientations. To properly understand this influence is not an easy task. The burning problems in this field are knowledge of an anisotropic flow law, i.e. the stretching-stress relationship, and the evolution of this anisotropy, i.e., the evolution of the distribution of the lattice orientations. A general rule for the anisotropy of polycrystalline

ice is that a uniformly random distribution of lattice orientations corresponds to the isotropic behaviour and the anisotropy is driven by a change of such a distribution. There are two reasons of this change. The first is that the deformations can induce a rotation of the crystallites towards given directions (grain rotation) and the second is that the boundaries between crystallites can move in such a way that certain orientations become privileged (Grain Boundary Migration or GBM). Thus, these two phenomena (i.e., grain rotation and GMB) are also reviewed in Chapter 2.

The occurrence of GBM is not guaranteed under all conditions. It is believed that the dislocation density (i.e., the length of linear defects per unit volume), must reach a certain threshold value. Therefore, the evolution of the dislocation density is also an important topic that is deeply discussed in the literature (see Section 2.7). In subsection 2.7.4, we will present a new model. This model is sufficiently general to comprehend the classical and the new contributions. The new contributions are due to the breaking of crystallites, i.e., to polygonization. We remark that this model is also sufficiently simple to provide an explicit and analytical solution for ρ_d.

We have already remarked that an analysis of the literature on anisotropic polycrystalline materials shows that there are two burning problems to be solved, namely:

1) Find an anisotropic flow law,

2) find the evolution of the anisotropy.

In Chapter 3 we present a novel theory that is able to give an important contribution to the solution of problem 1). We present, in fact, an anisotropic constitutive law for the stretching tensor of an incompressible polycrystalline material in terms of the deviatoric stress tensor and of the distribution of lattice orientations, that is able to comprehend the mechanical response for any state of deformation and that is valid in any frame of reference. The validity of the predictions of our model is checked by some remarkable examples.

In Section 5.3 we present a theory that solves the problem of the evolution of fabric, i.e., problem 2) on the evolution of the anisotropy. The evolution of fabrics (i.e., of the distribution of lattice orientations) is assumed to depend on grain rotation and on GBM. Two different constitutive functions, that appear in the generalized balance of mass for a Theory of Mixtures with Continuous Diversity (presented in Chapter 4), account for grain rotation and GBM, respectively. We remark that the constitutive function accounting for grain rotation is compatible with the Balance of Angular Momentum, as we will demonstrate in Chapter 6.

We pointed out that an explicit form for the anisotropic flow law for incompressible polycrystalline material and a suitable evolution equation for the distribution of the lattice orientations due to grain rotation and to GBM are two independent and very important results. As we will show in Chapter 2, the modelling of these two problems has not been ignored in the literature. However, we claim that some of these models are too simple to comprehend the mechanical behaviour of the ice in an ice sheet; on the other hand, other models exhibit the opposite problem, i.e., the number of parameters is so high that it is even difficult to find an independent number of experiments to be able to measure them. Moreover, the generality of some models does not allow to check the validity of the proposed assumptions. The model in this thesis has the suitable characteristics to depend only on 3 parameters.

The first parameter is a kind of scalar enhancement factor that is denoted by E. Any

mechanical test on an anisotropic sample of ice is able to identify a value for E, that, with the distribution of the lattice orientations, completely characterizes the anisotropic flow law presented in Chapter 3. Moreover, we will show that the value for E can easily be extrapolated from a mechanical test presented in 1989 by Jacka and Budd.

The second parameter quantifies the velocity of the rotation of the grains and is denoted by ι. Comparison with the analyses of the GRIP ice core will, in subsection 5.3.5, yield a rough estimate of its numerical value. We remark that in our model ι completely characterizes the evolution equation of the distribution of lattice orientations due to grain rotation.

The third parameter gives an estimate of the influence of GBM on fabrics and is denoted by $\hat{\Gamma}$, but the actual knowledge on this physical phenomenon has not allowed us to give a numerical value for it. A dependence of $\hat{\Gamma}$ on the dislocation density is, in fact, still not clear; on the other hand, such a dependence is believed to affect substantially the value of $\hat{\Gamma}$.

Generally, the dependences on temperature and dislocation density of these three parameters are believed to be important, but it is still not achieved in this work.

Besides the evolution of fabrics, Chapter 5 contains new results even for the evolution of texture, i.e., for the evolution of the distribution of grain size (see Section 5.2). Texture is assumed to depend on grain growth and polygonization. The occurrence of grain growth tends to increase the value of grain size. Polygonization, on the other hand, has the opposite effect. As for the fabric evolution, two different constitutive functions, that appear in the generalized balance of mass of a Theory of Mixtures with Continuous Diversity (presented in Chapter 4), drive the evolution of this distribution. In this case, however, they account for grain growth and for polygonization, respectively. Usually, models on the evolution of texture account only for the term due to grain growth, and that is suitable only for the evolution of the mean grain-size. Even the contributions aimed to include the effect of polygonization, that we review in Chapter 2, are constructed for an evolution equation of the mean grain-size. Even though experimental measurements of the distribution of grain sizes in the analyses of ice cores are known since almost 1996, our theoretical investigation on the evolution of this kind of distribution is completely new.

The parameterization of the evolution of texture and fabrics is achieved by equations that are not *ad hoc*. Their theoretical foundation lies on the Theory of Mixtures with Continuous Diversity and are nothing else that special forms of a generalized Balance of Mass. Chapter 4 is dedicated to the introduction of the basic concepts of this theory; it is presented in a form that is immediately suitable for application to polycrystalline materials.

On the basis of this theory, the distributions of grain sizes and lattice orientations are given by the size and by the orientation mass density, respectively. Such mass densities have different definitions with respect to their classical counterpart, i.e., the Crystal Size Distribution (CSD) and the Orientation Distribution Function (ODF). The advantages of the use of our definitions are not only theoretical, they are also of other nature. In fact, we will point out in Section 4.2, that the size mass density (and not the CSD) gives a definition of the mean grain-size that is independent of the sensitivity of the measuring instruments and that an uniformly random distributed orientation mass density guarantees the isotropic behaviour (we will prove that the ODF does not fulfil this property).

Another important characteristics of this Theory of Mixtures with Continuous Diversity is the form of the general Balance Equation. Besides the classical non convective fluxes, other kind of fluxes are introduced, i.e., the non convective interspecies fluxes. Their meaning will be explained in Section 4.4. The occurrence of interspecies fluxes in the mechanics of the ice in an ice sheet is evidenced in subsection 4.4.4, where a particular interspecies flux (the orientational couple stress $\varpi^{\triangleright}_{ij}$) is associated to the phenomenon of polygonization. We will also demonstrate that the explicit representation of the orientational couple stress by which polygonization is modelled will be the same representation that emerges from the application of the second Law of Thermodynamics on a more general form of $\varpi^{\triangleright}_{ij}$.

A further important aspect of the present work is that all results can be derived from a very general theory, of which the assumptions are explicit. The main assumptions come from the new Constitutive Theory, presented in Chapter 6. Besides the implementation of the Rules of Equipresence and the Principles of Determinism, Local Action and Material Frame Indifference, a novel Principle, called Principle of Global Action, is introduced to account for the new species assemblage variables (i.e., grain size and lattice orientation). The implementation of the Second Principle of Thermodynamics is given following the Method of Lagrange Multipliers of Liu and Müller. Moreover, Section 6.8 is dedicated to the implementation of the incompressibility condition; it is explicitely demonstrated, that all the results shown in this thesis for incompressible polycrystalline materials have a thermodynamic justification.

A new result, deduced from the application of the thermostatic equilibrium and from the incompressibility condition, is that the representation of the orientational couple stress, through which polygonization has been included, is connected with the classical concept of pressure.

The thesis is divided into chapters, which are divided into sections and the sections into subsections. For the sake of simplicity, when Cartesian tensor notation is used, the usual summation rule for repeated indices will be implemented with which the reader is supposed to be familiar. Parentheses, square brackets and angular parentheses define rules of symmetrization, antisymmetrization and traceless symmetrization, respectively, defined for a general tensor quantity A_{hij}, i.e.,

$$A_{h(ij)} \equiv \tfrac{1}{2}\left(A_{hij} + A_{hji}\right), \quad A_{h[ij]} \equiv \tfrac{1}{2}\left(A_{hij} - A_{hji}\right), \quad A_{h\langle ij\rangle} \equiv A_{h(ij)} - \tfrac{1}{3}A_{hkk}\delta_{ij}. \quad (1.1)$$

The list of the symbols we will use in this thesis is given in the following. We remark that the quantities listed in Table 4.2 and in the equation (4.56) are, generally, not listed here. Their meaning is given in the subsection 4.4.1. Further symbols yield from the application of the homogenization rules of Section 4.6. At the and of this chapter, we give also a list of the initials we will use.

Symbol	Description
a	Constitutive parameter of the creep response function and parameter defined in (3.13) and parameter defined in (5.13).
$\hat{a}$	Function defined in (3.13).
a_i	Terms of the entropy inequality in (6.26).
A	Age (Section 2.1) and Rate Factor and the scalar invariant defined in the equation (3.53).
A_S	Scalar invariant defined in (3.28).
A_{SS}	Scalar invariant defined in (3.29).
A_{SSSS}	Scalar invariant defined in (3.70).
A_j	Constitutive parameters of the rate factor.
A^T	Modified rate factor (see equation (2.20)).
A_{ij} and $\mathbf{A}$	Second order structure tensor.
$A_{ij}^{(i)}$ and $\mathbf{A}^{(i)}$	Second order structure tensor for the isotropic case.
$A_{ij}^{(gf)}$ and $\mathbf{A}^{(gf)}$	Second order structure tensor for the girdle fabric case.
b	Constitutive parameter of the creep response function and constitutive parameter defined in (5.13) and magnitude of the Burger Vector.
$\mathbf{b}$	Burger Vector.
b_i	Arbitrary vector defined in (6.14).
B	Material parameter defined in the equation (3.53).
B_{ijkl} and $\boldsymbol{B}$	Fourth order structure tensor.
$\boldsymbol{B}$	Left Cauchy–Green deformation tensor.
B_0	Constitutive parameter of the rate factor.
B_a	Functionals defined in (6.11).
$B_m^{\triangleright}$	Balance of mass defined in (6.17).
$B_{l\,i}^{\triangleright}$	Balance of linear momentum defined in (6.18).
$B_{a\,i}^{\triangleright}$	Balance of angular momentum defined in (6.19).
$B_e^{\triangleright}$	Balance of energy defined in (6.20).
$B_d^{\triangleright}$	Balance of dislocation defined in (6.21).
$B_\eta^{\triangleright}$	Balance of entropy defined in (6.22).
$\mathbf{B}^D$	Deviatoric part of the general tensor $\mathbf{B}$.
c	Constant.
$c_i^{(g)}$	Unit vector parallel to the c-axis of grain g.
C	Impurity Content.
$C^{\triangleright}$	Collective variable defined in (6.77).
dD	Elementary interval of $\mathcal{I}$.
d^2n	Elementary solid angle.
d_i, $i = 1, 2, 3$	Material parameters introduced in the equation (3.31).
$\tilde{d}_{ij}$	General function defined in subsection 3.2.2.
D	Grain size (Chapter 2) and dimensionless grain-size (Chapters 4, 5 & 6).
$\bar{D}$	Grain size in Chapters 4, 5 & 6.

Symbol	Description
$\bar{D}_M$	The size of the Representative Volume Element.
D_a and D_b	Given values of dimensionless grain-size.
D_c	Scalar invariant defined in (5.56).
D_m	Mean Value of grain size.
D_0	Grain size at time $t = 0$.
D_{ij} and $\mathbf{D}$	Stretching tensor.
$\mathbf{e}^{(r)}$	Eigenvectors of $\mathbf{B}$.
$\mathbf{e}_i$	Unit vectors parallel to the axes of a fixed frame of reference.
$\mathbf{e}_r$, $\mathbf{e}_\theta$ and $\mathbf{e}_\varphi$	Orthonormal vectors of the classical spherical coordinates.
e_i^W	Unit vector, normal to the surface where the jumps occur.
$e_{i\nu}$	Strain in the moving frame of reference (see subsection 2.5.5).
$\dot{e}_{i\nu}$	Strain rate in the moving frame of reference (see subsection 2.5.5).
E	Enhancement factor.
E_s	Enhancement factor for simple shear for single maximum fabric.
E_p	Enhancement factor for pure shear for girdle fabric.
f	Isotope Concentration (Section 2.1) and creep response function (in the rest of chapter 2) and phenomenological impurity factor (subsection 2.5.4).
f^*	Orientation Distribution Function.
F^*	The Orientation Distribution Function defined in the equation (4.5).
g	Velocity in which the grain size D reaches the steady state D_{eq} in the Fig. 2.11 and parameter defined in (3.13).
$\hat{g}$	Function defined in (3.13).
G	Shear Modulus and Functional defined in (6.7).
$\tilde{G}$	Functional defined in (6.10).
$\bar{G}_{ij}$ and $G_{ij}^{(g)}$	Tensors defined in (2.18).
h	Depth.
$\boldsymbol{H}_{\mathrm{I}}$	Isotropic part of the material response.
$\boldsymbol{H}_{\mathrm{A}}$	Anisotropic part of the material response.
$H_{ik}^{\triangleright}$	Relative spin tensor.
$\hat{\mathbf{i}}$	Unit vector parallel to the first axis of a fixed frame of reference.
I	Coefficient for the Isotropic Glen flow law (Chapter 3) and Rotational inertia (Chapters 4, 5 and 6).
I_2	Coefficient for the Isotropic two-dimensional Glen flow law.
I_3	Coefficient for the Isotropic three-dimensional Glen flow law.
$I_{\mathbf{B}}$, $II_{\mathbf{B}}$ and $III_{\mathbf{B}}$	Scalar invariants of a general tensor $\mathbf{B}$.
$\hat{\mathbf{j}}$	Unit vector parallel to the second axis of a fixed frame of reference.
$\hat{\mathbf{k}}$	Unit vector parallel to the third axis of a fixed frame of reference.

Symbol	Description
k_1 and k_3	Constitutive parameters of Ψ^*.
K	Grain boundary migration rate.
L	Functional defined in (6.24).
$L_{ij}^{\triangleright}$	Gradient of velocity.
$m_i^{(g)}$ and $\mathbf{m}^{(g)}$	Unit vector oriented towards the resolved shear stress on the basal plane.
M	Mass of the RVE.
M_f	Mass of the fluid part in the RVE.
M_s	Mass of the solid part in the RVE.
$M^{\blacktriangleright}(D)\,dD$	Mass of the crystallites with dimensionless grain-size between D and $D + dD$.
$\boldsymbol{M}^{(r)}$, $r = 1, 2, 3$	Structural Tensors.
$M_i^{\triangleright}$	Bending Moment.
M_i, $i = 1, 2$	Maxima in simple shear recrystallization fabrics.
n	Exponent in Glen flow law.
$n^{\blacktriangleright}$	Crystal Size Distribution.
n_i and $\mathbf{n}$	Unit vector parallel to the c-axis or to a general lattice orientation.
n_i^+ and $\mathbf{n}^+$, n_i^- and $\mathbf{n}^-$	Given lattice orientations.
N	Number of crystallites (subsection 2.5.5).
N_i and $\mathbf{N}$	Unit vector, normal to a surface in the classical three-dimensional Euclidian space.
N_{tot}	Total number of crystallites (Chapter 4).
$N^{\blacktriangleright}$	Crystal Size Distribution defined in the equation (4.4).
O_{ij}	Arbitrary orthogonal tensor defined in (6.14).
p	Exponent of grain size in the super-plastic flow law and macroscopic pressure.
$p^{\triangleright}$	Microscopic pressure and constitutive parameter of orientational couple stress.
P	Polygonization in the equation (2.45).
$q_{d\,i}$	Macroscopic density of non convective flux of dislocation.
s	Constitutive parameter of the rate factor.
$s_i^{\triangleright}$	Spin velocity.
$S^{\triangleright}$	General constitutive quantity.
$\overline{S}^{\triangleright}\,(t, x_i, n_j, D)$	General constitutive quantity.
$\hat{S}^{\triangleright}$	Functional defined in (6.13).
S_c	Scalar Invariant defined in the equation (3.46).
$S_{ij} = t_{\langle ij \rangle}$ and $\mathbf{S}$	Deviatoric stress tensor.
$\bar{S}$	Averaged Schmidt factor.
$\bar{S}_{ij}$ and $\bar{\mathbf{S}}$	Averaged Schmidt tensor.
S^g	Schmidt factor of grain g.
S_{ij}^g and $\mathbf{S}^g$	Schmidt tensor of grain g.
$S_{ik}^{\triangleright}$	Skew-symmetric tensor associated with the spin velocity $s_j^{\triangleright}$.
t	Time.

Symbol	Description
t_0	A given value for time and a material parameter defined in equation (3.52).
t_i, $i = 0, 1, 2$	Material parameters defined in equation (3.52).
t_{ij} and $\mathbf{t}$	Macroscopic Cauchy stress tensor.
$t_{ij}^{\triangleright}$	Microscopic Cauchy stress tensor.
$t_{ij}^{(g)}$ and $\mathbf{t}$	Cauchy stress tensor relative to the grain g.
$\mathbf{t}^D$	Deviatoric stress tensor.
T	Absolute temperature.
T_0 and T_r	Constitutive parameters of the rate factor.
T_j and $\mathbf{T}$	Unit vector, normal to a general hypersurface in the orientational space.
$T^{(g)}$	Resolved shear stress on the basal plane of the grain g.
$u_j^{\triangleright}$	Orientation transition rate.
V	Volume of the RVE.
V_f	Volume of the fluid part in the RVE.
V_s	Volume of the solid part in the RVE.
$V^{\blacktriangleright}(D)\,dD$	Dimensionless volume of the crystallites with dimensionless grain-size between D and $D + dD$.
$V^*(\theta)$	Relative volume of the crystals with the c-axis having an angle with the vertical that is larger than θ.
$w^{\triangleright}$	Size transition rate.
$W_{kh}^{\triangleright}$	Skew-symmetric part of the velocity gradient.
x	Collective variable defined in (6.30).
x_i	Position in the Eulerian description.
y	Collective variable defined in (6.30).
z	Collective variable defined in (6.30).
α	Coefficient exceeding 1 in equation (2.40).
α_j	Constitutive parameters of the rate factor.
$\alpha^{\blacktriangleright}(D)$	Shape factor of crystallites with dimensionless grain-size D.
$\tilde{\alpha}^{\blacktriangleright}(D)$	Modified shape factor (see equation (4.25)) of crystallites with dimensionless grain-size D.
β	Dimensionless parameter in equation (2.42).
β_a	Functionals defined in (6.11).
γ_a	Parameters defined in equation (2.33).
$\gamma^{\blacktriangleright}(D)$	True mass density of crystallites with dimensionless grain-size D.
$\bar{\gamma}$	A given true mass density.
δ	Dirac delta function.
$\delta^{\triangleright}$	Entropy production deviation.
δ_{ij}	Kronecker symbol.
δ_{xz}	Generalized Kronecker symbol defined in (6.31).
ϵ_{ij}^b	Strain of the bulk polycrystal in the fixed frame of reference (see subsection 2.5.5).
ϵ_{ij}^k	Strain of the crystallite k in the fixed frame of reference (see subsection 2.5.5).
ε	Strain.

Symbol	Description
ε^g	Strain of grain g.
ε_{ijk}	Permutational tensor.
η	Apparent viscosity.
θ	Final angle of c-axis with respect to the vertical and colatitude of a general lattice orientation and the misorientation angle between two subgrain.
θ_0	Initial angle of c-axis with respect to the vertical and latitude of girdle fabric.
$\tilde{\theta}$	Polar angle in the two-dimensional case.
$\tilde{\theta}_0$	A given value of the polar angle in the two-dimensional case.
ι^*	Constitutive scalar invariant.
λ_i, $i = 1, 2, 3$	Eigenvalues of $\mathbf{A}$.
ν_f	Volume fraction of the fluid part.
ν_s	Volume fraction of the solid part.
ξ_f	Mass fraction of the fluid part.
ξ_s	Mass fraction of the solid part.
ρ_d	Dislocation density.
$\rho_{d\,0}$	Dislocation density at time $t = 0$.
ρ_d^{sgb}	Dislocation density stored by the subgrain boundary.
ϱ	Mass density.
$\varrho^{\triangleright}$	Orientation-and-size mass density.
ϱ^*	Orientation mass density.
$\varrho^{\blacktriangleright}$	Size mass density.
ϱ_f	Partial mass density of the fluid part.
ϱ_s	Partial mass density of the solid part.
τ	Magnitude of the resolved stress tensor on the basal plane.
υ_i and $\mathbf{v}$	Velocity.
υ_i^W	Velocity field vector of the surface where the jumps occur.
ϕ	Final angle of c-axis with respect to the vertical.
ϕ_0	Initial angle of c-axis with respect to the vertical.
φ	Longitude of the lattice orientation.
χ	Arbitrary scalar defined in (6.14).
$\psi^{\triangleright}$	Helmholtz free energy.
σ	The secind invariant of $\mathbf{t}$ and standard deviation of CSD.
$\sigma_i^{\triangleright}$	Spin or microstructural angular momentum.
τ	Magnitude of the resolved shear stress on the basal plane.
τ_n	Magnitude of the resolved shear stress on the basal plane of the crystallites oriented as $\mathbf{n}$.
$\dot{\tau}_{i\nu}$	Deviatoric stress tensor in the moving frame of reference (see subsection 2.5.5).
$\omega_i^{\triangleright}$	Rotation vector.

Symbol	Description
ω_{ij}	Rotation from the external frame of reference $Oxyz$ to the reference frame $O\eta\mu\nu$ that matches the crystal orientation at the start of each time step (see subsection 2.5.5).
$\hat{\Gamma}$	Constitutive parameter.
Δt	Small time interval.
$\Lambda^{\triangleright}_{m}$	Lagrange multiplier relative to the balance of mass.
$\Lambda^{\triangleright}_{l\,i}$	Lagrange multiplier relative to the balance of linear momentum.
$\Lambda^{\triangleright}_{a\,i}$	Lagrange multiplier relative to the balance of ang. momentum.
$\Lambda^{\triangleright}_{e}$	Lagrange multiplier relative to the balance of energy.
$\Lambda^{\triangleright}_{d}$	Lagrange multiplier relative to the balance of dislocation.
Ψ	Dissipation potential of the polycrystal (Chapter 2).
$\mathcal{F}$	Collective variable defined in (4.78).
Ψ^{*}	Dissipation potential of crystallites (Chapter 2).
Ω	Term of the residual entropy inequality. Definition in (6.26).
$\Omega^{\triangleright}$	Intensity of bending moment.
$\mathcal{I}$	Grain-sizes range (or range of nondimensional grain-size).
$\bar{\mathcal{I}}$	Range of grain sizes.
$\mathbb{N}$	Positive natural numbers.
$\mathbb{R}$	Real numbers.
$\Re$	Collective variable defined in (6.9).
$\mathcal{S}^2$	Orientational space or range of lattice orientations.
$\mathbb{U}^{\triangleright}$	Ausiliar function defined in (4.73)
$\mathfrak{X}$	Collective variables defined in (6.35).
$\mathcal{X}$	Collective variable defined in (6.16).
$\mathcal{Y}_i$	List of variables defined in (6.27).
$\langle\bullet\rangle_{N}$	Mean value defined in (4.29).
$\langle D\rangle_{\varrho}$ and $\langle D\rangle$	Mean values defined in (4.29).
$\langle\bullet\rangle_{n}$	Mean value defined in subsection 5.3.6
$(\bullet)^{(a)}$, $a = 1, ..., 11$	All the quantities in Chapter 6 with the apix made of a number in brackets are general function of $\mathfrak{X}$.
$(\bullet)^{(b)}$	All the quantities in Chapter 6 with the apix made made of the letter b in brackets are defined in (6.34).

Initials	Description
CSD	Crystal Size Distribution.
GBM	Grain Boundary Migration.
GBS	Grain Boundary Sliding.
GRIP	Greenland Ice Core Project.
ODF	Orientation Distribution Function.
RVE	Representative Volume Element.
VPSC	Visco Plastic Self Consistent.

Chapter 2

A Critical Review of the Mechanics of Polycrystalline Ice

2.1 Introduction

The reconstruction of the climate on Earth from time series of the isotope ratios of O_2, D, CH_4, CO_2, and other trace gases (see, e.g., Fig. 2.1), which are determined by analyzing

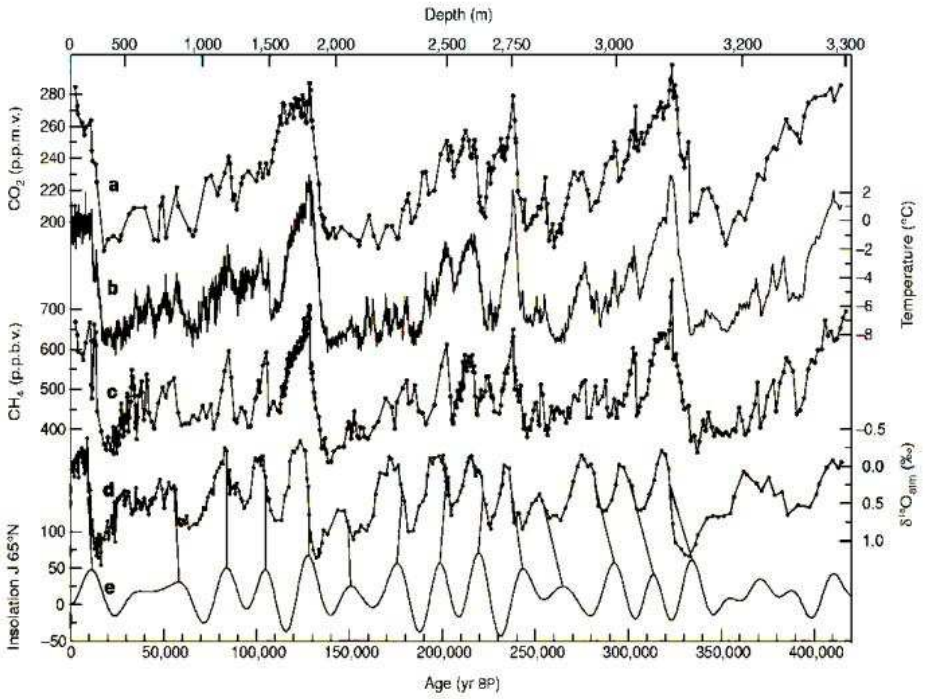

Figure 2.1: Time series of (a) atmospheric CO_2, (b) the surface temperature (deviation from today) reconstructed from D, (c) atmospheric CH_4, (d) $\delta^{18}O_{\mathbf{a}tm}$ of atmospheric oxygen and (e) the insolation at $65N$ as obtained from the Antarctic Vostok Ice core [112] for a time span of $420,000$ years into the past. Underlain photo of the drill camp: Todd Sowers, LDEO, Columbia University, Palisades, New York.

the ice and the air trapped within it from ice cores of Antarctica, Greenland and several glaciers, requires knowledge of the age of ice sample that was located at a certain position in an ice sheet, Fig. 2.2. The age of the the sample can be roughly defined as the difference between the times when the ice is analyzed in the laboratory and when it fell as snow on the surface of the ice sheet or glacier and started its motion along its own trajectory. Reconstructing the climate in the past approximate 500 000 years thus boils down to the determination in an ice core of the depth-age relationship, $h = h(t)$, that allows the transformation of an isotope-depth relation $f = \hat{f}(h)$ to an isotope-age relation $f = f(t)$. Since the deuterium D and the carbon-dioxide CO_2 isotope data are pretty good proxy-data of the mean temperature on Earth (app. $15°C$, today), ice cores are ideal objects to reconstruct the climate through the last ice ages.

Down to depths of 1500m or somewhat more (in Antarctica and Greenland) the $f(t)$-relation can fairly reliably be determined by methods of stratigraphy (e.g., counting layers, performing electrical conductivity measurements on the ice core, correlating dark impurity layers with volcanic eruptions, etc.). At large depths the annual layers are so thin ($< 100\mu m$) that computational methods, using, e.g., continuum mechanical methods, are needed to infer from them the age of the ice. This can be done by either solving the age equation $\dot{A} = 1$ (where A is the age, see [61]), more explicitly,

$$\frac{\partial A}{\partial t} + (\bigtriangledown A) \cdot \mathbf{v} = 1, \tag{2.1}$$

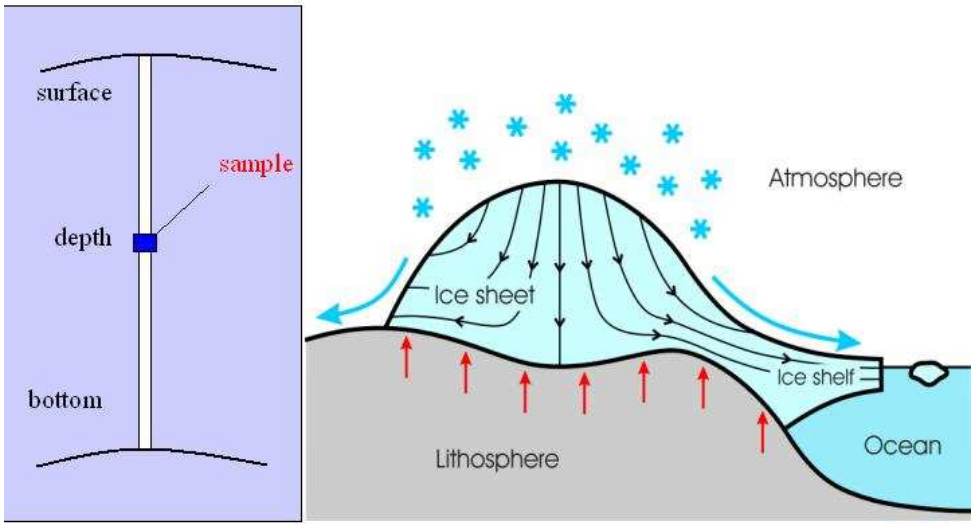

Figure 2.2: (a) Ice specimen at a certain depth of an ice core. (b) Ice sheet (with a core to be dated) and ice shelf bounded by the atmosphere, the ocean and the solid earth. The figure also shows the trajectories of the ice which falls as snow onto the free surface and is subsequently transported within the ice until it surfaces again and then melts or breaks off.

or by determining the ice particle trajectories from

$$\frac{d\mathbf{x}}{dt} = \mathbf{v}\left(\mathbf{x}, t\right), \qquad \mathbf{x}\left(t_0\right) = \mathbf{x}_0. \tag{2.2}$$

Both equations require knowledge of the velocity field $\mathbf{v}$ through the time t, and this is obtained by determining the motion of the ice through the space for all times. There are many subtleties that make this problem a very challenging one. Among these, a significant contribution to the uncertainty of the $h\left(t\right)$-relationship is an inadequate knowledge of the material behaviour of ice under thermomechanical creeping processes on geological time scales.

Classically, ice of the Earth's large ice masses has been treated as an heat conducting and non-Newtonian fluid with a power law viscosity, strongly dependent on temperature (see e.g., the equation (2.4) and the parameterization shown in (2.5)). The absence of privileged directions in the distribution of lattice orientations (i.e., fabric) is generally assumed and the isotropic mechanical response is inferred. On the other hand, fabric profiles in many ice cores show a transition with depth of the ice from isotropy to strong anisotropy and often, at very large depths, a near return to isotropy. Fig. 2.3 shows data

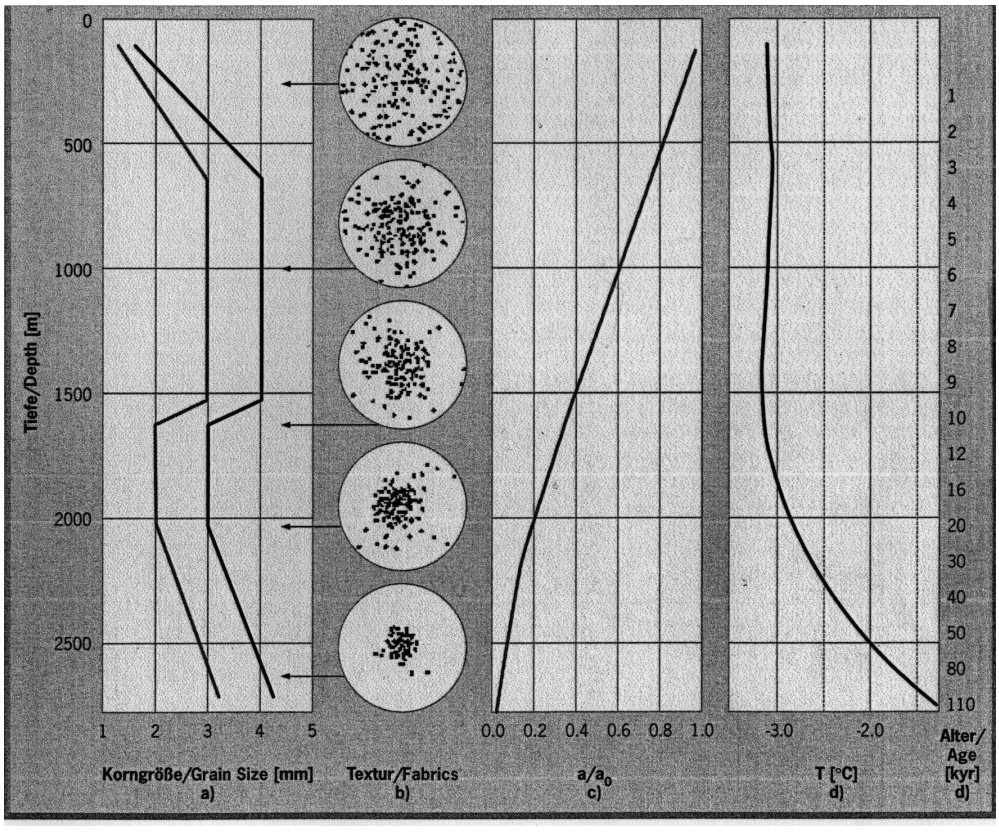

Figure 2.3: Data from the Greenland Ice Project (GRIP) drill core, 1990-1992. Diagrams depict (a) mean grain-size, (b) orientation of the c-axis of the crystals, (c) degree of anisotropy, and (d) temperature. Each point inside the circles shown in (b) is the vertex of a unit vector designating the c-axis direction of a crystal grain (a) so-called Schmidt diagram). (Courtesy: T. Thorsteinsson, [132, 134])

through the GRIP[1] ice core in Greenland with measured profiles for the mean grain-size and the Schmidt circles determined from analyses of thin sections of the samples. An anisotropic constitutive model that was constructed for this situation [94] showed that at certain depth (in GRIP below app. $2800m$) differences in age of the ice, computed with an isotropic and anisotropic stress-stretching relationship may differ by several tens of thousends of years (40000 to 100000 years, depending on basal topography). This makes the development on the theories about the material response of polycrystal *polar ice* an urgent and extremely challenging research topic.

This chapter reviews the efforts that have been taken since the early 80s of the last century to arrive at an adequate constitutive relation of a very complex anisotropic fluid. This review comprises works up to and including 2003. It demonstrates that there is very active research going on in the geophysical sciences that use the most advanced methods of mechanics and materials sciences. The paper begins with a review of laboratory experiments of uniaxial tension/compression and simple shear performed on polycrystalline ice samples and the parameterization of the Glen–Steinemann flow law in the geophysically relevant regime of temperatures, 210-273.15 K, and stresses, $1-5$ bars[2], (Section 2.2). The influence of the grain size to the flow law is reported and its parameterizations are discussed. These laws account only for a mean grain diameter. Studies on the GRIP ice core by Thorsteinsson [132, 134] have, with good accuracy, shown that grain sizes are log-normally distributed which ought to be accounted for (Section 2.3). Besides, the influence of lattice orientations is also discussed (Section 2.4).

In early studies of the flow law for polar ice, the orientation of the crystallites, the dust content, grain growth and grain size are only accounted for in the isotropic flow law by an enhancement factor, thus not accounting for the nonuniformity of the orientation distribution in a Representative Volume Element (RVE). In order to model the anisotropy induced by the applied load, both the Taylorand the Sachs assumptions have been used in the literature; thus, either the strain incompatibility or the stress incompatibility are avoided, but generally not both. One of the difficulties in the homogenization process of the polycrystalline polar ice consists in the fact that, in the crystal, basal gliding is about 60 times easier than pyramidal and prismatic gliding; this is the dominant factor why the Taylor hypothesis leads to an unrealistic assignment of the deformations to the five different gliding systems. This is apparently better done when stress compatibility is requested, but, of course, stretching incompatibilities then still remain. First formulas for a homogenized anisotropic flow law – a relation between Cauchy stress and stretching – make this relationship depending on the Schmidt tensor, but the distribution of the fabric must be known and no evolving fabric is possible (Section 2.5).

Macroscopic models, which assume a statistical distribution of the crystallites within the RVE are developed in glaciology, since approximately 1995. They are based on the assumption of an Orientation Distribution Function (ODF), which represents the probability density of the crystallites with c-axis orientation per solid angle. Theoretical models then consist of an evolution (Fokker–Planck) equation for the ODF, a set of constitutive equations for the macro quantities, including a certain number of anisotropy tensors of second and fourth order and a thermodynamic exploitation for the proposed constitutive

[1]Greenland Ice Core Project, drilling the core in the years 2000-2002. The core was taken at summit the highest point of the Greenland ice sheet. It is 3229 m long.

[2]In Fig.2.4 the range for stresses is even larger.

class (Section 2.6).

These models account for the crystal rotation but not the anisotropy produced by recrystallization, i.e. by normal and abnormal grain growth, by nucleation, polygonization and grain boundary migration. For this part of anisotropy the linear defects in the crystal lattice (namely dislocations) are responsible. This requires the description of the evolution of the dislocation density, whereby its growth rate must be attributed to the stretching, whilst its wastage is due to grain boundary migration and polygonization and both also depend on grain size (Section 2.7).

This is the state of the art that we shall further detail in the text that follows.

2.2 The Legacy of Isotropic Ice

In order to describe the flow of an ice sheet, polycrystalline ice is often considered as an isotropic very viscous fluid. This led to the celebrated Glen (or Glen–Steinemann) flow law [47, 129] and its representation as a three-dimensional viscous power law fluid [109],

$$D_{ij} = A\,(T)\;\sigma^{n-1}\;t_{\langle ij\rangle}, \tag{2.3}$$

valid for effective stresses in the range of 100 to 300 kPa where D_{ij} is the stretching (strain rate), $t_{\langle ij\rangle}$ the deviatoric part of the Cauchy stress tensor t_{ij}, $2\sigma^2 = t_{ij}t_{ij}$ is related to the second invariant of t_{ij}, and $A\,(T)$, a temperature dependent parameter, is also called the *rate factor*. Hence, as already observed by Steinemann [129] almost 50 years ago, the exponent n depends on σ (see also [2, 32, 38, 129, 144]). Besides this awkward dependence of power law exponent on stress, the mentioned Glen flow law suffers from its infinite apparent viscosity at zero stress deviator, $\eta = dt_{\langle ij\rangle}/dD_{ij} \to \infty$ (no sum over i,j) as $t_{ij} \to 0$. In laboratory experiments, when transient creep has not been fully eliminated, the apparent viscosity is a finite quantity; furthermore, this singularity would cause subtle difficulties whenever shallow ice approximation is considered [61]. Thus, it transpires that Glen's flow law need be generalized. Among others, Lliboutry [90], Colbeck and Evans [21], Hutter et al. [69, 70, 71] have amended the simple Glen's flow law by writing

$$D_{ij} = A\,(T) f\,(\sigma)\,t_{\langle ij\rangle}, \tag{2.4}$$

with $f(\sigma) > 0$ for all σ – called the *creep response function* or *fluidity* – obeying the finite viscosity requirement $0 < f(0) < \infty$ and $f(\sigma)$ otherwise chosen to match experiments in the entire stress range of 0 to 1 MPa. Parameterizations for the fluidity f and for the rate factor A are

$$f\,(\sigma) = \begin{cases} a\,\sigma^4 + b\,\sigma^2 + \eta^{-1}, \\ \sigma^{n-1} + \eta^{-1}, \\ \dfrac{1}{|\sigma|}\sinh^n(\alpha\sigma) + \eta^{-1}, \end{cases} \qquad A\,(T) = \begin{cases} A_0 \exp\left(-\dfrac{Q}{kT}\right), \\ \displaystyle\sum_{j=1}^{2} A_j \exp\left[\alpha_j\,(T - T_{\mathrm{M}})\right], \\ B_0 \exp\left\{\dfrac{T_0}{T} - \dfrac{C}{(T_r - T)^s}\right\}, \end{cases} \tag{2.5}$$

in which bounded $\eta \neq 0$ accounts for Newtonian behaviour at zero effective stress; k is the Boltzmann constant, T the absolute temperature and T_{M} its Melting point temperature, while a, b, n, α, A_j, α_j, B_0, T_r and s are temperature-independent parameters to

be identified by experiments. Specifically, the polynomial law, the first line of $(2.5)_1$ was recommended by Lliboutry [90] in 1969, while the second line of $(2.5)_1$ is a slight modification of (2.3) to account for finite apparent viscosity. The power-sinh law in the third line of $(2.5)_1$, also known as the Garofalo law [46], matches uniaxial compression tests by Barnes et al. [12] very well in the entire stress range $0 < \sigma < 1$ MPa (see Fig. 2.4). The Arrhenius relationship in the first line of $(2.5)_2$ represents measurements of Mellor and Testa [102] only for $T < 263\ K$, whilst the second line of $(2.5)_2$, due to Morland and Smith (see e.g. [70]) is valid also for higher temperatures. In 1981, Hooke proposed a different parameterization for $A(T)$, represented by the third line of $(2.5)_2$.

As shown by Hutter [70] it is possible to give a formal derivation of (2.4) from first principles of continuum mechanics by assuming that the polycrystalline ice is an incompressible non-linear viscous fluid. To this end, two other assumptions are necessary: the third invariant of the deviatoric stress has no effect on the material response and the stress deviator must be collinear to the strain rate tensor. The validity of the two assumptions is doubtful [11, 48, 70, 110, 140]; however the precision of the measurements is not clear and a conclusion that (2.4) would be inappropriate seems to be premature.

Notwithstanding, in attempts to achieve a better parameterization of the flow law (2.4), measurements often disagree with previous investigations, and so such contradictions still must be explained. The reason seems to be the high number of variables that

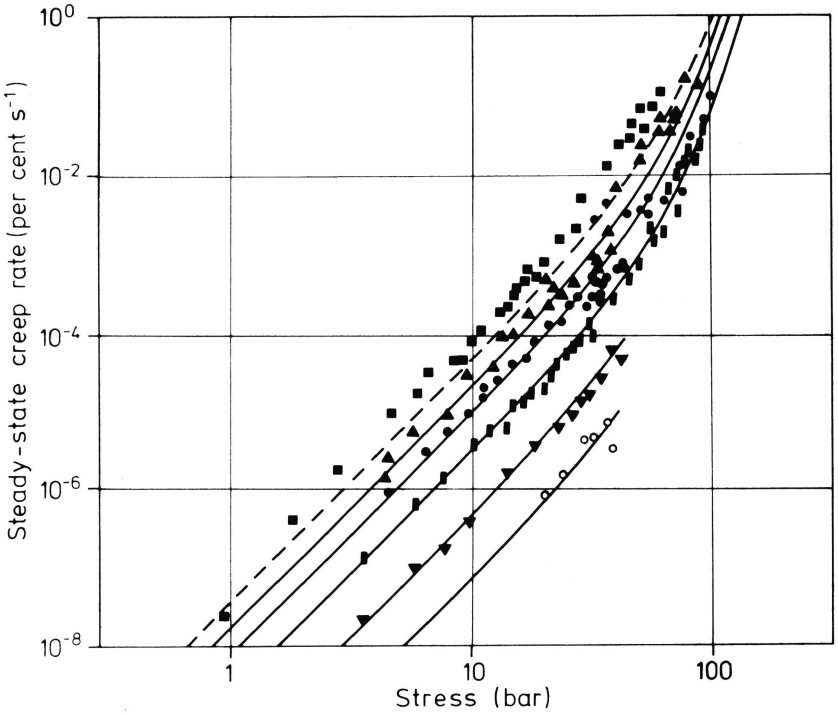

Figure 2.4: Steady-state creep for the secondary flow of polycrystalline ice in uniaxial compression against applied stress. ■ −2°C, ▲ −8°C, •−14°C, −22°C, ▼ −34°C, ○−48°C. The curves are calculated via sinh functions based on all experimental points between −2°C and −48°C. (from Barnes et al. [12], with modifications)

consistently affect equation (2.4), and these variables must be found in the microstructure. Impurity content, rock particles and grain sizes of all crystallites can in fact play a significant role. An important requirement in deformation studies is to understand such processes and to acquire knowledge of the conditions in which they occur. The target is, consequently, the prediction of the ice behaviour.

The usual method is to develop constitutive relations for the various microscopic deformation processes and to construct the so-called *deformation-mechanism map* to delineate the precise set of conditions where each individual mechanism is dominant [84]. Generally, it is convenient to plot the macroscopic variables (e.g. temperature, deviatoric stress, strain rate) as the axes for such maps, holding the microscopic variables (e.g. grain size, dislocation density etc.) constant [57]. A first classification of deformation mechanisms differentiates between boundary-mechanisms and lattice-mechanisms. The boundary-mechanisms are related to the behaviour of the grain boundary and therefore to grain size. The lattice-mechanisms refer to the behaviour of the crystalline structure, and since this presents a strong anisotropy for ice, a randomless distribution of the lattice orientations destroys the isotropic structure of the flow law (2.4). Therefore, the key parameters are related, in this case, to the lattice orientation of the grains.

2.3 The Influence of Grain Size

The concept of crystal size dependent rheology is not new in glaciology. In fact, in 1971 Barnes et al. [12] suggested a grain-size dependent deformation mechanism for temperatures higher than 263 K and attributed it to Grain Boundary Sliding (GBS). The experimental data indicate a marked softening of polycrystalline ice above that temperature, and a similar behaviour does not occur in creep of single crystal of ice. This and the formation, in that range of temperature, of liquid phase pockets at grain boundary sites suggest that the softening mechanism must be associated with GBS.

On the other hand, in 1995 de la Chappelle et al. [26] influenced the softening due to the formation of the liquid phase at grain boundaries as an attenuation of the internal stress field that should promote glide on basal planes, a deformation mechanism that is different from the sliding of grain boundaries. Moreover, in 1997 Goldsby and Kohlstedt [54] published results based on innovative laboratory techniques for fabricating ice samples with very fine grain size in such a way to be able to parameterize measurable[3] strain rates in terms of grain size. They proposed a new flow law for ice, namely a superplastic law[4] of the form

$$D_{ij} = A\,(T)\,\frac{\sigma^{n-1}}{D^{p}}\,t_{\langle ij\rangle}, \tag{2.6}$$

in which D is the grain size and the power exponent p is positive. This flow law is still of Glen type, i.e., it only applies to isotropic polycrystalline ice. Further investigations on grain-size control of the strain rate were conducted by the same authors in 2001 [56] and in 2000 by Cuffey et al. [22, 23]. These last two papers are interesting because they investigate the connection of the flow law with the impurity content and rock particles; this is also the subject in Thorsteinsson et al. [135] (see e.g. eq. (2.20)).

[3] We can observe from 2.6 that the higher the strain rate, the lower is the grain size.

[4] The terminology *plastic* and *viscous* is not as strict in materials science as it is in mechanics, where (2.6) would be called viscous.

Thus, the development of a grain-size dependent flow law, as equation (2.6), has always come parallel with investigations of its microscopic interpretation, about which there is no agreement in the glaciological community (see also [34, 55]). The main criticism concerns the compatibility between such a mechanism and the formation of fabrics, i.e., the change of the distribution of lattice orientations. We will see in the next section (cf. Figs. 2.6 and 2.7) that the development of a nonuniform distribution of lattice orientations is interpreted by another microscopic mechanism, namely crystal glide on basal planes.

Furthermore, we remark that, even if the main microscopic deformation mechanism can be classified as a lattice mechanism, the role of the dislocation density ρ_d, must not be forgotten, and, indeed, explicit evolution equations for ρ_d have always had grain size as one of the fundamental governing parameters (see e.g. subsections 2.7.3 and 2.7.4). Moreover, from a microscopic point of view, grain size varies abruptly from a crystallite to its neighbours; thus, the phenomenological description will obviously become very complicated if all grain sizes are accounted for. Generally, this difficulty is overcome by accounting in a Representative Volume Element (RVE) only for the mean value of the grain sizes of the crystallites present in the RVE. It is, however, the correct belief that this approximation is nevertheless too rough and one is forced to deal with the whole distribution of grain sizes. Measuring the grain-size distribution, also called texture, is now a common procedure in investigations of ice cores [132]. Generally, the distribution $n^{\blacktriangleright}(D)$ of grain sizes follows a log-normal distribution, i.e.,

$$n^{\blacktriangleright}(D) = \frac{1}{\sqrt{2\pi}\sigma D} \exp\left\{ -\frac{\left[\ln\left(\frac{D}{D_{\mathrm{m}}}\right)\right]^2}{2\sigma^2} \right\}, \tag{2.7}$$

where D_{m} and σ are the mean value and the standard deviation, respectively. Analyses of the properties of this kind of distribution can be found e.g. in the well-known work of Marsh published in 1988 [97].

On the other hand, the most important mechanism describing the creep deformation of ice in an ice sheet is glide on basal planes. Thus, we will analyse in the next section another distribution, the distribution of lattice orientations.

2.4 The Influence of Lattice Orientations

It is widely accepted that the reason of the mechanical anisotropy of polycrystalline ice lies in the microstructure and comes from the strong anisotropy of the monocrystals (see e.g. [15, 32, 38, 64, 95, 99, 110, 136, 141, 144]). Thus, the most important characteristic, generally believed to affect the flow law of polycrystalline ice, is the distribution of lattice orientations. If it is uniformly random, then the behaviour is isotropic and the framework of (2.4) or (2.6) is useful. On the other hand, deformations induce a change in such a distribution and an anisotropic flow law must be formulated (see Chapter 3). So, whereas formulas (2.4) or (2.6) indeed may match an individual strain rate component with an individual stress deviator component, their three-dimensional extrapolation is simply false. Nonetheless, early attempts to account for the differences of the fluidity in Holocene and Pleistocene ice maintained (2.4), amending it to incorporate an enhancement factor[5] E,

[5]The *strain rate enhancement* or *enhancement factor* is the ratio between the measured strain rate and the strain rate as considering by isotropic behaviour, i.e., the Glen flow law.

viz.,

$$D_{ij} = EA\,(T)\ f\,(\sigma)\ \ t_{\langle ij\rangle}, \tag{2.8}$$

and attributed to E all those properties one did not properly understand but is forced to account because of obvious observational evidence [2, 4, 10, 15, 19, 38, 43, 59, 60, 68, 78, 79, 93, 110, 114, 132, 134]. An early internal variable theory was also proposed to thermodynamically justify the introduction of E [72]. The failure of this kind of fudging procedure, in the analysis of the influence of lattice orientations, was quickly realized as with (2.8) no directional variation of the effective fluidity can be modelled. So, (2.8) is also a false three-dimensional amendment of the classical Glen flow law.

Single crystals deform in fact by slip along the crystallographic planes (Fig. 2.5), and for usual temperatures ($210\,\mathrm{K} < T < 273.15\,\mathrm{K}$) the slip resistance is up to 60 times smaller parallel to the basal planes than to the other slip planes of the system. Thus, as commented by McConnel [99] in 1891:

> "[...] *the crystal behaved as if it consisted of an infinite number of indefinitely thin sheets of paper, normal to the optic axis, attached to each other by some viscous substance which allowed one to slide over the next with great difficulty. This comparison proved to be the key to the whole question of the plasticity of a crystal of ice.*" (p. 325)

Following this simple idea, which has since then been repeatedly confirmed by experiments [32, 49, 64, 65, 96, 118, 129, 146] it is possible to comprehend the failure of the isotropy assumption through the Gedanken Experiments illustrated in Figs. 2.6 and 2.7.

The "thin sheets of paper" mentioned by McConnel can be envisaged as cards in a pile, with their normal vectors, representing the c-axis of the crystal, initially inclined by some angle (ϕ_0 in case (a), θ_0 in case (b)) with respect to the vertical. Independently of the value of this initial angle (ϕ_0 or θ_0), the c-axis of the crystal will tend to rotate towards the principal axis of compression, whenever a load is applied on the crystal. On the other hand, it is easy to show by a similar Gedanken Experiment, see Fig. 2.7, that the c-axes of the crystallites tend to rotate away from the principal axis of tension. This means that

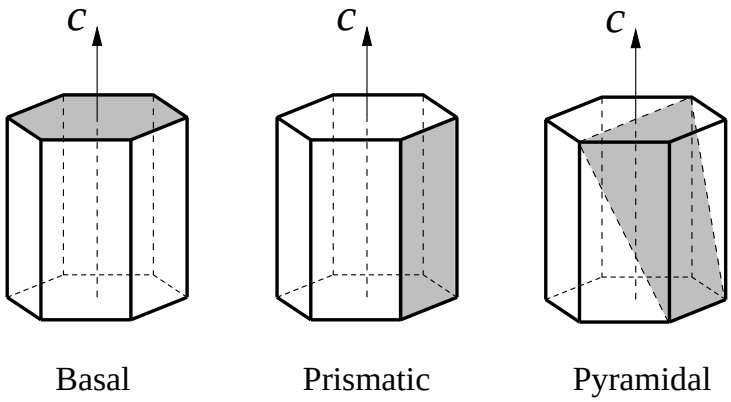

Figure 2.5: Sketch of a single ice crystal in the form of a right hexagonal prism. Three crystallographic planes are indicated

there is a connection between the sense of the rotational velocity of the crystallites and their strain rate. In Section 5.3 we will present a theory on the fabrics evolution that is coherent with the properties we have here pointed out.

As far as we have explained, only the deformation mechanism of glide along basal planes is coherent with the development of fabrics. On the other hand, the superplastic flow law represented in (2.6) is not compatible with such a mechanism. To overcome this problem Goldsby, Kohlstedt et al. [54, 111] suggested a compromise between the different mechanisms. However, a crucial experiment on the basis of which one could identify a mechanism that justifies equation (2.6) has not yet been found. We claim that a justification of (2.6) in terms of a microstructure process is not clear, but its validity in a certain range of the deformation mechanism map is supported by experimental data.

Mechanical tests on single crystals disclose behaviour similar to that of (2.4) for the components relative to the simple shear (i.e., D_{13} or D_{23} with the third axis parallel to the c-axis). Models and experiments of ice single crystals [32, 38, 64, 144, 146] lead in fact to creep rate equations having power law form and an Arrhenius type temperature dependence: since viscous sliding of the "cards" is driven by the resolved shear stress on the basal plane τ, the strain rate is proportional to τ^n, and the exponent is preferably $n = 2$ and less convincingly $n = 3$ [32, 49]. This supports, for a polycrystalline ice sample, the supposition that the controlling mechanism of deformation for $T < 263\,\mathrm{K}$ should also be basal sliding via dislocation glide. However, this raised for a long time a number

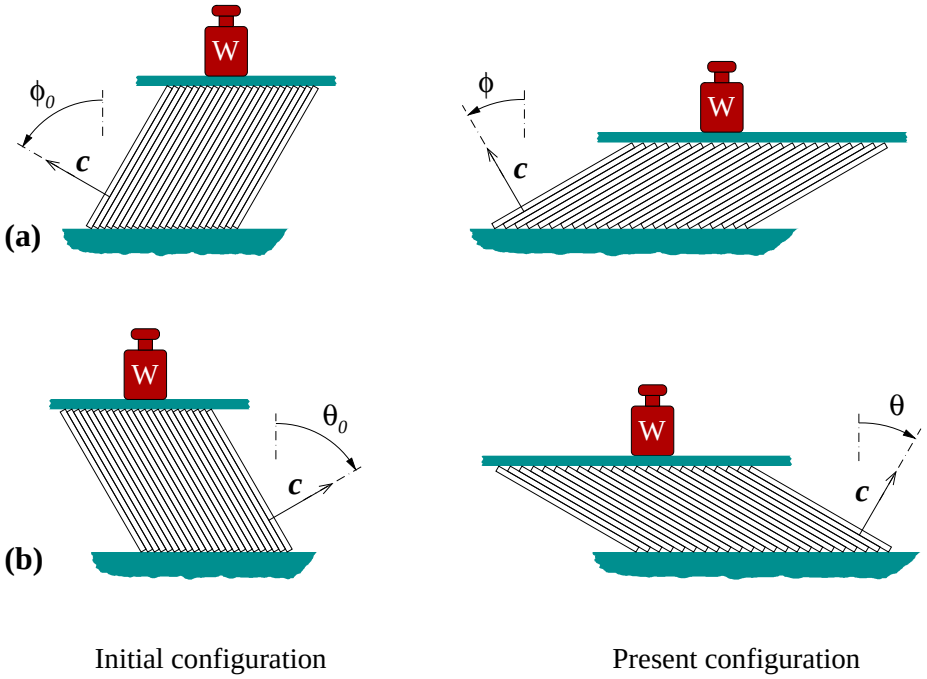

Figure 2.6: An ice crystal as a "deck of cards": when subjected to vertical compression due to the load W the crystal deforms by basal slip, forcing a rotation of its c-axis towards the principal compressive axis (vertical), regardless what the starting orientation of its c-axis in the initial configuration may be. In spite of some differences, the grains of a polycrystalline piece of ice are expected to deform in a somewhat similar manner, building so a concentration of c-axes about the vertical (called *single-maximum/single-pole fabric*)

of objections [33, 49, 64, 144]. Indeed, as we will discuss in the next section, the mere mismatch of the crystal orientations in a polycrystal seems to suggest that besides the planes of easy glide also the prismatic and pyramidal planes of hard glide should become active because of geometric compatibility (see e.g. the two-dimensional example in Fig. 2.8). This could qualitatively explain why polycrystalline ice is harder than a single crystal of ice under easy glide, whereas it is softer under hard glide conditions. It must be remarked here that the geometrical incompatibility between grains that are deformed only by glide on basal planes can be adjusted not only by the activation of pyramidal and prismatic planes, but also by the mobility of grain boundaries through the phenomenon of *grain boundary migration* (see, e.g. the Section 2.7).

Besides, the above arguments also make it obvious that the flow resistance will be orientation dependent according to the actual distribution of the crystal orientations within a sample.

We discussed the importance of grain size and orientation distributions and their role in the flow law. As we already pointed out, these concepts are often referred to in other words, namely as texture and fabric, respectively. Semantically, these two words have the same meaning. However, it is common to refer by fabric to a characterization of a distribution of orientations and by texture to a characterization of a distribution of grain sizes.

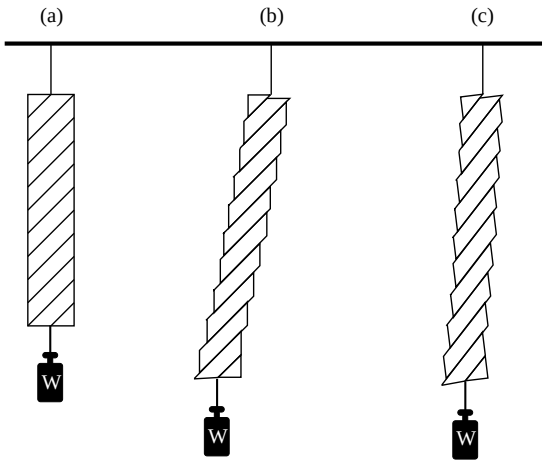

Figure 2.7: The analogue of Fig. 2.6 for the case of tension. It is evident that the crystallite tends to rotate away from the principal axis of tension. On the left-hand side of the figure (a), the crystallite is schematically represented as a rectangle. The lines in the rectangle represent the basal planes and the weight W generates a tension of the crystal. Since gliding along the basal planes is the only possible deformation mechanism, the rectangle can be deformed only as shown in part (b). In this position, the crystal is not in equilibrium, since a couple is acting on it. (c) Rigid body rotation re-establishes equilibrium and shows that under tension, the crystallites rotate away from the principal axis of tension.

2.5 Modelling Induced Anisotropy: Microscopic Models

2.5.1 The Taylor Hypothesis

If an incompressible body suffers uniform strain, it is obvious that stretches in five suitably distinct directions suffice to determine the whole deformation of the specimen simply because the strain rate tensor of a density preserving body has five independent components. This led von Mises [143] to conclude in 1928 that five independent slip systems[6] are required to impose an arbitrary strain in any crystal which deforms only by glide along these slip planes. Just ten years later, Taylor [131] used von Mises' inference to develop his celebrated theory of plastic strain in polycrystalline metals. *Taylor's hypothesis* can be reported as follows: *each crystal of the aggregate should suffer exactly the same strain as the bulk* (avoiding so the occurrence of microcracks and voids in the material due to incompatibilities among neighbouring grains). On these grounds he calculated deformation and fabric development of a polycrystalline medium in terms of its single crystalline rigid-plastic behaviour. In Fig. 2.8, we show a two-dimensional example. In this case the independent components of the strain rate of a density preserving body are only two. In the example the activation of the *basal* planes only causes a V-shaped void in Fig. 2.8b. On the other hand, the activation of both (*basal* and *prismatic*) planes avoids the occurrence of the geometrical incompatibility, see Fig. 2.8c.

Because of its simplicity, the model proposed by Taylor still continues to be widely used (sometimes with slight modifications) to predict the evolving anisotropy of polycrystals [4, 63, 142]. In spite of this, it is now recognized that the assumptions underlying Taylor's model build just a simplified picture of a commonly much more complex reality. Patchy deformations, grain boundary sliding and migration, shear and kink bands, diffusional flow, polygonization and dynamic recrystallization are just some of the presently known processes which can occur, allowing *inhomogeneous strains* [4, 29, 31, 54, 59, 62, 68, 96] and frustrating the requirement of five independent slip systems for each crystal [16, 92, 116, 139].

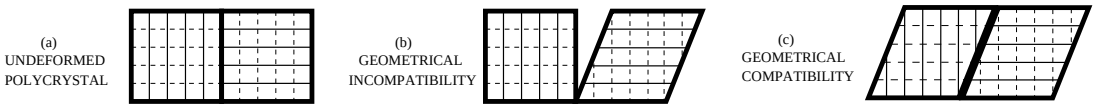

Figure 2.8: (a) A schematic two-dimensional picture of a polycrystal made of two crystallites. The thick lines represent the grain boundaries; the thin lines and the dashed lines represent the generalization of the *basal* and *prismatic* planes for a two-dimensional crystallite. (b) If the crystallite on the right-hand side is deformed via glide on the *basal* planes, then the geometrical compatibility cannot be fulfilled because the deformation of the other crystallite can not adjust the deformation of the first one, i.e., a V-shaped vacuum is created. (c) If the *prismatic* planes are active (i.e. the deformation is allowed also via glide on these *prismatic* planes), then compatibility of the deformation between the two crystallites can be achieved.

[6] A *slip system* is defined by the combination of a crystallographic plane and a particular slip direction on this plane.

2.5.2 The Sachs Hypothesis

When applied to ice, Taylor's model achieves a very deceptive performance [16, 18, 20]: it demands a contribution to the total strain of about 60% arising from non-basal slip and, consequently, it predicts strain rates which are too low in comparison with experimental data, as well as rather loose fabrics (i.e., low anisotropy). This outcome, added by the lack of experimental evidence on non-basal slip and the observation that hard glide is at least 60 times more difficult to activate than basal easy glide [32, 93], led glaciologists to prefer models which do not strictly require strain compatibility among neighbouring grains, with the hope that additional mechanisms (usually not considered in the modelling), like grain boundary migration or polygonization, can fulfil the necessity of coherence in the aggregate.

The simplest alternative is to reckon the deformation as being produced entirely by basal glide and to assume that stress, instead of strain, is homogeneous in the polycrystal. This last hypothesis, which can be traced back to Sachs [120] and Reuss [119], is commonly called *Sachs' hypothesis*. The Sachs' hypothesis has been considerably more successful for ice than Taylor's hypothesis: many of the already proposed models for anisotropic ice are based on such premises, even though some with modifications [17, 44, 45, 51, 52, 53, 92, 135, 141].

2.5.3 Models Including Fabric Evolution

A first effort to describe the fabric evolution of ice under prescribed uniaxial compressive strain was given by Azuma and Higashi [9]. Through direct observation of the crystallographic orientations in thin ice specimens compressed at constant rate, they found that the compressive strain $\varepsilon^{(g)}(< 0)$ in the grains was not the same, but correlated with the orientation of their c-axis, ϕ_0 given by the angle relative to the direction of compression of the sample (cf. Fig. 2.6a). Hence, crystals more favourably aligned for deformation by basal glide should exhibit larger strains. The fitting of their data led Azuma & Higashi to suggest an empirical relation between $\varepsilon^{(g)}$ and the bulk axial compressive strain ε, of the form

$$\varepsilon^{(g)} = \frac{S^{(g)}}{\bar{S}}\,\varepsilon, \tag{2.9}$$

where $S^{(g)} = \cos\phi_0 \sin\phi_0$ is the *Schmidt factor* (of the grain g, of which that c-axis is oriented at ϕ_0) and $\bar{S}$ is its average, viz.,

$$\bar{S} = \frac{1}{N}\sum_{g=1}^{N} S^{(g)}, \tag{2.10}$$

where N is the number of grains. To compute the rotation of the c-axis of a crystallite, they used the simple geometric relation valid for compression

$$\sin\phi = \left(1 + \varepsilon^{(g)}\right)\sin\phi_0, \tag{2.11}$$

where ϕ is the angle between the sample's axis of compression and the c-axis, after rotation (see e.g. [123, 132, 141]). This model was extended to uniaxial tension $\varepsilon^{(g)}(> 0)$ by Fujita

and others [43] and Lipenkov and others [87]: they used another simple geometric relation (see e.g. [123, 132, 141]) valid for tension, i.e.,

$$\cos\phi = \left(1+\varepsilon^{(g)}\right)^{-1}\cos\phi_0, \tag{2.12}$$

whereas Alley [1] generalized the model to pure shear by superimposing uniaxial tensile and compressive strains. Further, Alley also combined pure shear with a subsequent rigid body rotation to enable the simulation of simple shear. A weak point of these models is that the empirical law (2.9) is based on laboratory observations where the strain rate is almost four orders of magnitude larger than in ice sheets. On the other hand, laboratory tests can not be performed at such small strain rates: the time that one must wait to have reasonable strains would be simply too long[7].

The evolution of fabric is only part of the problem of the anisotropic behaviour. The other problem concerns directly the form of the flow law. In the next subsection, we analyse models built to this aim.

2.5.4 Homogenized Anisotropic Flow Laws

In 1994 Azuma [7] attempted to improve his early approach and presented in 1996, together with Goto-Azuma [8], an anisotropic generalization of Glen's flow law (2.3) in the form

$$D_{ij} = A\bar{S}_{(ij)}\left(\bar{S}_{(kl)}t_{kl}\right)^n, \tag{2.13}$$

with

$$A = A'\exp\left(-\frac{Q}{kT}\right), \qquad \bar{S}_{(ij)} = \frac{1}{2}\left(\bar{S}_{ij}+\bar{S}_{ji}\right), \qquad D_{kk} = \bar{S}_{jj} = 0. \tag{2.14}$$

In these equations, D_{ij} and $t_{ij} = t_{\langle ij\rangle}$ are, respectively, the stretching and the Cauchy stress deviator of the polycrystal, while $\bar{S}_{ij}$ denote the averaged Cartesian components of the *Schmidt tensor*, viz.,

$$\bar{S}_{ij} = \frac{1}{N}\sum_{g=1}^{N} S_{ij}^{(g)}, \qquad S_{ij}^{(g)} = m_i^{(g)}c_j^{(g)}, \tag{2.15}$$

where $c_i^{(g)}$ and $m_i^{(g)}$ are, respectively, unit vectors parallel to the c-axis and to the resolved shear stress in the basal plane of the g-th grain, viz.,

$$m_i^{(g)} = \frac{T_i^{(g)}}{\left(T_k^{(g)}T_k^{(g)}\right)^{\frac{1}{2}}}, \qquad T_i^{(g)} = t_{ij}c_j^{(g)} - \left(c_k^{(g)}t_{kl}c_l^{(g)}\right)c_i^{(g)}. \tag{2.16}$$

Thorsteinsson and others [134] suggested that the implicit idea of the above model should be to replace each crystallite of the aggregate by another one, of which the c-axis orientation is given by the averaged Schmidt tensor $\bar{\boldsymbol{S}}$. However, this claim is false because $\bar{\boldsymbol{S}}$ cannot be related to the c-axis of one crystallite. To prove this, it suffices to

[7] This is a dilemma of many attempts to identify the characteristic parameters of mechanical processes of geophysical time scales. They last much longer than human life spans.

give a simple example: imagine a polycrystal is made of two orthogonal crystallites with slip systems $\left(\boldsymbol{m}^{(1)}, \boldsymbol{c}^{(1)}\right)$, $\left(\boldsymbol{m}^{(2)}, \boldsymbol{c}^{(2)}\right)$ and respective Schmidt tensors $\boldsymbol{S}^{(1)}$, $\boldsymbol{S}^{(2)}$. For the sake of simplicity, consider matrix notation:

$$\boldsymbol{m}^{(1)} = (1,0)\,, \quad \boldsymbol{c}^{(1)} = (0,1)\,, \quad \boldsymbol{S}^{(1)} = \boldsymbol{m}^{(1)} \otimes \boldsymbol{c}^{(1)} = \begin{pmatrix} 0 & 1 \\ 0 & 0 \end{pmatrix};$$

$$\boldsymbol{m}^{(2)} = (0,1)\,, \quad \boldsymbol{c}^{(2)} = (1,0)\,, \quad \boldsymbol{S}^{(2)} = \boldsymbol{m}^{(2)} \otimes \boldsymbol{c}^{(2)} = \begin{pmatrix} 0 & 0 \\ 1 & 0 \end{pmatrix};$$

the averaged Schmidt tensor, $\bar{\boldsymbol{S}}$, is easily evaluated,

$$\bar{\boldsymbol{S}} = \frac{1}{2}\sum_{g=1}^{2} \boldsymbol{S}^{(g)} = \begin{pmatrix} 0 & \frac{1}{2} \\ \frac{1}{2} & 0 \end{pmatrix}; \tag{2.17}$$

its determinant is non-zero and so it is not a dyad, that means $\bar{\boldsymbol{S}}$ can not be represented by a tensor product between two vectors as every Schmidt tensor, e.g., $\boldsymbol{S}^{(1)}$ and $\boldsymbol{S}^{(1)}$ (see also the definition $(2.15)_2$). This implies that it is impossible to extract from $\bar{\boldsymbol{S}}$ the c-axis of the new (mesoscopic) crystallite.

The same authors also proposed that the model of Azuma–Goto-Azuma [8], mentioned above, could be derived from the usual Sachs hypothesis expressed in terms of the flow law

$$D_{ij} = A\bar{G}_{ij}, \qquad \text{where} \qquad G_{ij}^{(g)} = S_{(ij)}^{(g)} \left(S_{(kl)}^{(g)} t_{kl}\right)^n, \qquad t_{ij} = t_{ij}^{(g)}, \tag{2.18}$$

where $\bar{G}_{ij}$ denotes the average of $G_{ij}^{(g)}$ over all grains. The derivation is accomplished through replacing in (2.18) the average of the $(n+1)$-power tensorial product of the symmetric Schmidt tensor $S_{(ij)}^{(g)}$ by the $(n+1)$-power tensorial product of its averages; that is, for the case $n = 3$ (say):

$$\overline{S_{(ij)}^{(g)} S_{(kl)}^{(g)} S_{(pq)}^{(g)} S_{(rs)}^{(g)}} \;\Rightarrow\; \bar{S}_{(ij)} \bar{S}_{(kl)} \bar{S}_{(pq)} \bar{S}_{(rs)}. \tag{2.19}$$

Nevertheless, the validity of (2.19) is certainly questionable. Indeed, Thorsteinsson et al. [135] applied both models (Sachs' and Azuma's) to account for effects of anisotropy in the ice extracted from the Dye 3 borehole in Greenland and, as expected, sensible differences between the two approaches were observed, even though the authors could not identify which model had the best performance. They concluded also that no model was able to describe the strain rate enhancement at Dye 3 well. To justify the discrepancies of $\approx 25\%$, they replaced the rate factor A in (2.13) and in (2.18) by A^T, i.e.,

$$A^T = A\,(1+f)\,, \qquad f = \frac{C}{D} \tag{2.20}$$

where f is a phenomenological *impurity factor* depending in the most trivial manner on the impurity content C and grain size D. Besides, the analogy with the superpalstic flow law (2.6) with respect to the grain-size dependency is noted.

The weakest point in Azuma–Goto-Azuma's model [8] (as well as in its adaptations) is its inability to describe fabric *evolution*. More useful models are developed in fact with the target to solve both problems, i.e. the fabric evolution and the anisotropic flow law.

2.5.5 Complete Microscopic Models

One of the first approaches to reach the goal to describe, at the same time, the fabric evolution and the anisotropic flow law, was proposed by van der Veen and Whillans in 1994 [141]; they adopted Sachs' hypothesis and assumed that each crystal should deform only by basal slip driven by a viscous power law. The idea is the following: A certain state of stress is applied to the whole polycrystalline material. The Sachs hypothesis assures that this is transferred to all crystallites. The viscous power law that they assume for the single crystallite is the three-dimensional generalization of that derived by Weertman in 1973 [145], i.e.,

$$\dot{e}_{i\nu} = A\left(\tau_{\eta\nu}^2 + \tau_{\mu\nu}^2\right)^{\frac{n-1}{2}} \tau_{i\nu}, \qquad i = \eta, \mu \qquad \text{no summation over } \nu \tag{2.21}$$

where $\dot{e}_{i\nu}$ and $\tau_{i\nu}$ are the strain rate[8] and the stress tensors of the crystallite in the frame of reference $O\eta\mu\nu$, the third axis of which (with index ν) is parallel to the c-axis and coherent with the crystallite itself; A is a temperature-dependent rate factor and n is a parameter set equal to 3. Let us remark that the strain rate related to the other components ($\dot{e}_{\eta\eta}$, $\dot{e}_{\mu\mu}$, $\dot{e}_{\nu\nu}$, $\dot{e}_{\eta\mu} = \dot{e}_{\mu\eta}$) are zero. This reflects the assumption that each crystal is allowed to deform only by basal slip. If Δt is a small time interval, the strain of the single crystallite in the frame of reference $O\eta\mu\nu$ is simply given by

$$e_{ij} = \dot{e}_{ij}\Delta t. \tag{2.22}$$

The relation between e_{ij} and the strain ϵ_{ij}^k of the single crystallite with respect to the external frame of reference $Oxyz$ is

$$\epsilon_{ij}^k = \omega_{ki}\omega_{lj}e_{kl}, \tag{2.23}$$

where ω_{ij} is the rotation from the external frame of reference $Oxyz$ to the reference frame $O\eta\mu\nu$ that matches the crystal orientation at the start of each time step. The strain of the bulk polycrystal ε_{ij}^b is the mean of ε_{ij}^k, i.e.,

$$\epsilon_{ij}^b = \frac{1}{N}\sum_{k=1}^{N} \epsilon_{ij}^k, \tag{2.24}$$

where N is the number of crystallites. It is clear that the explicit definition of ω_{ij} is of great importance for the fabric evolution. At the initial step, ω_{ij} is defined by the latitude and the longitude of the single crystallite to which it is referred. At the second step these angles are defined again in order to be coherent not only with the bulk rigid rotation of the polycrystal but also with the rotation of the single crystallite due to the mechanism described in Figs. 2.6 and 2.7 (this additional rotation mechanism is called *tilt*). The routine is then done for many steps, each representing the evolution in the time interval Δt. The result is of course the development of fabric and of a numerical anisotropic flow law. Note that in a nonlinear theory integrating strain rate in time does not yield a strain measure. Accumulating strains by (2.24), therefore does not yield a strain tensor. So the entire process yielding (2.24) is dubious.

[8]We write $\dot{e}_{i\nu}$ for stretching and call it strain rate despite the fact that we used $D_{i\nu}$ before and prefer to call it stretching. We do it to make evident a common error that was also made when van der Veen and Whillans introduced their method.

In spite of some reasonable qualitative agreement of the numerical simulations with laboratory and field observations, some strong anomalies – as for example the minimum of the strain rate at about 10% of the strain, instead of 1% as observed in practice [15, 73, 78, 79] – evidenced the distinction between simulation and real mechanisms taking place during the deformation. Although the similarity of this approach with that of Azuma and Higashi [9] was recognized for simple regimes of deformation, the greatest merit of the van der Veen and Whillans model lies undoubtedly in their pioneering attempt to simulate dynamic recrystallization in polycrystalline ice, even though only numerically and through artificial criteria. We will discuss later on their approach to this problem.

A more sophisticated mechanical model for ice, capable also of describing fabric development, was proposed by Duval, Castelnau and co-workers [16, 18, 19, 20] through the adaptation of the so called *visco-plastic self-consistent* approach (VPSC) developed for metals by Lebensohn and Tomé [86]. In this method, both stress equilibrium and strain compatibility among neighbouring grains tend to be satisfied in a recursive manner. Each grain is assumed to be an inclusion embedded in an homogeneous matrix, which ought to represent an averaging of the polycrystalline environment. Hence, neither the stress nor the strain are constrained to be the same for all crystallites.

Despite the natural superiority of the VPSC approach in comparison with simpler methods of homogenization of the microstructural behaviour, some shortcomings still persist. For instance, the method is strictly limited to linear constitutive laws and requires the postulation of a constitutive equation for the response of the individual grains, and consequently, appropriate values for all the microscopic parameters involved in this equation must be determined, so as to provide physically acceptable results at the microscopic as well as at the macroscopic levels. In particular, a critical point is the stipulation of the yield shear stress for each slip system. For ice, the best fits of experimental data suggest a resistance to glide in non-basal planes 70 times greater than in the basal plane [16, 19]. Although this sounds tolerable for the case of prismatic slip (as commented before, the observed resistance of ice single crystals to hard glide is more than 60 times higher than for easy glide [32, 93]) the contribution of pyramidal slip to the polycrystalline deformation would be inadmissibly high: about 9%. This is rather unphysical, since the occurrence of pyramidal slip in polycrystalline ice is supported neither by theory nor by experiments [25, 65]. The probable reason for this unwanted result is the limited number of deformation mechanisms presently available in the VPSC: it considers only gliding on crystallographic planes, being therefore incapable of adequately treating inhomogeneous intracrystalline deformation (kink and deformation bands, polygonization, etc.) as well as recrystallization and intergranular interactions, which all are likely to occur in ice [54, 96, 147].

In order to account for this fault, even more sophisticated (and complex) descriptions of microstructural processes occurring in ice have been recently addressed. For instance, Meyssonnier and Philip [104] have utilized finite element simulations. In this case, each crystal is treated as a continuum, and complex inhomogeneous grain deformations can be simulated without violation of either strain compatibility or stress equilibrium. Due to its complexity, however, only a two-dimensional array with a little more than thousand grains was considered.

2.6 Modelling Induced Anisotropy: Macroscopic Models

2.6.1 Microscopic and Macroscopic Models

Common to all approaches discussed above is the fact that they constitute discrete models which reckon the polycrystal as an aggregate of a finite number of grains. The advantage of such discrete models is, of course, the potential accuracy of the description: each grain of the polycrystal is individually considered. The consequential disadvantage is that they can only handle a small number of ice crystals, since the required storage capacity and computational time tend to increase considerably with the dimension of the aggregate. In summary: they are definitively not suited for modelling the dynamics of large glaciers and ice sheets. In such cases the best alternative is to resort to a macroscopic continuum description, able to account somehow for the microstructural anisotropy of the medium.

2.6.2 Lliboutry's Model

One model of this sort has been proposed by Lliboutry in 1993 [91, 92]. He considered that the stress acting on every crystallite was the same (Sachs' hypothesis), assumed that each grain deforms only by basal glide and introduced for them the dissipation potential Ψ^*, i.e.,

$$\Psi^* = \tfrac{1}{2}k_1\tau_n^2 + \tfrac{1}{4}k_3\tau_n^4, \tag{2.25}$$

where τ_n is the respective resolved shear stress on the basal plane, while k_1 and k_3 are constants. For a given prescribed fabric, the model is suited to a homogenization procedure, i.e., the dissipation potential Ψ of the polycrystal is assumed to be the mean of Ψ^*, weighted by its relative volume. Thus,

$$\Psi = \int_0^{\pi/2} \Psi^*\ V^*(\theta)\ d\theta, \tag{2.26}$$

where $V^*(\theta)$ is the relative volume of the crystals with the c-axis having an angle with the vertical that is larger than θ.

The relevance of working with the dissipation potential is the form taken by the stretching tensor,

$$D_{ij} = \frac{\partial \Psi}{\partial S_{ij}}, \tag{2.27}$$

where $S_{ij} = t_{\langle ij \rangle}$ is the Cauchy stress deviator. Thus, Lliboutry obtains a three-dimensional anisotropic generalization of Glen's flow law of polynomial type, which contains a linear dependence on stress (and therefore viscous Newtonian behaviour) in addition to the usual cubic dependence of Glen's law. The greatest weakness of this theory is that it deals only with a static and prescribed fabric, being unable to determine its evolution.

2.6.3 The ODF Approach

To overcome the problem of the evolution of fabrics, two other approaches to describe the induced anisotropy of ice were proposed eight years ago by Meyssonnier and Philip

[103] and Svendsen and Hutter [130] through consideration of a continuous statistical distribution of crystallographic orientations within the polycrystal. The microstructural variable adopted in both works was a typical measure of anisotropy in complex media, namely, an *Orientation Distribution Function* $f^*(\mathbf{n})$ (ODF, see e.g. [82]) which gives the fraction of crystallites of which the c-axes are directed towards every particular orientation in space. More specifically, $f^*(\mathbf{n})\, d^2n$ represents the fraction of the number of crystallites that have orientations directed towards $\mathbf{n}$ within the solid angle d^2n, respectively. Thus, integration of the ODF over the unit sphere, $\mathcal{S}^2$, gives unity, i.e.,

$$\int_{\mathcal{S}^2} f^*(\mathbf{n})\, d^2n = 1. \tag{2.28}$$

It should be remarked that using a macroscopic continuum theory based on the concept of an ODF demands to regard each representative point of the body in the model as an assemblage of an "infinite" number of crystallites in order to ensure continuity of the ODF. This requirement is the so-called *continuum hypothesis*, and it is trivially satisfied for the large ice masses in Greenland and Antarctica, since their dimensions ($> 10^6\,\mathrm{m}$)[9] are by far much larger than the typical grain sizes ($\sim 10^{-3}\,\mathrm{m}$).

The first model, by Meyssonnier and Philip [103], employed a simpler version of the VPSC model already discussed in the previous section, by regarding each crystallite as a continuous transversely isotropic medium. Instead of treating the polycrystalline body as an aggregate of individual grains, they used the ODF to determine the fabric evolution. However, in order to simplify the calculations, only Newtonian viscous behaviour for the grains was considered. An even more simplified version of the Meyssonnier–Philip model was presented by Gagliardini and Meyssonnier [44, 45], with the aim at a numerical implementation to simulate ice sheet flow.

The second model, by Svendsen and Hutter [130], treated ice as a non-linear inelastic material, and utilized the conventional formalism of continuum mechanics [137, 138] to derive the fundamental equations of their model. They used a dissipation potential for the entire polycrystal (which was regarded as a transversely isotropic material) of the form

$$\Psi = \hat{\Psi}\left(t_{\langle ij\rangle}, A_{ij}, T\right) \tag{2.29}$$

where T is the absolute temperature, $t_{\langle ij\rangle}$ is the deviatoric stress tensor and A_{ij} is an additional symmetric tensor measuring the degree of transversal isotropy: the second moment of the ODF, named by different authors *alignment, conformation, anisotropy* or also *structure tensor* [24, 85],

$$A_{ij}(x_i, t) = \int_{\mathcal{S}^2} A^*_{ij}(n_i)\, f^*(x_i, n_i, t)\, d^2n, \qquad A^*_{ij} = n_i n_j, \tag{2.30}$$

where f^* is the ODF, n_i is a unit vector parallel to the c-axis of each crystallite and the integration is performed over the whole range of orientations $\mathcal{S}^2$. Implementing the general principle of material objectivity, equation (2.29) can be better represented by a simpler functional dependence, in which only scalar quantities are involved. It assumes

[9] Compare with the usual dimensions of common continuous bodies ($> 10^{-2}\,\mathrm{m}$) and their constituent molecules ($\gg 10^{-10}\,\mathrm{m}$)

that (2.29) is a scalar isotropic function of two symmetric tensors and of a scalar, and so

$$\Psi = \tilde{\Psi}\left(II_{\mathbf{t}^D}, III_{\mathbf{t}^D}, II_{\mathbf{A}}, III_{\mathbf{A}}, I_{\mathbf{t}^D\mathbf{A}}, I_{(\mathbf{t}^D)^2\mathbf{A}}, I_{\mathbf{t}^D\mathbf{A}^2}, I_{(\mathbf{t}^D)^2\mathbf{A}^2}, T\right), \tag{2.31}$$

where $I_{\mathbf{B}}$, $II_{\mathbf{B}}$, $III_{\mathbf{B}}$ denote the first, second and third scalar invariants of $\mathbf{B} = \mathbf{B}^T$ and $\mathbf{B}^D$ is the deviatoric part of a general tensor $\mathbf{B}$. Furthermore, neglecting the third scalar invariant of the Cauchy stress deviator is an approximation that is already employed in Glen's flow law; thus, they implement this approximation and assume, as Lliboutry did, the validity of equation (2.26). As a consequence, they are able to write a general form for the anisotropic flow law,

$$\mathbf{D} = \gamma_1\mathbf{t}^D + \gamma_2\mathbf{A}^D + \gamma_3\left[\mathbf{t}^D\mathbf{A} + \mathbf{A}\mathbf{t}^D\right]^D + \gamma_4\left(\mathbf{A}^2\right)^D + \gamma_5\left[\mathbf{t}^D\mathbf{A}^2 + \mathbf{A}^2\mathbf{t}^D\right]^D, \tag{2.32}$$

where [10]

$$\gamma_1 = \frac{\partial\Psi}{\partial II_{\mathbf{t}^D}}, \quad \gamma_2 = \frac{\partial\Psi}{\partial I_{\mathbf{t}^D\mathbf{A}}}, \quad \gamma_3 = \frac{\partial\Psi}{\partial II_{(\mathbf{t}^D)^2\mathbf{A}}}, \quad \gamma_4 = \frac{\partial\Psi}{\partial I_{\mathbf{t}^D\mathbf{A}^2}}, \quad \gamma_5 = \frac{\partial\Psi}{\partial I_{(\mathbf{t}^D)^2\mathbf{A}^2}}. \tag{2.33}$$

A common shortcoming of these two theories is that both reckon the polycrystalline ice as a transversely isotropic medium, hence restricting the fabric to remain axially symmetric; in other words, if one represents the unit vector n_i in spherical coordinates (θ, φ), the dependence of the orientation distribution function f^* is constrained to vary only with the latitude θ and not with the longitude φ.

The transversal isotropy of ice is in fact typical only of single crystals, and it cannot *a priori* be taken for granted for polycrystals. Hence, to overcome this problem, Svendsen and Hutter [130] suggested to introduce into the functional dependence of Ψ in (2.29) other structural tensors thereby being able, following Boehler [13], to take into account other kinds of anisotropies.

A different and even simpler approach to account for diverse anisotropies was suggested by Gödert and Hutter [52] by employing a homogenization technique similar to that used by Lliboutry [92]. They assigned a dissipation potential to each grain in the form of (2.25) and, using the ODF as a statistical distribution (see e.g. [66]), they proposed the dissipation potential for the entire polycrystal to be

$$\Psi\left(x_i, t\right) = \int_{\mathcal{S}^2} \Psi^*\left(x_i, n_i, t\right) f^*\left(x_i, n_i, t\right) d^2n. \tag{2.34}$$

This kind of connection between the microscopic and the macroscopic level is used systematically by the authors, e.g. for the structural tensor as in (2.30); besides, on the polycrystalline level, no compromise is made in this model with the degree of material anisotropy, which is given by the eigenvalues of A_{ij}, viz. λ_1, λ_2 and λ_3 as follows

$$\begin{aligned}
&\lambda_1 \neq \lambda_2 \neq \lambda_3 \neq \lambda_1 \quad \Longrightarrow \quad \text{orthotropic behaviour,}\\
&\lambda_1 \neq \lambda_2 = \lambda_3 \quad \Longrightarrow \quad \text{transversally isotropic behaviour,}\\
&\lambda_1 = \lambda_2 = \lambda_3 \quad \Longrightarrow \quad \text{isotropic behaviour.}
\end{aligned}$$

[10] We remark that in the paper a simplified version of the general anisotropic flow law comes from an incorrect evaluation of the tensor $\mathbf{A}^2$, the square of the structure tensor.

Motivated by the ideas of the VPSC approach [20], the same authors [51, 53] introduced interactions among neighbouring grains and implemented their model numerically in a coupled finite element–finite volume scheme. Comparison of the results of their model with the GRIP ice-core data and the predictions of the VPSC were performed. Curiously, in spite of the fact that Gödert and Hutter [51, 53] employed simply a linear (i.e. Newtonian) viscous relationship between stress and strain rate for basal slip, they showed that their model could better fit the GRIP data than the non-linear VPSC method. However, the authors find that the maximum increase of the fluidities due to crystal alignments does not achieve the value observed in laboratory tests. They claim that this is due to an overestimation of the shear viscosity in the application of this model to the case of single maximum fabric; they in fact suggest that the observed flow law changes according to the loading and alignment.

In chapter 3 we will give our proposal for the solution of this problem.

2.6.4 The Morland–Staroszczyk Model

A purely phenomenological approach to anisotropic ice dynamics, which ignores any micromechanical processes and microscopic interactions at the grain level, was proposed in a series of papers by Morland and Staroszczyk [107, 125, 126, 127, 128]. The fundamental idea behind this theory lies in the expectation to obtain a sketchy picture of the anisotropy of the polycrystal from its *instantaneous* state of deformation (Fig. 2.9) without any explicit reference to fabric or grain size. More precisely, the model is based on the following flow law,

$$\boldsymbol{t}^D = \boldsymbol{H}_{\mathrm{I}}\left(\boldsymbol{D}\right) + \boldsymbol{H}_{\mathrm{A}}\left(\boldsymbol{D}, \boldsymbol{B}, \boldsymbol{M}^{(r)}\right), \quad \boldsymbol{H}_{\mathrm{A}}\left(\boldsymbol{D}, \boldsymbol{I}, \boldsymbol{M}^{(r)}\right) = \boldsymbol{0}, \quad (r = 1, 2, 3) \qquad (2.35)$$

where $\boldsymbol{t}^D$ is the Cauchy stress deviator, $\boldsymbol{H}_{\mathrm{I}}$ and $\boldsymbol{H}_{\mathrm{A}}$ are, respectively, the isotropic and the anisotropic part of the material response, $\boldsymbol{D}$ is the stretching tensor, $\boldsymbol{B}$ is the left

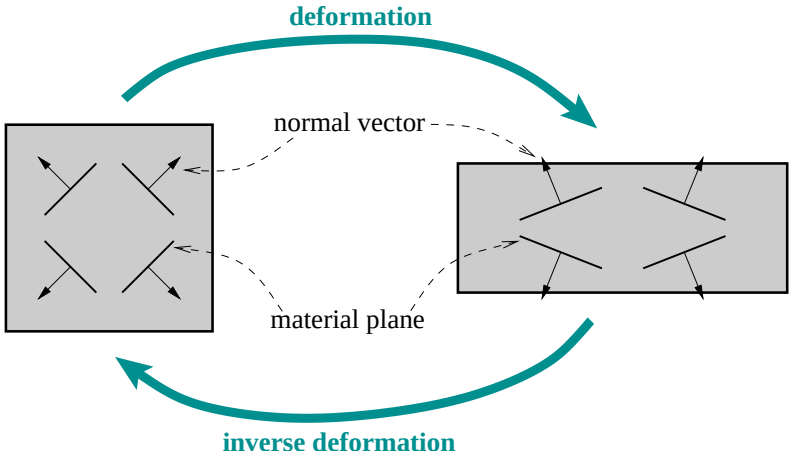

Figure 2.9: Cubic sample subjected to an arbitrary cyclic deformation. The panels show material planes arranged diagonally, with their respective normal vectors. At the initial configuration, the orientational distribution of planes is assumed isotropic. During deformation, an anisotropic distribution of normal vectors is induced, but at the end of the cycle this distribution becomes isotropic again, as the final configuration returns to the identical initial one.

Cauchy–Green deformation tensor and $\boldsymbol{M}^{(r)}$ are the three structural tensors that take into account the anisotropy, and are related to the principal directions of $\boldsymbol{B}$,

$$\mathbf{M}^{(r)} = \mathbf{e}^{(r)} \otimes \mathbf{e}^{(r)}, \tag{2.36}$$

where $\mathbf{e}^{(r)}$ are the eigenvectors of $\mathbf{B}$. Hence, whenever $\boldsymbol{B} = \boldsymbol{I}$ (i.e., no instantaneous deformation), the material response is isotropic. The assumption that the evolving anisotropy does *not* depend on the deformation history ensures the straightforwardness of the model, but it implies also unpleasant consequences, like the reversibility of the induced anisotropy (see Fig. 2.9). In fact, according to the Morland–Staroszczyk model, described by (2.35) and Fig. 2.9, an initially isotropic sample of ice, deformed by any cyclic process (of shear, compression/tension, etc.), such that $\boldsymbol{B} = \boldsymbol{I}$ at the final configuration, would manifest again an isotropic mechanical behaviour. This does agree neither with experience nor with the mechanisms of basal slip depicted in Figs. 2.6 and 2.7.

Of course, the supposition of a direct correlation between polycrystalline deformation and induced anisotropy is not new, it can be traced back at least to the early model of Azuma and Higashi [9] and of van der Veen and Whillans [141]. The difference is that, in this phenomenological approach, no compromise with microscopic mechanisms is assumed.

The combination of simplicity and flexibility found in this model is in fact its greatest attractiveness, but also its principal weakness. While it presents itself as a suitable approach to model ice sheet flow with comparatively low computational costs, it is in fact physically feeble: the microscopic processes occurring within the ice – including changes in grain size and shape, as well as in the fabric itself – are all cryptically subsumed in rheological coefficients, in a way somewhat similar to the case of the pre-exponential coefficient A of Glen's law (2.3).

2.7 The Anisotropy Induced by Recrystallization

2.7.1 The Role of Dislocations

As we have already pointed out, the macroscopic description of polycrystalline ice is influenced by the microstructure. We have also remarked that the crystalline structure of natural ice is hexagonal (see Fig. 2.5). In spite of the symmetry of this structure, the mechanical behaviour of a *real crystal* is very different from that of a hypothetically *perfect crystal*. In 1926 Frenkel [42] put forward a simple method of estimating the theoretical shear strength of perfect crystals and found that it is much larger than the observed values. As commented by Kittel [81], this cannot be explained without the presence of defects.

The defects may be grouped into different types according to the dimension of the region where the crystalline structure is destroyed [50]: if this region is a point, its dimension is zero and we refer to it as a *point defect*; if it is a line, the dimension is one and we refer to it as a *line defect* or *dislocation*. Two-dimensional regions of defects are called *plane defects* and larger defects, where the structure is seriously disrupted in a three-dimensional region, are called *gross defects*.

We have pointed out that dislocation is a line defect. On the other hand, a working definition for the word *dislocation* is: The total lenght of line defects. In this way, the

dislocation density ρ_d is, by definition, the dislocation per unit volume or, equivalently, the total length of line defects per unit volume and its physical dimension is the inverse of a surface, i.e., m^{-2}. The curve on which the line defect lies is the domain of a vector field, the Burgers vector $\mathbf{b}$, that defines the displacement which a perfect crystal must fulfil to have that structure. Depending upon whether $\mathbf{b}$ is parallel or orthogonal to that line, we call the dislocation *screw* or *edge*, respectively. Hybrid dislocations (combinations of screw and edge types) are also frequent.

Since the early works on dislocations, many attempts were concerned with the experimental verification of the idea that dislocations should not only occur, but must also play a central role in the deformation of polycrystalline material. The deformation mechanism of glide on basal planes suggests in fact a relation between the total deformation (the strain ε) and the stored dislocation density in the material. This is actually done by the Orowan relation, i.e.,

$$\varepsilon = \rho_d \, b \, D, \tag{2.37}$$

where b is the length of the Burgers vector of a certain dislocation that moves the distance D, approximately identified by the grain size[11].

Moreover, the mobility of dislocations has often some relation with the softness of the material. We remarked that a perfect crystal is very hard and the introduction of dislocations makes the material softer. Thus, in principle, the larger the dislocation density, the greater will be the ductility of the material. However, this simple correlation is proved to fail in many cases, including ice. The *interaction* of dislocations plays in fact a very important role, e.g. dislocations can pile-up, thus their mobility decreases and the material becomes harder. Therefore, it is customary to use a relation between the stress, σ, and the dislocation density as follows:

$$\sigma = c \, G \, b \, \sqrt{\rho_d}, \tag{2.38}$$

where c is a constant generally equal to $1/2$ and G is the shear modulus. Relation (2.38) has been shown to be valid for a wide range of materials by McElroy and Szkopiaz [101]; however, Montagnat and Duval have pointed out that it only represents an upper bound for ice because of the occurrence of Grain Boundary Migration (GBM) [105]. GBM makes, in fact, ρ_d smaller but has practically no effect on σ. It is a phenomenon belonging to the general class of recrystallization mechanisms, that we will discuss in the next subsection.

2.7.2 Phenomena Related to Recrystallization

Recrystallization is a word associated with a wide number of processes, and there is no agreement on its precise definition. The reason lies perhaps in the high complexity of the physical phenomena that scientists want to refer to with this word and the impossibility to build a mathematical theory that associates to it a measurable quantity. In this paper, we try to associate with this word all the phenomena that can be interpreted by what the word itself suggests. Initially, the ice is assumed to be already crystallized. The term recrystallization will be used whenever the grains change their shape or position in the microstructure, in the sense that crystallization occurs for a second time.

A first example is given when a portion of mass belonging to a given crystallite in a polycrystal is transferred to a neighbouring crystallite. In this case we say that the

[11] The grain size is in fact the upper bound of the distance that a dislocation can be displaced.

boundary between the two crystallites has moved (see e.g. Fig. 2.10). We call this process *grain boundary migration* and regard it as a recrystallization phenomenon. Notice that grain boundary migration can easily adjust the geometrical incompatibility shown in Fig. 2.8b without the necessity to make active the pyramidal and the prismatic planes.

The migration of grain boundaries is driven essentially by the reduction of the Gibbs free energy stored either in the grain boundaries or within the grains by dislocations. The migration of grain boundaries driven by the grain boundary energy is generally quite uniform, implying that certain crystallites grow while others shrink. This process is *Normal grain growth*. If only a few grains grow in a very accelerated pace, then we refer to this as *abnormal grain growth*; in this case the microstructure becomes unstable and a few grains may grow excessively. The driving force for abnormal grain growth is a reduction in grain boundary energy. This is the same force that drives normal grain growth. However, an important question to consider is whether or not normal or abnormal grain growth can occur. In a three-dimensional polycrystalline material (i.e., excluding thin films) the main factors which lead to abnormal grain growth are impurities and fabrics.

Impurities are in fact generally considered to prevent the growth; they provide a pinning pressure against the usual pressure that drives the growth. However, this pinning pressure, also called the *Zener pinning pressure*, is inversely proportional to the grain size; this means that the larger the grain size, the lower the Zener pinning pressure. Thus, the crystallites with large grain sizes are favoured to grow and those with small grain sizes are favoured to be pinned by the impurities.

An important characteristics of the grain boundary energy is that it is proportional to the angle between the lattice orientations of the crystallites that such a boundary lies. If the grain boundary divides crystallites with very close lattice orientations, then it is called a low angle grain boundary. If the crystallites that the grain boundary divide have conspicuously different lattice orientations, then we call the boundary a high angle grain boundary. Therefore also strong fabrics, such as a single maximum fabric, can drive abnormal grain growth; this is possible because in a sample with a single maximum fabric we have mostly low angle grain boundaries which posses low energy and low mobility. On the other hand, if some grains with relatively different lattice orientations are present, then these introduce high angle grain boundaries (possessing high energy and high mobility) and these grains may grow preferentially, providing room for the abnormal grain growth.

The phenomenon of *nucleation* is closely related to abnormal grain growth. Generally

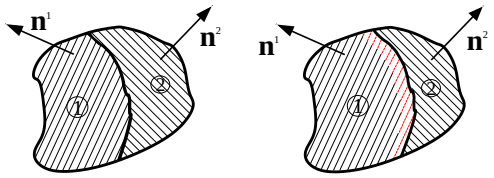

Figure 2.10: Schematic two-dimensional illustration of grain boundary migration. The boundary between grains "1" and "2" migrates so that grain "1" grows while grain "2" shrinks. The parallel thin lines represent the basal planes of the two grains. Besides, where the boundary passes, the dislocation density decreases to almost zero value. Basal planes represented by thin dashed lines indicate, in this figure, the fact that the dislocation density in that region is very low.

we refer to it when a new crystallite nucleates and rapidly grows within a polycrystalline matrix from which it is separated by a high angle grain boundaries.

Polygonization is a rather different phenomenon but nevertheless quite common in ice sheets. When a polycrystal is deformed, dislocations are produced and start to move. The tendency of dislocations to be arranged into a state of lower energy configuration makes possible the formation of regular arrays of dislocations. Such arrays generate low angle grain boundaries, also called subgrain boundary. Thus, the crystallite is bent or twisted, subgrain boundaries are formed and subsequently the grain is broken (it is said that it is polygonized); the newly formed low angle grain boundaries divide the new crystallites. The result is that the mean grain-size is reduced. Moreover, the new boundaries decrease the amount of dislocations – hence, the formation of subgrain boundaries is also a recovery process.

Recovery is a general characterization of recrystallization phenomena. In fact, in all processes where the grain boundary moves (i.e., grain boundary migration, normal and abnormal grain growth and nucleation), the recrystallized material has, in the end, almost vanishing dislocation density. Thus, we can claim that where the boundary passes the dislocation density will decrease to almost zero value. In Fig. 2.10 we explain this recovery process with grain boundary migration.

Other recovery mechanisms, such as dislocation annihilation, are supposed to be of minor importance in polar ice sheets, see e.g. [25].

2.7.3 The Dislocation Density Dynamics

In this subsection we discuss some models developed in the literature to predict the dynamics of dislocation density. For the sake of simplicity, we will review only the models that are proposed for ice.

We have seen that the dislocation density increases with deformation. From the Orowan relation (2.37) one can easily derive an equation for the time rate of change of the dislocation density by straining (see e.g. [25, 31, 105, 106])

$$\frac{d\rho_d^+}{dt} = \frac{|\dot{\varepsilon}|}{b\,D}, \tag{2.39}$$

where $\dot{\varepsilon}$ is the strain rate and the superscript "+" indicates that the production of dislocations due to straining is always positive. To generalize this to the multidimensional case, Morland [106] suggested to replace $\dot{\varepsilon}$ with the positive square root of the second invariant of the stretching, $\sqrt{D_{hk}D_{hk}}$.

The negative contribution to the rate of the stored dislocation density is given by the recovery processes of recrystallization. The mechanisms that are generally taken into account are those explained in the previous section, i.e., grain boundary migration (including also nucleation and for normal and abnormal grain growth) and polygonization.

The reduction in the dislocation density due to grain boundary migration is generally modelled by the following formula, proposed by many authors [25, 31, 105, 106], i.e.,

$$\frac{d\rho_d^-}{dt} = -\frac{\alpha\rho_d K}{D^2}, \tag{2.40}$$

where α is a coefficient exceeding 1, which makes possible to take into account a higher dislocation density near the grain boundaries, and K is the grain boundary migration

rate. The superscript "$-$" indicates that the production of dislocations due to GBM is always negative.

The *grain boundary migration rate* K is a typical parameter related, for example, to normal grain growth. It was introduced in metallurgy in 1948 by Smith [124] and its adequacy for polar ice was supported by Gow [58] in 1969, who fitted a parabolic growth relationship between grain size and time for several sites in Antarctica and Greenland, i.e.,

$$D^2 = D_0^2 + Kt \qquad \Longrightarrow \qquad \frac{dD}{dt} = \frac{K}{2D}. \tag{2.41}$$

It should be remarked here that even expression (2.40) for the reduction of the dislocation density due to grain boundary migration can be easily derived from the Orowan relation (2.37), if (2.41) is taken into account.

Montagnat and Duval [105] in 2000 noted that a combination of equations (2.39) and (2.40), by assuming the usual evolution equation for normal grain growth (2.41), would provide a continuous increase of dislocation density and grain size. An equilibrium for them can be reached only when polygonization is taken into account. It provides in fact new boundaries formed by dislocations that are subtracted from the interior of the crystallites. A relation between the dislocation density ρ_d^{sgb} stored by the subgrain boundary, the misorientation angle θ formed by it, the magnitude of the Burger vector b of dislocations and the averaged grain size D has been proposed in 1972 by Dillamore et al. [29] for metals, and reads

$$\rho_d^{sgb} = \beta \frac{\theta}{bD}, \tag{2.42}$$

where β is a dimensionless parameter, that Dillamore et al. [29] set equal to 1, i.e., $\beta = 1$. Montagnat and Duval [105] use $\beta = 2$, applied this relation to ice and deduce a reduction of dislocation density due to polygonization by simply differentiating (2.42). Thus, loss of dislocations by polygonization is assumed to be expressed by the following formula,

$$\frac{d\rho_d^{-(pol)}}{dt} = -\frac{d\rho_d^{sgb}}{dt} = \frac{2\theta}{bD^2}\left[\frac{dD}{dt}\right], \tag{2.43}$$

where θ is the mean misorientation angle of the subgrains.

2.7.4 A Note on Dislocation Density Dynamics

The weak point of the formulation by Montagnat and Duval is that they use the expression (2.41) for the rate dD/dt of (2.43), which is valid for normal grain growth but not for polygonization. They in fact did not use (2.43) as contributing to the dislocation loss, but rather only to establishing a condition for the steady state of the dislocation density and grain size, viz.,

$$\frac{d\rho_d^{-(pol)}}{dt} + \frac{d\rho_d^{-}}{dt} = \frac{d\rho_d^{+}}{dt}. \tag{2.44}$$

We think, a more convenient and realistic model can be provided as follows.

In 1994 Jacka and Jun [75] proposed a differential equation having the ingredients of an evolution equation of grain size. This equation was able to reproduce the steady state grain size that realistically occurs in the middle part of an ice sheet, i.e.,

$$\frac{dD}{dt} = \frac{K}{D} - PD. \tag{2.45}$$

In 2004 we proposed [115] to assign to P the physical meaning of polygonization. For constant K and P, (2.45) is easily integrated and the graph of $D(t)$ is shown in Fig. 2.11. Together with an explicit comparison of the data from the Byrd ice core. There remains to suggest a formula stating that the decrease of dislocation density during polygonization is proportional to that necessary to build the new subgrain boundaries. With this in mind, we propose to replace the rate of grain size dD/dt in (2.43) by the expression in (2.45) that is explicitly related to polygonization, i.e., with $-P\,D$. Therefore from (2.42) we have

$$\frac{d\rho_d^{(pol)}}{dt} = -\frac{d\rho_d^{sgb}}{dt} = \beta\frac{\theta}{bD^2}(-PD) = -\beta\frac{\theta}{bD}P. \tag{2.46}$$

This equation gives a negative contribution to the dislocation density that is exactly what we expect.

Collecting all contributions, we finally arrive at a system of differential equations for grain size and dislocation density that can be represented as follows,

$$\begin{cases} \dfrac{dD}{dt} = \dfrac{K}{D} - PD, \\ \dfrac{d\rho_d}{dt} = \dfrac{\dot{\varepsilon}}{bD} - \alpha\dfrac{\rho_d K}{D^2} - \beta\dfrac{\theta P}{bD}. \end{cases} \tag{2.47}$$

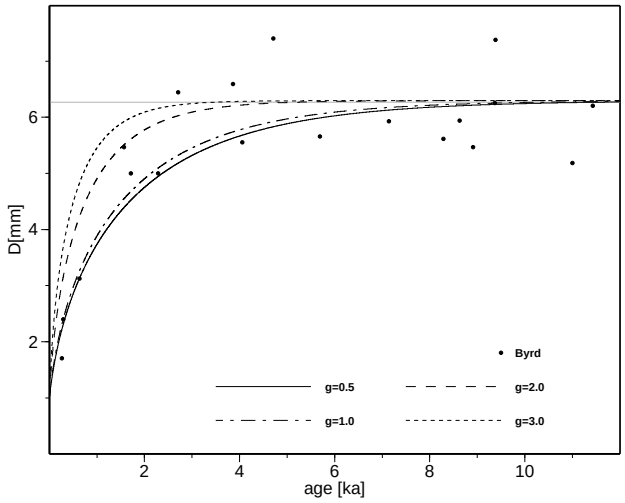

Figure 2.11: The curves based on (2.45) fit well the experimental data given for grain size of the ice core at Byrd Station, Antarctica. The values $k = g\hat{k}$ and $P = g\hat{P}$ with $\hat{k} = 9mm^2ka^{-1}$ and $\hat{P} = g0.2ka^{-1}$ guarantee that they all reach the same steady state $D_{eq} = 6.3mm$ for each value of the nondimensional factor g. Let us remark that the figure gives us the physical interpretation of this nondimensional factor: it is the velocity in which the grain size D reaches the steady state D_{eq}.

For constant K, P, $\dot{\varepsilon}$ and θ, it can be solved analytically. The results are

$$\begin{cases} D^2 = D_0^2 \exp\left(-2Pt\right) + \dfrac{K}{2P}\left[1 - \exp\left(-2Pt\right)\right], \\ \rho_d = \dfrac{bPD_0\rho_{d0} - \dot{\varepsilon} + P\beta\theta}{b\sqrt{P}\sqrt{D_0^2 P - \alpha\dfrac{K}{2}\left[1 - \exp\left(2Pt\right)\right]}} - \dfrac{-\dot{\varepsilon} + P\beta\theta}{b\sqrt{P}\sqrt{\alpha\dfrac{K}{2} + \left[D_0^2 P - \alpha\dfrac{K}{2}\right]\exp\left(-2Pt\right)}}, \end{cases} \tag{2.48}$$

where ρ_{d0} and D_0 are the values of dislocation density and of grain size at time $t = 0$. It is straightforward to compute the limit of (2.48) when polygonization is not taken into account ($P \to 0$) and then derive (2.41) for the evolution equation of grain size and the blow-up of the dislocation density already noticed by Montagnat and Duval in 2000 [105].

2.7.5 A Review of the Models Including Recrystallization

In this subsection, we review some models for polar ice which take recrystallization into account. The problem one needs to solve is the determination of the fabric and the mechanical response of ice after the occurrence of nucleation and abnormal grain growth.

The main idea is that the polycrystal tends to assume a microstructural configuration with a minimum amount of free energy. A general correlation between the onset of nucleation and abnormal grain growth and the acceleration in creep rate (i.e., an acceleration of the strain-rate) is generally accepted in the literature. This can be attributed to crystal reorientations produced by nucleation and abnormal grain growth [80]: the newly formed crystals and those that grow abnormally have orientations that are favourable for intracrystalline plastic flow, and the orientations preferentially eliminated are those for which intracrystalline plastic flow is more difficult. The glide for the crystallites so oriented is easier and the microstructural configuration is more stable. This means that it is very important to understand which directions are well oriented for deformation in any state of the stress deviator or stretching. In the states of compression or extension such orientations are those at 45° from the principal axes of deformation (see Fig. 2.12a). In Fig. 2.12b, we show a simple graphical method to extract this information even for simple shear. Moreover, it has been recognized that, to describe the recrystallization processes, we need a parameter able to switch them on, e.g. dislocation density or its associated lattice distortion energy.

As we have already pointed out, a first attempt to achieve this goal was done by van der Veen and Whillans in 1994 [141]. The parameter that switched the recrystallization on was for them the accumulated strain. This means that those crystallites reaching a certain threshold value for the strain were constrained to be recrystallized, and the recrystallization replaced strained crystals with new ones at the optimum orientation for basal glide. In uniaxial compression, for example, the new crystallites had a c-axis oriented at 45° with respect to the axis of compression. The authors recognized the following problem: the crystals unfavourably oriented for basal glide do not accumulate any strain and they do not recrystallize. On the other hand, it is believed that in nature awkwardly aligned crystals are stressed more than others and they are the first ones to recrystallize. However the Sachs model, that they used, does not allow to distinguish between different states of stress. To overcome this problem the authors proposed that it is not the strain

that must reach a certain threshold value to allow recrystallization, but the difference of this and the mean strain. A second problem arises when the recrystallization fabric was analyzed for simple shear. Experiments [67, 80] on the ice samples subjected to simple shear show a two-maxima fabric. The first maximum is normal to the shear plane and is called M_1. The second maximum is inclined at about 70° from M_1 and is called M_2. The main characteristic is that M_1 is stronger than M_2. The failure of the model of van der Veen and Whillans is that M_1 is weaker than M_2. The reason is the following: in principle the two maxima should place M_1 normal to the shear plane and M_2 at 90° from M_1 (see the Fig. 2.12). These are in fact two easy-glide orientations for simple shear. However the tilt-rotation of the crystallites (shown in Fig. 2.12 by curved arrows) and the whole rotation of the polycrystal (in the simple shear test shown in Fig. 2.12 such a rotation is not present because we do not show the form of the sample after the deformation) determine a net clockwise rotation for M_2 and a negligible rotation for M_1, when the experimental apparatus is such that the rotation of the polycrystal is clockwise. This means that the crystallites oriented in M_1 accumulate more strain than those in M_2, and they are more easily recrystallized. Thus, the residence time of crystals in M_2 is larger, and this maximum appears to be stronger. To overcome this problem, van der Veen and Whillans assumed that new crystals are formed preferentially in the direction containing most crystals. Thus, recrystallized grains are formed at the easy-glide orientations not with equal probability but in proportion to the number of crystals that are already near that orientation. The easy-glide orientation relative to the M_2 maximum is at 90° from M_1 and does not correspond to that maximum because of the effect of the tilt and the bulk rotations; it contains fewer grains than the other easy-glide orientation, that is in fact the place of the maximum M_1. Therefore, M_1 is favoured by this third mechanism and ultimately all crystals accumulate on this maximum. The criteria shown in this paper seem to be artificial. However, they represent a first approach of the problem and were of great importance in the development of this field.

Another step for the understanding of the recrystallization processes in the dynamics of polycrystalline ice is done by Faria, Ktitarev et al. [41, 83]. In this case the method of approach is essentially numerical and based on a cellular automaton algorithm to simulate simultaneously grain growth and fabric evolution, including recrystallization and polygonization processes.

Furthermore, recrystallization processes have been included in 2001 in the Morland–Staroszczyk model [128], but through an artificial mechanism: a smooth scaling function, dependent on temperature and on the second invariant of strain rate (not strain!), such that it is unity for low strain rates that falls off to zero when the strain rate surpasses a prescribed critical value. When this scaling function vanishes, the fabric of the medium becomes isotropic again. In 2002 Morland [106] generalized the model and replaced the smooth scaling function by the lattice distortion energy. An evolution equation for the lattice distortion energy was proposed of the same form as the equation for the dislocation density (2.39) and (2.40) to take into account the effects of work hardening and grain boundary migration. The effect of polygonization was, however, not accounted for.

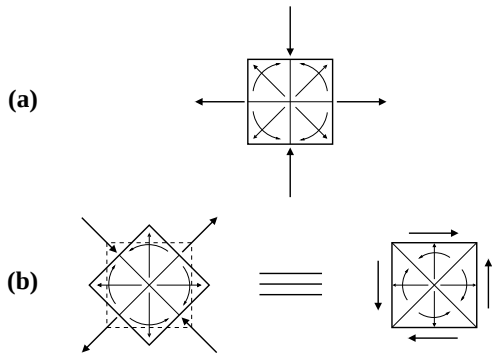

Figure 2.12: Schematic, two-dimensional representation of a volume element. Straight arrows inside the polycrystal stand for the c-axes of crystallites well oriented for deformation. Curved arrows indicate the rotational motion of such crystallites, due to the *tilt* mechanism explained in Figs. 2.6 and 2.7. The arrows outside the volume element indicate the state of the deviatoric stress or stretching acting on it. In case (a), the state of deviatoric stress (or stretching) is pure shear. The c-axes are well oriented at 45° with respect to the axes of tension and compression and the *tilt* mechanism rotates the crystallites towards the axis of compression and away the axis of tension. In (b) an anticlockwise rotation of the volume element is performed. The result is a sample subjected to a simple shear state of deformation. The situation exposed in panel (b) is shown by two equivalent volume elements.

Chapter 3

An Anisotropic Flow Law for Incompressible Polycrystalline Materials

3.1 Introduction

The anisotropic description of polycrystals is a very important field for material science (see e.g. [36, 37, 68, 93, 107, 115, 125, 126, 127, 128]). Experimental evidence tells us that the anisotropy may affect the material response considerably (see e.g. [2, 4, 15, 19, 32, 38, 43, 64, 78, 79, 114, 110, 132, 134]). The state of the art is as follows: Many authors try to solve the problem via numerical simulations that are valid for a certain material and in a given situation [7, 8, 9, 16, 18, 19, 20, 86, 123, 132, 134, 135, 141]. Thus, every application must be analyzed with its own numerical simulation. On the other hand, authors interested in the general problem of anisotropy [36, 37, 52, 89, 91, 92, 114, 130] often stop their analyses at a level that is so high that neither experimentalists nor numerical analysts are able to extract any useful information from their works. The level of generality may be so far distant from any single application that it may even be difficult to judge whether the level of complexity is sufficient or must be further extended. The modern philosophy of science prescribes, in fact, a bijective mapping between the space of the ideas, where models are built and where the model assumptions have no restrictions, and the space where we live. It is the duty to give this bijective mapping that drives the construction of models. Authors aimed to find such a relationship have found their roles in the field of anisotropic description of polycrystals. The problems of their model, however, is always the same: The parameters involved are so many that their experimental evaluation is difficult.

In this chapter, we will present two general anisotropic flow laws: one for the two- and the other for the three-dimensional case. The framework is that of a continuum theory of polycrystals at the microlevel of which the orientation is statistically distributed and described by an ODF. In subsection 2.5.3, a review was given on the literature of this field. In Section 3.2 we will analyse a very important shortcoming that emerges from the use of a second order structure tensor and propose a simple generalization that is able to overcome the problem. Explicit forms of the anisotropic flow law for the two- and three-dimensional cases will be shown in Sections 3.3 and 3.4. The reader not interested

in the method can directly pass to the two relevant equations (3.38) and (3.57). The two subsections following these equations confirm their adequacy by some examples. In Section 3.5 we analyse the limit of the three-dimensional anisotropic flow law in (3.57) for the two-dimensional case. The result is another version of a two-dimensional anisotropic flow law, the equation (3.71). Comparison between the different proposed two-dimensional anisotropic flow laws is given in the subsection that follows equation (3.71).

3.2 A Note on the Classical Theory

3.2.1 The Second-order Structure Tensor

Although the procedures related to the use of the second-order structure tensor seem to be sufficiently general to comprehend a large class of anisotropic behaviour, we now wish to point out one of its awkward properties and prove with an example that the general anisotropic flow law (2.32) is able to predict a single value of the strain rate, for at least two different orientation distributions and regardless of the specific assumption on the parameters γ_a, $a = 1, ..., 5$. Thus, (2.32) can be accepted or refused by performing a laboratory experiment.

In order to deduce this result from (2.32), let us derive the form of the second-order structure tensor in the two cases represented in Fig. 3.1: the isotropic case and the case in which the c-axes are oriented towards all the directions that are inclined by an angle θ_0 from the vertical, i.e., the case of a girdle fabric. We use spherical coordinates. Thus, the unit vector n_i, parallel to the c-axis, is represented by

$$n_1 = \sin\theta\cos\varphi, \qquad n_2 = \sin\theta\sin\varphi, \qquad n_3 = \cos\theta, \tag{3.1}$$

and the range, $\mathcal{S}^2$, of orientations is

$$\theta \in [0, \pi]\,, \qquad \varphi \in [0, 2\pi]\,. \tag{3.2}$$

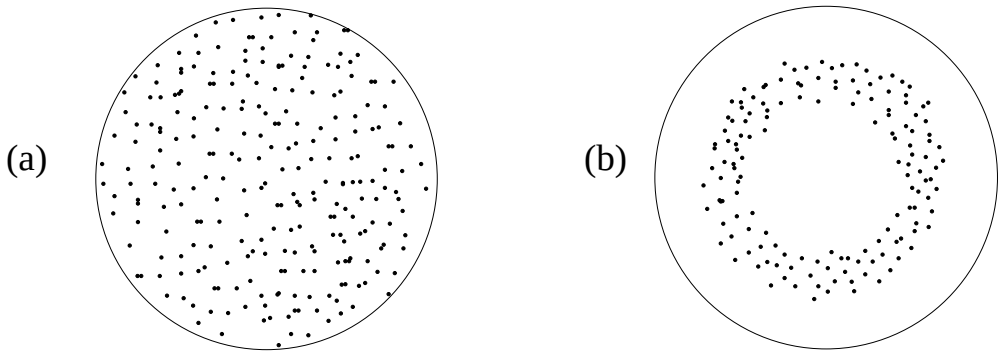

Figure 3.1: Schmidt diagrams for random (a) and for girdle (b) fabric distributions. Dots in the Schmidt diagram represent the orthogonal projection on the horizontal plane of dots at top of unit vectors **n**, when their bases coincide with the center of the diagram. Samples with the Schmidt diagram (a) on the left-hand side are assumed to generate isotropic mechanical response. It is reasonable to suppose that samples with the Schmidt diagram (b) on the right-hand side have a mechanical anisotropic response. The reason is that glide on the plane orthogonal to **n** is assumed to be softer than glide on other planes of the crystallite represented by **n**.

Therefore, integrations over $\mathcal{S}^2$ will be performed using the Jacobian of the transformation (3.1). Thus,

$$\int_{\mathcal{S}^2} (\cdot)\, d^2n = \int_0^{\pi} \sin\theta \left[\int_0^{2\pi} (\cdot)\, d\varphi \right] d\theta.$$

As we have already pointed out, the isotropic behaviour is prescribed by a uniformly random distribution of the c-axes (see Fig. 3.1a) and can be modelled by a constant ODF, e.g., $f^{*(i)}$. Thus, from the normalization condition (2.28), we have,

$$f^{*(i)} = \frac{1}{4\pi}. \tag{3.3}$$

Inserting (3.3) into (2.30) yields the second-order structure tensor, $A^{(i)}_{hk}$, in the isotropic case; its matrix representation is,

$$\mathbf{A}^{(i)} = \frac{1}{3} \begin{pmatrix} 1 & 0 & 0 \\ 0 & 1 & 0 \\ 0 & 0 & 1 \end{pmatrix}. \tag{3.4}$$

For an ideal girdle fabric (see Fig. 3.1b) the angles between the c-axes and the vertical are θ_0, and the ODF, e.g. $f^{*(gf)}$, is proportional to the Dirac Delta function, $\delta(\theta - \theta_0)$. Using the normality condition (2.28), the exact form of $f^{*(gf)}$ can be established, i.e.,

$$f^{*(gf)} = \frac{1}{2\pi \sin\theta_0} \delta(\theta - \theta_0). \tag{3.5}$$

This, together with (2.30), determines the following matrix representation of the second-order structure tensor, $A^{(gf)}_{hk}$ for the girdle fabric, i.e.,

$$\mathbf{A}^{(gf)} = \frac{1}{2} \begin{pmatrix} (\sin\theta_0)^2 & 0 & 0 \\ 0 & (\sin\theta_0)^2 & 0 \\ 0 & 0 & 2(\cos\theta_0)^2 \end{pmatrix}. \tag{3.6}$$

Now, we easily recognize from (3.4) and (3.6) that there exists an angle θ_0 for which the two structure tensors (3.4) and (3.6) are the same, i.e.,

$$\mathbf{A}^{(i)} = \mathbf{A}^{(gf)} \qquad \Longrightarrow \qquad \theta_0 = \arccos\left(\frac{1}{\sqrt{3}}\right) \simeq 0.955\ rad = 54.7\ ^\circ \tag{3.7}$$

Thus, irrespective of the general form (2.32) of the anisotropic flow law, expression (3.7) implies that for every deviatoric stress tensor, the strain rates for the isotropic case and for the case of a girdle fabric with $\theta_0 \simeq 54.7\ ^\circ$ are the same. This means that validity of (2.32) implies the impossibility to distinguish by a mechanical test a sample of polycrystalline ice with a random distribution of c-axes from another sample with a girdle fabric distribution with $\theta_0 \simeq 54.7^\circ$.

Although we have not found in the literature the results of mechanical tests on samples with this particular girdle fabric, their isotropy is questionable, e.g., for ice. An alternative procedure is the use of the fourth-order structure tensor.

3.2.2 The Fourth-order Structure Tensor

We define the fourth-order structure tensor by

$$B_{hklm} \equiv \int_{\mathcal{S}^2} f^* n_h n_k n_l n_m d^2 n = \int_0^{2\pi} \int_0^{\pi} f^* n_h n_k n_l n_m \sin\theta d\theta d\varphi, \tag{3.8}$$

and propose to change (2.32) to

$$D_{ij} = \tilde{d}_{ij}\left(B_{hklm}, S_{ab}\right), \tag{3.9}$$

where $\tilde{d}_{ij}$ is a general function of the fourth-order structure tensor, B_{hklm}, and of the deviatoric stress tensor, S_{ab}. In order to prove that this new form of the anisotropic flow law is able to overcome the problem analysed above, we need to evaluate the fourth-order structure tensor for a uniform distribution of c-axes, $B^{(i)}_{hklm}$, and for a girdle fabric distribution, $B^{(gf)}_{hklm}$, i.e.,

$$\left.\begin{aligned} B^{(i)}_{hklm} &= \frac{1}{4\pi} \int_0^{2\pi} \int_0^{\pi} n_h n_k n_l n_m \sin\theta d\theta d\varphi, \\ B^{(gf)}_{hklm} &= \frac{1}{2\pi \sin\theta_0} \int_0^{2\pi} \int_0^{\pi} \delta\left(\theta - \theta_0\right) n_h n_k n_l n_m \sin\theta d\theta d\varphi. \end{aligned}\right\} \tag{3.10}$$

Among the 30 independent components of these two symmetric fourth-order tensors, it is sufficient to show the values of the following four:

$$B^{(i)}_{1111} = \tfrac{1}{5}, \quad B^{(i)}_{3333} = \tfrac{1}{5}, \quad B^{(gf)}_{1111} = \tfrac{3}{8}\left(\sin\theta_0\right)^4, \quad B^{(gf)}_{3333} = \left(\cos\theta_0\right)^4. \tag{3.11}$$

Thus, (3.11) proves that no angle θ_0 allows the two tensors in (3.10) to be equal. This means that (3.9) does not imply any mechanical equivalence between samples with a certain girdle fabric distribution and samples in which the distribution of the c-axes is uniformly random, as desired.

Another possibility of overcoming the same problem is to use the Theory of Mixtures with Continuous Diversity. In the next chapter we will analyse how to achieve this goal.

3.2.3 The Basic Assumptions Underlying the Approach to Anisotropy

In the next two sections we show an alternative and new technique for the construction of a general anisotropic flow law for the two-dimensional and three-dimensional cases, respectively.

The idea is taken from the Theory of Mixtures with Continuous Diversity[1], but it can be derived independently. For the sake of simplicity, we will assume collinearity between the deviatoric stress tensor, S_{ij}, and the stretching tensor, D_{ij}, i.e.,

$$D_{ij} = g\, S_{ij}. \tag{3.12}$$

[1] see next Chapters.

The anisotropy will be taken into account through the explicit form of the function g, that will be given as follows,

$$g = \hat{g}\,(a) \qquad a = \int_{\mathcal{S}^2} f^*\,\hat{a}\,(n_a, S_{ab})\,d^2n. \tag{3.13}$$

Let us remark that if $\hat{g}$ is the identity function, $\hat{g}\,(a) = a$, and if a is proportional to the second invariant of the deviatoric stress tensor, $\hat{a}\,(n_a, S_{ab}) = I\,S_{ab}S_{ab}$, then (3.12) takes the form of the isotropic Glen flow law. Moreover, the function $\hat{a}\,(n_a, S_{ab})$ must fulfil the requirements of the principle of material objectivity. This means that $\hat{a}$ can be a function only of the scalar invariants of n_a and S_{ab}. Thus,

$$a = \hat{a}\,(n_a, S_{ab}) = \tilde{a}\,(S_{ab}S_{ab}, S_{ab}S_{bc}S_{ca}, S_{ab}n_an_b, S_{ab}n_bS_{ac}n_c)\,. \tag{3.14}$$

3.3 A Two-dimensional Anisotropic Flow Law

3.3.1 General Remarks

In this section we wish to find a two-dimensional anisotropic flow law. In this scheme, the unit vector, n_j, parallel to the c-axis has only two components, namely

$$n_1 = \cos\,\tilde{\theta}, \qquad\qquad n_2 = \sin\,\tilde{\theta}. \tag{3.15}$$

The range of possible orientations in $\mathcal{S}^2$, is the interval $\tilde{\theta} \in [0, 2\pi]$. The Jacobian of (3.15) is unity and the second-order structure tensor is defined by

$$A_{ij} = \int_0^{2\pi} f^* n_i n_j d\tilde{\theta}. \tag{3.16}$$

The most simple scalar invariant including the unit vector n_a and the stress deviator, S_{ab}, is, from (3.14),

$$S_{ab}n_an_b = S_{12}\sin 2\tilde{\theta} - S_{22}\cos 2\tilde{\theta}. \tag{3.17}$$

After integration, according to (3.16), it has the form

$$tr\,(\mathbf{AS}) = A_{ij}S_{ij} = \int_0^{2\pi} f^* S_{ij} n_i n_j d\tilde{\theta}. \tag{3.18}$$

In two dimensions, pure shear is given by the stress deviator

$$\mathbf{S} = \begin{pmatrix} -S_{22} & 0 \\ 0 & S_{22} \end{pmatrix}. \tag{3.19}$$

Thus, the scalar invariant in (3.18) is

$$tr\,(\mathbf{AS}) = \int_0^{2\pi} f^* S_{22}\,(n_2n_2 - n_1n_1)\,d\tilde{\theta} = -S_{22}\int_0^{2\pi} f^* \cos 2\tilde{\theta} d\tilde{\theta}. \tag{3.20}$$

A single maximum distribution is represented by the ODF

$$f^* = \delta\left(\tilde{\theta} - \tilde{\theta}_0\right), \tag{3.21}$$

and if it is at $\tilde{\theta}_0 = 0$ or $\tilde{\theta}_0 = \pi/2$ we have

$$\tilde{\theta}_0 = 0 \qquad \Longrightarrow \qquad tr\,(\mathbf{AS}) = -S_{22}, \tag{3.22}$$

and

$$\tilde{\theta}_0 = \tfrac{\pi}{2} \qquad \Longrightarrow \qquad tr\,(\mathbf{AS}) = S_{22}, \tag{3.23}$$

respectively. However, the behaviour of samples with the single maximum distributions represented by (3.22) and (3.23) must be the same, i.e., from Fig. 3.2, the material, in these configurations, should be hard to deform. To overcome the above discrepancy (i.e., the difference in signs), the most simple modification is to take the square of such a scalar invariant, i.e.,

$$(A_{hk}S_{hk})^2 = \left(\int_0^{2\pi} f^* S_{ij} n_i n_j d\tilde{\theta}\right)^2. \tag{3.24}$$

In this way eqn. (3.24) yields the same value for the previous two situations. Thus, from (3.22) and (3.23), the scalar invariant in (3.24) has the same value, i.e.,

$$(A_{hk}S_{hk})^2 = (S_{22})^2. \tag{3.25}$$

However, this proposition does not solve the problem. For the two-maxima distribution (see Fig. 3.2c) with the first maximum at $\tilde{\theta}_0 = 0$ and the second at $\tilde{\theta}_0 = \pi/2$, the ODF takes the form

$$f^* = \tfrac{1}{2}\delta(\tilde{\theta}) + \tfrac{1}{2}\delta(\tilde{\theta} - \frac{\pi}{2}), \tag{3.26}$$

For this distribution and for pure shear, the mechanical behaviour of the sample must be the same as that of the previous two situations (see Fig. 3.2). However, the scalar invariant (3.24) for the two-maxima distribution (3.26) takes the value

$$(A_{hk}S_{hk})^2 = \left(\tfrac{1}{2}S_{22} - \tfrac{1}{2}S_{22}\right)^2 = 0, \tag{3.27}$$

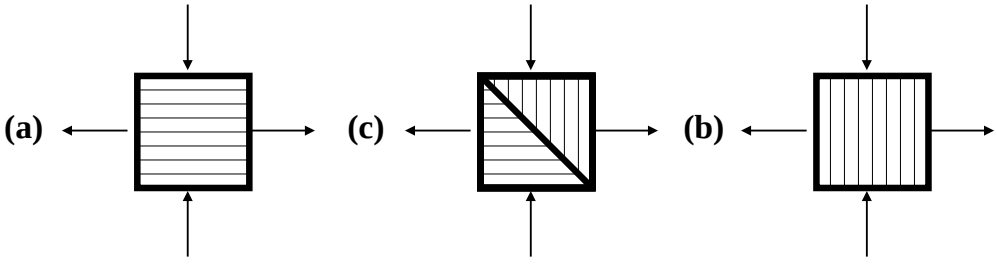

Figure 3.2: Schematic representation of pure shear tests in the two-dimensional case for three samples: the thin lines are parallel to the basal planes of the crystallites in the polycrystal: (a) the single maximum distribution is at $\tilde{\theta}_0 = \pi/2$ (the first and the second axes of the frame of reference represent always the horizontal and the vertical orientations, respectively); (b) the single maximum distribution is at $\tilde{\theta}_0 = 0$; (c) here two maxima arise: the first maximum is at $\tilde{\theta}_0 = 0$, whilst the second maximum is at $\tilde{\theta}_0 = \pi/2$. The deformation mechanism of only basal slip explained in Figs. 2.6 and 2.7 implies nondeformability for these three samples.

different from (3.25). Thus, we have found again two situations that ought to be identical from the mechanical point of view but for which the chosen scalar invariant (e.g., (3.24)) does not generate the same result. The problem is that the crystallites orientated at $\tilde{\theta} = 0$ are able, for the evaluation of (3.24), to cancel the contribution of the crystallites orientated at $\tilde{\theta} = \pi/2$. These difficulties suggest the following considerations. The scalar invariants that we can choose for an ODF-dependent anisotropic flow law (e.g. (3.12)) are always an integral over (or, if we discretize the integral, the sum of) the regions of orientations, $\mathcal{S}^2$, of a quantity (see e.g. (3.13)) evaluated for all the possible orientations. Since every orientation is representative of the crystallites with that lattice orientation, we may postulate that the contribution of the deformation of every crystallite (i.e., of every orientation) must have the same sign[2]: thus, we must assure that the deformation of the crystallites with a given orientation can not be cancelled by the deformation of the crystallites with another orientation. Therefore, we propose to change the scalar invariant of equation (3.24) by the two scalar invariants

$$A_S = \int_0^{2\pi} f^* \left| S_{cd} n_c n_d \right| d\tilde{\theta}, \tag{3.28}$$

and

$$A_{SS} = \int_0^{2\pi} f^* \left| S_{cd} n_c n_d \right|^2 d\tilde{\theta}. \tag{3.29}$$

The adequacy of this choice of scalar invariants can be checked only *a posteriori*. On the other hand, it is easy to recognize that (3.28) and (3.29) fulfil the requested properties: in these cases, in fact, the sum over all the orientations is done for quantities $|S_{cd} n_c n_d|$ or $|S_{cd} n_c n_d|^2$ that are always positive. Moreover, for the pure shear test represented by (3.19), the three situations proposed in Fig. 3.2 provide the same value, as shown in Table 3.1.

Another important property that a scalar invariant should fulfil in order to qualify for use in a flow law is the following: if the mode of deformation is pure shear then the orientations that are symmetric with respect to $\tilde{\theta} = \pi/2$ must give the same contribution.

Table 3.1: Values of the scalar invariants A_S and A_{SS}, shown schematically for the three different fabrics in Fig. 3.2 and for the pure shear test (3.19). In these three situations, the deformation is assumed equally hard. The usefulness of the scalar invariants represented in (3.28) and (3.29) follows from the equivalence of the expressions in the second and the third columns.

f^*	A_S	A_{SS}
$\delta(\tilde{\theta})$	$\lvert S_{22}\rvert$	$(S_{22})^2$
$\delta(\tilde{\theta} - \frac{\pi}{2})$	$\lvert S_{22}\rvert$	$(S_{22})^2$
$\frac{1}{2}\delta(\tilde{\theta}) + \frac{1}{2}\delta(\tilde{\theta} - \frac{\pi}{2})$	$\lvert S_{22}\rvert$	$(S_{22})^2$

[2]Such an assumption can be heavily criticized from a microscopic point of view. However, its validity must be checked only *a posteriori* and for large polycrystalline materials.

This is a requirement dictated by symmetry (see, e.g., Fig. 3.3). It can be shown that its occurrence is guaranteed for all scalar invariants proposed in this section. In Fig. 3.3, a two-maxima fabric distribution made of two orientations that are symmetric with respect to $\tilde{\theta} = \pi/2$ is shown. This is the analog of the three-dimensional girdle fabric and can be represented by the ODF

$$f^* = \tfrac{1}{2}\delta(\tilde{\theta} - \tilde{\theta}_0) + \tfrac{1}{2}\delta(\tilde{\theta} - \pi + \tilde{\theta}_0). \tag{3.30}$$

In Table 3.2 we explicitly state the expressions for the scalar invariants represented in (3.28) and (3.29), including the second invariant of the stress deviator, $S_{ab}S_{ab}$, evaluated for a given mode of deformation and for a given fabric.

All ingredients to build a two-dimensional anisotropic flow law are now prepared. Besides the collinearity between the stretching tensor and the stress deviator, we will, for the sake of simplicity, assume that the stress exponent will be fixed at $n = 3$. Thus, we claim that

$$D_{ij} = S_{ij}\left[d_1 S_{ab}S_{ab} + d_2\left(A_S\right)^2 + d_3 A_{SS}\right] \tag{3.31}$$

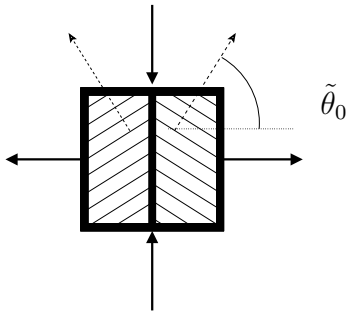

Figure 3.3: Two-dimensional girdle fabric distribution. Thin lines are parallel to the basal planes of the crystallites in the polycrystal. In this sample only two orientations, evidenced by the dashed arrows and symmetric with respect to $\tilde{\theta} = \pi/2$, are present. The sample is subject to pure shear, as shown by the solid outside arrows. The symmetry between the state of deviatoric stress and the two orientations in the polycrystal implies that the contributions of the two crystallites to the stretching must be the same.

Table 3.2: Expressions for three important scalar invariants for specific distributions of the lattice orientations, denoted in the first row, and for the indicated mode of deformation, denoted in the second row.

Fabrics	**Random distribution**	**Girdle**: $\tilde{\theta} = \tilde{\theta}_0$	**Girdle**: $\tilde{\theta} = \tilde{\theta}_0$
Mode of deformation	*General*	*Pure Shear*	*Simple Shear*
$S_{ab}S_{ab}$	$2\left[\left(S_{22}\right)^2 + \left(S_{12}\right)^2\right]$	$2\left(S_{22}\right)^2$	$2\left(S_{12}\right)^2$
A_S	$\frac{1}{\pi}\sqrt{\lvert 2S_{ab}S_{ab}\rvert}$	$\left\lvert S_{22}\cos 2\tilde{\theta}_0\right\rvert$	$\left\lvert S_{12}\sin 2\tilde{\theta}_0\right\rvert$
A_{SS}	$\frac{1}{4}\left(S_{ab}S_{ab}\right)$	$\left(S_{22}\right)^2\left(\cos 2\tilde{\theta}_0\right)^2$	$\left(S_{12}\right)^2\left(\sin 2\tilde{\theta}_0\right)^2$

is a suitable two-dimensional anisotropic flow law. The values of the three material parameters d_1, d_2 and d_3 have to be chosen by a set of three Gedanken Experiments that we show in the next subsection.

3.3.2 Evaluation of the Material Parameters

In order to make explicit the three material parameters d_1, d_2 and d_3, three independent equations are needed, that will be derived from a set of three independent Gedanken Experiments. It should be noted that the results of these "experiments" must be known: they will be constructed for a random distribution (isotropic case), for the single maximum distribution (in a hard configuration) and for the girdle fabric distribution (in a soft configuration), respectively. A similar strategy will be used in the next section for the evaluation of the material parameters of the three-dimensional anisotropic flow law.

From Table 3.2 and from (3.31), it is straightforward to derive the analogue of Glen's flow law with $n = 3$ when the distribution of the lattice orientations is random. For the sake of simplicity we introduce the parameter I to write such a two-dimensional isotropic flow law, namely

$$D_{ij} = I_2 S_{ij} \left(S_{hk} S_{hk} \right). \tag{3.32}$$

Thus, we can perform the first Gedanken Experiment for this isotropic case, assume that the numerical value of I is known and derive the first equation for the evaluation of the three material parameters d_1, d_2 and d_3 from Table 3.2, (3.31) and (3.32),

$$d_1 + \tfrac{2}{\pi^2} d_2 + \tfrac{1}{4} d_3 = I_2. \tag{3.33}$$

The second Gedanken Experiment can be performed in the regime of pure shear and for a girdle fabric distribution[3]. As already pointed out, if the angle $\tilde{\theta}_0$ of this distribution equals $\pi/2$, the deformation for the pure shear test is hard and zero stretching can be assumed. Therefore, we can derive the second equation from Table 3.2 and (3.31), i.e.,

$$2d_1 + d_2 + d_3 = 0. \tag{3.34}$$

The third equation comes from a Gedanken Experiment for a girdle fabric at $\tilde{\theta}_0 = \pi/4$. In this configuration (see e.g. Fig. 3.3a) the deformation for the pure shear test represented in (3.19) is very easy and we assume that the stretching is E times the stretching for the isotropic case. Thus, the third equation is,

$$2d_1 = 2I_2 E, \tag{3.35}$$

where E is an enhancement factor.

We will prove in the next subsection that this third Gedanken Experiment is the analogue of the simple shear test performed on a sample where one single maximum is present at $\tilde{\theta}_0 = \pi/2$. Thus, E is the enhancement factor that Jacka and Budd [74] measured in 1989. They found that its value is,

$$E \cong 8. \tag{3.36}$$

[3]Note from equation (3.30) that a girdle fabric distribution with $\tilde{\theta}_0 = \pi/2$ can also be called the vertical single maximum distribution.

The combination of (3.33), (3.34) and (3.35) is a well posed system of linear equations that can be easily solved to yield

$$d_1 = I_2 E, \quad d_2 = I_2 \pi^2 \left[\frac{2E-4}{\pi^2-8}\right], \quad d_3 = 4I_2 \left[\frac{4E+\pi^2-E\pi^2}{\pi^2-8}\right]. \tag{3.37}$$

Thus, the final form of the anisotropic flow law takes the form

$$D_{ij} = S_{ij}\left\{EI_2 S_{ab}S_{ab} + I_2\pi^2\left[\frac{2E-4}{\pi^2-8}\right](A_S)^2 + 4I_2\left[\frac{4E+\pi^2-E\pi^2}{\pi^2-8}\right]A_{SS}\right\}. \tag{3.38}$$

3.3.3 Verification of the Anisotropic Flow Law

It can be easily recognized from Table 3.2 that for a uniformly random distribution, (3.38) gives the isotropic flow law (3.32) and for a girdle fabric distribution, it is no longer isotropic. It is furthermore remarkable that, in this girdle fabric case and in a pure shear test (see, e.g. Fig. 3.3), (3.38) provides the following expression for the related component of the stretching,

$$\begin{aligned} D_{22} &= (S_{22})^3\left\{2EI_2 + I_2\pi^2\left[\frac{2E-4}{\pi^2-8}\right]\left(\cos 2\tilde{\theta}_0\right)^2 + 4I_2\left[\frac{4E+\pi^2-E\pi^2}{\pi^2-8}\right]\left(\cos 2\tilde{\theta}_0\right)^2\right\} \\ &= (S_{22})^3 I_2\left\{2E - 2E\left(\cos 2\tilde{\theta}_0\right)^2\right\} = (S_{22})^3\, 2I_2 E\left(\sin 2\tilde{\theta}_0\right)^2, \end{aligned} \tag{3.39}$$

where $\sin 2\tilde{\theta}_0$ is the analogue of the Schmidt factor $S^{(g)}$ in equation (2.9) introduced to describe the mechanical behaviour of a single crystal. The nondeformability under a pure shear test of a sample with a girdle fabric distribution at $\tilde{\theta}_0 = 0$, $\tilde{\theta}_0 = \pi/2$ and $\tilde{\theta}_0 = \pi$ can be easily corroborated from (3.39). Moreover, the stretching, in this configuration, is maximum if the girdle fabric is at $\tilde{\theta}_0 = \pi/4$.

Another important result is the form of the flow law in a simple shear test and for a girdle fabric,

$$D_{12} = (S_{12})^3\left\{2EI_2 + I_2\pi^2\left[\frac{2E-4}{\pi^2-8}\right]\left(\sin 2\tilde{\theta}_0\right)^2 + 4I_2\left[\frac{4E+\pi^2-E\pi^2}{\pi^2-8}\right]\left(\sin 2\tilde{\theta}_0\right)^2\right\},$$

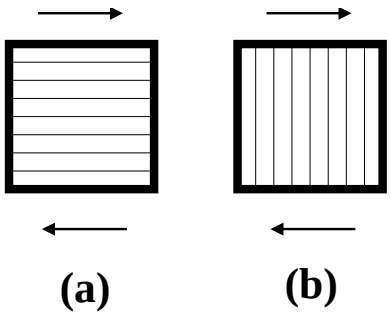

Figure 3.4: Two simple shear tests performed on two single maximum distributions at $\tilde{\theta} = \tilde{\theta}_0$: (a) $\tilde{\theta}_0 = \pi/2$; (b) $\tilde{\theta}_0 = 0$. The thin lines are parallel to the basal planes of the crystallites in the polycrystal. It is pleasing that equation (3.40) produces the same flow law (3.41) for these two cases.

or

$$D_{12} = (S_{12})^3 I_2 \left\{ 2E - 2E \left(\sin 2\tilde{\theta}_0 \right)^2 \right\} = (S_{12})^3 I_2 2E \left(\cos 2\tilde{\theta}_0 \right)^2 . \tag{3.40}$$

Thus, if $\tilde{\theta}_0 = 0$ or $\tilde{\theta}_0 = \pi/2$ we have,

$$D_{12} = E \left[2I_2 (S_{12})^3 \right] . \tag{3.41}$$

The equivalence of these two cases, also represented in Fig. 3.4, must not surprise. We already showed in Fig. 2.12 that the vertical and the horizontal orientations are, for the simple shear mode of deformation, equivalent. Moreover, we proved in (3.41) the equivalence of this simple shear test of a single maximum fabric at $\tilde{\theta}_0 = \pi/2$ with the third Gedanken Experiment. Finally, expression (3.40) shows that the stretching for the simple shear mode of deformation on a sample with girdle fabric distribution at $\tilde{\theta}_0 = \pi/4$ is zero.

A more important result is to achieve an explicit anisotropic generalization of Glen's flow law for the three-dimensional case. This is a more difficult task, for which we dedicate the next section.

3.4 A Three-dimensional Anisotropic Flow Law

3.4.1 General Remarks

A three-dimensional generalization of the anisotropic flow law is not trivial. The most simple scalar invariant, $S_{ab} n_a n_b$, that we can build from the unit vector, n_j, parallel

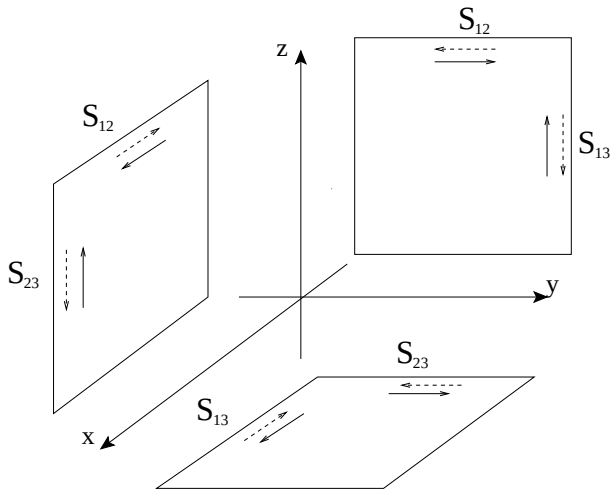

Figure 3.5: Schematic representation of the physical meaning of the three components (S_{12}, S_{13} and S_{23}) of the deviatoric stress tensor S_{ij}. Three orthogonal planes are shown; the normals of these planes are the three unit vectors $\mathbf{e}_1 = \hat{\mathbf{i}}$, $\mathbf{e}_2 = \hat{\mathbf{j}}$ and $\mathbf{e}_3 = \hat{\mathbf{k}}$ parallel to the three axes of the frame of reference with respect to which the components S_{ij} are evaluated. S_{ij} is the shear stress acting on the plane orthogonal to $\mathbf{e}_i$ in the direction $\mathbf{e}_j$, if i is different from j. Balance of angular momentum guarantees the symmetry of the stress tensor.

to the c-axis and from the deviatoric stress tensor, S_{ij}, and that was employed for the two-dimensional case is not useful. The reason is as follows:

We use for this three-dimensional case the classical spherical coordinate system defined in (3.1), i.e.,

$$n_1 = \sin\theta\cos\varphi, \quad n_2 = \sin\theta\sin\varphi, \quad n_3 = \cos\theta,$$

and then can easily evaluate

$$\begin{aligned} S_{ab}n_a n_b &= S_{11}\left(\sin\theta\cos\varphi\right)^2 + S_{22}\left(\sin\theta\sin\varphi\right)^2 + S_{33}\left(\cos\theta\right)^2 \\ &\quad + S_{13}\cos\varphi\sin 2\theta + S_{23}\sin\varphi\sin 2\theta + S_{12}\left(\sin\theta\right)^2\sin 2\varphi. \end{aligned} \tag{3.42}$$

For vertical orientation ($\theta = 0$), we have

$$\theta = 0, \quad \Longrightarrow \quad S_{ab}n_a n_b = S_{33} = -S_{11} - S_{22}. \tag{3.43}$$

Since we want to use this scalar invariant in the flow law, we must provide its physical interpretation. The component S_{33}, that emerges in (3.43) in the evaluation of $S_{ab}n_a n_b$ at the vertical orientation, represents a compression (or tension) along the third (i.e., vertical) direction of the actual frame of reference. We know that such a component is not able to produce any stretching for a crystallite with vertical c-axis orientation. Therefore we can assign a preliminary physical meaning to $S_{ab}n_a n_b$: the higher the deformation is, the lower will be the value of $S_{ab}n_a n_b$. On the other hand, S_{12} is neither able to give any measurable deformation for a crystal that is oriented with $\theta = 0$, as we can recognize from its interpretation explained in Fig. 3.5. Thus, the use of the scalar invariant $S_{ab}n_a n_b$ gives in (3.43) an unwanted discrimination between the two components, S_{12} and S_{33}, which for the crystallites with vertical orientation have theoretically the same physical response. This implies that the preliminary physical meaning that we have assigned above to the scalar invariant $S_{ab}n_a n_b$ is not correct. In fact, if we make an experiment in which the only component S_{12} is different from zero, the scalar invariant $S_{ab}n_a n_b$ for $\theta = 0$ is zero as well as the deformation of this experiment.

Such a problem did not arise in two dimensions. In fact, from (3.17), the vertical orientation ($\tilde{\theta} = \pi/2$) selected S_{22}, that was the only component unable to produce measurable stretching. In this two-dimensional scheme the other component, S_{12}, of the stress deviator is, on the other hand, the only component that is able to produce measurable stretching.

In order to avoid this problem, let us analyse for this three-dimensional case another scalar invariant,

$$\begin{aligned} S_{ab}n_b S_{ah}n_h &= \left[\left(S_{11}\right)^2 + \left(S_{12}\right)^2 + \left(S_{13}\right)^2\right]\left(\sin\theta\cos\varphi\right)^2 \\ &\quad + \left[\left(S_{12}\right)^2 + \left(S_{22}\right)^2 + \left(S_{23}\right)^2\right]\left(\sin\theta\sin\varphi\right)^2 \\ &\quad + \left[\left(S_{13}\right)^2 + \left(S_{23}\right)^2 + \left(S_{33}\right)^2\right]\left(\cos\theta\right)^2 \\ &\quad + \left[S_{12}S_{23} - S_{22}S_{13}\right]\cos\varphi\sin 2\theta \\ &\quad + \left[S_{13}S_{12} - S_{11}S_{23}\right]\sin\varphi\sin 2\theta \\ &\quad + \left[S_{23}S_{13} - S_{33}S_{12}\right]\left(\sin\theta\right)^2\sin 2\varphi. \end{aligned} \tag{3.44}$$

Note that this invariant can be used only in a three-dimensional context. The proof is as follows: If we neglect all stress components involving the third direction, set $\theta = \pi/2$ and $S_{11} = -S_{22}$, then we have

$$S_{11} = -S_{22}, \quad S_{13} = S_{23} = S_{33} = 0, \quad \theta = \tfrac{\pi}{2}, \quad \Longrightarrow \quad S_{ab}n_b S_{ah}n_h = \left(S_{22}\right)^2 + \left(S_{12}\right)^2.$$

This is not independent of the second invariant of the deviatoric stress tensor in the two-dimensional case. Thus, use of $S_{ab}n_bS_{ah}n_h$ as an invariant in a two-dimensional context is not forbidden, it is simply useless. The value of this scalar invariant for vertical orientation ($\theta = 0$) is

$$\theta = 0, \quad \Longrightarrow \quad S_{ab}n_bS_{ah}n_h = (S_{13})^2 + (S_{23})^2 + (S_{33})^2 . \tag{3.45}$$

In this case we have another unwanted situation: for a vertical c-axis, the two components that produce high strain rates (i.e., S_{13} and S_{23}) are operating together with another component (i.e., S_{33}), that is unable to produce them. However, considering (3.43) and (3.45), the solution of the problem can be achieved if we define another scalar invariant, $S_c(\theta, \varphi)$, by a combination of (3.42) and (3.44), as follows

$$S_c(\theta, \varphi) \equiv S_{ab}n_bS_{ah}n_h - (S_{ab}n_an_b)^2 . \tag{3.46}$$

The value of S_c for vertical orientation, $S_c(0, \varphi)$, is remarkable,

$$\mathbf{n} = \hat{\mathbf{k}} \quad \theta = 0, \quad \Longrightarrow \quad S_c(0, \varphi) = (S_{13})^2 + (S_{23})^2 , \tag{3.47}$$

where $\left(\hat{\mathbf{i}}, \hat{\mathbf{j}}, \hat{\mathbf{k}}\right)$ is the unit basis of the Cartesian coordinate system. Thus, for the orientation at $\theta = 0$ ($\mathbf{n} = \hat{\mathbf{k}}$), the scalar invariant S_c produces the selection of the two components that are able to give the highest stretching values, i.e., S_{13} and S_{23}. Moreover, the principle of material objectivity guarantees the validity of the following properties,

$$\mathbf{n} = \hat{\mathbf{i}} \quad \Longrightarrow S_c\left(\tfrac{\pi}{2}, 0\right) = (S_{12})^2 + (S_{13})^2 ; \quad \mathbf{n} = \hat{\mathbf{j}} \quad \Longrightarrow S_c\left(\tfrac{\pi}{2}, \tfrac{\pi}{2}\right) = (S_{12})^2 + (S_{23})^2 . \tag{3.48}$$

The properties revealed by (3.47) and (3.48) are remarkable in conection with Fig. 3.5: $S_c(\theta, \varphi)$ gives the sum of the squares of the components of the stress deviator that are better able to deform the crystallites oriented with θ and φ. The general physical response of S_c is, therefore, the following: the higher the deformation is, the higher will be the value of S_c !

For pure shear, the usefulness of $S_c(\theta, \varphi)$ is equally confirmed by the expression

$$S_{11} = S_{22} = -\tfrac{1}{2}S_{33}, \quad S_{12} = S_{13} = S_{23} = 0, \quad \Longrightarrow \quad S_c(\theta, \varphi) = \left(\tfrac{3}{4}S_{33}\sin 2\theta\right)^2 . \tag{3.49}$$

The presence of the Schmidt factor $\sin 2\theta$ guarantees an analogy with the case of a single crystal. Moreover, the orientation that gives the greatest value for S_c is $\theta = \pi/4$; this is the orientation for which the deformation is easiest. Therefore, the response of S_c is, even in this case, physically meaningful. For simple shear (e.g., $S_{13} \neq 0$), the explicit value of S_c is more puzzling; indeed, if

$$S_{13} \neq 0 \qquad S_{11} = S_{22} = S_{33} = S_{12} = S_{23} = 0, \tag{3.50}$$

then

$$S_c(\theta, \varphi) = (S_{13})^2 \left[(\cos\theta)^2 - (1 + 2\cos 2\theta)(\cos\varphi)^2 (\sin\theta)^2\right] .$$

However, in the plane $1-3$, where $\varphi = 0$ or $\varphi = \pi$, we have the following simplification,

$$S_{11} = S_{22} = S_{33} = S_{12} = S_{23} = 0, \quad \Longrightarrow \quad S_c(\theta, 0) = [S_{13}(\cos 2\theta)]^2 . \tag{3.51}$$

All these results confirm the adequacy of the physical response of S_c: the higher the value of S_c is, the larger will be the deformation !

The three-dimensional generalization of the anisotropic flow law will include this scalar invariant. In fact we will choose the representation

$$D_{ij} = S_{ij}\left[t_0 S_{hk}S_{hk} + t_1 A + t_2 B\right], \tag{3.52}$$

where

$$A = \int_{\mathcal{S}^2} |S_c|\, f^* d^2 n, \quad B = \sqrt{\int_{\mathcal{S}^2} \left[S_c\right]^2 f^* d^2 n}. \tag{3.53}$$

In Table 3.3, we calculate values of A and B for some typical situations.

In Table 3.3, for the sake of synthesis, we have used the definition,

$$B_{ss}\left(\theta_0\right) \equiv \frac{\left(S_{13}\right)^2}{8}\sqrt{22 + 18\cos 2\theta_0 + 19\cos 4\theta_0 + 2\cos 6\theta_0 + 3\cos 8\theta_0}.$$

3.4.2 Evaluation of the Material Parameters

For this three-dimensional case again a set of three Gedanken Experiments must be performed in order to determine the values of the material parameters t_0, t_1 and t_2. If the three-dimensional generalization of (3.32) is written as

$$D_{ij} = I_3 S_{ij}\left(S_{hk}S_{hk}\right),$$

and the first Gedanken Experiment is given for a sample with (uniform) random orientation distribution, then, from Table 3.3, (3.32) and (3.52), we have,

$$t_0 + \frac{1}{5}t_1 + \sqrt{\frac{2}{35}}t_2 = I_3. \tag{3.54}$$

In analogy with the two-dimensional case, the second Gedanken Experiment is performed for a sample that is very hard to deform for the given state of deviatoric stress. We will make the following choice: vertical single maximum distribution ($\theta = 0$) and a state of pure shear as given on the left-hand side of (3.49). Thus, from Table 3.3 and (3.49), we get $S_c = 0$ and, consequently, $A = 0$, $B = 0$, so that (3.52) yields

$$t_0 = 0. \tag{3.55}$$

In the third Gedanken Experiment the sample will be very soft to deform and we use the enhancement factor (3.36). Therefore, we can choose the same sample; the mode

Table 3.3: Expressions for the scalar invariants defined in (3.53) for typical distributions of the lattice orientations for particular modes of deformation.

Fabrics	**Random**	**Girdle**:$\theta = \theta_0$	**Girdle**:$\theta = \theta_0$
Mode of deformation	*General*	*Simple Shear (3.51)*	*Pure Shear (3.49)*
A	$\frac{1}{5}S_{hk}S_{hk}$	$\frac{\left(S_{13}\right)^2}{4}\left(2 + \cos 2\theta_0 + \cos 4\theta_0\right)$	$\left(\frac{3}{4}S_{33}\sin 2\theta_0\right)^2$
B	$\sqrt{\frac{2}{35}}S_{hk}S_{hk}$	$B_{ss}\left(\theta_0\right)$	$\left(\frac{3}{4}S_{33}\sin 2\theta_0\right)^2$

of deformation will, consequently, be simple shear expressed, e.g., in (3.50). Thus, from Table 3.3 and (3.52),

$$2t_0 + t_1 + t_2 = 2EI_3. \tag{3.56}$$

Combination of (3.54), (3.55) and (3.56) defines a well posed system of linear equations that can be solved to give the final three-dimensional generalization of the anisotropic flow law, i.e.,

$$D_{ij} = \frac{I_3}{\sqrt{70} - 7} \left[\left(2E\sqrt{70} - 35 \right) A + 7\,(5 - 2E)\,B \right] S_{ij}. \tag{3.57}$$

3.4.3 Verification of the Anisotropic Flow Law

We begin the verification of (3.57) by remarking that for a (uniform) random distribution of the c-axes, from Table 3.3 and (3.57), the classical isotropic Glen flow law (2.3) in the form (3.4.2) is obtained.

Moreover, the simple shear test (3.50) on a sample with vertical single maximum distribution may be deduced from the third column of Table 3.3 and (3.57), and yields

$$D_{13} = E \left[2I_3 \left(S_{13} \right)^3 \right]. \tag{3.58}$$

In the isotropic case the value of D_{13} is simply given by the expression in the square bracket of (3.58). Therefore, the enhancement factor E_s for simple shear is

$$E_s = E. \tag{3.59}$$

For pure shear, represented by the left-hand side of (3.49), the expression for D_{33}, in the isotropic case, is

$$D_{33} = \tfrac{3}{2} I_3 \left(S_{33} \right)^3. \tag{3.60}$$

For a girdle fabric and pure shear as represented on the left-hand side of (3.49) and from the fourth column of Table 3.3, the anisotropic flow law (3.57) yields the expression

$$D_{33} = \left[\tfrac{3}{2} I \left(S_{33} \right)^3 \right] \tfrac{3}{4} E \left(\sin 2\theta_0 \right)^2. \tag{3.61}$$

Comparison between (3.60) and (3.61) identifies the enhancement factor E_p for pure shear on a girdle fabric, i.e.,

$$E_p = \tfrac{3}{4} E \left(\sin 2\theta_0 \right)^2. \tag{3.62}$$

Jacka and Budd [74] measured the enhancement factor $E_s \cong 8$ (see (3.36)) for simple shear for a vertical single maximum distribution. Furthermore, they obtained an enhancement factor $E_p \cong 3$ for pure shear for a strong small-circle girdle fabric. Unfortunately, they do not specify the value of the angle θ_0 and so we can not verify this aspect of the theory. On the other hand, we mention that, in order the theory to be coherent with these measurements, from (3.62), the strong small-circle girdle fabric of their experiments should have the following value for θ_0:

$$E_p = 3, \quad E = E_s = 8, \quad \Longrightarrow \quad \theta_0 = \tfrac{1}{2} \arcsin \tfrac{1}{\sqrt{2}} = \tfrac{\pi}{8}. \tag{3.63}$$

Besides, a very important conclusion can be made. If the angle θ_0 of the girdle fabric is $\theta_0 = \frac{\pi}{4}$, the enhancement factor E_p in (3.62) assures its maximum, i.e.,

$$E_p = \tfrac{3}{4}\ E. \tag{3.64}$$

Therefore, E_p does not reach the value $E_s = E$ (see (3.59)) derived for simple shear for a vertical single maximum distribution. This seems to be incoherent with the equivalences between the vertical orientation in simple shear and the 45° from the vertical orientation in pure shear evidenced in Fig. 2.12 and the analogy shown at the end of Section 3.3 between simple shear on single maximum fabric and pure shear on girdle fabric. However those results are developed in a two-dimensional context and the explanation of this spurious contradiction is as follows: In the two-dimensional case, for pure shear on a girdle fabric at $\tilde{\theta}_0 = \frac{\pi}{4}$ the strain rate is enhanced in the same way as it is for simple shear on the single maximum distribution at $\tilde{\theta}_0 = \frac{\pi}{2}$, because all crystallites are well oriented for both modes of deformation. In the three-dimensional case this is not so. In fact, even though the state of stress represented by the component S_{33} meets all the crystallites well oriented for deformation (i.e., at 45° from the vertical), the deformation caused by the state of stress represented by the components S_{11} and S_{22} is not favoured by all crystallites of that girdle fabric. If, e.g., an orientation of this girdle fabric is at 45° with respect to $\boldsymbol{e}_1$, then the same orientation can neither be at 45° with respect to $\boldsymbol{e}_2$.

3.5 The Derivation of Another Two-dimensional Flow Law

3.5.1 Two-dimensional Limit of (3.57)

The aim of this section is to derive a second two-dimensional anisotropic flow law as the limit of the three-dimensional equation (3.57). It is easy to recognize that (3.57) can be written in the following form

$$D_{ij} = S_{ij} \frac{7\, I_3}{\sqrt{70} - 7} \left[5\,(B - A) + 2E \frac{\sqrt{70} A - 7B}{7} \right]. \tag{3.65}$$

From the definition of the scalar invariant S_c in (3.46), if we neglect all components involving the third direction and set the latitude θ equal to $\frac{\pi}{2}$ in order to constraint the unit vector n_i to lie in the plane generated by the first and the second axes of the frame of reference, it is straightforward to derive

$$\theta = \tfrac{\pi}{2},\ S_{13} = S_{23} = S_{33} = 0 \quad \Longrightarrow \quad S_c = \left[(S_{22})^2 + (S_{12})^2 \right] - \left[S_{12} \sin 2\varphi - S_{22} \cos 2\varphi \right]^2, \tag{3.66}$$

where the traceless condition on the deviatoric stress tensor is already taken into account. If the longitude φ is identified with the angle $\tilde{\theta}$ introduced for the two-dimensional case, then the scalar invariant S_c can be represented as

$$S_c = \tfrac{1}{2} S_{ab} S_{ab} - \left[S_{cd} n_c n_d \right]^2, \tag{3.67}$$

and its square is

$$S_c^2 = \tfrac{1}{4} \left[S_{ab} S_{ab} \right]^2 + \left[S_{cd} n_c n_d \right]^4 - \left[S_{ab} S_{ab} \right] \left[S_{cd} n_c n_d \right]^2, \tag{3.68}$$

where the value of the indices can only be 1 or 2. Therefore, the scalar functions A and B introduced in (3.53) to build the three-dimensional anisotropic flow law (3.57), can be

written, in the two-dimensional limit, as

$$A = \tfrac{1}{2} S_{ab} S_{ab} - A_{SS}, \qquad B = \sqrt{\tfrac{1}{4} \left[S_{ab} S_{ab} \right]^2 + A_{SSSS} - S_{ab} S_{ab} A_{SS}}, \tag{3.69}$$

where

$$A_{SSSS} = \int_0^{2\pi} f^* \left| S_{cd} n_c n_d \right|^4 d\tilde{\theta}. \tag{3.70}$$

Substitution of (3.69) into (3.57) or (3.65), yields the target of this subsection, i.e., another proposal of the two-dimensional anisotropic flow law,

$$\begin{aligned} D_{ij} \;=\; & \frac{I\left(2E\sqrt{70} - 35\right)}{\sqrt{70} - 7} \left[\tfrac{1}{2} S_{ab} S_{ab} - A_{SS} \right] S_{ij} \\ & + 7 \frac{I\left(5 - 2E\right)}{\sqrt{70} - 7} \left[\sqrt{\tfrac{1}{4} \left[S_{ab} S_{ab} \right]^2 + A_{SSSS} - S_{ab} S_{ab} A_{SS}} \right] S_{ij}. \end{aligned} \tag{3.71}$$

3.5.2 Comparison with (3.38)

As we can easily recognize, the two anisotropic flow laws (i.e., (3.38) and (3.71)) are built for the same two-dimensional case and are different. The presence of the new scalar invariant A_{SSSS} and the absence of A_S make (3.71) more complicated. Moreover, the numerical evaluation of A_{SSSS} needs a larger computational time than that for A_S. For this reason, we propose to continue to use (3.38) in a pure two-dimensional context. On the other hand, (3.71) must fulfil the general properties that were verified for (3.38) in subsection 3.3.3. The corroboration of these properties will be, in fact, a further guarantee of the validity of (3.57). To this end, we remark that, in the analogy of Table 3.2, the scalar invariant A_{SSSS} for pure and simple shear tests on a girdle fabric sample have, respectively, the forms

$$A_{SSSS} = \left(S_{22} \cos 2\tilde{\theta}_0 \right)^4 \quad \text{and} \quad A_{SSSS} = \left(S_{12} \sin 2\tilde{\theta}_0 \right)^4, \tag{3.72}$$

where $\tilde{\theta}_0$ is the angle that all the c-axes of the girdle fabric have with respect to the second axis of the frame of reference. Insertion of the results of the third column of Table 3.2 and $(3.72)_1$ for pure shear on a two-dimensional girdle fabric yields (3.39). On the other hand, insertion of the results of the fourth column of Table 3.2 and $(3.72)_2$ for simple shear on a two-dimensional girdle fabric yields (3.40). Thus, we have proved that the limit of (3.57) in the two-dimensional case is coherent in these two simple situations with the other proposed parameterization, (3.38).

3.6 Conclusion

Equations (3.38) and (3.57) are two anisotropic constitutive flow laws valid for those incompressible polycrystals with transversely isotropic crystallites in the two- and three-dimensional cases, respectively. The validity of (3.38) and (3.57) is ensured in any frame of reference and for any state of deformation. If the deformation mechanism of the crystallites in the polycrystal is glide on planes (basal planes) orthogonal to $\mathbf{n}$ and if this

is a unique deformation mechanism in the polycrystal, then the anisotropy of each material that fulfils these properties can be characterized by only one parameter, that we called E to remind that it is a kind of enhancement factor. The theory is built in such a way that experimental evaluation of this parameter can be achieved from the results on any anisotropic sample for which the ODF is known. However, it is convenient to use the anisotropic sample such that the stretching is the largest, in order to reduce to a minimum the experimental error on E. We remark, for example, that the enhancement factor E for terrestrial ice of ice sheets is already measured and we used a simple shear test, in the third Gedanken Experiment, on a single maximum fabric. The parameterization of E with respect to temperature is not done for the lack of available experimental data. However, this fundamental knowledge is needed to allow this theory to be used in a polythermal body such as an ice sheets. Another important outlook is the knowledge of the evolution of the ODF with respect to the phenomena of grain rotation and recrystallization.

The approach on anisotropy that we have discussed in this chapter is new and it is developed for one specific material, i.e., polycrystalline ice of terrestrial ice sheets. However, the generality of the method makes us confident to believe that its application for other materials, of which the anisotropy is driven by an ODF, is possible. The model presented in this paper is valid for those polycrystals, of which the crystallites are characterized by a unique unit vector that is orthogonal to the plane on which the glide is easier. This is a situation that is typical for ice and ensures the usefulness of the scalar invariant S_c. Another material with these characteristics will be modelled simply by a different value of the enhancement factor E. On the other hand, if the active planes are more than the planes of easy glide, the anisotropy is more complicated and the scalar S_c must be changed accordingly to the mechanical behaviour of the new material. We finally remark that the compatibility of the equations presented in this paper with the Second Law of Thermodynamics is not ensured by the structure of (3.57) for any kind of ODF. The overcoming of this weak point is nevertheless fundamental for the suitability of this model for any possible applications.

Chapter 4

Balance Equations for Polycrystalline Materials

4.1 The Theory of Mixtures with Continuous Diversity

The variety of possible applications of the Theory of Mixtures with Continuous Diversity is underlined in the introduction of the first paper on it in 2001 by Faria [36]. As in any general theory, care should be observed to avoid the risk that, because of the generality of the theory, inferences that can be drawn from it are too weak to be informative. However, the Theory of Mixtures with Continuous Diversity is actually more than a theory, it is a framework in which new theories can be developed. In this chapter we will analyse polycrystalline materials and show how useful this framework is for such a modelling. To this end, the characterization of the RVE is essential. As we have already pointed out in the first chapter, the lattice orientation and the grain size[1] play a fundamental role in the mechanics of ice and, in general, of polycrystalline materials. Therefore, the RVE will be provided by a large number of crystallites with their own grain sizes and lattice orientations. In the Theory of Mixtures with Continuous Diversity, this is transferred into a particular definition of the *species assemblage*. In the present case each species of the mixture will be the representative of those crystallites with a certain grain size and lattice orientation. Thus, the species assemblage is characterized by the range in which grain sizes and lattice orientations are allowed to be varied.

In polycrystalline materials with a transversal isotropic microstructure[2], the lattice orientation of a crystallite is represented by a unit vector, n_j, belonging to the two-dimensional space of the unit sphere $\mathcal{S}^2$, i.e.,

$$n_j \in \mathcal{S}^2.$$

On the other hand, grain size $\bar{D}$ can not vary arbitrarily; the size of the RVE (say, $\bar{D}_M$) is the greatest admissible value of $\bar{D}$, i.e.,

$$\bar{D} \in \left[0, \bar{D}_M\right] =: \bar{\mathcal{I}} \subset \mathbb{R}.$$

[1] In this chapter $\bar{D}$ is the symbol of grain size. D is the symbol of the nondimensional grain-size, defined in equation (4.1).

[2] The microstructure of ice is, from Fig. 2.5, approximated as transversal isotropic.

Note that the maximum value of the grain size varies from point to point and is different from $\bar{D}_M$[3]; $\bar{D}_M$ is in fact fixed, and it must be chosen in such a way to be always greater than the largest grain size and smaller than the characteristic length of the body. Moreover, for reasons of dimensionality it is advantageous to introduce a dimensionless grain-size variable, D, according to

$$D = \frac{\bar{D}}{\bar{D}_M}. \tag{4.1}$$

Clearly, as $\bar{D} \in \bar{\mathcal{I}}$ varies from 0 to $\bar{D}_M$, the dimensionless grain-size D,

$$D \in \mathcal{I} := [0, 1]$$

varies from 0 to 1. Henceforth, we shall only work with $D \in \mathcal{I}$. We shall also call $\mathcal{I}$ the *grain-size range* and will assume that all functions have now compact support with respect to $\mathcal{I}$: this means that all functions of the nondimensional grain-size D are continuous and vanish outside the grain-size range.

4.2 Mass Densities

4.2.1 General Remarks

The above considerations should make it clear that we wish the species assemblage to consist of the union of the possible values of nondimensional grain-sizes, $\mathcal{I}$, and orientations, $\mathcal{S}^2$, i.e., $\mathcal{S}^2 \cup \mathcal{I}$. Moreover, the species assemblage consists of the direct sum of subassemblages describing different physical subprocesses. In fact, grain sizes and orientations can have different distributions within any one RVE. In the Theory of Mixtures with Continuous Diversity this difference is explicitly expressed in terms of distinct *mass densities*, i.e., for every time t and position x_i the *orientation-and-size mass density* $\varrho^{\triangleright}(x_i, t, n_j, D)$ is defined such that when integrated over $\mathcal{I}$, the *orientation mass density* $\varrho^{*}(x_i, t, n_j)$, and when integrated over $\mathcal{S}^2$ the *size mass density* $\varrho^{\blacktriangleright}(x_i, t, D)$ are obtained , i.e.,

$$\varrho^{*}(x_i, t, n_j) = \int_{\mathcal{I}} \varrho^{\triangleright}(x_i, t, n_j, D)\, dD, \quad \varrho^{\blacktriangleright}(x_i, t, D) = \int_{\mathcal{S}^2} \varrho^{\triangleright}(x_i, t, n_j, D)\, d^2n, \tag{4.2}$$

respectively. In the same way, the *mass density* of the mixture $\varrho(x_i, t)$ (i.e., of the polycrystal) is given by the chain of identities,

$$\varrho(x_i, t) = \int_{\mathcal{S}^2}\int_{\mathcal{I}} \varrho^{\triangleright}(x_i, t, n_j, D)\, dD d^2n = \int_{\mathcal{I}} \varrho^{\blacktriangleright}(x_i, t, D)\, dD = \int_{\mathcal{S}^2} \varrho^{*}(x_i, t, n_j)\, d^2n, \tag{4.3}$$

where dD and d^2n are the increments of length for the grain-size range $\mathcal{I}$ and of solid angle for the unit surface $\mathcal{S}^2$, respectively. The definitions of the size mass density, $\varrho^{\blacktriangleright}$, the orientation mass density, ϱ^{*}, and the orientation-and-size mass density, $\varrho^{\triangleright}$, as stated in (4.2) and (4.3) have very important meanings: the product

$$\varrho^{\blacktriangleright}(D)\, dD$$

[3]Each point represents a certain RVE and each RVE can have a certain maximum value for the grain size.

is that part of the mass density due to crystallites with dimensionless grain-sizes between D and $D + dD$, the product

$$\varrho^{*}\left(n_j\right) d^2n$$

is that part of the mass density due to crystallites with lattice orientations directed toward n_j within the solid angle d^2n and the product

$$\varrho^{\triangleright}\left(n_j, D\right) dD d^2n$$

is that part of the mass density due to crystallites with lattice orientations directed toward n_j within the solid angle d^2n and dimensionless grain-sizes between D and $D + dD$. It is for the definitions of $\varrho^{\blacktriangleright}$ and ϱ that the dimensionless grain-size variable D has been introduced in (4.1), for only with the use of D (instead of $\bar{D}$) do $\varrho^{\blacktriangleright}$ and ϱ have both the physical dimension of a mass density.

The analogy of $\varrho^{\blacktriangleright}$ and ϱ^{*} with the Crystal Size Distribution (CSD) $n^{\blacktriangleright}(D)$ (see, e.g., [3, 6, 35, 76, 97, 100, 113, 121, 122, 132, 133]) and the Orientation Distribution Function (ODF) $f^{*}\left(n_j\right)$ (see, e.g., [44, 45, 117]), respectively, is as follows. If N_{tot} is the total number of crystallites within the RVE, then

$$N_{tot} n^{\blacktriangleright}(D)\, dD =: N^{\blacktriangleright}(D)\, dD \tag{4.4}$$

is the number of crystallites with dimensionless grain-sizes between D and $D + dD$ and

$$N_{tot} f^{*}\left(n_j\right) d^2n =: F^{*}\left(n_j\right) d^2n \tag{4.5}$$

gives the number of crystallites with lattice orientations directed toward n_j within the solid angle d^2n. Consequently, whilst CSD and ODF give the distributions of grain sizes and orientations in terms of numbers of crystallites, $\varrho^{\blacktriangleright}$ and ϱ^{*} give it in terms of mass density. Moreover, it can be proved that, whereas a relation between CSD and $\varrho^{\blacktriangleright}$ can be established once the so-called true mass density [14] and the shape factor are given, f^{*} and ϱ^{*} are two different quantities with no mathematical relation connecting them. As we shall see, the advantage of our definitions (4.2) and (4.3) is the possibility to use the Theory of Mixtures with Continuous Diversity and to employ the generalized equation for the balance of mass as the evolution equation for such distributions. A more specific analysis of these mass densities will be treated in the next two subsections; it reveals other advantages of $\varrho^{\blacktriangleright}$ and ϱ^{*}, i.e., $\varrho^{\blacktriangleright}$ (and not $n^{\blacktriangleright}$) gives a definition of the mean grain-size that is independent of the sensitivity of the measuring instruments and ϱ^{*} describes the anisotropy of a sample of polycrystalline material better than f^{*}.

4.2.2 CSD and Size Mass Density

In this subsection, we prove a relation between CSD and size mass density in terms of the so-called true mass density, $\gamma^{\blacktriangleright}$, and of the shape factor, $\alpha^{\blacktriangleright}$. The concept of the true mass density is borrowed from those theories on the mechanics of porous materials where the volume fraction is taken into account, e.g., a porous material saturated with a fluid. This case is generally treated as a binary mixture of one solid and one fluid. If ν_s is the volume fraction of the solid part and ν_f is the volume fraction of the fluid part, we have,

$$\nu_s + \nu_f = 1. \tag{4.6}$$

If ξ_s is the mass fraction of the solid part and ξ_f is the mass fraction of the fluid part, we have,

$$\xi_s + \xi_f = 1. \tag{4.7}$$

On the other hand, if ϱ is the mass density of the mixture and ϱ_s and ϱ_f are the partial mass densities of the solid and of the fluid parts, respectively, then we have,

$$\varrho = \varrho_s + \varrho_f. \tag{4.8}$$

Let us assume that V and M are the volume and the mass of the RVE of the mixture. Then, we have,

$$\varrho = \frac{M}{V}. \tag{4.9}$$

Since V_s and V_f are the relative volumes of the solid and of the fluid parts inside the RVE, respectively, we have from (4.6),

$$\nu_s = \frac{V_s}{V}, \qquad \nu_f = \frac{V_f}{V}, \qquad V = V_s + V_f. \tag{4.10}$$

Analogously, if M_s and M_f are the masses of the solid and of the fluid, respectively, inside the RVE, we have,

$$\xi_s = \frac{M_s}{M}, \qquad \xi_f = \frac{M_f}{M}, \qquad M = M_s + M_f. \tag{4.11}$$

Thus, the interpretation of the quantities involved in (4.8) in terms of masses and volumes in the RVE, is as follows,

$$\varrho_s = \frac{M_s}{V}, \quad \varrho_f = \frac{M_f}{V}. \tag{4.12}$$

Therefore, ϱ_s and ϱ_f are the masses of the given components of the mixture per unit volume of the mixture. The mass of a given component of the mixture per unit volume of the same component is given by the so-called true mass density, i.e.,

$$\gamma_s = \frac{M_s}{V_s}, \quad \gamma_f = \frac{M_f}{V_f}. \tag{4.13}$$

In the Theory of Mixtures with Continuous Diversity, the number of components is no longer two or countably finite, it is non-countably infinite and the interpretation must be done with care. Let $V^{\blacktriangleright}(D)$ and $M^{\blacktriangleright}(D)$ be the dimensionless volume (i.e., the volume divided by $\bar{D}_M^3$) and the mass of the crystallites with the dimensionless grain-size equal to D, respectively. The true mass density is defined, in analogy to (4.13), as follows,

$$\gamma^{\blacktriangleright}(D) = \frac{M^{\blacktriangleright}(D)}{V^{\blacktriangleright}(D)\ \bar{D}_M^3}. \tag{4.14}$$

The concept of the shape factor, $\alpha^{\blacktriangleright}(D)$, is fundamental to obtain the relationship between the CSD and the size mass density. The shape factor gives the non-dimensional volume of a single crystallite with dimensionless grain-size equal to D. Such a dimensionless volume is,

$$\alpha^{\blacktriangleright}(D)\, D^3. \tag{4.15}$$

If the only crystallite with dimensionless grain-size D has the shape of a sphere and D is its dimensionless diameter (i.e., the diameter divided by $\bar{D}_M$), we have,

$$V^{\blacktriangleright}(D) = \tfrac{\pi}{6} D^3, \quad \alpha^{\blacktriangleright}(D) = \tfrac{\pi}{6}. \tag{4.16}$$

If the shape of the crystallite is a cube and D is the value the dimensionless side (i.e., the side divided by $\bar{D}_M$), then,

$$V^{\blacktriangleright}(D) = D^3, \quad \alpha^{\blacktriangleright}(D) = 1, \tag{4.17}$$

and if it is a parallelepiped with the fundamental dimensionless sides equal to D, D and $2D$, respectively, we have,

$$V^{\blacktriangleright}(D) = 2D^3, \quad \alpha^{\blacktriangleright}(D) = 2, \tag{4.18}$$

If there are ten crystallites with dimensionless grain-size D and their shape is a sphere with dimensionless diameter D, then the shape factor is the same as in (4.16) but the volume is ten times larger, i.e.,

$$V^{\blacktriangleright}(D) = 10\,\tfrac{\pi}{6} D^3, \quad \alpha^{\blacktriangleright}(D) = \tfrac{\pi}{6}. \tag{4.19}$$

To have a relationship between the shape factor $\alpha^{\blacktriangleright}(D)$ and the volume $V^{\blacktriangleright}(D)$ we need the information of the number of grains present in the polycrystal. In order to assure the continuity of the functions, the number of crystallites, in the Theory of Mixtures with Continuous Diversity, is assumed to be infinite. However, for the sake of simplicity and without loss of generality, we may fix this number and set it equal to N_{tot}. Thus, an integration of $N^{\blacktriangleright}(D)$, defined in equation (4.4), over the grain size yields

$$N_{tot} = \int_{\mathcal{I}} N^{\blacktriangleright}(D)\, dD. \tag{4.20}$$

As we have already pointed out, $N^{\blacktriangleright}(D)\, dD$ is the number of crystallites in the RVE with the nondimensional grain-sizes between D and $D + dD$. Therefore, the dimensionless volume of these crystallites, $V^{\blacktriangleright}(D)\, dD$, is the product of their number, $N^{\blacktriangleright}(D)\, dD$, and the volume of one of them. Thus, from (4.15), we have,

$$V^{\blacktriangleright}(D)\, dD = \alpha^{\blacktriangleright}(D)\, D^3 N^{\blacktriangleright}(D)\, dD. \tag{4.21}$$

From (4.14), the mass of the same crystallites is,

$$M^{\blacktriangleright}(D)\, dD = \gamma^{\blacktriangleright}(D)\, \alpha^{\blacktriangleright}(D)\, D^3\, \bar{D}_M^3 N^{\blacktriangleright}(D)\, dD, \tag{4.22}$$

whilst from (4.22) the mass and from (4.21) the dimensionless volume of the RVE are

$$M = \int_{\mathcal{I}} M^{\blacktriangleright}(D)\, dD = \int_{\mathcal{I}} \gamma^{\blacktriangleright}(D)\, \alpha^{\blacktriangleright}(D)\, D^3\, \bar{D}_M^3 N^{\blacktriangleright}(D)\, dD, \tag{4.23}$$

$$V = \int_{\mathcal{I}} V^{\blacktriangleright}(D)\, dD = \int_{\mathcal{I}} \alpha^{\blacktriangleright}(D)\, D^3 N^{\blacktriangleright}(D)\, dD. \tag{4.24}$$

The dimensionless volume, V, of the RVE is assumed to be much larger than the dimensionless volume of a given crystallite and much smaller than the dimensionless volume of the whole polycrystal. If we define another shape factor, $\tilde{\alpha}^{\blacktriangleright}(D)$, as follows,

$$\tilde{\alpha}^{\blacktriangleright}(D) = \frac{\alpha^{\blacktriangleright}(D)\ \bar{D}_M^3}{V}, \tag{4.25}$$

then using (4.9), (4.23), (4.24) and (4.25), the mass density of the RVE takes the form

$$\varrho = \frac{M}{V} = \int_{\mathcal{I}} \gamma^{\blacktriangleright}(D)\, \tilde{\alpha}^{\blacktriangleright}(D)\, D^3 n^{\blacktriangleright}(D)\, dD. \tag{4.26}$$

Comparing this with $(4.3)_3$, an explicit relation between the CSD and the size mass density is obtained, namely

$$\varrho^{\blacktriangleright} = N^{\blacktriangleright} \tilde{\alpha}^{\blacktriangleright} D^3 \gamma^{\blacktriangleright}. \tag{4.27}$$

For the purposes of this subsection, we will also assume that the true mass density does not vary within the RVE; then,

$$\gamma^{\blacktriangleright}(D) = \bar{\gamma}. \tag{4.28}$$

In principle, the choice of one of the two distributions ($N^{\blacktriangleright}$ or $\varrho^{\blacktriangleright}$) is arbitrary and their relationship is equation (4.27). However the mean grain-sizes computed with these two functions are different. We will call $\langle D \rangle_N$ and $\langle D \rangle_\varrho$, respectively, the mean grain-sizes computed by using $N^{\blacktriangleright}$ and $\varrho^{\blacktriangleright}$, i.e.,

$$\langle D \rangle_N = \int_{\mathcal{I}} D \frac{N^{\blacktriangleright}}{N_{tot}} dD, \qquad \langle D \rangle_\varrho = \int_{\mathcal{I}} D \frac{\varrho^{\blacktriangleright}}{\varrho} dD. \tag{4.29}$$

Our main aim here is to make clear that the evaluation of the mean grain-size $\langle D \rangle_N$ exhibits a very weak property; it strongly depends upon the sensitivity of the measuring instruments. Let us demonstrate this with a very simple example: It is shown in Fig. 4.1 and shows two polycrystals consisting of idealized spherical crystallites of two sizes. The first (A) is made of 2 crystallites, the second (B) is made of 11 crystallites. Their

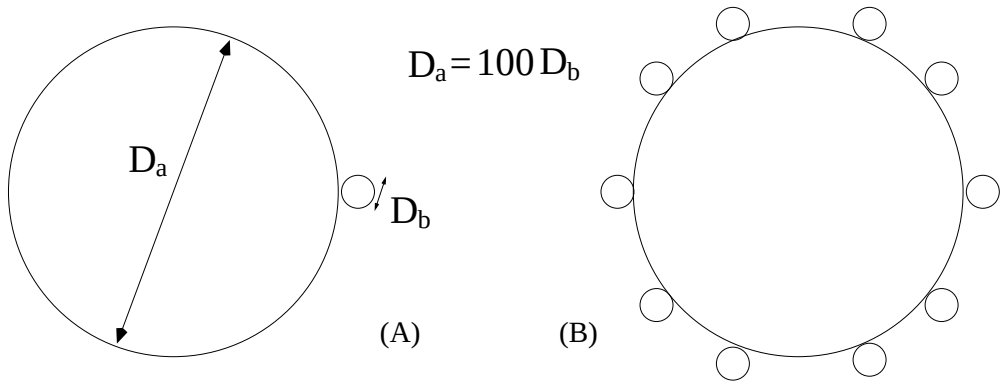

Figure 4.1: Schematic representation of two polycrystal: Two kinds of crystallites are present: those with the dimensionless grain-size $D = D_a$ and those with the dimensionless grain-size $D = D_b$. Relation (4.30) between D_a and D_b is also shown.

number is so chosen for simplicity and the grain-size range is composed by two points, i.e., $D = D_a$ and $D = D_b$, such that,

$$D_a = 100 D_b, \tag{4.30}$$

again for convenience. It follows that all integrations must[4] be transformed into sums, i.e.,

$$\int_{\mathcal{I}} \hat{g}\,(D)\, dD = \sum_{i=a,b} \hat{g}\,(D_i)\,. \tag{4.31}$$

Because of the sphericity of the individual crystals their shape factor $\alpha^{\blacktriangleright}(D)$ is constant and equal to $\pi/6$. If we set the quantities V and $\bar{D}_M$ also equal to 1, then $\tilde{\alpha}^{\blacktriangleright}(D) = \pi/6$ as well. Consequently, the CSD, the total number of grains, the size mass density, the mass density of the polycrystal and the two mean grain-sizes defined above can be subsumed in Table 4.1.

The derivation of the mean grain-sizes for sample (1) is

$$\langle D \rangle_{_N} = \frac{D_a + D_b}{2} \simeq \frac{D_a}{2}, \qquad \langle D \rangle_{_\varrho} = \frac{D_a^4 + D_b^4}{D_a^3 + D_b^3} \simeq D_a, \tag{4.32}$$

and for sample (2) is

$$\langle D \rangle_{_N} = \frac{D_a + 10 D_b}{11} = \frac{D_a}{10}, \qquad \langle D \rangle_{_\varrho} = \frac{D_a^4 + 10 D_b^4}{D_a^3 + 10 D_b^3} \simeq D_a. \tag{4.33}$$

We remark that eqs. (4.32) and (4.33) are deduced from (4.29-4.31) and Table 4.1. It follows from (4.32) and (4.33), that $\langle D \rangle_{_\varrho}$ in the two cases has nearly the same value, whilst for $\langle D \rangle_{_N}$ they differ substantially from one another. Heuristically, it is clear that we would assign to both cases similar grain sizes. So we are tempted to use $\langle D \rangle_{_\varrho}$ as the adequate definition of the mean grain-size. Objectively, this does not mean that one value is better than the other, in fact, the choice is only a question of conventionality. However, we wish

Table 4.1: Second and third columns list the values of the quantities represented in the first column relative to the sample (A) and (B) of Fig. 4.1.

	Sample (A)	Sample (B)
D_a, D_b	$D_a = 100 D_b$	$D_a = 100 D_b$
$N^{\triangleright}(D_a)$	1	1
$N^{\triangleright}(D_b)$	1	10
N_{tot}	2	11
$\langle D \rangle_{_N}$	$\frac{D_a}{2}$	$\frac{D_a}{11}$
$\varrho^{\triangleright}(D_a)$	$\frac{\pi}{6}\bar{\gamma} D_a^3$	$\frac{\pi}{6}\bar{\gamma} D_a^3$
$\varrho^{\triangleright}(D_b)$	$\frac{\pi}{6}\bar{\gamma} D_b^3$	$10\frac{\pi}{6}\bar{\gamma} D_b^3$
ϱ	$\frac{\pi}{6}\bar{\gamma}\,(D_a^3 + D_b^3)$	$\frac{\pi}{6}\bar{\gamma}\,(D_a^3 + 10 D_b^3)$
$\langle D \rangle_{_\varrho}$	D_a	D_a

[4] Alternatively, we could use the tool of the Dirac Delta function.

to point out a problem that becomes evident when we attempt to measure grain size by two different instruments. Assume that the small grains may be detectable by the first instrument but not by the second. Using the second instrument one would thus conclude

$$\langle D\rangle_{_N} = \langle D\rangle_{_\varrho} = D_a, \tag{4.34}$$

i.e., $\langle D\rangle_{_N}$ is equal to $\langle D\rangle_{_\varrho}$. On the other hand, $\langle D\rangle_{_N}$ would differ from $\langle D\rangle_{_\varrho}$ when the first measurement device were used. The conclusion is that the mean grain-size $\langle D\rangle_{_N}$ depends upon the sensitivity of the measuring instruments while this unpleasant property does not appear for the mean grain-size $\langle D\rangle_{_\varrho}$. In other words, the presence of tiny grains, detectable or not detectable by the microscope, has a great influence on the experimental value of $\langle D\rangle_{_N}$, whilst on the other hand, $\langle D\rangle_{_\varrho}$ is almost independent of them.

Therefore, the mean grain-size, $\langle D\rangle$, that we choose in this thesis is

$$\langle D\rangle \equiv \langle D\rangle_{_\varrho} = \int\limits_{\mathcal{I}} D\frac{\varrho^{\blacktriangleright}}{\varrho}dD. \tag{4.35}$$

Finally, from (4.27) we have a very important condition for the size mass density,

$$\varrho^{\blacktriangleright}(0) = 0. \tag{4.36}$$

This condition can not be obtained for the CSD.

4.2.3 ODF and Orientation Mass Density

Relation (4.27) was derived because the grain size of a crystallite has an implicit connection with its mass. A similar relation can not be derived between the ODF and the orientation mass density because the lattice orientation of a crystallite is not related to its mass. The ODF and orientation mass density are independent quantities and which one of the two distributions is chosen is arbitrary but non conventional. One can look at one single problem to judge advantages and shortcomings, and we represent such an example in Fig. 4.2. We make here clear that the ODF has a weak point which can be overcome by using the orientation mass density.

Generally, the mechanical response of polycrystalline materials is primarily related to the distribution of the lattice orientations of their crystallites (see, e.g., the third chapter of this thesis). An important characteristic is that an uniformly random distribution must correspond to isotropic behaviour. In the example of Fig. 4.2, we demonstrate that the ODF does not fulfil this property. The main point is that the ODF can not include the largeness of each crystallite in its form. On the other hand, the orientation mass density, somehow, contains this information. In Fig. 4.2a we show an academic sample of a polycrystal having the Schmidt diagram of the panel a of Fig. 3.1 and in which the crystallite oriented towards $\tilde{\theta} = \pi/2$ [5] is larger than the others. Therefore, the ODF is uniform and the mechanical behaviour of the polycrystal is anisotropic. However, an uniformly random distribution in terms of the ODF could not correspond to the isotropic behaviour. On the other hand, the orientation mass density, ϱ^*, of the same sample is nonuniform. Moreover, the distribution revealed by the orientation mass density is

[5] We use the same angle as in (3.15) and choose the two coordinate axes horizontally and vertically.

coherent with its mechanical behaviour and its use is more indicative of the mechanical description. Thus, all the results of the third chapter should be interpreted, in a more convenient way with the following substitution, i.e.,

$$f^* \qquad \longrightarrow \qquad \frac{\varrho^*}{\varrho}. \tag{4.37}$$

4.3 The Basic Variables

The basic variables x_i, t, n_j and D define position, time, orientation and dimensionless grain-size in the Eulerian description. As with other models, the idea of motion, and consequently the introduction of a Lagrangian description, is questionable for structured materials. On the other hand, some kinematic quantities must be defined in order to describe the evolution in time of position, orientation and dimensionless grain-size. We will do this by considering *velocity*, *orientation transition rate* and *size transition rate* as these kinematic rates, i.e.,

$$v_i^{\triangleright}\left(x_i, t, n_j, D\right), \qquad u_j^{\triangleright}\left(x_i, t, n_j, D\right), \qquad w^{\triangleright}\left(x_i, t, n_j, D\right), \tag{4.38}$$

respectively, and regard the quantities in (4.38) as fundamental. The interpretations of these fundamental quantities will be demonstrated later on. Here we remark that $v_i^{\triangleright}$ is the

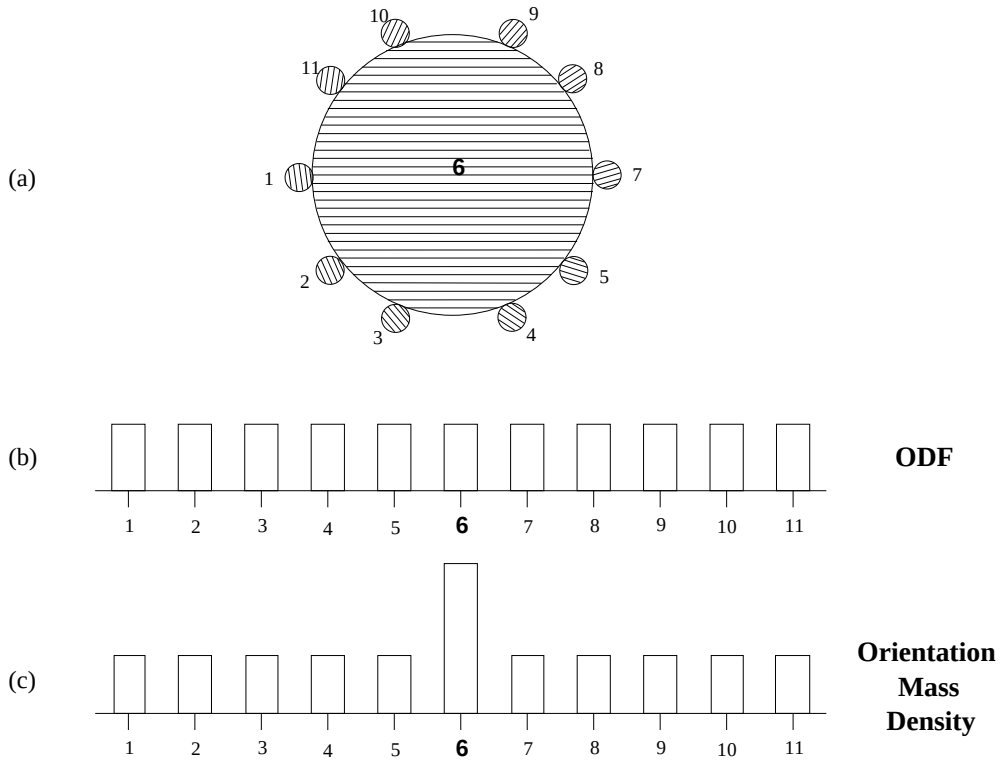

Figure 4.2: (a) Schematic representation of the same polycrystal as in Fig. 4.1b. Here, we add, inside every grain, thin lines representing the planes of easy glide. In ice they are parallel to the basal planes. Each crystal is denoted with a number and the grain with number 6 is larger than the other ones. Therefore, the mechanical behaviour of the sample is anisotropic. The lower panels show the histograms related to the ODF (b) and to the Orientation Mass Density (c).

classical velocity and represents the transition of mass from a given position x_i to a neighbouring position. Analogously, the orientation transition rate $u_j^{\triangleright}$ and the size transition rate $w^{\triangleright}$ represent, respectively, the transition of mass from a certain orientation n_j to a neighbouring orientation and from a certain dimensionless grain-size D to a neighbouring dimensionless grain-size.

As demonstrated by Faria [36], the normality condition,

$$n_i n_i = 1,$$

makes the orientation transition rate $u_j^{\triangleright}$ to lie on the unit sphere $\mathcal{S}^2$; consequently it is orthogonal to n_j, i.e.,

$$u_i^{\triangleright} n_i = 0. \tag{4.39}$$

Besides, the species assemblage suggests the following differential operators useful to be defined: for a general field $A^{\triangleright}(x_i, t, n_j, D)$, we adopt the definitions

$$A^{\triangleright}_{,i} \equiv \frac{\partial A^{\triangleright}}{\partial x_i}, \quad \partial_i A^{\triangleright} \equiv \frac{\partial A^{\triangleright}}{\partial n_i} - n_i n_j \frac{\partial A^{\triangleright}}{\partial n_j}, \quad \partial_D A^{\triangleright} \equiv \frac{\partial A^{\triangleright}}{\partial D}. \tag{4.40}$$

Of these relations, $(4.40)_1$ is the classical spatial gradient operator, $(4.40)_2$ is the orientational gradient operator[6] and $(4.40)_3$ is the size gradient operator of the general field $A^{\triangleright}(x_i, t, n_j, D)$, respectively.

In classical continuum theories partial and total time derivatives play important roles. Here, we must distinguish between five different time derivatives, defined for a general field $A^{\triangleright}(x_i, t, n_j, D)$,

$$\left.\begin{aligned}
&\partial_t A^{\triangleright} \equiv \frac{\partial A^{\triangleright}}{\partial t},\\
&\dot{A}^{\triangleright} \equiv \frac{\partial A^{\triangleright}}{\partial t} + \frac{\partial A^{\triangleright}}{\partial x_i} v_i^{\triangleright},\\
&\grave{A}^{\triangleright} \equiv \frac{\partial A^{\triangleright}}{\partial t} + A^{\triangleright}_{,i} v_i^{\triangleright} + (\partial_i A^{\triangleright})\, u_i^{\triangleright} = \dot{A}^{\triangleright} + (\partial_i A^{\triangleright})\, u_i^{\triangleright},\\
&\mathring{A}^{\triangleright} \equiv \frac{\partial A^{\triangleright}}{\partial t} + A^{\triangleright}_{,i} v_i^{\triangleright} + (\partial_D A^{\triangleright})\, w^{\triangleright} = \dot{A}^{\triangleright} + (\partial_D A^{\triangleright})\, w^{\triangleright},\\
&\acute{A}^{\triangleright} \equiv \frac{\partial A^{\triangleright}}{\partial t} + A^{\triangleright}_{,i} v_i^{\triangleright} + (\partial_i A^{\triangleright})\, u_i^{\triangleright} + (\partial_D A^{\triangleright})\, w^{\triangleright},\\
&\quad = \dot{A}^{\triangleright} + (\partial_i A^{\triangleright})\, u_i^{\triangleright} + (\partial_D A^{\triangleright})\, w^{\triangleright} = \grave{A}^{\triangleright} + (\partial_D A^{\triangleright})\, w^{\triangleright} = \mathring{A}^{\triangleright} + (\partial_i A^{\triangleright})\, u_i^{\triangleright}.
\end{aligned}\right\} \tag{4.41}$$

The first is the time derivative of $A^{\triangleright}$ keeping x_i, n_j and D fixed; in the second n_j and D are held constant; in the third D is kept unchanged; in the fourth n_j remains unchanged;

[6]The explicit form, stated in $(4.40)_2$, can be obtained from the gradient operator in spherical coordinates, setting the radius equal to 1 and transforming the result into Cartesian variable. Thus, since $n_i \partial_i = 0$, this operator is tangential to $\mathcal{S}^2$.

and in the fifth all basic variables can vary. In the literature [36, 37, 40], the nomenclature is set with a species assemblage without the grain-size range $\mathcal{I}$ and the first three definitions of (4.41) are called partial, total and co-transitional time derivatives, respectively. Although denotations should be assigned coherently with the literature, here we have the complication of an enlarged species assemblage and the co-transitional time derivative is a name more appropriate for the fifth definition in (4.41). Thus, we will call the five different time derivatives defined in (4.41), partial, total, co-transition-orientation, co-transition-size and co-transitional time derivatives[7], respectively. Keeping this in mind we can evaluate the co-transitional time derivative of the basic variables x_i, n_j and D and rewrite (4.38) as follows,

$$\acute{x}_i = v_i^{\triangleright}, \qquad \acute{n}_j = u_j^{\triangleright}, \qquad \acute{D} = w^{\triangleright}. \tag{4.42}$$

The first and the third equations in (4.42) are obvious, once one regards the basic variables x_i, t, n_j and D as independent (as they are); to verify $(4.42)_2$, it is sufficient to apply $(4.41)_5$ to n_j, take into account the orthogonality condition (4.39) and from (4.40) the following expression relative to the orientational gradient of orientation, i.e.,

$$\partial_i n_j = \frac{\partial n_j}{\partial n_i} - n_i n_h \frac{\partial n_j}{\partial n_h} = \delta_{ij} - n_i n_j. \tag{4.43}$$

The definitions of five time derivatives in (4.41) involve the fundamental quantities introduced in (4.38). The physical interpretation that we have given for these quantities is confirmed by eqn. (4.42). In chapter 6, we will build a constitutive theory for the problem that we are treating. In this regard, we remark that whereas velocity $v_i^{\triangleright}$ and orientation transition rate $u_j^{\triangleright}$ are connected from to the balance equations of linear and angular momentum, respectively, the size transition rate can not deduced from any balance equations. Therefore, $w^{\triangleright}$ will be assumed as a constitutive quantity.

The microstructural angular momentum (or simply spin) $\sigma_i^{\triangleright}$ is considered also as a fundamental quantity and the spin velocity $s_i^{\triangleright}$ is associated to it through the rotational inertia I of the crystallites. For reasons of simplicity, the shape of the crystallites is considered not important and the rotational inertia, usually represented by a tensor, is here just a material constant, i.e.,

$$I = const.$$

Thus $\sigma_i^{\triangleright}$ and its co-transitional time derivative are

$$\sigma_i^{\triangleright} = I s_i^{\triangleright}, \quad \acute{\sigma}_i^{\triangleright} = I \acute{s}_i^{\triangleright}, \tag{4.44}$$

respectively. It is evident that the spin velocity $s_i^{\triangleright}$ and the orientation transition rate $u_i^{\triangleright}$ are related. Faria [36] suggested that $u_i^{\triangleright}$ determines the part of $s_i^{\triangleright}$ that is orthogonal to n_j as follows,

$$s_j^{\triangleright} - n_j s_i^{\triangleright} n_i = \varepsilon_{jhk} n_h u_k^{\triangleright}; \tag{4.45}$$

furthermore, the rotation of the material, in which the crystallite is embedded, determines its parallel part, i.e.,

$$s_i^{\triangleright} n_i = n_i \omega_i^{\triangleright} = \tfrac{1}{2} n_i \varepsilon_{ihk} v_{k,h}^{\triangleright}, \tag{4.46}$$

[7]The symbols for co-transition-orientation and co-transitional time derivative look similar; however, they have different meanings as one can see in $(4.41)_3$ and $(4.41)_5$. Moreover, the co-transitional time derivative could also be called the orientation-and-size time derivative.

where $\omega_i^{\triangleright}$ is the usual rotation vector, i.e., the vector associated with the skew-symmetric part of the velocity gradient $W_{kh}^{\triangleright} \equiv v_{[k,h]}^{\triangleright}$, i.e.,

$$W_{kh}^{\triangleright} = \varepsilon_{ihk}\omega_i^{\triangleright}, \quad \omega_j^{\triangleright} = \tfrac{1}{2}\varepsilon_{jhk}W_{kh}^{\triangleright}. \tag{4.47}$$

If $S_{ik}^{\triangleright}$ is the skew-symmetric tensor associated with the spin velocity $s_j^{\triangleright}$,

$$S_{ik}^{\triangleright} = \varepsilon_{ijk}s_j^{\triangleright}, \quad s_j^{\triangleright} = \tfrac{1}{2}\varepsilon_{kjb}S_{kb}^{\triangleright}, \tag{4.48}$$

then, after multiplying equation (4.45) by $\varepsilon_{ijl}n_l$, the following two expressions emerge

$$\varepsilon_{ijl}n_l\left[s_j^{\triangleright} - n_j s_i^{\triangleright}n_i\right] = \varepsilon_{ijl}n_l s_j^{\triangleright} - \varepsilon_{ijl}n_l n_j s_i^{\triangleright}n_i = \varepsilon_{ijl}n_l s_j^{\triangleright} = S_{il}^{\triangleright}n_l, \tag{4.49}$$

$$\varepsilon_{ijl}n_l\varepsilon_{jhk}n_h u_k^{\triangleright} = \left(-\delta_{ih}\delta_{lk} + \delta_{lh}\delta_{ik}\right)n_l u_k^{\triangleright}n_h = -n_k u_k^{\triangleright}n_i + n_h u_i^{\triangleright}n_h = u_i^{\triangleright}, \tag{4.50}$$

that are equal. Moreover, from (4.43), (4.45), (4.49) and (4.50), we may show that

$$u_i^{\triangleright} = \varepsilon_{ijl}s_j^{\triangleright}n_l = S_{il}^{\triangleright}n_l, \quad \partial_i u_i^{\triangleright} = \left(\partial_i S_{ik}^{\triangleright}\right)n_k + S_{ik}^{\triangleright}\partial_i n_k = \left(\partial_i S_{ik}^{\triangleright}\right)n_k, \tag{4.51}$$

and from (4.45) and (4.48), we can find useful relations for the spin velocity $s_j^{\triangleright}$, i.e.,

$$\left.\begin{aligned} s_{j,i}^{\triangleright} = \tfrac{1}{2}\varepsilon_{kjb}S_{kb,i}^{\triangleright}, \quad \partial_i s_j^{\triangleright} = \tfrac{1}{2}\varepsilon_{kjb}\partial_i S_{kb}^{\triangleright}, \\ \varepsilon_{jis}n_s\partial_i s_j^{\triangleright} = \varepsilon_{jis}n_s\tfrac{1}{2}\varepsilon_{kjb}\partial_i S_{kb}^{\triangleright} = \tfrac{1}{2}\left(-\delta_{ik}\delta_{sb} + \delta_{sk}\delta_{ib}\right)n_s\partial_i S_{kb}^{\triangleright} \\ = -\tfrac{1}{2}n_b\partial_k S_{kb}^{\triangleright} + \tfrac{1}{2}n_k\partial_b S_{kb}^{\triangleright} = n_k\partial_b S_{kb}^{\triangleright}. \end{aligned}\right\} \tag{4.52}$$

With the definition of the relative spin velocity tensor

$$H_{ij}^{\triangleright} \equiv S_{ij}^{\triangleright} - W_{ij}^{\triangleright}, \tag{4.53}$$

the first of equations (4.51) and the two equations in the first line of (4.52) can be written as

$$u_i^{\triangleright} = \left(H_{ij}^{\triangleright} + W_{ij}^{\triangleright}\right)n_j, \quad s_{j,i}^{\triangleright} = \tfrac{1}{2}\varepsilon_{kjb}H_{kb,i}^{\triangleright} + \tfrac{1}{2}\varepsilon_{kjb}W_{kb,i}^{\triangleright}, \quad \partial_i s_j^{\triangleright} = \tfrac{1}{2}\varepsilon_{kjb}\partial_i H_{kb}^{\triangleright} + \tfrac{1}{2}\varepsilon_{kjb}\partial_i W_{kb}^{\triangleright}. \tag{4.54}$$

These relations will henceforth regularly be used.

4.4 Formulation of the Balance Equations

4.4.1 General Remarks

In order to characterize the range of phenomena for which the present theory can be used, together with the definition of the species assemblage, it is important to assign a set of balance and constitutive equations. For this reason it is convenient, at this level, to be general and to apply the theory to a particular case later. The balance equations in a Theory of Mixtures with Continuous Diversity are stated in Faria [36] for a general

Table 4.2: Definition of field quantities for the fundamental physical laws to be substituted in (4.55), in order to obtain the balance equations for the quantities marked in the first coloumn.

Density of the	Quantity	Flux	Orientation -flux	Size -flux	Production rate	External supply
	$\Psi^{\triangleright}$	$\Phi_j^{\triangleright}$	$\Upsilon_j^{\triangleright}$	$\Delta^{\triangleright}$	$\Xi^{\triangleright}$	$\Sigma^{\triangleright}$
Mass	$\varrho^{\triangleright}$	0	0	0	$\varrho^{\triangleright}\Gamma^{\triangleright}$	0
Linear Momentum	$\varrho^{\triangleright}v_i^{\triangleright}$	$-t_{ij}^{\triangleright}$	$-\tau_{ij}^{\triangleright}$	$-F_i^{\triangleright}$	$\varrho^{\triangleright}\kappa_i^{\triangleright}$	$\varrho^{\triangleright}g_i^{\triangleright}$
Total Angular Momentum	$\varrho^{\triangleright}L_i^{\triangleright}$	$-M_{ij}^{\triangleright}$	$-\Pi_{ij}^{\triangleright}$	$-A_i^{\triangleright}$	$\varrho^{\triangleright}N_i^{\triangleright}$	$\varrho^{\triangleright}K_i^{\triangleright}$
Total Energy	$\varrho^{\triangleright}E^{\triangleright}$	$Q_j^{\triangleright}$	$\Xi_j^{\triangleright}$	$H^{\triangleright}$	$\varrho^{\triangleright}P^{\triangleright}$	$\varrho^{\triangleright}R^{\triangleright}$
Entropy	$\varrho^{\triangleright}\eta^{\triangleright}$	$\phi_j^{\triangleright}$	$\varphi_j^{\triangleright}$	$n^{\triangleright}$	$\varrho^{\triangleright}\varsigma^{\triangleright}$	$\varrho^{\triangleright}s^{\triangleright}$
Dislocation	$\rho_d^{\triangleright}$	$q_{dj}^{\triangleright}$	$\gamma_{dj}^{\triangleright}$	$\Delta_d^{\triangleright}$	$\Pi^{\triangleright}$	0

species assemblage and for a general additive quantity. The specification for the species assemblage defined above is as follows

$$\partial_t \Psi^{\triangleright} + \left(\Psi^{\triangleright} v_j^{\triangleright} + \Phi_j^{\triangleright}\right)_{,j} + \partial_j \left(\Psi^{\triangleright} u_j^{\triangleright} + \Upsilon_j^{\triangleright}\right) + \partial_D \left(\Psi^{\triangleright} w^{\triangleright} + \Delta^{\triangleright}\right) = \Xi^{\triangleright} + \Sigma^{\triangleright}, \tag{4.55}$$

where $\Psi^{\triangleright}$ is the density, $\Phi_j^{\triangleright}$ is the non-convective flux density, $\Upsilon_j^{\triangleright}$ and $\Delta^{\triangleright}$ are the so-called interspecies flux densities in the spaces of orientations, $\mathcal{S}^2$, and grain-size range, $\mathcal{I}$, respectively, $\Xi^{\triangleright}$ is the density of production rate, and $\Sigma^{\triangleright}$ the density of external supply for that quantity.

The classical form for an equation of the type (4.55) can be achieved by setting to zero the two transition rates $u_j^{\triangleright}$ and $w^{\triangleright}$ and the two interspecies flux densities $\Upsilon_j^{\triangleright}$ and $\Delta^{\triangleright}$. The physical interpretation of the terms in (4.55) involving these four quantities are the analogue of the terms relating the usual three-dimensional space, but this time, they are related to the species assemblage: If $\Psi^{\triangleright} v_j^{\triangleright}$ and $\Phi_j^{\triangleright}$ account for convective and non convective flux in the classical three-dimensional space, respectively, then $\Psi^{\triangleright} u_j^{\triangleright}$ and $\Upsilon_j^{\triangleright}$ account for convective and non convective flux in the orientational space and $\Psi^{\triangleright} w^{\triangleright}$ and $\Delta^{\triangleright}$ account for convective a non convective flux in the grain-size range. The convective terms are always associated to a transfer of the additive quantity, for which the balance equation is formulated, due to a transfer of mass and they always incorporate a transition rate term, i.e., $v_i^{\triangleright}$, $u_j^{\triangleright}$ or $w^{\triangleright}$. On the other hand the non convective terms are, by definition, associated to a transfer of the same additive quantity but with no transfer of mass.

A suitable generalization of the cases presented in [36, 37, 40] allows us to make the substitutions stated in Table 4.2 to obtain balance equations of mass, momenta, energy, entropy and dislocation.

The nomenclature of the quantities in Table 4.2 is somewhat complicated. The main rule is that the words "specific" and "density" mean "per unit mass" and "per unit volume", respectively. Thus, $\varrho^{\triangleright}$ and $\rho_d^{\triangleright}$ are the densities of mass and dislocations, respectively; $v_i^{\triangleright}$, $L_i^{\triangleright}$, $E^{\triangleright}$ and $\eta^{\triangleright}$ are the specific linear momentum ($v_i^{\triangleright}$ is also called velocity), total angular momentum, total energy and entropy, respectively; $-t_{ij}^{\triangleright}$, $-M_{ij}^{\triangleright}$, $Q_j^{\triangleright}$, $\phi_j^{\triangleright}$ and $q_{dj}^{\triangleright}$ are the non convective flux densities of linear momentum ($t_{ij}^{\triangleright}$ is also called Cauchy stress tensor), total angular momentum ($M_{ij}^{\triangleright}$ is also called total couple stress), total energy ($Q_j^{\triangleright}$ is also called total heat flux density), entropy and dislocation, respectively; $-\tau_{ij}^{\triangleright}$,

$-\Pi^{\triangleright}_{ij}$, $\Xi^{\triangleright}_{j}$, $\varphi^{\triangleright}_{j}$ and $\gamma^{\triangleright}_{dj}$ are the orientation-flux densities of linear momentum ($\tau^{\triangleright}_{ij}$ is also called orientational stress), total angular momentum ($\Pi^{\triangleright}_{ij}$ is also called orientational total couple stress), total energy, entropy and dislocation, respectively; $-F^{\triangleright}_{i}$, $-A^{\triangleright}_{i}$, $H^{\triangleright}$, $n^{\triangleright}$ and $\Delta^{\triangleright}_{d}$ are the size-flux densities of linear momentum, total angular momentum, total energy, entropy and dislocation, respectively; $\Gamma^{\triangleright}$, $\kappa^{\triangleright}_{i}$, $N^{\triangleright}_{i}$, $P^{\triangleright}$ and $\varsigma^{\triangleright}$ are the specific production rates of mass, linear momentum ($\kappa^{\triangleright}_{i}$ is also called specific interaction force), total angular momentum ($N^{\triangleright}_{i}$ is also called specific total interaction couple), total energy and entropy, respectively; $\Pi^{\triangleright}$ is the density of the production rate of dislocation; $g^{\triangleright}_{i}$, $K^{\triangleright}_{i}$, $R^{\triangleright}$ and $s^{\triangleright}$ are the specific external supplies of linear momentum ($g^{\triangleright}_{i}$ is also called specific external force), total angular momentum ($K^{\triangleright}_{i}$ is also called specific total external couple), total energy and entropy, respectively.

Faria and Hutter [37] noted that the quantities involved in the balances of angular momentum and energy can be additively decomposed as follows:

$$\left.\begin{array}{ll} L^{\triangleright}_{i} = \sigma^{\triangleright}_{i} + \varepsilon_{ijk}x_j\upsilon^{\triangleright}_{k}, & E^{\triangleright} = e^{\triangleright} + \frac{1}{2}\upsilon^{\triangleright}_{i}\upsilon^{\triangleright}_{i} + \frac{1}{2}\sigma^{\triangleright}_{i}s^{\triangleright}_{i}, \\ M^{\triangleright}_{ij} = m^{\triangleright}_{ij} + \varepsilon_{ihk}x_h t^{\triangleright}_{kj}, & Q^{\triangleright}_{i} = q^{\triangleright}_{i} - t^{\triangleright}_{ji}\upsilon^{\triangleright}_{j} - m^{\triangleright}_{ji}s^{\triangleright}_{j}, \\ \Pi^{\triangleright}_{ij} = \varpi^{\triangleright}_{ij} + \varepsilon_{ihk}x_h\tau^{\triangleright}_{kj}, & \Xi^{\triangleright}_{i} = \xi^{\triangleright}_{i} - \tau^{\triangleright}_{ji}\upsilon^{\triangleright}_{j} - \varpi^{\triangleright}_{ji}s^{\triangleright}_{j}, \\ A^{\triangleright}_{i} = a^{\triangleright}_{i} + \varepsilon_{ijk}x_j F^{\triangleright}_{k}, & H^{\triangleright} = h^{\triangleright} - F^{\triangleright}_{j}\upsilon^{\triangleright}_{j} - a^{\triangleright}_{j}s^{\triangleright}_{j}, \\ N^{\triangleright}_{i} = \nu^{\triangleright}_{i} + \varepsilon_{ijk}x_j\kappa^{\triangleright}_{k}, & P^{\triangleright} = \epsilon^{\triangleright} + \kappa^{\triangleright}_{i}\upsilon^{\triangleright}_{i} + \nu^{\triangleright}_{i}s^{\triangleright}_{i}, \\ K^{\triangleright}_{i} = c^{\triangleright}_{i} + \varepsilon_{ijk}x_j g^{\triangleright}_{k}, & R^{\triangleright} = r^{\triangleright} + g^{\triangleright}_{i}\upsilon^{\triangleright}_{i} + c^{\triangleright}_{i}s^{\triangleright}_{i}. \end{array}\right\} \tag{4.56}$$

Here $\sigma^{\triangleright}_{i}$ is the specific spin and $e^{\triangleright}$ is the specific internal energy; $-m^{\triangleright}_{ij}$ and $q^{\triangleright}_{i}$ are the non-convective flux densities of angular momentum ($m^{\triangleright}_{ij}$ is also called the Voigt couple stress) and heat; $-\varpi^{\triangleright}_{ij}$ and $\xi^{\triangleright}_{i}$ are the orientation-flux densities of angular momentum ($\varpi^{\triangleright}_{ij}$ is also called the orientational couple stress) and heat, respectively; $-a^{\triangleright}_{i}$ and $h^{\triangleright}$ are the size-flux densities of angular momentum and heat, respectively; $\nu^{\triangleright}_{i}$ and $\epsilon^{\triangleright}$ are the specific production rates of angular momentum ($\nu^{\triangleright}_{i}$ is also called the specific interaction couple) and internal energy, respectively; $c^{\triangleright}_{i}$ and $r^{\triangleright}$ are the specific external supplies of angular momentum ($c^{\triangleright}_{i}$ is also called the specific external couple) and internal energy, respectively.

In the next subsection, we will analyse the balance of dislocation in detail and prove, from [40], that the non-convective flux of dislocation can be neglected for large scale polycrystalline materials.

4.4.2 The Non-convective Flux of Dislocation

The word "dislocation" is intended to refer to the length of linear defects, of every kind, present in the polycrystal. Thus, the dislocation density $\rho^{\triangleright}_{d}$ is consequently that length per unit volume and its unit of measure is the inverse of a surface: $[\rho^{\triangleright}_{d}] = \frac{1}{m^2}$. In Table 4.2, the assumption is stated that no external supply for dislocation can occur. On the other hand, a production rate term is present, for which a constitutive assumption must be given. An example of constitutive assumption for the density of production rate of dislocation (i.e., for $\Pi^{\triangleright}$) is given on the right-hand side of equation $(2.47)_2$. In this subsection we will prove

that the non-convective flux of dislocation, $q^{\triangleright}_{d\,j}$, can be neglected for a *huge* polycrystalline material[8].

The non-convective flux of a certain quantity is different from zero only if the quantity under question is removed from a given RVE to the neighbouring one without any transfer of mass. This removal, for momenta, energy and entropy, is allowed. In the case of mass it is, by definition, forbidden. For dislocation we need to give more details. A single dislocation can move inside a crystallite, but only until it reaches the grain boundary. Therefore, the transfer of dislocations, without any transfer of mass, is allowed only if it occurs inside a single grain but it is forbidden from a crystallite to another crystallite. Thus, a non-convective flux of dislocation can occur only if the crystallite in which the dislocation is assumed to move is present in two neighbouring Representative Volume Elements. Now, if the polycrystal represented by the RVE is big enough, then the possibility that a crystallite belongs to two Representative Volume Elements is low: The reason is

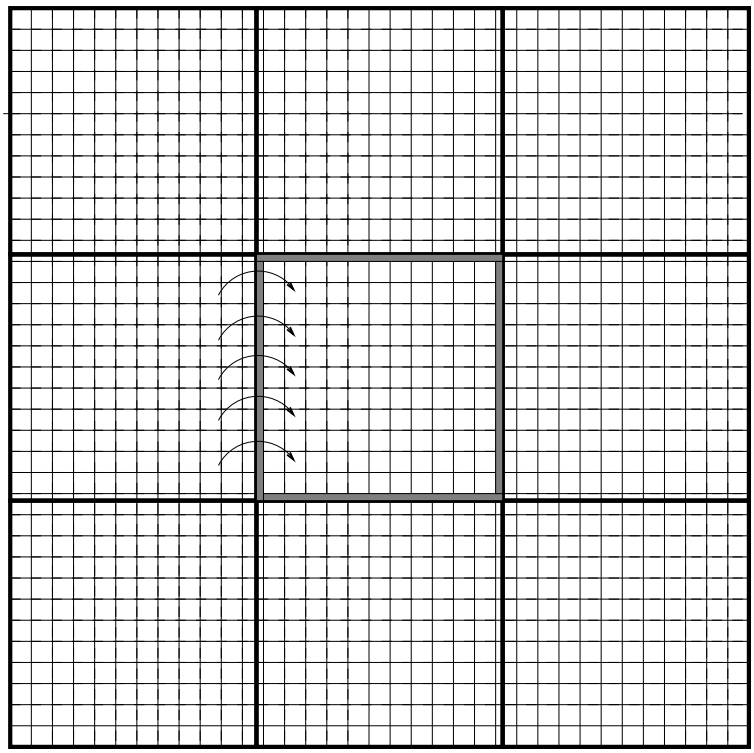

Figure 4.3: Schematic representation of a two-dimensional polycrystal. Thick lines divide the region into 9 parts. Each part represents a given position x_j and is composed by a certain RVE. Thus, only 9 Representative Volume Elements are drawn. Thin lines represent the boundaries between crystallites. If a given additive quantity shifts from one RVE to the neighbouring RVE, then the non-convective flux of this quantity is non zero and is represented by the curved arrows. The shadowed region marks the part of the central RVE composed of those crystallites that belong, contemporarily, to neighbouring Representative Volume Elements. If the size of the crystallites is fixed, then the larger the RVE, the smaller will be the contribution of the shadowed region.

[8]By *huge* is meant that a typed RVE contains a huge number of crystallites, practically infinite.

explained in Fig. 4.3, where we explain that the larger the polycrystal represented by a single RVE is, the smaller will be the possibility that one crystallite belongs to two different Representative Volume Elements.

Therefore, in the case of a huge polycrystalline material, we have made clear that the non-convective flux of dislocation can be neglected.

4.4.3 The Non-convective Interspecies Fluxes

The interspecies flux densities $\Upsilon_j^{\triangleright}$ and $\Delta^{\triangleright}$ have been introduced above rather formally and must be specified and physically interpreted. We have remarked that the non-convective terms represent the transfer of a given additive quantity without any transfer of mass. This transfer, for the interspecies flux densities, is intended to occur in the species assemblage. Generally a flux is associated with the surface through which the transfer of the additive quantity is performed. For this reason, some authors denote these fluxes as *surface* interactions. The *volume* interactions are, on the other hand, associated with all the other kinds of interactions due, e.g., to gravitational or electrostatic forces.

The theorem of Cauchy states that any flux density, acting on a given surface, must be linearly dependent with the normal vector of the respective surface. In the usual three-dimensional space, the normals to these surfaces can be denoted by N_j and are represented in Fig. 4.4a. Therefore, if the additive quantity is the linear momentum, the angular momentum, the energy or the entropy, the quantity associated with their fluxes are

$$t_{ij}^{\triangleright} N_j, \qquad m_{ij}^{\triangleright} N_j, \qquad q_j^{\triangleright} N_j, \qquad \phi_j^{\triangleright} N_j, \tag{4.57}$$

respectively.

The surfaces in the species assemblage are better called hypersurfaces: hypersurfaces in the orientational space $\mathcal{S}^2$ (see, e.g., Fig. 4.4b), are simply lines on the unit sphere, and hypersurfaces in the grain-size range $\mathcal{I}$, are in fact only points in that interval. $\Upsilon_j^{\triangleright}$ is intended to denote a flux for the first kind of hypersurfaces and pertains to interactions

Figure 4.4: (a) Contact interaction in the usual three-dimensional space acting on the usual surface in $\mathbb{R}^3$. A general body is drawn together with a frame of reference. A surface in that body has the normal denoted by $\mathbf{N}$. Each point of this body, in the Theory of Mixture with Continuous Diversity, is associated with a RVE. (b) Contact interactions in the orientational space are acting on hypersurfaces in $\mathcal{S}^2$, i.e., on curves that lie on the unit sphere $\mathcal{S}^2$. The normal of this hypersurface is denoted by $\mathbf{T}$. Two close lattice orientations, $\mathbf{n}^+$ and $\mathbf{n}^-$, are also shown. The hypersurface divides such two lattice orientations. These two lattice orientations are the representative of the same lattice orientations shown in Fig. 4.5b.

between parts of polycrystal with very close lattice orientations and $\Delta^{\triangleright}$ denotes a flux for the second kind of hypersurfaces and pertains to the interactions between crystallites with very close dimensionless grain-sizes, respectively. In the orientational space, $\mathcal{S}^2$, the hypersurfaces are lines on $\mathcal{S}^2$, of which the normal, in Fig. 4.4b, is denoted by T_j. The application of the Theorem of Cauchy yields that the additive quantity associated with the fluxes of linear momentum, angular momentum, energy, entropy and dislocation are equal to

$$\tau_{ij}^{\triangleright}T_j, \qquad \varpi_{ij}^{\triangleright}T_j, \qquad \xi_j^{\triangleright}T_j, \qquad \varphi_j^{\triangleright}T_j, \qquad \gamma_{dj}^{\triangleright}T_j, \tag{4.58}$$

respectively. The size-fluxes do not (yet) have physical interpretations. Therefore, they will eventually be neglected. On the other hand, the physical interpretation of the orientation-fluxes can be associated with the occurrence of the bending of crystallites (or with their polygonization) and will be analyzed in the next subsection

4.4.4 On the Inclusion of Polygonization

One situation in which two parts of a polycrystal with very close lattice orientations can interact occurs, for example, when one crystallite is subjected to bending. Bending is produced by couples acting on the grain. When a grain, see e.g. Fig. 4.5a, is slightly bent, one may imagine that the crystallite is characterized by "two lattice orientations very close to each other", say n_i^+ and n_i^-, and its average orientation n_i may be given by their mean. These three unit vectors form the plane of bending (in Fig. 4.5, this plane is simply the plane of the figure). If the crystallite suffers further bending, then the "two close lattice orientations" n_i^+ and n_i^- will rotate in different directions or at least with different transition rates, i.e., $u_i^{\triangleright}\left(n_j^+\right) \neq u_i^{\triangleright}\left(n_j^-\right)$; this implies that $u_i^{\triangleright}$ should not be a constant function of n_j; in fact the bending is likely proportional to the variation of the transition rate $u_i^{\triangleright}$ with orientation n_j[9]. Obviously, in this simple situation we know that the vector denoting the bending moment must be orthogonal to the bending plane. So, if we denote the intensity of this bending moment by $\Omega^{\triangleright}$ and introduce a unit vector T_j,

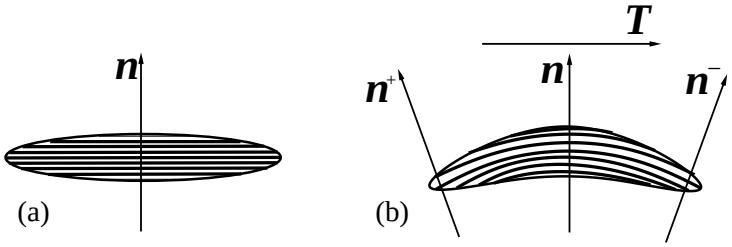

Figure 4.5: (a) Single crystal with its basal planes all parallel to one another and with its c-axis given by the unit vector n_i. (b) The crystal is then subjected to a bending moment $M_i^{\triangleright}$ orthogonal to the plane of the picture and the bent crystal is represented by the "two close orientations" n_i^+ and n_i^- orthogonal to the end cross sections of the bent crystal. For further bending, the orientation-transition rates of the "two close orientations" n_i^+ and n_i^- have to be different: $u_i^{\triangleright}\left(n_j^+\right) \neq u_i^{\triangleright}\left(n_j^-\right)$. Furthermore, T_i is a unit vector orthogonal to n_i and parallel to the difference $n_i^- - n_i^+$ that lies in the bending plane.

[9] At the end of this subsection we will give a further comment on this topic.

orthogonal to n_i and lying in the bending plane, then the bending moment required to bend (and eventually polygonize) the crystallite is given by

$$M_i^{\triangleright} = \Omega^{\triangleright} \varepsilon_{ijk} n_k T_j. \tag{4.59}$$

Note that the unit vector T_j agrees with that of equation (4.58). Eqn. (4.59) shows that $M_i^{\triangleright}$ is an example of orientational flux density of angular momentum. Now, reverting to densities instead of a single crystal, we replace $\Omega^{\triangleright}$ by $p^{\triangleright}$ and $M_i^{\triangleright}$ by $\varpi_{ij}^{\triangleright} T_j^{\triangleright}$ (see $(4.58)_2$). This then yields

$$\varpi_{ij}^{\triangleright} = p^{\triangleright} \varepsilon_{ijk} n_k. \tag{4.60}$$

Thus, a clear physical interpretation of $\varpi_{ij}^{\triangleright}$ has been found; it represents the bending moment associated with polygonization. Needless to say that a constitutive theory for polycrystalline materials should be consistent with (4.60), i.e., yield a representation for $\varpi_{ij}^{\triangleright}$ which conforms with the right-hand side of (4.60). This will be demonstrated later on.

At last, we remark that the flux of lattice orientations across the above mentioned hyper-surface in $\mathcal{S}^2$ with normal vector $T_j^{\triangleright}$ is described by the scalar product $u_j^{\triangleright} T_j^{\triangleright}$. When this product has the same value for all orientations, then only a rigid lattice rotation is occurring along the hypersurface; on the other hand, when this scalar product varies with n_i, bending of crystallites might be taking place. Therefore, the orientational divergence of $u_i^{\triangleright}$, i.e., $\partial_i u_i^{\triangleright}$, cannot vanish during polygonization (see [39]).

4.4.5 Elucidation of the Balance Equations

If we insert (4.56) in the entries of Table 4.2 and perform the substitutions in (4.55), we arrive at the following new set of balance equations:

$$\frac{\partial \varrho^{\triangleright}}{\partial t} + \left(\varrho^{\triangleright} v_j^{\triangleright}\right)_{,j} + \partial_j \left(\varrho^{\triangleright} u_j^{\triangleright}\right) + \partial_D \left(\varrho^{\triangleright} w^{\triangleright}\right) = \varrho^{\triangleright} \Gamma^{\triangleright}, \tag{4.61}$$

$$\varrho^{\triangleright} \acute{v}_i^{\triangleright} - t_{ij,j}^{\triangleright} - \partial_j \tau_{ij}^{\triangleright} - \partial_D F_i^{\triangleright} = \varrho^{\triangleright} \left(\kappa_i^{\triangleright} - \Gamma^{\triangleright} v_i^{\triangleright}\right) + \varrho^{\triangleright} g_i^{\triangleright}, \tag{4.62}$$

$$\varrho^{\triangleright} \acute{\sigma}_i^{\triangleright} - m_{ij,j}^{\triangleright} - \partial_j \varpi_{ij}^{\triangleright} - \partial_D a_i^{\triangleright} = \varepsilon_{ijk} t_{kj}^{\triangleright} + \varrho^{\triangleright} c_i^{\triangleright} + \varrho^{\triangleright} \left(\nu_i^{\triangleright} - \Gamma^{\triangleright} \sigma_i^{\triangleright}\right), \tag{4.63}$$

$$\begin{aligned} &\varrho^{\triangleright} \acute{e}^{\triangleright} + q_{i,i}^{\triangleright} + \partial_i \xi_i^{\triangleright} + \partial_D h^{\triangleright} + t_{kj}^{\triangleright} \left(H_{kj}^{\triangleright} - D_{kj}^{\triangleright}\right) - \tau_{ji}^{\triangleright} \partial_j v_j^{\triangleright} - F_j^{\triangleright} \partial_D v_j^{\triangleright} - m_{ji}^{\triangleright} s_{j,i}^{\triangleright} \\ &- \varpi_{ji}^{\triangleright} \partial_i s_j^{\triangleright} - a_j^{\triangleright} \partial_D s_j^{\triangleright} = \varrho^{\triangleright} \left(\epsilon^{\triangleright} - e^{\triangleright} \Gamma^{\triangleright}\right) + \varrho^{\triangleright} r^{\triangleright} + \varrho^{\triangleright} \Gamma^{\triangleright} \left(\frac{v_i^{\triangleright} v_i^{\triangleright}}{2} + \frac{\sigma_i^{\triangleright} s_i^{\triangleright}}{2}\right), \end{aligned} \tag{4.64}$$

$$\varrho^{\triangleright} \acute{\eta}^{\triangleright} + \phi_{j,j}^{\triangleright} + \partial_j \varphi_j^{\triangleright} + \partial_D n^{\triangleright} = \varrho^{\triangleright} \left(\varsigma^{\triangleright} - \Gamma^{\triangleright} \eta^{\triangleright}\right) + \varrho^{\triangleright} s^{\triangleright}, \tag{4.65}$$

$$\frac{\partial \rho_d^{\triangleright}}{\partial t} + \left(\rho_d^{\triangleright} v_j^{\triangleright}\right)_{,j} + \partial_j \left(\rho_d^{\triangleright} u_j^{\triangleright}\right) + \partial_D \left(\rho_d^{\triangleright} w^{\triangleright}\right) + \partial_j \gamma_{dj}^{\triangleright} + \partial_D \Delta_d^{\triangleright} = \Pi^{\triangleright}. \tag{4.66}$$

The calculations to obtain these are explicitly done in subsection, 4.4.6.

Finally, we also note, in analogy with (4.39), and as already pointed out by Faria et al. [36, 37], that the densities of orientation fluxes (say $\Upsilon_j^{\triangleright}$) satisfy the following constraint properties,

$$\tau_{ij}^{\triangleright} n_j = \varpi_{ij}^{\triangleright} n_j = \xi_i^{\triangleright} n_j = \varphi_j^{\triangleright} n_j = \gamma_{dj}^{\triangleright} n_j = 0. \tag{4.67}$$

This completes the presentation of the balance laws.

4.4.6 Derivation of the Balance Equations

Insertion of (4.56) in Table 4.2 and substitution of the resulting entries into (4.55) yields the balance equations in the form (4.61-4.66). In this section we want to demonstrate this passage.

The balances of mass (4.61), entropy (4.65) and dislocation (4.66) are left unchanged. The balance of linear momentum (4.62) is transformed by substituting the balance of mass (4.61). The balances of angular momentum (4.63) and energy (4.64) have the complication of the insertion of (4.56). Thus, we will analyse these two cases in detail. Inserting (4.61) and then introducing the co-transitional time derivative $(4.41)_5$ leads to the balance of angular momentum in the form

$$\varrho^{\triangleright}\acute{L}_i^{\triangleright} - M_{ij,j}^{\triangleright} - \partial_j\Pi_{ij}^{\triangleright} - \partial_{\scriptscriptstyle D}A_i^{\triangleright} = \varrho^{\triangleright}\left(N_i^{\triangleright} - \Gamma^{\triangleright}\sigma_i^{\triangleright}\right) + \varrho^{\triangleright}K_i^{\triangleright}. \tag{4.68}$$

Now, we insert the definitions on the left-hand side of (4.56) and take (4.62) into account. This will lead to the balance of angular momentum in the form stated in (4.63).

In much the same way, we may insert (4.61) and the definition of the co-transitional time derivative $(4.41)_5$ into (4.64) and then obtain the following formula for the balance of energy:

$$\varrho^{\triangleright}\acute{E}^{\triangleright} + Q_{j,j}^{\triangleright} + \partial_j\Xi_j^{\triangleright} + \partial_{\scriptscriptstyle D}H^{\triangleright} = \varrho^{\triangleright}\left(P^{\triangleright} - \Gamma^{\triangleright}E^{\triangleright}\right) + \varrho^{\triangleright}R^{\triangleright}. \tag{4.69}$$

The quantities on the right-hand side of (4.56) contain three terms and are all involved in (4.69). Thus, we can rewrite formula (4.69) by regrouping it as three different contributions: the first, the second and the third of these three contributions trace back to the first, the second and the third of these three terms. Therefore, equation (4.69) is transformed in the following statement

$$\begin{aligned}
&\varrho^{\triangleright}\acute{e}^{\triangleright} + q_{j,j}^{\triangleright} + \partial_j\xi_j^{\triangleright} + \partial_{\scriptscriptstyle D}h^{\triangleright} - \varrho^{\triangleright}\left(\epsilon^{\triangleright} - \Gamma^{\triangleright}e^{\triangleright}\right) - \varrho^{\triangleright}r^{\triangleright} \\
&+\varrho^{\triangleright}v_i^{\triangleright}\acute{v}_i^{\triangleright} - \left(t_{ji}^{\triangleright}v_j^{\triangleright}\right)_{,i} - \partial_i\left(v_j^{\triangleright}\tau_{ji}^{\triangleright}\right) - \partial_{\scriptscriptstyle D}\left(v_j^{\triangleright}F_j^{\triangleright}\right) - \varrho^{\triangleright}\left(\kappa_i^{\triangleright}v_i^{\triangleright} - \frac{1}{2}\Gamma^{\triangleright}v_i^{\triangleright}v_i^{\triangleright}\right) - \varrho^{\triangleright}g_i^{\triangleright}v_i^{\triangleright} \\
&\varrho^{\triangleright}s_i^{\triangleright}\acute{\sigma}_i^{\triangleright} - \left(m_{ji}^{\triangleright}s_j^{\triangleright}\right)_{,i} - \partial_i\left(s_j^{\triangleright}\varpi_{ji}^{\triangleright}\right) - \partial_{\scriptscriptstyle D}\left(s_j^{\triangleright}a_j^{\triangleright}\right) - \varrho^{\triangleright}\left(\nu_i^{\triangleright}s_i^{\triangleright} - \frac{1}{2}\Gamma^{\triangleright}\sigma_i^{\triangleright}s_i^{\triangleright}\right) - \varrho^{\triangleright}c_i^{\triangleright}s_i^{\triangleright} = 0.
\end{aligned} \tag{4.70}$$

Now, insertion of (4.62) into the second line of (4.70) and of (4.63) into the third line, generates the result

$$\begin{aligned}
&\varrho^{\triangleright}\acute{e}^{\triangleright} + q_{j,j}^{\triangleright} + \partial_j\xi_j^{\triangleright} + \partial_{\scriptscriptstyle D}h^{\triangleright} - \varrho^{\triangleright}\left(\epsilon^{\triangleright} - \Gamma^{\triangleright}e^{\triangleright}\right) - \varrho^{\triangleright}r^{\triangleright} \\
&- \tfrac{1}{2}\varrho^{\triangleright}\Gamma^{\triangleright}v_i^{\triangleright}v_i^{\triangleright} - t_{ji}^{\triangleright}v_{j,i}^{\triangleright} - \tau_{ji}^{\triangleright}\partial_i V_j^{\triangleright} - F_j^{\triangleright}\partial_{\scriptscriptstyle D}v_j^{\triangleright} \\
&+ s_j^{\triangleright}\varepsilon_{jik}t_{ki}^{\triangleright} - \tfrac{1}{2}\varrho^{\triangleright}\Gamma^{\triangleright}\sigma_j^{\triangleright}s_j^{\triangleright} - m_{ji}^{\triangleright}s_{j,i}^{\triangleright} - \varpi_{ji}^{\triangleright}\partial_i s_j^{\triangleright} - a_j^{\triangleright}\partial_{\scriptscriptstyle D}s_j^{\triangleright} = 0.
\end{aligned} \tag{4.71}$$

Finally, substituting (4.48), decomposing the gradient of the velocity, $L_{ij}^{\triangleright}$, into the symmetric, $D_{ij}^{\triangleright}$, and skew-symmetric, $W_{ij}^{\triangleright}$, parts,

$$L_{ij}^{\triangleright} = D_{ij}^{\triangleright} + W_{ij}^{\triangleright}, \tag{4.72}$$

and introducing the definition (4.53) of the relative spin tensor, $H_{ij}^{\triangleright}$, yields the balance equation of energy in the form (4.64).

4.5 Jump Conditions

Classically, the derivation of jump conditions is clear; here jumps can in principle occur also within $\mathcal{S}^2$ and $\mathcal{I}$. However, for the sake of simplicity we will neglect jumps in the species assemblage and consider only surfaces without intrinsic properties. Whereas e_i^W and v_i^W are the unit normal and the velocity field vectors of the surface where the jumps occur, using Faria and Hutter [37] we can easily derive the equations

$$\left.\begin{aligned}
[[\mathbb{U}^{\triangleright}]] = [[\varrho^{\triangleright}\,(v_i^{\triangleright} - v_i^W)]]\, e_i^W = 0,\\
[[\mathbb{U}^{\triangleright} v_i^{\triangleright}]] - \left[\left[t_{ij}^{\triangleright}\right]\right] e_j^W = 0,\\
[[\mathbb{U}^{\triangleright}\,(\varepsilon_{ijk} x_j v_k^{\triangleright} + \sigma_i^{\triangleright})]] - \left[\left[\varepsilon_{ihk} x_h t_{kj}^{\triangleright} + m_{ij}^{\triangleright}\right]\right] e_j^W = 0,\\
\left[\left[\mathbb{U}^{\triangleright}\left(e^{\triangleright} + \tfrac{1}{2} v_i^{\triangleright} v_i^{\triangleright} + \tfrac{1}{2}\sigma_i^{\triangleright} s_i^{\triangleright}\right)\right]\right] + \left[\left[q_i^{\triangleright} - t_{ji}^{\triangleright} v_j^{\triangleright} - m_{ji}^{\triangleright} s_j^{\triangleright}\right]\right] e_i^W = 0,\\
[[\mathbb{U}^{\triangleright}\eta^{\triangleright}]] + [[\phi_i^{\triangleright}]]\, e_i^W = 0,\\
[[\rho_d^{\triangleright}\,(v_i^{\triangleright} - v_i^W)]]\, e_i^W = 0,
\end{aligned}\right\} \tag{4.73}$$

in which $[[f]] \equiv f^+ - f^-$, where, for a general function f, evaluation on the surface where the jump occurs yields f^+ on the side into which the normal e_j^W points, and f^- on the other side.

If we deal with impermeable surfaces ($v_j^{\triangleright} e_j^W = v_j^W e_j^W$) and if the tangential component of the velocity vanishes on both sides of the wall ($v_i^{\triangleright} - v_j^{\triangleright} e_j^W e_i^W = 0$), then (4.73) can be simplified as follows:

$$\left[\left[t_{ij}^{\triangleright}\right]\right] e_j^W = 0, \quad \left[\left[m_{ij}^{\triangleright}\right]\right] e_j^W = 0, \quad [[q_i^{\triangleright}]]\, e_i^W - \left[\left[m_{ji}^{\triangleright} s_j^{\triangleright}\right]\right] e_i^W = 0, \quad [[\phi_i^{\triangleright}]]\, e_i^W = 0. \tag{4.74}$$

These define flux continuity conditions across the surface where the jump occurs.

4.6 Rules of Homogenization

The next step is to connect the microscopic fields with their macroscopic counterparts. This process will define rules of homogenization. The micro-quantities are the fields that depend on the variables belonging to the species assemblage (and are denoted by "$\triangleright$", "$*$" or "$\blacktriangleright$")[10]. On the other hand, the macro-quantities are the usual quantities in the classical continuum theory, and the balance equations for them have to be postulated; here we assume the validity of the balance equations of mass, momenta, energy and entropy,

[10] One may call "$*$" and "$\blacktriangleright$" symbols identifying meso scales

for a general polar continuum, i.e.,

$$\left.\begin{aligned}
\frac{\partial \varrho}{\partial t} + \left(\varrho \upsilon_i\right)_{,i} &= 0, \\
\frac{\partial \varrho \upsilon_i}{\partial t} + \left(\varrho \upsilon_i \upsilon_j - t_{ij}\right)_{,j} &= \varrho g_i, \\
\frac{\partial \varrho L_i}{\partial t} + \left(\varrho L_i \upsilon_j - M_{ij}\right)_{,j} &= \varrho K_i, \\
\frac{\partial \varrho E}{\partial t} + \left(\varrho E \upsilon_i + Q_i\right)_{,i} &= \varrho R, \\
\frac{\partial \varrho \eta}{\partial t} + \left(\varrho \eta \upsilon_j + \phi_j\right)_{,j} &= \varrho \varsigma + \varrho s,
\end{aligned}\right\} \tag{4.75}$$

where the quantities without the notation "$\triangleright$", "$*$" or "$\blacktriangleright$" denote the macro-quantities of the respective micro-quantities defined before. Integration of (4.61)-(4.65) over the species assemblage and comparison with the respective equations in (4.75) yield these micro-macro relations. The results are stated here as follows:

$$\left.\begin{aligned}
\mathcal{F}^{\blacktriangleright} = \int\limits_{\mathcal{S}^2} \mathcal{F}^{\triangleright} d^2 n, \quad \mathcal{F}^{*} = \int\limits_{\mathcal{I}} \mathcal{F}^{\triangleright} dD, \\
\mathcal{F} = \int\limits_{\mathcal{S}^2} \int\limits_{\mathcal{I}} \mathcal{F}^{\triangleright} dD d^2 n = \int\limits_{\mathcal{I}} \mathcal{F}^{\blacktriangleright} dD = \int\limits_{\mathcal{S}^2} \mathcal{F}^{*} d^2 n,
\end{aligned}\right\} \tag{4.76}$$

$$\left.\begin{aligned}
\Phi_j^{\blacktriangleright} &= \int\limits_{\mathcal{S}^2} \left[\Phi_j^{\triangleright} - \varrho^{\triangleright} \left(\Psi^{\triangleright} - \Psi^{\blacktriangleright}\right) \left(\upsilon_j^{\triangleright} - \upsilon_j^{\blacktriangleright}\right)\right] d^2 n, \\
\Phi_j^{*} &= \int\limits_{\mathcal{I}} \left[\Phi_j^{\triangleright} - \varrho^{\triangleright} \left(\Psi^{\triangleright} - \Psi^{*}\right) \left(\upsilon_j^{\triangleright} - \upsilon_j^{*}\right)\right] dD, \\
\Phi_j &= \int\limits_{\mathcal{S}^2} \int\limits_{\mathcal{I}} \left[\Phi_j^{\triangleright} - \varrho^{\triangleright} \left(\Psi^{\triangleright} - \Psi\right) \left(\upsilon_j^{\triangleright} - \upsilon_j\right)\right] dD d^2 n, \\
\Phi_j &= \int\limits_{\mathcal{I}} \left[\Phi_j^{\blacktriangleright} - \varrho^{\blacktriangleright} \left(\Psi^{\blacktriangleright} - \Psi\right) \left(\upsilon_j^{\blacktriangleright} - \upsilon_j\right)\right] dD, \\
\Phi_j &= \int\limits_{\mathcal{S}^2} \left[\Phi_j^{*} - \varrho^{*} \left(\Psi^{*} - \Psi\right) \left(\upsilon_j^{*} - \upsilon_j\right)\right] d^2 n,
\end{aligned}\right\} \tag{4.77}$$

where

$$\left.\begin{aligned}
\mathcal{F} = \left\{\Psi, \Sigma, \Xi, \rho_d, \Pi, \varrho\, u_j, \varrho\, w\right\}., \\
\Gamma = \kappa_j = N_i = P = 0,
\end{aligned}\right\} \tag{4.78}$$

and the definitions of Table 4.2 are taken into account. The additive quantities $\mathcal{F}$ are averaged by simple integrals over the respective species assemblage, whilst the non-convective flux densities $\Phi_j^{\triangleright}$ are homogenized by accounting also for convective difference fluxes. The orientation transition rate, $u_j^{\triangleright}$, and the size transition rate, $w^{\triangleright}$, are homogenized as the

field of velocity, $v_i^{\triangleright}$. The dislocation density $\rho_d^{\triangleright}$ and its production rate $\Pi^{\triangleright}$ are additive quantities by definition.

The interspecies flux densities $\Upsilon_j^{\triangleright}$ and $\Delta^{\triangleright}$ can not be defined as macro quantities. However, $\partial_j \Upsilon_j^{\triangleright}$ and $\partial_D \Delta^{\triangleright}$ can be considered additive quantities $\mathcal{F}$, once one notes that

$$\Upsilon_j^{\triangleright} n_j = 0 \quad \Rightarrow \quad \int_{\mathcal{S}^2} \partial_j \Upsilon_j^{\triangleright} d^2 n = 0, \tag{4.79}$$

$$\int_{\mathcal{I}} \partial_D \Delta^{\triangleright} dD = 0. \tag{4.80}$$

Relation $(4.79)_1$, as well as its implication, $(4.79)_2$, are derived by Faria [36] . The rule stated in (4.79) is in fact valid not only for orientation fluxes, but for every field. Relation (4.80) is valid for all fields that have compact support on the interval $\mathcal{I}$.

The balance of dislocation from a macroscopic point of view is not postulated and is obtained by integration of (4.66) over the species assemblage, thereby obeying the rules (4.79) and (4.80). Thus,

$$\frac{\partial \rho_d}{\partial t} + \int_{\mathcal{S}^2} \int_{\mathcal{I}} \left\{ \rho_d^{\triangleright} \left(v_i^{\triangleright} - v_i \right) + \rho_d^{\triangleright} v_i \right\}_{,i} dD \, d^2 n = \Pi.$$

Therefore we have

$$\frac{\partial \rho_d}{\partial t} + \left(v_i \rho_d \right)_{,i} + \left(q_{di} \right)_{,i} = \Pi, \tag{4.81}$$

where the macroscopic density of non-convective flux of dislocation q_{di} is here defined by

$$q_{di} \equiv \int_{\mathcal{S}^2} \int_{\mathcal{I}} \rho_d^{\triangleright} \left(v_i^{\triangleright} - v_i \right) dD d^2 n. \tag{4.82}$$

In subsection 4.4.2 we neglected the microscopic non-convective flux of dislocation for huge polycrystalline materials. Eqn. (4.82) shows that the macroscopic counterpart can be different from zero if the velocity has a microscopic dependence. If the velocity has no microstructural dependence ($v_i^{\triangleright} = v_i$), then the balance of dislocation looses also the macroscopic non-convective flux term ($q_{di} = 0$) and takes the simpler form,

$$\frac{\partial \rho_d}{\partial t} + \left(v_i \rho_d \right)_{,i} = \Pi. \tag{4.83}$$

4.7 Homogenization of the Cauchy Stress Tensor

In the previous chapter, we have given a constitutive equation for the stretching in (3.12-3.14), that can be compressed as

$$D_{ij} = \hat{g}\left(a\right) \, S_{ij}, \quad a = \int_{\mathcal{S}^2} \frac{\varrho^*}{\varrho} \tilde{a} \left(S_{ab} S_{ab}, S_{ab} S_{bc} S_{ca}, S_{ab} n_a n_b, S_{ab} n_b S_{ac} n_c \right) d^2 n, \tag{4.84}$$

where the principle of material frame indifference is already taken into account. From the point of view of the Theory of Mixtures with Continuous Diversity, a constitutive

equation should be given, however, for the Cauchy stress and not for the stretching. On the other hand, for polar ice, we can assume microscopic independence of the velocity and incompressibility of the polycrystal,

$$v_i^{\triangleright} = v_i, \qquad v_{i,i} = D_{aa} = 0, \tag{4.85}$$

and the macroscopic deviatoric stress and the stretching have the same mathematical (traceless) structure. Therefore, postulating a constitutive equation for the stretching or for the deviatoric stress is equivalent and we can rewrite the third chapter assuming not the eqn. (4.84), but

$$S_{ij} = \hat{g}\,(a)\; D_{ij}, \quad a = \int\limits_{\mathcal{S}^2} \frac{\varrho^*}{\varrho} \tilde{a}\,(D_{ab}D_{ab}, D_{ab}D_{bc}D_{ca}, D_{ab}n_a n_b, D_{ab}n_b D_{ac}n_c)\, d^2n, \tag{4.86}$$

where we have systematically interchanged the symbols for stretching D_{ij} and stress deviator S_{ij}.

As we have already pointed out, the microscopic Cauchy stress tensor is a non-convective flux and its homogenization rules are given in equation (4.77). If we assume the validity of (4.85) and ignore grain-size dependence, homogenization of the deviatoric part of the Cauchy stress tensor is the operation

$$S_{ij} = \int\limits_{\mathcal{S}^2} S_{ij}^*\; d^2n. \tag{4.87}$$

In the Theory of Mixtures with Continuous Diversity, a constitutive equation must be given for the microscopic deviatoric stress tensor S_{ij}^* and in the last chapter, we will prove compatibility between (4.86) and (4.87). Thus, a complete justification of the results explained in the third chapter will be proved in terms of the Theory of Mixtures with Continuous Diversity.

Chapter 5

The Evolution of Texture and Fabrics

5.1 General Remark

In the third chapter, we pointed out that the anisotropic behaviour is driven by f^*, the Orientation Distribution Function (ODF). In the fourth chapter, we proved that a better representation of the distribution of lattice orientations of the crystallites in a polycrystal, for the purposes of its mechanical behaviour, is the orientation mass density ϱ^* (see eqn. (4.37)). The deformation mechanism of glide on basal planes described in Figs. 2.6 and 2.7 and various mechanical tests on polycrystalline materials suggest that the structure of the anisotropy, i.e. the ODF or the orientational mass density, changes in accordance with the deformation. In subsection 2.4.3, a review was given on the literature of this field. The main idea is that the unit vector n_j parallel to the c-axis and orthogonal to the (basal) plane on which the glide is easiest, goes towards the axis of compression, away from the axis of tension and the rule for simple shear can be extracted from Fig. 2.12.

In the present application of the Theory of Mixtures with Continuous Diversity, the evolution of fabrics, as well as the evolution of texture, is given by the evolution of the orientation-and-size mass density. One of the advantages of the use of this concept, is to regard the balance of mass as the equation that gives the evolutions of texture and fabric. Let us resume the final form of this balance equation from (4.61),

$$\frac{\partial \underset{\triangleright}{\varrho}}{\partial t} + \left(\underset{\triangleright}{\varrho} \underset{\triangleright}{v_j}\right)_{,j} + \partial_j \left(\underset{\triangleright}{\varrho} \underset{\triangleright}{u_j}\right) + \partial_D \left(\underset{\triangleright}{\varrho} \underset{\triangleright}{w}\right) = \underset{\triangleright}{\varrho} \underset{\triangleright}{\Gamma}.$$

Integration over $\mathcal{S}^2$ is sufficient to formally arrive at an evolution equation of the size mass density. In fact, from (4.61), (4.76) and (4.78), we have,

$$\frac{\partial \underset{\blacktriangleright}{\varrho}}{\partial t} + \left(\underset{\blacktriangleright}{\varrho} \underset{\blacktriangleright}{v_j}\right)_{,j} + \partial_D \left(\underset{\blacktriangleright}{\varrho} \underset{\blacktriangleright}{w}\right) = \underset{\blacktriangleright}{\varrho} \underset{\blacktriangleright}{\Gamma}. \tag{5.1}$$

On the other hand, integration of (4.61) over the grain-size range, $\mathcal{I}$, yields a formal evolution equation for the orientation mass density. In fact, from (4.61), (4.76) and (4.78), we have,

$$\frac{\partial \varrho^*}{\partial t} + \left(\varrho^* v_j^*\right)_{,j} + \partial_j \left(\varrho^* u_j^*\right) = \varrho^* \Gamma^*. \tag{5.2}$$

In the next two sections we will give our contribution to the solution of the problem of texture and fabric evolution by the use of equations (5.1) and (5.2), respectively. Moreover, for the sake of simplicity, we will assume in this chapter, (i) incompressibility of the polycrystal and (ii) absence of a microstructural dependence of the velocity, i.e.,

$$v_j^{\triangleright} = v_j \qquad \text{and} \qquad v_{j,j} = D_{jj} = 0. \tag{5.3}$$

Later, these restrictions will be relaxed.

5.2 Evolution of Texture

5.2.1 General Remark

A more convenient way to write equation (5.1) with the approximation (5.3) already taken into account is the following,

$$\mathring{\varrho}^{\blacktriangleright} = \varrho^{\blacktriangleright}\Gamma^{\blacktriangleright} - \varrho^{\blacktriangleright}\partial_D w^{\blacktriangleright}. \tag{5.4}$$

From the definition of the size time derivative (4.41) and from (5.4) it is visible that the evolution of the size mass density is driven by the size transition rate, $w^{\blacktriangleright}$, and by the specific size production rate of mass, $\Gamma^{\blacktriangleright}$. The size transition rate $w^{\blacktriangleright}$ is the rate at which the mass in the RVE performs a continuous transition from a certain dimensionless grain-size, D, to another dimensionless grain-size that is near to D. The specific size production rate of mass, $\Gamma^{\blacktriangleright}$, is the rate at which the mass in the RVE performs a (not necessarily continuous) transition from a certain dimensionless grain-size D to another dimensionless grain-size (that is not necessarily near to D).

The phenomenon of grain growth can be explained as a continuous transition of a crystallite with dimensionless grain-size D to a crystallite with dimensionless grain-size $D + dD$. Thus, grain growth can be modelled by the size transition rate, $w^{\blacktriangleright}$. For polygonization, on the other hand, if a crystallite is broken into two equal parts, its old dimensionless grain-size, e.g. D, is transformed into a dimensionless grain-size equal to $D/2$. Therefore this is a discontinuous transition inside the grain-size range that can be interpreted with the specific size production rate of mass $\Gamma^{\blacktriangleright}$. Finally, a restriction on $\Gamma^{\blacktriangleright}$ is set by eqn. (4.77) of the homogenization procedure of the fourth chapter, namely,

$$\int_{\mathcal{I}} \varrho^{\blacktriangleright}\Gamma^{\blacktriangleright} dD = 0. \tag{5.5}$$

Its physical meaning is as follows: If the production of mass for a certain dimensionless grain-size is positive, then the same amount of mass is lost by other crystallites with other values of D. If a crystallite with dimensionless grain-size D is polygonized into two crystallites with dimensionless grain-size $D/2$, then the production of mass evaluated in D is negative and that evaluated in $D/2$ is positive, in such a way that $\Gamma^{\blacktriangleright}(D) = -\Gamma^{\blacktriangleright}(D/2)$. In other words, (5.5) guarantees conservation of mass.

5.2.2 Evolution of the Mean Grain-size

In the second chapter we reviewed an evolution equation for the mean grain-size of polycrystalline ice under conditions that occur in an ice-sheet (2.45). In this subsection, we

want to connect this result with the evolution of the size mass density (5.4). Before embarking into details we note that, in this context, the time t and the dimensionless grain-size D are two independent variables; so, to establish a relation between them is not possible. On the other hand, the mean grain-size, $\langle D\rangle$, is defined in (4.35) and its evolution equation is related to the size mass density. Moreover, in the ensuing development we need a generalization of eqn. (4.35) for a general field $A^{\blacktriangleright}(D)$, i.e.,

$$\langle A^{\blacktriangleright}\rangle_{D} \equiv \int_{\mathcal{I}} A^{\blacktriangleright}\frac{\varrho^{\blacktriangleright}}{\varrho}dD. \tag{5.6}$$

If we multiply equation (5.4) by D/ϱ, then we can write,

$$\frac{1}{\varrho}\frac{\partial D\varrho^{\blacktriangleright}}{\partial t}+\frac{1}{\varrho}\frac{\partial D\varrho^{\blacktriangleright}}{\partial x_i}\upsilon_i+\frac{1}{\varrho}\frac{\partial D\left(\varrho^{\blacktriangleright}w^{\blacktriangleright}\right)}{\partial D}-\frac{1}{\varrho}\varrho^{\blacktriangleright}w=D\frac{1}{\varrho}\varrho^{\blacktriangleright}\Gamma$$

or

$$\frac{\partial}{\partial t}\left(D\frac{\varrho^{\blacktriangleright}}{\varrho}\right)+D\frac{\varrho^{\blacktriangleright}}{\varrho^2}\frac{\partial\varrho}{\partial t}+\frac{\partial}{\partial x_i}\left(D\frac{\varrho^{\blacktriangleright}}{\varrho}\right)\upsilon_i+D\frac{\varrho^{\blacktriangleright}}{\varrho^2}\frac{\partial\varrho}{\partial x_i}\upsilon_i+\frac{1}{\varrho}\frac{\partial D\left(\varrho^{\blacktriangleright}w^{\blacktriangleright}\right)}{\partial D}=\frac{\varrho^{\blacktriangleright}}{\varrho}w+D\frac{\varrho^{\blacktriangleright}}{\varrho}\Gamma^{\blacktriangleright}. \tag{5.7}$$

if one regards x_i, D and t as independent variables (as they are!). Validity of the classical (macroscopic) balance of mass $(4.75)_1$, integration of (5.7) over the grain-size range $\mathcal{I}$, application of the rule (4.80) and the general definition (5.6) yield

$$\frac{d}{dt}\langle D\rangle=\langle w^{\blacktriangleright}\rangle_{D}+\langle D\Gamma^{\blacktriangleright}\rangle_{D}\,. \tag{5.8}$$

Once we interpret the size transition rate, $w^{\blacktriangleright}$, as a grain growth term and the specific size production of mass, $\Gamma^{\blacktriangleright}$, as a polygonization term, then comparison between (2.45) and (5.8) yields

$$\langle w^{\blacktriangleright}\rangle_{D}=\frac{K}{\langle D\rangle}, \tag{5.9}$$

and

$$\langle D\,\Gamma^{\blacktriangleright}\rangle_{D}=-P\,\langle D\rangle\,. \tag{5.10}$$

The goal of this subsection is to achieve an explicit form for $w^{\blacktriangleright}$ and $\Gamma^{\blacktriangleright}$. It is clear that such a parameterization must be consistent with (5.9) and (5.10). From the analyses of ice-cores it is evident that the Crystal Size Distribution (CSD) has always the form of a Log-normal Distribution (see e.g. Section 2.2). Therefore, if we assign the following expression for the size transition rate,

$$w^{\blacktriangleright}=\frac{K}{D},\qquad\Longrightarrow\qquad\langle w^{\blacktriangleright}\rangle_{D}=\left\langle\frac{K}{D}\right\rangle_{D}\simeq\frac{K}{\langle D\rangle}, \tag{5.11}$$

then coherence with (5.9) for the mean grain-size is guaranteed, but not for the Crystal Size Distribution (CSD) deduced from the analyses of ice-cores in polar ice. In fact, if we assume the validity of (5.11), then all the tiny grains in the distribution of grain size are forced to grow faster than the others. More specifically, the size transition rate $w^{\blacktriangleright}$ in $(5.11)_1$ tends to infinity when the dimensionless grain-size D tends to zero. This means

that, once a certain amount of time has elapsed, the Log-normal Distribution is disrupted. Thus, we propose a better parameterization of the size transition rate, i.e.,

$$w^{\blacktriangleright} = \frac{K}{\langle D \rangle}, \tag{5.12}$$

We remark that $w^{\blacktriangleright}$, as parameterized by (5.12), does not tend to infinity when D tends to zero, since it depends on the global variable $\langle D \rangle$ and is independent of the dimensionless grain-size D. Therefore, the tiny grains have now the same size transition rate as the larger grains, they are not forced to grow with different velocity and the Log-normal Distribution revealed in the analyses of ice-cores is not disrupted.

There are two conditions on the specific size production rate of mass that must be fulfilled, namely (5.5) and (5.10). Thus, we may assume a linear form with respect to the dimensionless grain-size D and write

$$\Gamma^{\blacktriangleright} = a + b\, D. \tag{5.13}$$

The two parameters a and b can be fixed, then, by (5.5) and (5.10). Indeed, the closed system of linear equations may be deduced from (5.5) and (5.10), reads

$$a + b\, \langle D \rangle = 0, \qquad a\, \langle D \rangle + b\, \left\langle D^2 \right\rangle_D + P\, \langle D \rangle = 0, \tag{5.14}$$

and possesses the solution

$$a = P \frac{\langle D \rangle^2}{\left\langle D^2 \right\rangle_D - \langle D \rangle^2}, \qquad b = P \frac{\langle D \rangle}{\langle D \rangle^2 - \left\langle D^2 \right\rangle_D}. \tag{5.15}$$

Thus, the explicit form of the specific size production rate of mass is given by

$$\Gamma^{\blacktriangleright} = (\langle D \rangle - D)\, \frac{P\, \langle D \rangle}{\left\langle D^2 \right\rangle_D - \langle D \rangle^2}. \tag{5.16}$$

We remark that, even for the specific size production rate of mass $\Gamma^{\blacktriangleright}$, we have a dependence on global variables, the mean grain-size $\langle D \rangle$ and the mean of the square of dimensionless grain-size $\left\langle D^2 \right\rangle_D$. Finally, the denominator of the right-hand side of equation (5.16) is also called the variance of the distribution $\varrho^{\blacktriangleright}/\varrho$.

5.3 The Evolution of Fabrics

5.3.1 General Remarks

In this section we analyse the problem of how the anisotropy in a polycrystal evolves and how this is induced by deformations. We begin this discussion by writing equation (5.2) with the approximation (5.3) taken into account; then

$$\mathring{\varrho}^* = \varrho^* \Gamma^* - \varrho^* \partial_j u_j^*, \tag{5.17}$$

where the definition of the orientation time derivative (4.41) has been introduced. In much the same way as with the evolution equation of size mass density, the evolution of

orientation mass density is driven by the orientation transition rate, u_j^*, and by the specific orientation rate of mass production, Γ^*. Moreover, the orientation transition rate, u_j^*, is the rate at which the mass of the RVE performs a continuous transition from a certain orientation, n_j, to another orientation that is close to n_j. The specific orientation rate of mass production, Γ^*, is the rate at which the mass in the RVE performs a (not necessarily continuous) transition from a certain orientation n_j to another orientation (that is, therefore, not necessarily near to n_j). The phenomenon of grain rotation described in Figs. 2.6 and 2.7 can be explained as a continuous transition of mass from a crystallite with orientation n_j to a crystallite with an orientation that is close to n_j. Thus, the rotation of crystallites can be modelled by the orientation transition rate, u_j^*. Grain Boundary Migration (GBM), following the definition given in the second chapter, can be interpreted as the rate of specific orientation production of mass Γ^*. In fact, in the example shown in Fig. 2.10, part of the mass of the crystallite with orientation n_i^2 is transferred into the crystallite with orientation n_i^1. In such an example the mathematical interpretation is

$$\Gamma^*\left(n_i^1\right) > 0, \quad \Gamma^*\left(n_i^2\right) < 0, \tag{5.18}$$

or in a form that is suitable for generalization,

$$\varrho^*\left(n_i^1\right)\Gamma^*\left(n_i^1\right) + \varrho^*\left(n_i^2\right)\Gamma^*\left(n_i^2\right) = 0. \tag{5.19}$$

This is the discretization for the situation represented in Fig. 2.10 of the general form of the homogenization procedure presented in chapter 4 in eqn. (4.77), that takes, for the rate of specific orientation production of mass, the form

$$\int_{\mathcal{S}^2} \varrho^*\,\Gamma^*\,d^2n = 0. \tag{5.20}$$

This equation is of the same type as (5.5). Both have the same meaning. The mass of the entire polycrystal does not change and the loss and the gain of mass of certain crystallites are balanced by the respective gain and loss of mass of other crystallites.

5.3.2 Grain Rotation

The deformation mechanism described in Figs. 2.6 and 2.7 implies that the c-axis of a crystallite, in a polycrystal, rotates towards the axis of compression and away from the axis of tension. At the end of the second chapter we showed in Fig. 2.12 a simple graphical method to evaluate the direction of the rotation even for simple shear. In this subsection we show how to insert this information into the present application of the Theory of Mixtures with Continuous Diversity. We already pointed out that the grain rotation can be modelled from the orientation transition rate. A general form for the orientation transition rate u_i^*, that is coherent with the Principle of Material Objectivity and that guarantees the orthogonality with respect to the orientation n_j is,

$$u_j^* = 2\iota^* D_{h[j}n_{k]}n_h n_k, \tag{5.21}$$

In symbolic notation, this can be written as

$$\mathbf{u}^* = \iota^*\left[\mathbf{Dn} - (\mathbf{Dn}\cdot\mathbf{n})\,\mathbf{n}\right]. \tag{5.22}$$

In Chapter 6 we will demonstrate how to motivate equations (5.21) or (5.22) for the orientation transition rate from the balance of Angular Momentum. There, we will also prove that ι^* can be taken as a very general function of some scalar invariants, i.e.,

$$\iota^* = \iota^* \left\{ \varrho^*, D_{hk}D_{hk}, D_{hk}D_{km}D_{mh}, n_h D_{hk} n_k, n_h D_{hk} D_{kl} n_l \right\}. \tag{5.23}$$

The orthogonality between the orientation transition rate u_i^* and the orientation n_j can be written as

$$\mathbf{u}^* \cdot \mathbf{n} = u_j^* n_j = 0. \tag{5.24}$$

and is a consequence of the expression (5.21) or (5.22). Dafalias [27] noted that, if the value of ι^* is equal to one, then the unit vector n_j remains along a material line element and the rotation is defined an *affine rotation*. However the occurrence of non-affine rotations in the dynamic of an ice sheet can not *a priori* be neglected. The advantages of the present macroscopic approach is the possibility to perform a parameterization of ι^*, that is not deduced, here, from any microscopic model. In fact, we will demonstrate that a suitable value for ι^* for the description of grain rotation in the GRIP ice core is different from unity. In this subsection we will impose a very strong approximation that can be checked *a posteriori*: the function ι^* is simply a positive constant, i.e.,

$$\iota^* = \iota \geqslant 0. \tag{5.25}$$

To verify the validity of this assumption, it is sufficient to perform a Gedanken Experiment. As we did in the third chapter, the Gedanken Experiment will be so selected that the result is known. We choose a pure shear test with a vertical compression and isotropic horizontal tension that can be modelled by the following stretching tensor,

$$\mathbf{D} = \begin{pmatrix} -\frac{D_{33}}{2} & 0 & 0 \\ 0 & -\frac{D_{33}}{2} & 0 \\ 0 & 0 & D_{33} \end{pmatrix}, \tag{5.26}$$

where D_{33} is positive. The orientation n_i will be represented by spherical coordinates so that in vectorial form

$$\mathbf{n} = \begin{pmatrix} \sin\theta\cos\varphi \\ \sin\theta\sin\varphi \\ \cos\theta \end{pmatrix}. \tag{5.27}$$

From (5.22), (5.26) and (5.27) we can derive the explicit form for the orientation transition rate; it is given by

$$\mathbf{u}^* = \frac{3}{4}\iota \sin 2\theta D_{33} \begin{pmatrix} -\cos\varphi\cos\theta \\ -\sin\varphi\cos\theta \\ \sin\theta \end{pmatrix}. \tag{5.28}$$

It is easy to recognize that the orthogonality condition expressed in (5.24) is fulfilled. Furthermore, (5.28) exhibits an explicit dependence on the Schmidt factor that Azuma and Higashi [9] already recognized in equations (2.11) and (2.12) in 1985. Besides, the presence of the Schmidt factor guarantees that crystallites with vertical and horizontal lattice orientations do not rotate and those at 45° from the vertical yield the maximum magnitude of the orientation transition rate. The direction of the rotation is also guaranteed because the third component of the orientation transition rate is positive when

$\theta < \pi/2$ and negative when $\theta > \pi/2$. Furthermore, a change in the sign of D_{33} produces in (5.28) a change in the sign of $\mathbf{u}^*$ and this agrees with experimental data. This guarantees that the choice of ι as a positive constant is coherent with the actual knowledge of the grain rotation. Moreover, if the crystallite is in the plane composed of the first and the third axes of the frame of reference, we have,

$$\varphi = 0 \quad \Rightarrow \quad \mathbf{u}^* = \frac{3}{4}\iota \sin 2\theta D_{33} \begin{pmatrix} -\cos\theta \\ 0 \\ \sin\theta \end{pmatrix}, \tag{5.29}$$

and if it belongs to the plane composed of the second and the third axes of the frame of reference, we have,

$$\varphi = \frac{\pi}{2} \quad \Rightarrow \quad \mathbf{u}^* = \frac{3}{4}\iota \sin 2\theta D_{33} \begin{pmatrix} 0 \\ -\cos\theta \\ \sin\theta \end{pmatrix}. \tag{5.30}$$

In the derivation of equation (5.21), the requirements of the Principle of Material Objectivity is already observed. Therefore, the expression for the orientation transition rate for other pure shear tests can be developed by the same considerations that have been for pure shear test represented in (5.26). Anyhow, it is straightforward to derive that for pure shear represented by,

$$\mathbf{D} = \begin{pmatrix} D_{11} & 0 & 0 \\ 0 & -\frac{D_{11}}{2} & 0 \\ 0 & 0 & -\frac{D_{11}}{2} \end{pmatrix}, \tag{5.31}$$

the orientation transition rate takes the form

$$\mathbf{u}^* = \iota D_{11} \begin{pmatrix} \sin\theta\cos\varphi - A_1(\theta,\varphi)\sin\theta\cos\varphi \\ -\frac{1}{2}\sin\theta\sin\varphi - A_1(\theta,\varphi)\sin\theta\sin\varphi \\ -\frac{1}{2}\cos\theta - A_1(\theta,\varphi)\cos\theta \end{pmatrix}, \tag{5.32}$$

once one defines

$$A_1(\theta,\varphi) \equiv \sin\theta\cos\varphi\sin\theta\cos\varphi - \tfrac{1}{2}\sin\theta\sin\varphi\sin\theta\sin\varphi - \tfrac{1}{2}\cos\theta\cos\theta.$$

It is easy to check that in the plane composed of the first and the third axes of the frame of reference,

$$\varphi = 0 \quad \Rightarrow \quad \mathbf{u}^* = \frac{3}{4}\iota \sin 2\theta D_{11} \begin{pmatrix} \cos\theta \\ 0 \\ -\sin\theta \end{pmatrix}, \tag{5.33}$$

or in the plane composed of the first and the second axes of the frame of reference,

$$\theta = \frac{\pi}{2} \quad \Rightarrow \quad \mathbf{u}^* = \frac{3}{4}\iota \sin 2\theta D_{11} \begin{pmatrix} \sin\varphi \\ -\cos\varphi \\ 0 \end{pmatrix}. \tag{5.34}$$

If the pure shear test takes the form

$$\mathbf{D} = \begin{pmatrix} -\frac{D_{22}}{2} & 0 & 0 \\ 0 & D_{22} & 0 \\ 0 & 0 & -\frac{D_{22}}{2} \end{pmatrix}, \tag{5.35}$$

then the orientation transition rate is

$$\mathbf{u}^{*} = \iota D_{22} \begin{pmatrix} -\frac{1}{2}\sin\theta\cos\varphi - A_2(\theta,\varphi)\sin\theta\cos\varphi \\ \sin\theta\sin\varphi - A_2(\theta,\varphi)\sin\theta\sin\varphi \\ -\frac{1}{2}\cos\theta - A_2(\theta,\varphi)\cos\theta \end{pmatrix}, \tag{5.36}$$

once one defines

$$A_2(\theta,\varphi) \equiv -\frac{1}{2}\sin\theta\cos\varphi\sin\theta\cos\varphi + \sin\theta\sin\varphi\sin\theta\sin\varphi - \frac{1}{2}\cos\theta\cos\theta.$$

In the plane composed of the second and the third axes of the frame of reference this is given by,

$$\varphi = \frac{\pi}{2} \quad \Rightarrow \quad \mathbf{u}^{*} = \frac{3}{4}\iota\sin 2\theta D_{22} \begin{pmatrix} 0 \\ \cos\theta \\ -\sin\theta \end{pmatrix}, \tag{5.37}$$

and in the plane composed of the first and the second axes of the frame of reference (5.36) becomes

$$\theta = \frac{\pi}{2} \quad \Rightarrow \quad \mathbf{u}^{*} = \frac{3}{4}\iota\sin 2\varphi D_{22} \begin{pmatrix} -\sin\varphi \\ \cos\varphi \\ 0 \end{pmatrix}. \tag{5.38}$$

We also note that the magnitude of the orientation transition rate in equations (5.29), (5.30), (5.33), (5.34), (5.37) and (5.38) can be increased if the pure shear test is conducted in another way. In fact, the components D_{11} and D_{22} of the stretching tensor in (5.26), for example, do not contribute to the same direction of rotation. In order to increase the magnitude of $\mathbf{u}^{*}$ we can take the same pure shear with vertical compression but now with an anisotropic horizontal tension, e.g. only towards the first axis of the frame of reference. The stretching can be represented by the equation

$$\mathbf{D} = \begin{pmatrix} -D_{33} & 0 & 0 \\ 0 & 0 & 0 \\ 0 & 0 & D_{33} \end{pmatrix}, \tag{5.39}$$

and the orientation transition rate becomes

$$\mathbf{u}^{*} = \iota D_{33} \begin{pmatrix} -\left[1 - \sin\theta\cos\varphi\sin\theta\cos\varphi + \cos\theta\cos\theta\right]\sin\theta\cos\varphi \\ 0 \\ -\sin\theta\sin\theta\left[-1 - \cos\varphi\cos\varphi\right]\cos\theta \end{pmatrix}, \tag{5.40}$$

that, in the plane composed of the first and the third axes of the frame of reference, is

$$\varphi = 0 \quad \Rightarrow \quad \mathbf{u}^{*} = \iota\sin 2\theta D_{33} \begin{pmatrix} -\cos\theta \\ 0 \\ \sin\theta \end{pmatrix}. \tag{5.41}$$

Thus, we see that the magnitude of the orientation transition rate in (5.41) is larger than the magnitude expressed in (5.29). The two expressions (5.29) and (5.41) are in fact evaluated for the crystallites of the same plane but for different pure shear tests with vertical compression. The orientation transition rate (5.29) is for isotropic horizontal tension and the related stretching tensor is stated in (5.26), and the orientation transition

rate (5.41) is for an anisotropic horizontal tension and the related stretching tensor is stated in (5.39).

For simple shear we can either perform a certain rotation of the frame of reference or perform the calculation of the orientation transition rate from (5.21) and use the stretching tensor related to the wanted simple shear. The graphical method illustrated at the end of Chapter 2 can also be used.

5.3.3 A Three-dimensional Application

In this subsection our goal is to derive an explicit evolution equation for the orientation mass density, by assuming the constitutive equation (5.22) for the orientation transition rate, i.e.,

$$u_j^* = \iota^* \left[D_{jh} n_h - D_{hk} n_h n_k n_j \right]. \tag{5.42}$$

If we neglect the production term Γ^* and any dependence of ϱ^* on the position x_i, then the evolution equation (5.17) takes a simplified form, namely

$$\frac{\partial \varrho^*}{\partial t} + \partial_j \left(\varrho u_j^* \right) = \frac{\partial \varrho^*}{\partial t} + \frac{\partial}{\partial n_j} \left(\varrho u_j^* \right) - n_j n_h \frac{\partial}{\partial n_h} \left(\varrho u_j^* \right) = 0. \tag{5.43}$$

The combination of (5.42) and (5.43) yields the remarkable result

$$\frac{\partial \varrho^*}{\partial t} + \iota D_{jh} n_h \partial_j \varrho^* - 3\iota \varrho^* D_{kh} n_h n_k = 0. \tag{5.44}$$

Equation (5.44) holds for any state of stretching. We have already pointed out that for the state of stretching (5.26) of pure shear, the respective orientation transition rate is expressed by (5.29). To achieve our goal, we state that

$$\mathbf{D} = D_{33} \begin{pmatrix} -\frac{1}{2} & 0 & 0 \\ 0 & -\frac{1}{2} & 0 \\ 0 & 0 & 1 \end{pmatrix}, \ \mathbf{Dn} = D_{33} \begin{pmatrix} -\frac{1}{2} \sin\theta \cos\varphi \\ -\frac{1}{2} \sin\theta \sin\varphi \\ \cos\theta \end{pmatrix}, \ D_{hk} n_h n_k = D_{33} \left[\frac{3}{2} \cos^2\theta - \frac{1}{2} \right]. \tag{5.45}$$

Moreover, if we recall the explicit expression for the orientational gradient operator in spherical coordinates (see e.g. (7.1)), and if we observe that the state of stretching is axially symmetric, then

$$D_{jh} n_h \partial_j \varrho^* = -\frac{3}{2} D_{33} \sin\theta \cos\theta \frac{\partial \varrho^*}{\partial \theta}$$

once it is assumed that also the initial fabric is axially symmetric, e.g., uniformly randomly distributed. Thus, the evolution equation of fabric, (5.44) yields

$$\frac{\partial \varrho^*}{\partial t} - \iota \frac{3}{4} D_{33} \sin 2\theta \frac{\partial \varrho^*}{\partial \theta} - 3\iota \varrho^* D_{33} \left[\frac{3}{2} \cos^2\theta - \frac{1}{2} \right] = 0.$$

or

$$\frac{\partial \varrho^*}{\partial t} - \iota \frac{3}{4} D_{33} \left[\frac{\partial \sin 2\theta \varrho^*}{\partial \theta} + 2\varrho^* \cos^2\theta \right] = 0. \tag{5.46}$$

To corroborate the suitability of this equation, we perform an integration over the unit sphere which must vanish; thus,

$$\int_0^{\pi} \left[\frac{\partial \varrho^*}{\partial t} - \iota \frac{3}{4} D_{33} \left[\frac{\partial \sin 2\theta \varrho^*}{\partial \theta} + 2\varrho^* \cos^2 \theta \right] \right] \sin \theta d\theta = 0. \tag{5.47}$$

One can verify that (5.47) is fulfilled for any orientational mass density.

In the next subsection we will prove that the two-dimensional limit can not be derived from (5.46). On the other hand, the evolution equation, in that limit, is simpler and an analytical solution can be found.

5.3.4 The Two-dimensional Limit

In the two-dimensional case, the evolution equation of ϱ^* is simplified. (5.43) is still valid, but now it implies

$$\frac{\partial \varrho^*}{\partial t} + \iota D_{jh} n_h \partial_j \varrho^* - 2\iota \varrho^* D_{kh} n_h n_k = 0. \tag{5.48}$$

If we use the polar coordinate system (3.15), we have

$$\mathbf{D} = D_{22} \begin{pmatrix} -1 & 0 \\ 0 & 1 \end{pmatrix}, \quad \mathbf{Dn} = D_{22} \begin{pmatrix} -\cos\hat{\theta} \\ \sin\hat{\theta} \end{pmatrix}, \quad D_{hk} n_h n_k = -D_{22} \cos 2\hat{\theta}. \tag{5.49}$$

Setting all components related to the third direction equal to zero, choosing the latitude $\theta = \pi/2$ and the longitude φ equal to the angle $\tilde{\theta}$, evaluation of the orientational gradient operator can explicitly be performed. The result is

$$\frac{\partial \varrho^*}{\partial t} + \iota D_{22} \frac{\partial}{\partial \tilde{\theta}} \left(\varrho^* \sin 2\tilde{\theta} \right) = 0. \tag{5.50}$$

From (5.46) and (5.50), we confirm that the two-dimensional limit is simpler than the axisymmetric three-dimensional case. Moreover, the solution of (5.50) can be constructed with the method of characteristics (see e.g. [117]) and yields the following result

$$\varrho^* = \frac{\varrho}{2\pi \left(e^{2\iota D_{22} t} \left(\cos\tilde{\theta} \right)^2 + e^{-2\iota D_{22} t} \left(\sin\tilde{\theta} \right)^2 \right)}, \tag{5.51}$$

provided the initial orientation mass density is assumed to be uniformly random. The verification of (5.51) as a solution of (5.50) is straightforward. Rashid [117] remarked that the validity of this solution, with $\iota = 1$, depends upon only three things: (i) the two-dimensionality of the polycrystal, (ii) the Taylor assumption (see subsection 1.5.2) and (iii) the rigid-plastic response of the individual crystallites. The last two assumptions are consequences of the microscopic model that Rashid uses. The theory that here is presented, however, avoids any micromechanical suppositions and is a purely phenomenological continuum theory. The advantages are that the hypotheses (ii) and (iii) can be relaxed and that the parameterization of ι is possible. This flexibility is, in fact, the main advantage of this approach; it is therefore more appropriate for the (non-numerical !) simulation of the evolution of the ODF along the first 2100 meters of the GRIP ice core, than any preceding approach.

5.3.5 The GRIP Ice Core

Experimental verification of the evolution equations of the orientational mass density presented in this chapter is not easy. The problem is that if the magnitude of the stretching (e.g. D_{33}) is too big, then the approximation of excluding the phenomena related to Grain Boundary Migration (GBM) and, consequentely, the term Γ^* is irrealistic. On the other hand, if the magnitude of the stretching is too small, the time required to reach a measurable change of the orientation mass density surpasses the life time of a human scientist. Experience shows that a compromise on a suitable value for the stretching is not possible. One possibility is to find in Nature a body in which the conditions that we wish to reproduce in the laboratory have been satisfied for thousands of years necessary to generate a significant change in the distribution of lattice orientations. Such conditions can be found in an ice-sheet. The GRIP ice core at the summit of Greenland is one of these an ideal instruments. It comes from a dome and the state of stretching can be assumed to be represented by (5.26). The trajectory of the particles of the ice is assumed, therefore, to be vertical from the top to the bottom. The value of the strain rate[1], $\simeq 2.5 \times 10^{-12}$ seconds^{-1}, is believed to be sufficiently low to avoid the occurrence of recrystallization phenomena related to GBM. If we analyse the upper 2000m, then the time elapsed from the time when the ice was deposited on the surface of the ice-sheet as a snow flake is sufficiently high. It needs almost 30000 years, to have a significant change in the distribution of lattice orientations. From Thorsteinsson's report in 1996 [132], the available experimental data on the development of fabric in the GRIP ice core are given in the fabric diagrams as percentages of the number of c-axes within each 10° interval from the vertical. In the two-dimensional scheme, for reasons of symmetry, these percentages are, from (5.51),

$$P_m(t) = 400 \int_{\frac{m-1}{18}\pi}^{\frac{m}{18}\pi} \frac{\varrho^*}{\varrho} d\tilde{\theta} = \frac{200}{\pi} \left[\arctan\left(e^{-2D_{22}t\iota} \tan\frac{m\pi}{18} \right) - \arctan\left(e^{-2D_{22}t\iota} \tan\frac{(m-1)\pi}{18} \right) \right]. \tag{5.52}$$

The nine functions P_m, $m = 1, ..., 9$ are graphically displayed in Fig. 5.1.

The figures show that at the beginning, all the nine 10° intervals of the fabric diagrams are populated in the same way and the percentage values are all equal to $P_m(0) \simeq 11\%$. This characteristics can not be revealed in the experimental data shown on the right-hand side. Greenland is, in fact, a three-dimensional body and such intervals (i.e. P_m) for a uniformly random distribution of c-axes are not uniformly populated. Besides, the intervals that comprehend crystallites with more than 45° inclination from the vertical (i.e., P_1, P_2, P_3 and P_4) decrease their population and the intervals that comprehend crystallites with less than 45° inclination from the vertical (i.e., P_6, P_7, P_8 and P_9) begin to increase their population. After some time, however, even these populations tend to decrease. Only P_9 maintains a constant tendency to grow. We remark, in fact, that the functions P_m are percentages and their sum is always 100%. We remark that these last characteristics can be revealed, on the other hand, from the measured data of Thorsteinsson [132] reported on the right-hand side of Fig. 5.1. We remarked that an ice sheet is a three-dimensional

[1]This value is assumed to be equal to the square root of the second invariant of the stretching tensor, i.e., $\sqrt{D_{hk}D_{hk}} \simeq 2.5 \times 10^{-12}$ seconds^{-1}.

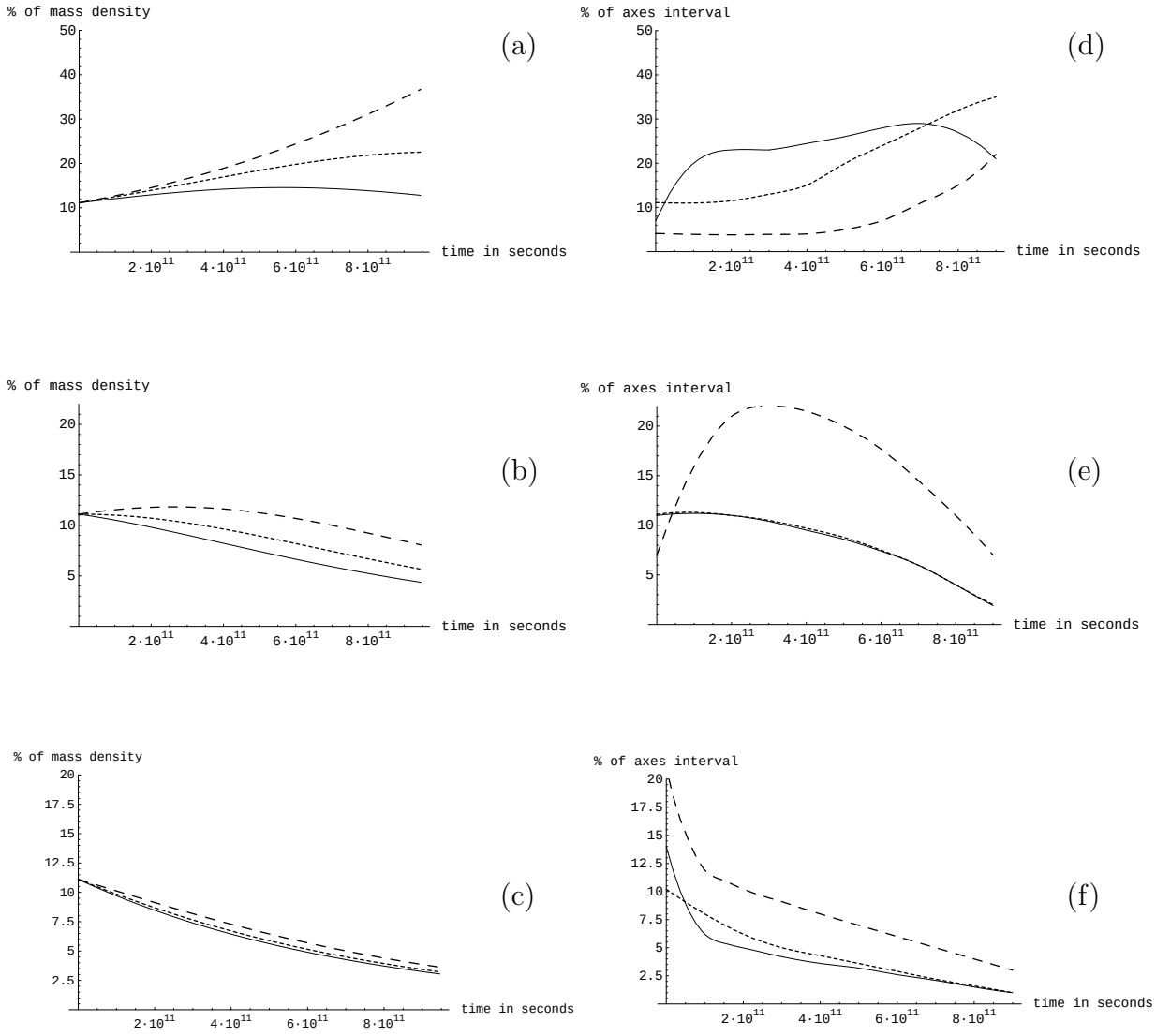

Figure 5.1: On the left-hand side, we show the percentages of mass density due to the crystallites with c-axes within 10° intervals of the fabric diagrams in the upper 2100m of the GRIP ice core. The curves represent the analytical functions $P_m(t)$ with $m = 1, ..., 9$. (a) Dashed line: $0 - 10^\circ$ from the vertical, i.e., the function $P_9(t)$; dotted line: $10 - 20^\circ$ from the vertical, i.e., the function $P_8(t)$; full line: $20 - 30^\circ$ from the vertical, i.e., the function $P_7(t)$; (b) Dashed: $30 - 40^\circ$ from the vertical, i.e., the function $P_6(t)$; dotted line: $40 - 50^\circ$ from the vertical, i.e., the function $P_5(t)$; full line: $50 - 60^\circ$ from the vertical, i.e., the function $P_4(t)$; (c) Dashed line: $60 - 70^\circ$ from the vertical, i.e., the function $P_3(t)$; dotted line: $70 - 80^\circ$ from the vertical, i.e., the function $P_2(t)$; full line: $80 - 90^\circ$ from the vertical, i.e., the function $P_1(t)$. The values of the parameters are explained in equations (5.53) and (5.54). On the right-hand side we show the respective experimental data from [132]. (d) is the analog of (a), (e) is the analogue of (b) and (f) is the analogue of (c). Among a qualitative agreement, we can see that not only a three-dimensional model but also a more refined parameterization of ι is needed.

body and equation (5.50) is valid only in a two-dimensional context. The evolution equation that is suitable for a detailed comparison is therefore the more complicated equation (5.46), for which an appropriate numerical simulation is needed. Anyhow, from [132] we can derive, for example, that

$$P_1(T)+P_2(T)\simeq 59\%,\quad T=30000 \text{ years}\simeq 10^{12} \text{ seconds},\quad D_{22}\simeq 1.8\times 10^{-12} \text{ seconds}^{-1}, \tag{5.53}$$

and, from (5.52), we thus deduce a rough parameterization of ι,

$$\iota\simeq 0.4. \tag{5.54}$$

For a two-dimensional model the value of the paramer ι, in the simulation of the upper part of the Greenland ice-sheet, can be set as given in (5.54). Further parameterizations with respect to temperature and dislocation density are believed to be also needed. For a three-dimensional context, use of (5.46), instead of (5.50), is suggested.

Notwithstanding, the value of ι is considerably different from unity and we claim non-validity, in the upper part of the Greenland ice-sheet, of the microscopic models from which the value $\iota=1$ is deduced (see e.g. [117]).

Apart from the use of a simple two-dimensional scheme, another simplification seems to be incorrect, namely, the assumption that the value of the stretching is constant. This is a standard assumption in these kind of simplified models. However, its validity is doubtful if we take the anisotropy into account.

We remark that once the value of ι is known, one can use the most general formula (5.22) as a constitutive equation for the orientational transition rate and predict the fabric of any sample for which the history of the stretching is known.

5.3.6 The Recrystallization Fabrics

In the second chapter we reviewed the recrystallization models that were able to deduce the anisotropic behaviour of polycrystalline ice. There, we pointed out that GBM is the basic process that drives the different distributions of lattice orientations due to recrystallization. The main rule of GBM is that the crystallites which suffer the smaller amount of deformation are the first ones to recrystallize into another crystallite that is better oriented for deformation. In this chapter we remarked that the specific orientation production rate of mass, Γ^*, is able to model GBM: equation (5.18) models the GBM, schematically represented in Fig. 2.10. In order to achieve the goal to obtain a general form of the specific production rate of mass Γ^* it is important to build a scalar invariant by which we can extract the information on the lattice orientations that are better-oriented for deformation. To this end, use may be made of the results of the third chapter of this thesis. In that chapter, the scalar invariant able to give the same information was S_c. However, in Chapter 6, we will prove that the specific production rate of mass, Γ^*, is a constitutive function of the same form as ι^* (see (5.23)), namely,

$$\Gamma^*=\Gamma^*\left\{\varrho^*, D_{hk}D_{hk}, D_{hk}D_{km}D_{mh}, n_hD_{hk}n_k, n_hD_{hk}D_{kl}n_l\right\}. \tag{5.55}$$

Therefore, instead of S_c (a scalar invariant of the deviatoric stress tensor), we need a scalar invariant of the stretching tensor. Thus, because of the collinearity between the deviatoric stress and stretching, the analogue of the scalar invariant, D_c, of the stretching

tensor may be introduced. In analogy with definition of S_c in eqn. (3.46), we will define the following scalar invariant,

$$D_c\left(n_j\right) \equiv n_h D_{hk} D_{kl} n_l - \left(n_h D_{hk} n_k\right)^2, \tag{5.56}$$

that enjoys the property to be maximum for the orientations that represent the crystallites for which the deformation is largest and zero for the orientations that represent the crystallites for which the deformation is zero. In order to fulfil the conservation of mass in the form of equation (5.20), the most simple representation for the specific production rate of mass is the following,

$$\Gamma^* = \hat{\Gamma} \times \left(D_c - \varrho \langle D_c \rangle_n\right), \tag{5.57}$$

where the mean $\langle D_c \rangle_n$ is introduced in analogy with (5.6), i.e.,

$$\langle D_c \rangle_n \equiv \int_{\mathcal{S}^2} \frac{\varrho^*}{\varrho} D_c \, d^2 n. \tag{5.58}$$

In a first approximation, we can take $\hat{\Gamma}$ as a positive constant. The reason for this is simplicity and because the available experimental data can not guarantee verification of another more refined expression. The positiveness of $\hat{\Gamma}$ is, on the other hand, coherent with the actual experimental data. In fact, only if $\hat{\Gamma}$ is positive, we can guarantee that the production of mass is positive for the grains better-oriented for deformation and negative for the grains for which the deformation is more difficult. We remark that the explicit form of the specific orientation production rate of mass Γ^* of equation (5.57) is not coherent with the general form illustrated in eqn. (5.55). As for the explicit form of the specific size production rate of mass, $\Gamma^{\blacktriangleright}$, and of size transition rate, $w^{\blacktriangleright}$, Γ^* has a global dependence with respect to the variables belonging to the species assemblage. We will justify this in detail in Chapter 6, where all results will be derived from the general assumptions of a complete constitutive theory for this Mixture with Continuous Diversity.

An other important consideration must be addressed in this subsection. Experimental data give us the information that GBM does not occur in the whole ice-sheet. It is believed that the parameters able to switch on GBM are temperature and dislocation density. Therefore an explicit form for $\hat{\Gamma}$ must take temperature and dislocation density into account. In Chapter 6, we will explain how to include this dependence.

5.4 Conclusion

In the introduction of Chapter 2 we remarked how important it is to reach a relationship between age and depth of an ice core. We claim that an important step has been achieved in this direction of the solution of this problem. In fact, if the evolution equations for the distribution of lattice orientations discussed in this chapter are coupled with the anisotropic constitutive equations for the stretching discussed in chapter 3, then a simulation of the dynamics of an anisotropic ice-sheet can be achieved. Therefore, we claim that, once the parameterization of E, ι and $\hat{\Gamma}$ are performed with respect to temperature and dislocation density, then the problem to find a depth-age relationship, valid in any site of an anisotropic ice-sheet, can be considered to be solved from a theoretical point view. In other words, at that stage, a numerical simulation will be able to produce the required depth-age relationship.

Chapter 6

Constitutive Equations for Polycrystalline Materials

6.1 Introduction

The aim of this chapter is to find a thermodynamic justification of the results given in this thesis within the framework of the Theory of Mixtures with Continuous Diversity. To this end we analyse the Second Law of Thermodynamics and its restrictions on the Constitutive Equations. A constitutive theory is also presented and the analysis of Thermodynamic Equilibrium and the specialization to incompressible polycrystalline materials will conclude the Chapter.

6.2 The Second Law of Thermodynamics

The Second Law of Thermodynamics is stated as follows: for any thermodynamic process the specific (macroscopic) production rate of entropy ς is non-negative. Of course, an entropy balance can be established on every level of formulation, be this a micro or macro state, however, the inequality – namely that the entropy production is non-negative ($\varsigma \geqslant 0$) – must be satisfied at the highest level of homogenization that one applies, because the inequality contains the fields at that level. Thus, from (4.76), (4.78) and Table 4.2, we have

$$\varrho\left(x_i,t\right)\varsigma\left(x_i,t\right)=\int\limits_{\mathcal{S}^2}\int\limits_{\mathcal{I}}\varrho^{\triangleright}\left(x_i,t,n_j,D\right)\varsigma^{\triangleright}\left(x_i,t,n_j,D\right)dDd^2n\geqslant 0. \tag{6.1}$$

The imbalance (6.1) is the homogenized form of the Second Law of Thermodynamics. In order to deduce the explicit restrictions of this law on the level of constitutive equations (i.e., on the microscopic level), its local (microscopic) form is needed. To this end, by following Faria [36], we consider the case in which the RVE is composed only of crystallites with orientation $n_j=\tilde{n}_j$ and dimensionless grain-size $D=\tilde{D}$. Such a distribution can be mathematically represented by an orientation-and-size mass density $\varrho^{\triangleright}$ in terms of the Dirac delta function, i.e.,

$$\varrho^{\triangleright}\left(x_i,t,n_j,D\right)=\delta\left(n_j-\tilde{n}_j,D-\tilde{D}\right)\varrho\left(x_i,t\right).$$

In this case, the specific (microscopic) production rate of entropy will be denoted by $\varsigma^{\triangleright P}(x_i, t, n_j, D)$, for which we then deduce the entropy inequality from (6.1), viz.,

$$\int_{\mathcal{S}^2}\int_{\mathcal{I}} \delta\left(n_j - \tilde{n}_j, D - \tilde{D}\right) \varsigma^{\triangleright P}(x_i, t, n_j, D)\, dD d^2n = \varsigma^{\triangleright P}\left(x_i, t, \tilde{n}_j, \tilde{D}\right) \geqslant 0. \tag{6.2}$$

The above Gedanken Experiment can be done for all values of $\tilde{n}_j$ and $\tilde{D}$ in the species assemblage. So we may drop the tildes and simply write

$$\varsigma^{\triangleright P}(x_i, t, n_j, D) \geqslant 0. \tag{6.3}$$

If we then define the *entropy-production deviation* by

$$\delta^{\triangleright} \equiv \varsigma^{\triangleright} - \varsigma^{\triangleright P}, \tag{6.4}$$

then we have the wanted local (microscopic) form of the entropy inequality, i.e.,

$$\varsigma^{\triangleright} \geqslant \delta^{\triangleright}. \tag{6.5}$$

Equation (6.4) introduces a new function, $\delta^{\triangleright}$, defined at the micro level that may have either sign and eventually will have to be prescribed by a constitutive relation. This function is the result of the rescaling and expresses the fact that on the micro level the sign of the entropy production is not constrained.

6.3 Postulates of Constitutive Equations

6.3.1 Introduction

The constitutive theory we present in this section is general enough to comprehend all the results exposed in this thesis. Among the classical principles (the Rule of Equipresence, Determinism, Local Action and Material Indifference), we need another special postulate to take the new variables of the species assemblage into account, i.e., the Principle of Global Action.

The balance equations introduced in Chapter 4 need to be complemented by a set of constitutive equations. In fact (4.61-4.66) are a system of partial differential equations that is not closed and some quantities, called constitutive quantities, namely

$$S^{\triangleright} = \left\{w^{\triangleright}, \Gamma^{\triangleright}, t^{\triangleright}_{ij}, \tau^{\triangleright}_{ij}, F^{\triangleright}_i, \kappa^{\triangleright}_i, m^{\triangleright}_{il}, \varpi^{\triangleright}_{il}, a^{\triangleright}_i, \nu^{\triangleright}_i, e^{\triangleright}, q^{\triangleright}_i, \xi^{\triangleright}_i, h^{\triangleright}, \epsilon^{\triangleright}, \eta^{\triangleright}, \phi^{\triangleright}_j, \varphi^{\triangleright}_j, n^{\triangleright}, \Pi^{\triangleright}, \gamma^{\triangleright}_{dj}, \Delta^{\triangleright}_d, \delta^{\triangleright}\right\}, \tag{6.6}$$

have to be prescribed phenomenologically. As we have remarked in Chapter 4, the size transition rate, $w^{\triangleright}$, is a constitutive quantity. It can not, in fact, be related to any balance equation.

6.3.2 General Remarks and Rule of Equipresence

The prescription of the general constitutive quantity $S^{\triangleright}$ is connected only with the choice of the material. For this reason, the external supplies are not considered constitutive quantities; they are in fact related to external driving mechanisms. A general constitutive

quantity, say $S^{\triangleright}$, has a certain value once one fixes a point in the time-position-species assemblage (t, x_i, n_j, D); from this point of view $S^{\triangleright}$ is a function of t, x_i, n_j and D, i.e.,

$$S^{\triangleright} = \overline{S}^{\triangleright}(t, x_i, n_j, D).$$

However, experience shows that a material can not be characterized by the prescription of such a function. A very general assumption is to regard the constitutive quantity $S^{\triangleright}$ at a given point (t, x_i, n_j, D) as a function of the following functions (i.e., as a functional G): of a general point in the time-position-species assemblage $\left(\breve{t}, \breve{x}_i, \breve{n}_j, \breve{D}\right)$ (to be distinguished from (t, x_i, n_j, D)), of velocity $v_i^{\triangleright}\left(\breve{t}, \breve{x}_i, \breve{n}_j, \breve{D}\right)$, of orientation-transition rate $u_i^{\triangleright}\left(\breve{t}, \breve{x}_i, \breve{n}_j, \breve{D}\right)$, of orientation-and-size mass density $\varrho^{\triangleright}\left(\breve{t}, \breve{x}_i, \breve{n}_j, \breve{D}\right)$, of temperature $T^{\triangleright}\left(\breve{t}, \breve{x}_i, \breve{n}_j, \breve{D}\right)$ and of dislocation density $\rho_d^{\triangleright}\left(\breve{t}, \breve{x}_i, \breve{n}_j, \breve{D}\right)$. We remark that, in this way, the *rule of equipresence* is automatically fulfilled. Thus, the representation of a general constitutive quantity $S^{\triangleright}$ for a given point (t, x_i, n_j, D) is as follows:

$$\overline{S}^{\triangleright}(t, x_i, n_j, D) = G\left(\begin{array}{c} \breve{t}, \breve{x}_i, \breve{n}_j, \breve{D}; v_i^{\triangleright}\left(\breve{t}, \breve{x}_i, \breve{n}_j, \breve{D}\right), u_i^{\triangleright}\left(\breve{t}, \breve{x}_i, \breve{n}_j, \breve{D}\right), \\ \varrho^{\triangleright}\left(\breve{t}, \breve{x}_i, \breve{n}_j, \breve{D}\right), T^{\triangleright}\left(\breve{t}, \breve{x}_i, \breve{n}_j, \breve{D}\right), \rho_d^{\triangleright}\left(\breve{t}, \breve{x}_i, \breve{n}_j, \breve{D}\right) \end{array}\right). \tag{6.7}$$

6.3.3 The Principle of Determinism and Local Action

The *Principle of Determinism* implies that the value of $S^{\triangleright}$ at time t can depend on the times $\breve{t}$ such that $\breve{t} \leq t$. Generally, such a dependence is assumed to hold only for times $\breve{t}$ that are very close to t. This implies that a Taylor series expansion with respect to time can be applied to the functional G in (6.7). We will interrupt such an expansion[1] at zeroth order, i.e., we will approximate the functional G by its value at $\breve{t} = t$.

The *Principle of Local Action* implies that the dependence upon $\breve{x}_i$ should be restricted to the neighbourhood of x_i. This implies that we can apply a similar Taylor series expansion, but this time with respect to $\breve{x}_i$ (instead of $\breve{t}$) and in the neighbourhood of x_i (instead of t), of the functional G in (6.7). We will terminate such expansions at zeroth order for all fields on the right-hand side of (6.7) except for the velocity and temperature, for which the expansion will terminate at the first order.

Generally, the Principles of Determinism and of Local Action determine a change and a simplification of the set of fields appearing on the right-hand side of (6.7). Table 6.1 has been built to illustrate these changes. We now explain how such a reduction works for the velocity field, but omit the other cases because the reasonings are analogous. The Principle of Determinism approximates the velocity field $v_i^{\triangleright}\left(\breve{t}, \breve{x}_i, \breve{n}_j, \breve{D}\right)$ evaluated at $\breve{t}$ with the same field evaluated at t. This causes a trivial change from $v_i^{\triangleright}\left(\breve{t}, \breve{x}_i, \breve{n}_j, \breve{D}\right)$ to $v_i^{\triangleright}\left(t, \breve{x}_i, \breve{n}_j, \breve{D}\right)$ that is illustrated in Table 6.1 in the passage from the first to the third column. In the second column the arrow $\overset{t}{\rightarrow}$ has the meaning to recall a Taylor series expansion with respect to time. The Principle of Local Action approximates the velocity

[1] We remark that $\breve{x}_i$, $\breve{n}_i$ and $\breve{D}$ are not functions of $\breve{t}$ (they are independent variables!) and we will not expand them.

Table 6.1: Scheme explaining how the functions on the right-hand side of (6.7) change when the Principles of Determinism and Local Action are accounted for. The explanation for the velocity field is stated in the text. The arguments for the other cases are analogous.

$\breve{t}$	$\overset{t}{\rightarrow}$	t	$\overset{x}{\rightarrow}$	t
$\breve{x}_i$	$\overset{t}{\rightarrow}$	$\breve{x}_i$	$\overset{x}{\rightarrow}$	x_i
$\breve{n}_j$	$\overset{t}{\rightarrow}$	$\breve{n}_j$	$\overset{x}{\rightarrow}$	$\breve{n}_j$
$\breve{D}$	$\overset{t}{\rightarrow}$	$\breve{D}$	$\overset{x}{\rightarrow}$	$\breve{D}$
$v_i^{\triangleright}\left(\breve{t},\breve{x}_i,\breve{n}_j,\breve{D}\right)$	$\overset{t}{\rightarrow}$	$v_i^{\triangleright}\left(t,\breve{x}_i,\breve{n}_j,\breve{D}\right)$	$\overset{x}{\rightarrow}$	$\begin{cases} v_i^{\triangleright}\left(t,x_i,\breve{n}_j,\breve{D}\right) \\ L_{ij}^{\triangleright}\left(t,x_i,\breve{n}_j,\breve{D}\right) \end{cases}$
$u_i^{\triangleright}\left(\breve{t},\breve{x}_i,\breve{n}_j,\breve{D}\right)$	$\overset{t}{\rightarrow}$	$u_i^{\triangleright}\left(t,\breve{x}_i,\breve{n}_j,\breve{D}\right)$	$\overset{x}{\rightarrow}$	$u_i^{\triangleright}\left(t,x_i,\breve{n}_j,\breve{D}\right)$
$\varrho^{\triangleright}\left(\breve{t},\breve{x}_i,\breve{n}_j,\breve{D}\right)$	$\overset{t}{\rightarrow}$	$\varrho^{\triangleright}\left(t,\breve{x}_i,\breve{n}_j,\breve{D}\right)$	$\overset{x}{\rightarrow}$	$\varrho^{\triangleright}\left(t,x_i,\breve{n}_j,\breve{D}\right)$
$T^{\triangleright}\left(\breve{t},\breve{x}_i,\breve{n}_j,\breve{D}\right)$	$\overset{t}{\rightarrow}$	$T^{\triangleright}\left(t,\breve{x}_i,\breve{n}_j,\breve{D}\right)$	$\overset{x}{\rightarrow}$	$\begin{cases} T^{\triangleright}\left(t,x_i,\breve{n}_j,\breve{D}\right) \\ T_{,i}^{\triangleright}\left(t,x_i,\breve{n}_j,\breve{D}\right) \end{cases}$
$\rho_d^{\triangleright}\left(\breve{t},\breve{x}_i,\breve{n}_j,\breve{D}\right)$	$\overset{t}{\rightarrow}$	$\rho_d^{\triangleright}\left(t,\breve{x}_i,\breve{n}_j,\breve{D}\right)$	$\overset{x}{\rightarrow}$	$\rho_d^{\triangleright}\left(t,x_i,\breve{n}_j,\breve{D}\right)$

field $v_i^{\triangleright}\left(t,\breve{x}_i,\breve{n}_j,\breve{D}\right)$ evaluated at $\breve{x}_i$ by a Taylor series expansion in the neighbourhood of x_i truncated at first order. If we define the gradient of velocity by

$$L_{ij}^{\triangleright}\left(t,x_i,n_j,D\right) \equiv \left[v_i^{\triangleright}\left(t,x_i,n_j,D\right)\right]_{,j},$$

then such a Taylor series expansion is given by

$$v_i^{\triangleright}\left(t,\breve{x}_i,\breve{n}_j,\breve{D}\right) = v_i^{\triangleright}\left(t,x_i,\breve{n}_j,\breve{D}\right) + \left(\breve{x}_k - x_k\right) L_{ik}^{\triangleright}\left(t,x_i,\breve{n}_j,\breve{D}\right) + O\left(|\breve{x}_i - x_i|^2\right). \quad (6.8)$$

Generally we try to avoid a dependence of the constitutive quantity $\overline{S}^{\triangleright}\left(t,x_i,n_j,D\right)$ on positions $\breve{x}_i$ different from x_i. For this reason we can split the dependence upon the right-hand side of (6.8) into the two fields $v_i^{\triangleright}\left(t,x_i,\breve{n}_j,\breve{D}\right)$ and $L_{ik}^{\triangleright}\left(t,x_i,\breve{n}_j,\breve{D}\right)$, that have the suitable characteristics to be evaluated at x_i. The splitting is illustrated in Table 6.1 from the third to the fifth column. In the fourth column the arrow $\overset{x}{\rightarrow}$ is to recall a Taylor series expansion with respect to position.

Thus, the representation for the general constitutive quantity $S^{\triangleright}$ in equation (6.7) changes according to the rules of Table 6.1. Each column of this table introduces a new and simpler constitutive class. We restrict considerations to the simplest class exhibited by the last column, that we will denote by $\mathfrak{R}$, i.e.,

$$\mathfrak{R} = \breve{\mathfrak{R}}\left(\breve{n}_j,\breve{D}\right) \equiv \begin{pmatrix} t,x_i,\breve{n}_j,\breve{D};v_i^{\triangleright}\left(t,x_i,\breve{n}_j,\breve{D}\right),L_{ij}^{\triangleright}\left(t,x_i,\breve{n}_j,\breve{D}\right),u_i^{\triangleright}\left(t,x_i,\breve{n}_j,\breve{D}\right), \\ \varrho^{\triangleright}\left(t,x_i,\breve{n}_j,\breve{D}\right),T^{\triangleright}\left(t,x_i,\breve{n}_j,\breve{D}\right),T_{,i}^{\triangleright}\left(t,x_i,\breve{n}_j,\breve{D}\right),\rho_d^{\triangleright}\left(t,x_i,\breve{n}_j,\breve{D}\right) \end{pmatrix}. \quad (6.9)$$

Thus, the general constitutive equation (6.7) is simplified as follows:

$$\overline{S}^{\triangleright}\left(t, x_i, n_j, D\right) = \tilde{G}\left(\Re\right), \tag{6.10}$$

where $\tilde{G}$ is a functional (generally different from G) of the functions $\Re$ listed in (6.9).

6.3.4 The Principle of Global Action

An extended Principle of Local Action should also be formulated for the species assemblage variables $\breve{n}_j$ and $\breve{D}$. However, whereas it is reasonable that the interaction between positions that are very close to each other[2] can affect constitutive relations, the interaction in the species assemblage is unrelated to the distance in the species assemblage itself. In fact, crystallites with very close positions can interact with each other because they are in contact and the Principle of Local Action makes sense in the space of positions. On the other hand, crystallites with very close orientations and grain sizes, generally, are unrelated and the validity of a similar Principle of Local Action also for the species assemblage is questionable. This was recognized since the first paper on the Theory of Mixtures with Continuous Diversity by Faria [36] and to overcome this problem he introduces, instead of a Principle of Local Action, a sort of *Principle of Global Action*. In this chapter, we will assume the validity of this principle but we formulate it in a different way in order to deduce the results achieved in Chapters 3, 4 & 5. In the previous subsection, we have seen that the Principle of Determinism and Local Action implied a simplification for the class of variables from which the constitutive function, $S^{\triangleright}$, depends. Here, we substitute the class $\breve{\Re}\left(\breve{n}_j, \breve{D}\right)$, evaluated in $\breve{n}_j$ and $\breve{D}$, by the same variables $\breve{\Re}\left(n_j, D\right)$, evaluated in n_j and D, and by the set of global variables $\beta_a\left(t, x_i\right)$, defined as follows,

$$\beta_a\left(t, x_i\right) = \int_{\mathcal{S}^2}\int_{\mathcal{I}} \mathrm{B}_a\left[\breve{\Re}\left(\breve{n}_j, \breve{D}\right)\right] d\breve{D}d^2\breve{n}. \tag{6.11}$$

The number of functions β_a (i.e., the number of values that $a \in \mathbb{N}$ can have) is arbitrary and must be chosen in the solution of the given problem. The definitions of the functions β_a depend on the definitions of the functionals B_a. In the following we give four examples.

$$\begin{aligned}
&\mathrm{B}_0 = \varrho^{\triangleright}\left(t, x_i, \breve{n}_j, \breve{D}\right) && \Longrightarrow \beta_0\left(t, x_i\right) = \varrho\left(t, x_i\right), \\
&\mathrm{B}_1 = D_c\left(\breve{n}_j\right)\varrho^{\triangleright}\left(t, x_i, \breve{n}_j, \breve{D}\right) && \Longrightarrow \beta_1\left(t, x_i\right) = \varrho\left(t, x_i\right)\left\langle D_c\left(\breve{n}_j\right)\right\rangle_{\breve{n}}, \\
&\mathrm{B}_2 = \breve{D}\ \varrho^{\triangleright}\left(t, x_i, \breve{n}_j, \breve{D}\right) && \Longrightarrow \beta_2\left(t, x_i\right) = \left\langle D\right\rangle \varrho\left(t, x_i\right), \\
&\mathrm{B}_3 = \breve{D}^2\varrho^{\triangleright}\left(t, x_i, \breve{n}_j, \breve{D}\right) && \Longrightarrow \beta_3\left(t, x_i\right) = \left\langle D^2\right\rangle_D \varrho\left(t, x_i\right),
\end{aligned} \tag{6.12}$$

where all the symbols have been introduced before. We observe that β_0 is the classical (macroscopic) mass density. With β_1, we easily derive the scalar invariant $\langle D_c\rangle_n$ introduced in (5.58) and used in the constitutive equation (5.57) for the orientation production rate of mass to model recrystallization phenomena related to Grain Boundary Migration (GBM). The variable β_1 also allows us to derive the analog of the scalar invariant defined in Chapter 3 in equation (3.53) if a stress-formulation of the flow law is implemented

[2] In other words, positions between which the distance is very small.

instead of the stretching-formulation[3]. Besides, β_2 and β_3 allows us to derive those variables we used in Chapter 5 to give the constitutive relations (5.12) and (5.16) for the size transition rate and for the size production rate of mass, respectively. Finally, we observe that the dependence of the gradient of the velocity $L^{\triangleright}_{ij}$ can be split into two contributions: the respective symmetric part (strain rate or stretching tensor) $D^{\triangleright}_{ij} \equiv L^{\triangleright}_{(ij)}$ and the skew-symmetric part (the rotation tensor of equation (4.47)), $W^{\triangleright}_{ij} = L^{\triangleright}_{[ij]}$. Furthermore, $(4.51)_1$ allows us to use the skew-symmetric tensor $S^{\triangleright}_{ij}$ associated with the spin velocity instead of the orientation-transition rate $u^{\triangleright}_i$. Thus, the functional (6.7) or (6.10) is simplified as expressed by the following relation,

$$\overline{S}^{\triangleright}\left(t, x_i, n_j, D\right) = \hat{S}^{\triangleright}\left(t, x_i, n_j, D, v^{\triangleright}_i, D^{\triangleright}_{ij}, W^{\triangleright}_{ij}, S^{\triangleright}_{ij}, \varrho^{\triangleright}, \beta_a, T^{\triangleright}, T^{\triangleright}_{,i}, \rho^{\triangleright}_d\right). \tag{6.13}$$

6.3.5 The Principle of Material Frame Indifference

The *Principle of Material Frame Indifference* will provide further restrictions. The transformation rules, obeyed by the quantities involved in (6.6) and (6.13) under Euclidean changes of the reference frames, are

$$\left\{\begin{array}{l}
t' = t + \chi, \quad x'_i = b_i + O_{ij}x_j, \quad n'_i = O_{ij}n_j, \quad D' = D, \\
v^{\triangleright\prime}_i = \dot{b}_i + \dot{O}_{ij}x_j + O_{ij}v^{\triangleright}_j, \quad D^{\triangleright\prime}_{ij} = O_{ik}D^{\triangleright}_{kl}O_{lj}, \\
W^{\triangleright\prime}_{ij} = O_{ik}O_{jl}W^{\triangleright}_{kl} + \dot{O}_{ik}O_{jk}, \quad S^{\triangleright\prime}_{ij} = O_{ik}O_{jl}S^{\triangleright}_{kl} + \dot{O}_{ik}O_{jk}, \\
\varrho^{\triangleright\prime} = \varrho^{\triangleright}, \quad \beta'_a = \beta_a, \quad T^{\triangleright\prime} = T^{\triangleright}, \quad T^{\triangleright\prime}_{,i} = O_{ij}T^{\triangleright}_{,j}, \quad \rho^{\triangleright\prime}_d = \rho^{\triangleright}_d, \quad w^{\triangleright\prime} = w^{\triangleright}, \\
\Gamma^{\triangleright\prime} = \Gamma^{\triangleright}, \quad t^{\triangleright\prime}_{ij} = O_{ik}t^{\triangleright}_{kl}O_{lj}, \quad \tau^{\triangleright\prime}_{ij} = O_{ik}\tau^{\triangleright}_{kl}O_{lj}, \quad F^{\triangleright\prime}_i = O_{ij}F^{\triangleright}_j, \quad \kappa^{\triangleright\prime}_i = O_{ij}\kappa^{\triangleright}_j, \\
m^{\triangleright\prime}_{ij} = sO_{ik}m^{\triangleright}_{kl}O_{lj}, \quad \varpi^{\triangleright\prime}_{ij} = sO_{ik}\varpi^{\triangleright}_{kl}O_{lj}, \quad a^{\triangleright\prime}_i = sO_{ij}a^{\triangleright}_j, \quad \nu^{\triangleright\prime}_i = sO_{ij}\nu^{\triangleright}_j, \\
e^{\triangleright\prime} = e^{\triangleright}, \quad q^{\triangleright\prime}_i = O_{ij}q^{\triangleright}_j, \quad \xi^{\triangleright\prime}_i = O_{ij}\xi^{\triangleright}_j, \quad h^{\triangleright\prime} = h^{\triangleright}, \quad \epsilon^{\triangleright\prime} = \epsilon^{\triangleright}, \\
\eta^{\triangleright\prime} = \eta^{\triangleright}, \quad \phi^{\triangleright\prime}_i = O_{ij}\phi^{\triangleright}_j, \quad \varphi^{\triangleright\prime}_i = O_{ij}\varphi^{\triangleright}_j, \quad n^{\triangleright\prime} = n^{\triangleright}, \\
\Pi^{\triangleright\prime} = \Pi^{\triangleright}, \quad \gamma^{\triangleright\prime}_{di} = O_{ij}\gamma^{\triangleright}_{dj}, \quad \Delta^{\triangleright\prime}_d = \Delta^{\triangleright}_d, \quad \delta^{\triangleright\prime} = \delta^{\triangleright},
\end{array}\right. \tag{6.14}$$

where χ, $b_i(t)$, $O_{ij}(t)$ are an arbitrary scalar, vector and orthogonal tensor, respectively, that define the change of the frame of reference. The accented quantities are evaluated in the moving frame of reference and s is the determinant, $s = \det \mathbf{O}$, of the orthogonal tensor O_{ij}. The arbitrariness of χ, $b_i(t)$ and $O_{ij}(t)$ implies, together with the first and second relations of the first row of (6.14) and with the third row of (6.14) that t and x_i have to be excluded in the list of functions on the right-hand side of (6.13) and that $W^{\triangleright}_{ij}$ and $S^{\triangleright}_{ij}$ have to be taken into account only through their difference $S^{\triangleright}_{ij} - W^{\triangleright}_{ij}$, i.e., through the relative spin tensor, $H^{\triangleright}_{ij} = S^{\triangleright}_{ij} - W^{\triangleright}_{ij}$, defined in (4.53). The condition $D^{\triangleright}_{hh} = 0$ (in case of no microstructural dependence of the velocity field, $v^{\triangleright}_i = v_i$, is compelling due

[3]In Section 4.7 we have remarked that the two formulations are analogous.

to incompressibility and) will henceforth not explicitly be incorporated, but this will be done implicitly, and so it will not be assumed *ab initio* that $D^{\triangleright}_{hh}$ vanishes. However, to put the $D^{\triangleright}_{hh}$-dependence in evidence, it is convenient to split the stretching tensor $D^{\triangleright}_{ij}$ in (6.13) into its deviatoric part $D^{\triangleright}_{\langle ij\rangle}$, according to the notation stated in (1.1), and its trace $D^{\triangleright}_{hh}$, i.e.,

$$D^{\triangleright}_{ij} = D^{\triangleright}_{\langle ij\rangle} + \frac{1}{3}\delta_{ij} D^{\triangleright}_{hh}. \tag{6.15}$$

We remark that the assumption that the global variables β_a are scalar invariants, $\beta'_a = \beta_a$, implies the impossibility to take into account an explicit dependence of the constitutive quantities $S^{\triangleright}$ with respect to diffusive terms such as $v^{\triangleright}_i - v_i$. However, this can not be considered a weak point of the present formulation because we will assume later on, as it is obvious for polycrystalline materials, the microstructural independence of the velocity field, i.e. $v^{\triangleright}_i = v_i$. Thus, the constitutive relations (6.13) can be written as follows

$$\bar{S}^{\triangleright}\left(t, x_i, n_j, D\right) = J^{\triangleright}\left(n_j, D; \varrho^{\triangleright}, \beta_a, D^{\triangleright}_{\langle ij\rangle}, D^{\triangleright}_{hh}, H^{\triangleright}_{ij}, T^{\triangleright}, T^{\triangleright}_{,i}, \rho^{\triangleright}_d\right) \equiv J^{\triangleright}\left(\mathcal{X}\right).\mathcal{X} \tag{6.16}$$

All variables in (6.6) transform under a Euclidian change of frame as objective polar or axial tensors (of zeroth, first or second rank). Thus, further restrictions of the Principle of Material Frame Indifference will be given by the application of the representation theorem of isotropic functions. We will analyse this problem in Section 6.5.

Further restrictions follow from the Second Law of Thermodynamics (6.5). We will analyse them in the next section.

6.4 Exploitation of the Second Law of Thermodynamics

We exploit the 2nd Law of Thermodynamics by following the method of Lagrange multipliers proposed by Liu [88]. To this end, as we have remarked in the previous section, the restrictions of this law to the Constitutive Equations are independent upon the external supplies. Thus, in this section, we will set them equal to zero. If we substitute $S^{\triangleright}_{ij}$ everywhere following the definition of the relative spin tensor (4.53), replace $D^{\triangleright}_{jk}$ by (6.15), use the formulae (4.51), $(4.54)_{1,2}$ and (6.5), the balance equations (4.61-4.66) can be written as follows:

$$\begin{gathered} B^{\triangleright}_{m} \equiv \partial_t \varrho^{\triangleright} + \varrho^{\triangleright}_{,i} v^{\triangleright}_i + \varrho^{\triangleright} v^{\triangleright}_{i,i} + \left(\partial_i \varrho^{\triangleright}\right) u^{\triangleright}_i \\ + \varrho^{\triangleright}\left(\partial_i H^{\triangleright}_{ik}\right) n_k + \varrho^{\triangleright}\left(\partial_i W^{\triangleright}_{ik}\right) n_k + \left(\partial_D \varrho^{\triangleright}\right) w^{\triangleright} + \varrho^{\triangleright} \partial_D w^{\triangleright} - \varrho^{\triangleright} \Gamma^{\triangleright} = 0, \end{gathered} \tag{6.17}$$

$$\begin{gathered} B^{\triangleright}_{l\,i} \equiv \varrho^{\triangleright} \partial_t v^{\triangleright}_i + \varrho^{\triangleright} v^{\triangleright}_{i,j} v^{\triangleright}_j + \varrho^{\triangleright}\left(\partial_j v^{\triangleright}_i\right) u^{\triangleright}_j + \varrho^{\triangleright}\left(\partial_D v^{\triangleright}_i\right) w^{\triangleright} \\ - t^{\triangleright}_{ij,j} - \partial_j \tau^{\triangleright}_{ij} - \partial_D F^{\triangleright}_i - \varrho^{\triangleright}\left(\kappa^{\triangleright}_i - v^{\triangleright}_i \Gamma^{\triangleright}\right) = 0, \end{gathered} \tag{6.18}$$

$$\begin{gathered} B^{\triangleright}_{a\,i} \equiv \varrho^{\triangleright} \partial_t \sigma^{\triangleright}_i + \varrho^{\triangleright} \sigma^{\triangleright}_{i,j} v^{\triangleright}_j + \varrho^{\triangleright}\left(\partial_j \sigma^{\triangleright}_i\right) u^{\triangleright}_j + \varrho^{\triangleright}\left(\partial_D \sigma^{\triangleright}_i\right) w^{\triangleright} \\ - \varepsilon_{ilk} t^{\triangleright}_{kl} - m^{\triangleright}_{il,l} - \partial_l \varpi^{\triangleright}_{il} - \partial_D a^{\triangleright}_i - \varrho^{\triangleright}\left(\nu^{\triangleright}_i - \sigma^{\triangleright}_i \Gamma^{\triangleright}\right) = 0, \end{gathered} \tag{6.19}$$

$$
\begin{aligned}
B_e^{\triangleright} \equiv\ & \varrho^{\triangleright}\partial_t e^{\triangleright} + \varrho^{\triangleright} e^{\triangleright}_{,i} v_i^{\triangleright} + \varrho^{\triangleright}\left(\partial_j e^{\triangleright}\right) u_j^{\triangleright} + \varrho^{\triangleright}\left(\partial_{D} e^{\triangleright}\right) w^{\triangleright} + q^{\triangleright}_{i,i} \\
& - m^{\triangleright}_{ji}\left(\tfrac{1}{2}\varepsilon_{kjb} H^{\triangleright}_{kb,i} + \tfrac{1}{2}\varepsilon_{kjb} W^{\triangleright}_{kb,i}\right) + \partial_i \xi_i^{\triangleright} - \varpi^{\triangleright}_{ji}\left(\tfrac{1}{2}\varepsilon_{kjb}\partial_i H^{\triangleright}_{kb} + \tfrac{1}{2}\varepsilon_{kjb}\partial_i W^{\triangleright}_{kb}\right) \\
& + H^{\triangleright}_{jk} t^{\triangleright}_{[jk]} - D^{\triangleright}_{\langle jk\rangle} t^{\triangleright}_{\langle jk\rangle} - \frac{1}{3} D^{\triangleright}_{aa} t^{\triangleright}_{(bb)} - \tau^{\triangleright}_{ji}\left(\partial_i v_j^{\triangleright}\right) - \tfrac{1}{2}\varrho^{\triangleright}\Gamma^{\triangleright} v_i^{\triangleright} v_i^{\triangleright} - \tfrac{1}{2}\varrho^{\triangleright}\Gamma^{\triangleright}\sigma_i^{\triangleright} s_i^{\triangleright} \\
& + \partial_{D} h^{\triangleright} - F_j^{\triangleright}\partial_{D} v_j^{\triangleright} - a_j^{\triangleright}\partial_{D} s_j^{\triangleright} - \varrho^{\triangleright}\left(\epsilon^{\triangleright} - \Gamma^{\triangleright} e^{\triangleright}\right) = 0,
\end{aligned}
\tag{6.20}
$$

$$
\begin{aligned}
B_d^{\triangleright} \equiv\ & \partial_t \rho_d^{\triangleright} + \rho^{\triangleright}_{d,i} v_i^{\triangleright} + \rho_d^{\triangleright} v^{\triangleright}_{i,i} + \left(\partial_i \rho_d^{\triangleright}\right) u_i^{\triangleright} + \rho_d^{\triangleright}\left(\partial_i H^{\triangleright}_{ik}\right) n_k \\
& + \rho_d^{\triangleright}\left(\partial_i W^{\triangleright}_{ik}\right) n_k + \left(\partial_{D}\rho_d^{\triangleright}\right) w^{\triangleright} + \rho_d^{\triangleright}\partial_{D} w^{\triangleright} + \partial_j \gamma^{\triangleright}_{jd} + \partial_{D}\Delta_d^{\triangleright} - \Pi^{\triangleright} = 0,
\end{aligned}
\tag{6.21}
$$

$$
\begin{aligned}
B_\eta^{\triangleright} \equiv\ & \varrho^{\triangleright}\partial_t \eta^{\triangleright} + \varrho^{\triangleright}\eta^{\triangleright}_{,i} v_i^{\triangleright} + \varrho^{\triangleright}\left(\partial_j^{\triangleright}\eta^{\triangleright}\right) u_j^{\triangleright} + \varrho^{\triangleright}\left(\partial_{D}\eta^{\triangleright}\right) w^{\triangleright} \\
& + \phi^{\triangleright}_{j,j} + \partial_j \varphi_j^{\triangleright} + \partial_{D} n^{\triangleright} - \varrho^{\triangleright}\delta^{\triangleright} + \varrho^{\triangleright}\Gamma^{\triangleright}\eta^{\triangleright} \geq 0.
\end{aligned}
\tag{6.22}
$$

With these definitions the prescription in Liu [88] for the exploitation of the 2nd Law of Thermodynamics is given by the statement

$$
B_\eta^{\triangleright} - \Lambda_m^{\triangleright} B_m^{\triangleright} - \Lambda_{l\,i}^{\triangleright} B_{l\,i}^{\triangleright} - \Lambda_{a\,i}^{\triangleright} B_{a\,i}^{\triangleright} - \Lambda_e^{\triangleright} B_e^{\triangleright} - \Lambda_d^{\triangleright} B_d^{\triangleright} \geq 0, \quad \text{(no sum over } m,\ l,\ a,\ e \text{ and } d\text{)} \tag{6.23}
$$

where $\Lambda_m^{\triangleright}$, $\Lambda_{l\,i}^{\triangleright}$, $\Lambda_{a\,i}^{\triangleright}$, $\Lambda_e^{\triangleright}$ and $\Lambda_d^{\triangleright}$ are the Lagrange multipliers, the sum is intended only on the index i and where the independent field variables in (6.23) are unconstrained and may have any value. The Lagrange multipliers must be determined in the process of exploiting the Entropy Principle. However, they can have *ab initio* an arbitrary form regardless of the validity of the inequality (6.23): they can be constant or they can depend upon every variables appearing in the Balance Equations in their form (6.17-6.22). This last case is very complicated to handle, but the restrictions are complete. On the other hand, the case in which the Lagrange multipliers are constant is simpler, but the results are too restrictive. A satisfactory compromise is to assume for them the same dependence as for the constitutive quantities, i.e.,

$$
\left\{\Lambda_m^{\triangleright}, \Lambda_{l\,i}^{\triangleright}, \Lambda_{a\,i}^{\triangleright}, \Lambda_e^{\triangleright}, \Lambda_d^{\triangleright}\right\} = L\left(n_j, D; \varrho^{\triangleright}, \beta_a, D^{\triangleright}_{\langle ij\rangle}, D^{\triangleright}_{hh}, H^{\triangleright}_{ij}, T^{\triangleright}, T^{\triangleright}_{,i}, \rho_d^{\triangleright}\right) = L\left(\mathcal{X}\right). \tag{6.24}
$$

Moreover, experience with simpler systems has shown that the Lagrange multiplier $\Lambda_e^{\triangleright}$ of the energy balance is in those cases a universal function of the empirical temperature. Motivated by this, we shall now assume that this is so here too and set $\Lambda_e^{\triangleright}$ equal to a non-constant function of the temperature $T^{\triangleright}$, i.e.,

$$
\frac{\partial \Lambda_e^{\triangleright}}{\partial T^{\triangleright}} \neq 0 \tag{6.25}
$$

If we substitute (6.17-6.22) into (6.23) and perform all derivative operations that follow from applying the chain rule of differentiation when formally substituting the constitutive relations in the form of (6.16), then the entropy inequality takes the form

$$
a_i \mathcal{Y}_i + \Omega \geq 0, \quad \text{where} \quad a = \hat{a}_i\left(\mathcal{X}\right), \quad \Omega = \hat{\Omega}\left(\mathcal{X}\right); \tag{6.26}
$$

this inequality is linear in $\mathcal{Y}_i$ given by the following very long list of variables, i.e.,

$$\mathcal{Y}_i = \left\{ \begin{array}{c} \partial_t \varrho^{\triangleright}, \partial_t \beta_a, \partial_t v_i^{\triangleright}, \partial_t D^{\triangleright}_{\langle ij\rangle}, \partial_t D^{\triangleright}_{kk}, \partial_t H^{\triangleright}_{ij}, \partial_t s_i^{\triangleright}, \partial_t T^{\triangleright}, \partial_t T^{\triangleright}_{,i}, \partial_t \rho_d^{\triangleright}, \\ \\ \varrho^{\triangleright}_{,i}, \beta_{a\,,i}, D^{\triangleright}_{\langle hk\rangle,i}, D^{\triangleright}_{kk,i}, W^{\triangleright}_{kb,i}, H^{\triangleright}_{kb,i}, T^{\triangleright}_{,hi}, \rho^{\triangleright}_{d,i}, \\ \\ \partial_j \varrho^{\triangleright}, \partial_i v_j^{\triangleright}, \partial_j D^{\triangleright}_{\langle hk\rangle}, \partial_j D^{\triangleright}_{kk}, \partial_j W^{\triangleright}_{hk}, \partial_j H^{\triangleright}_{hk}, \partial_j T^{\triangleright}, \partial_j T^{\triangleright}_{,i}, \partial_j \rho_d^{\triangleright}, \\ \\ \partial_D \varrho^{\triangleright}, \partial_D v_i^{\triangleright}, \partial_D s_i^{\triangleright}, \partial_D D^{\triangleright}_{\langle hk\rangle}, \partial_D D^{\triangleright}_{kk}, \partial_D H^{\triangleright}_{hk}, \partial_D T^{\triangleright}, \partial_D T^{\triangleright}_{,i}, \partial_D \rho_d^{\triangleright}. \end{array} \right. \tag{6.27}$$

Proposition (6.26) must be identically satisfied for every value of $\mathcal{Y}_i$ listed in (6.27). This means that $a_i \equiv 0$, which are the so-called Liu Equations, that can be shown to be explicitly given by[4]

$$\left. \begin{array}{c} \Lambda^{\triangleright}_{li} = 0, \quad \Lambda^{\triangleright}_{a\,i} = 0, \quad m^{\triangleright}_{ji} = 0, \quad \tau^{\triangleright}_{ji} = 0, \quad F^{\triangleright}_{j} = 0, \quad a^{\triangleright}_{j} = 0, \\ \\ \tfrac{1}{2}\Lambda^{\triangleright}_{e}\varpi^{\triangleright}_{aj}\varepsilon_{hak} = \left(\Lambda^{\triangleright}_{m}\varrho^{\triangleright} + \Lambda^{\triangleright}_{d}\rho^{\triangleright}_{d}\right)\delta_{j[h}n_{k]}, \end{array} \right\} \tag{6.28}$$

and

$$\left. \begin{array}{c} \dfrac{\partial \eta^{\triangleright}}{\partial x} - \Lambda^{\triangleright}_{e}\dfrac{\partial e^{\triangleright}}{\partial x} = \dfrac{\Lambda^{\triangleright}_{m}}{\varrho^{\triangleright}}\delta_{x\varrho^{\triangleright}} + \dfrac{\Lambda^{\triangleright}_{d}}{\varrho^{\triangleright}}\delta_{x\rho^{\triangleright}_{d}}, \quad \dfrac{\partial \phi^{\triangleright}_{i}}{\partial y} - \Lambda^{\triangleright}_{e}\dfrac{\partial q^{\triangleright}_{i}}{\partial y} = 0, \\ \\ \dfrac{\partial \varphi^{\triangleright}_{j}}{\partial z} - \Lambda^{\triangleright}_{e}\dfrac{\partial \xi^{\triangleright}_{j}}{\partial z} - \Lambda^{\triangleright}_{d}\dfrac{\partial \gamma^{\triangleright}_{j\,d}}{\partial z} = 0, \quad \dfrac{\partial n^{\triangleright}}{\partial z} - \Lambda^{\triangleright}_{e}\dfrac{\partial h^{\triangleright}}{\partial z} - \Lambda^{\triangleright}_{d}\dfrac{\partial \Delta^{\triangleright}_{d}}{\partial z} = \left(\Lambda^{\triangleright}_{m}\varrho^{\triangleright} + \Lambda^{\triangleright}_{d}\rho^{\triangleright}_{d}\right)\dfrac{\partial w^{\triangleright}}{\partial z}, \end{array} \right\} \tag{6.29}$$

in which x, y and z are the collective variables

$$\left. \begin{array}{l} x = \left\{\varrho^{\triangleright}, \beta_a, D^{\triangleright}_{ij}, H^{\triangleright}_{ij}, T^{\triangleright}, T^{\triangleright}_{,i}, \rho^{\triangleright}_{d}\right\}, \\ \\ y = \left\{\varrho^{\triangleright}, \beta_a, D^{\triangleright}_{ij}, H^{\triangleright}_{ij}, T^{\triangleright}_{,i}, \rho^{\triangleright}_{d}\right\}, \\ \\ z = \left\{\varrho^{\triangleright}, D^{\triangleright}_{ij}, H^{\triangleright}_{ij}, T^{\triangleright}, T^{\triangleright}_{,i}, \rho^{\triangleright}_{d}\right\}, \end{array} \right\} \tag{6.30}$$

and the Kronecker symbols $\delta_{x\varrho^{\triangleright}}$ and $\delta_{x\rho^{\triangleright}_{d}}$ have the usual meaning, i.e.,

$$\delta_{xz} = \left\{ \begin{array}{lll} 1 & \text{if} & x = z, \\ 0 & \text{if} & x \neq z. \end{array} \right. \tag{6.31}$$

It is evident, the Liu Equations (6.28) and (6.29) are the first set of restrictions implied by the 2nd Law of Thermodynamics, the second being the following residual entropy

[4]Notice that some of the variables listed in (6.27) are symmetric (e.g. $D^{\triangleright}_{\langle ij\rangle}$, $\partial D^{\triangleright}_{\langle ij\rangle}/\partial t$) and others are skew-symmetric (e.g. $H^{\triangleright}_{ij}$, $\partial_t H^{\triangleright}_{ij}$) tensors. In such cases, of course, only the symmetric or skew-symmetric parts of the prefactors in $a_i\mathcal{Y}_i + \Omega \geq 0$, respectively, vanish.

inequality (6.23), $\Omega \geq 0$, i.e.,

$$\left[\frac{\partial \phi_i^{\triangleright}}{\partial T^{\triangleright}} - \Lambda_e^{\triangleright}\frac{\partial q_i^{\triangleright}}{\partial T^{\triangleright}}\right] T_{,i}^{\triangleright} - \left(\varrho^{\triangleright}\Lambda_m^{\triangleright} + \rho_d^{\triangleright}\Lambda_d^{\triangleright}\right) T^{\triangleright}\left(\hat{\partial}_D w^{\triangleright} + v_{i,i}^{\triangleright}\right)$$
$$- \varrho^{\triangleright}\delta^{\triangleright} + \varrho^{\triangleright}\Gamma^{\triangleright}\eta^{\triangleright} + \Lambda_m^{\triangleright}\varrho^{\triangleright}\Gamma^{\triangleright} - \Lambda_e^{\triangleright}H_{jk}^{\triangleright}t_{[jk]}^{\triangleright} + \Lambda_e^{\triangleright}D_{\langle jk\rangle}^{\triangleright}t_{\langle jk\rangle}^{\triangleright} + \frac{1}{3}\Lambda_e^{\triangleright}\delta_{jk}D_{aa}^{\triangleright}t_{(jk)}^{\triangleright} + \Lambda_e^{\triangleright}\varrho^{\triangleright}\epsilon^{\triangleright}$$
$$- \Lambda_e^{\triangleright}\varrho^{\triangleright}\Gamma^{\triangleright}e^{\triangleright} + \Lambda_e^{\triangleright}\frac{1}{2}\varrho^{\triangleright}\Gamma^{\triangleright}v_i^{\triangleright}v_i^{\triangleright} + \Lambda_e^{\triangleright}\frac{1}{2}\varrho^{\triangleright}\Gamma^{\triangleright}\sigma_i^{\triangleright}s_i^{\triangleright} + \Lambda_d^{\triangleright}\Pi^{\triangleright}$$
$$+ \varrho^{\triangleright}\left(\hat{\partial}_i\eta^{\triangleright}\right)u_i^{\triangleright} + \varrho^{\triangleright}\left(\hat{\partial}_D\eta^{\triangleright}\right)w^{\triangleright} + \hat{\partial}_i\varphi_i^{\triangleright} + \hat{\partial}_D n^{\triangleright} - \Lambda_d^{\triangleright}\hat{\partial}_j\gamma_{dj}^{\triangleright} - \Lambda_d^{\triangleright}\hat{\partial}_D\Delta_d^{\triangleright}$$
$$- \Lambda_e^{\triangleright}\varrho^{\triangleright}\left(\hat{\partial}_i e^{\triangleright}\right)u_j^{\triangleright} - \Lambda_e^{\triangleright}\varrho^{\triangleright}\left(\hat{\partial}_D e^{\triangleright}\right)w^{\triangleright} - \Lambda_e^{\triangleright}\hat{\partial}_j\xi_j^{\triangleright} - \Lambda_e^{\triangleright}\hat{\partial}_D h^{\triangleright} \geq 0,$$

where

$$\hat{\partial}_i S^{\triangleright} \equiv \left[\partial_i S^{\triangleright}\right]_z, \qquad \hat{\partial}_D S^{\triangleright} \equiv \left[\partial_D S^{\triangleright}\right]_z \tag{6.32}$$

and $S^{\triangleright}$ represents any constitutive quantity in (6.6), and the subscript z indicates that the quantities in $(6.30)_3$ are kept constant. The derivation of (6.28-6.30) is tedious and is deferred to the Appendix, where an extended and more readable form of the Liu Equations, (7.2-7.6), is given.

In order to obtain further restrictions on the constitutive quantities from the 2^{nd} Law of Thermodynamics, we will consider in the next section the completion of rules implied by the Principle of Material Frame Indifference in a change of frame of reference. Transformation properties are listed in (6.14), and suitable isotropic function representations will be given below.

6.5 Representation Theorems

The constitutive relations (6.16) comprise a large number of equations involving many variables. When formulated relative to different frames, the variables of these relations transform as listed in (6.14). We will subsequently assume that a change in the direction of n_j does not affect the physics of the problem. This is reasonable, because in most cases the orientation of the crystallites is defined by a line and not by the orientation along this line. This means that two crystallites oriented toward n_j and $-n_j$, respectively, are considered to have the same behaviour, i.e., n_j and $-n_j$ are equivalent. This implies that the balance equations (6.17-6.22) must not be affected by orientations of the direction represented by n_j. Thus, some physical quantities change their sign under a change of orientation, others do not, e.g. $B(n_j) = -B(-n_j)$ and $A(n_j) = A(-n_j)$, respectively. All variables arising in (6.6) and on the right-hand side of (6.16) are listed in Table 6.2 as members of these two classes[5].

Apart from this, we assume linearity of the constitutive quantities in (6.6) with respect to the gradient of the temperature, $T_{,i}^{\triangleright}$ and to the relative spin tensor, $H_{ij}^{\triangleright}$. We will also restrict the non-linearity of the scalar invariants and generators to second order with respect to the stretching $D_{ij}^{\triangleright}$. Moreover, we will neglect all possible vector products in the scalar invariants[6]. We, however, emphasize that this restriction is not applied for

[5]Let us remark that the orientation gradient operator ∂_i defined in $(4.40)_2$ changes sign when n_i changes the direction of orientation.

[6]For a clear definition of the notion of scalar invariants and generators see e.g. Liu [89] and Böhler [13].

the entropy production deviation $\delta^{\triangleright}$, see e.g. Faria [36]. Under these hypotheses, and using the tables in the book of Liu [89], the scalar invariants and generators affecting the constitutive relations (i.e., of those variables on the right-hand side of (6.16)) are collected and classified in the Table 6.3.

Table 6.2 and Table 6.3, together with the linearity of the scalar invariant $n_i T^{\triangleright}_{,i}$ and the properties (4.39) and (4.67) for the orientational quantities, allow the following rep-

Table 6.2: Transformation properties of constitutive variables (6.6) and (6.16) under changes of orientation:$n_j \to -n_j$. We have also remarked the case when the constitutive variable vanishes because of the Liu Equation (6.28).

	$A(n_j) = A(-n_j)$	$B(n_j) = -B(-n_j)$
Absolute Scalar Invariants	$w^{\triangleright}, \Gamma^{\triangleright}, e^{\triangleright}, h^{\triangleright}, \epsilon^{\triangleright}, \eta^{\triangleright}, n^{\triangleright}, \Pi^{\triangleright}, \Delta^{\triangleright}_d, \delta^{\triangleright}, D, \varrho^{\triangleright}, \beta_a, T^{\triangleright}, \rho^{\triangleright}_d$	/ /
Absolute Vectors	$\kappa^{\triangleright}_i, q^{\triangleright}_i, \phi^{\triangleright}_j, T^{\triangleright}_{,i}; \quad F^{\triangleright}_j = 0$	$\xi^{\triangleright}_i, \varphi^{\triangleright}_j, \gamma^{\triangleright}_{dj}, n_j$
Axial Vectors	$\nu^{\triangleright}_i; \quad a^{\triangleright}_j = 0$	/
Absolute Symmetric Tensors	$t^{\triangleright}_{(ij)}, D^{\triangleright}_{ij}$	$\tau^{\triangleright}_{(ji)} = 0$
Absolute Skew Symmetric Tensors	$t^{\triangleright}_{[ij]}, H^{\triangleright}_{ij}$	$\tau^{\triangleright}_{[ji]} = 0$
Axial Symmetric Tensors	$m^{\triangleright}_{(ji)} = 0$	$\varpi^{\triangleright}_{(il)}$
Axial Skew Symmetric Tensors	$m^{\triangleright}_{[ji]} = 0$	$\varpi^{\triangleright}_{[il]}$

Table 6.3: Scalar Invariants and Generators selected from the tables presented by Liu [89] and classified in the two sets defined in Table 6.2. The rules of selection are stated in the text and are resumed here: we consider Scalar Invariants and Generators only up to second order in the stretching $D^{\triangleright}_{ij}$ and linear in the gradient of the temperature $T^{\triangleright}_{,i}$ and relative spin tensor $H^{\triangleright}_{jk}$. We also neglect all Scalar Invariants involving vector products.

*	$A(n_j) = A(-n_j)$	$B(n_j) = -B(-n_j)$
Scalar Invariants	$D, \varrho^{\triangleright}, \beta^{\triangleright}_a, T^{\triangleright}, \rho^{\triangleright}_d, D^{\triangleright}_{kk}, D^{\triangleright}_{ij} D^{\triangleright}_{ji}, n_i D^{\triangleright}_{ij} n_j, n_i D^{\triangleright}_{ij} D^{\triangleright}_{ja} n_a$	$n_i T^{\triangleright}_{,i}$
Absolute Vector Generators	$T^{\triangleright}_{,i}$	$n_j, H^{\triangleright}_{ij} n_j, D^{\triangleright}_{ij} n_j$
Axial Vector Generators	$\varepsilon_{ijk} H^{\triangleright}_{jk}; \varepsilon_{il(e} n_{h)} n_l D^{\triangleright}_{eh}$	$\epsilon_{ijk} n_{[j} T_{,k]}$
Absolute Symmetric Tensor Generators	$\delta_{ij}, n_i n_j, D^{\triangleright}_{ij}, D^{\triangleright}_{ih} D^{\triangleright}_{hj}, D^{\triangleright}_{h(i} n_{j)} n_h, D^{\triangleright}_{ia} D^{\triangleright}_{jb} n_a n_b$ $H^{\triangleright}_{h(i} n_{j)} n_h$	$n_{(i} T^{\triangleright}_{,j)}$
Absolute Skew-Symmetric Tensor Generators	$H^{\triangleright}_{ij}, D^{\triangleright}_{h[i} n_{j]} n_h,$ $n_{[i} D^{\triangleright}_{j]a} D^{\triangleright}_{ab} n_b, H^{\triangleright}_{h[i} n_{j]} n_h$	$n_{[i} T^{\triangleright}_{,j]}$
Axial Symmetric Tensor Generators	$\varepsilon_{ab(i} n_{j)} n_a T^{\triangleright}_{,b}$	$\varepsilon_{ab(i} n_{j)} H^{\triangleright}_{ab}, n_l D^{\triangleright}_{h(i} \varepsilon_{j)lh},$ $\varepsilon_{hb(j} D^{\triangleright}_{i)a} D^{\triangleright}_{ab} n_h$ $n_{(i} \varepsilon_{j)ab} D^{\triangleright}_{ac} n_b n_c$
Axial Skew-Symmetric Tensor Generators	$\varepsilon_{ijk} T^{\triangleright}_{,k}$	$\varepsilon_{ijk} n_k, \varepsilon_{ijk} D^{\triangleright}_{kl} n_l,$ $\varepsilon_{ijk} D^{\triangleright}_{ka} D^{\triangleright}_{ab} n_b, \varepsilon_{ijk} H^{\triangleright}_{kl} n_l$

resentations for the non-vanishing constitutive quantities:

$$\left.\begin{aligned}
&w^{\triangleright} = w^{\triangleright(1)}, \quad \Gamma^{\triangleright} = \Gamma^{\triangleright(1)}, \quad e^{\triangleright} = e^{\triangleright(1)}, \quad h^{\triangleright} = h^{\triangleright(1)}, \quad \epsilon^{\triangleright} = \epsilon^{\triangleright(1)},\\
&\eta^{\triangleright} = \eta^{\triangleright(1)}, \quad n^{\triangleright} = n^{\triangleright(1)}, \quad \Pi^{\triangleright} = \Pi^{\triangleright(1)}, \quad \Delta_d^{\triangleright} = \Delta_d^{\triangleright(1)},\\
&\kappa_i^{\triangleright} = \kappa_{ij}^{\triangleright(b)} T_{,j}^{\triangleright}, \quad q_i^{\triangleright} = q_{ij}^{\triangleright(b)} T_{,j}^{\triangleright}, \quad \phi_i^{\triangleright} = \phi_{ij}^{\triangleright(b)} T_{,j}^{\triangleright}\\
&\xi_i^{\triangleright} = \xi_{ij}^{\triangleright(b)} T_{,j}^{\triangleright}, \quad \varphi_j^{\triangleright} = \varphi_{ij}^{\triangleright(b)} T_{,j}^{\triangleright}, \quad \gamma_{dj}^{\triangleright} = \gamma_{dij}^{\triangleright(b)} T_{,j}^{\triangleright}\\
&\nu_i^{\triangleright} = \nu^{\triangleright(1)} \varepsilon_{ijk} H_{jk}^{\triangleright} + \nu^{\triangleright(2)} \varepsilon_{il(e} n_{h)} n_l D_{eh}^{\triangleright},\\
&t_{ij}^{\triangleright} = t^{\triangleright(1)} \delta_{ij} + t^{\triangleright(2)} n_i n_j + t^{\triangleright(3)} D_{ij}^{\triangleright} + t^{\triangleright(4)} D_{ih}^{\triangleright} D_{hj}^{\triangleright} + t^{\triangleright(5)} D_{h(i}^{\triangleright} n_{j)} n_h\\
&\quad + t^{\triangleright(6)} D_{ih}^{\triangleright} D_{jb}^{\triangleright} n_h n_b + t^{\triangleright(7)} H_{h(i}^{\triangleright} n_{j)} n_h + t^{\triangleright(8)} H_{ij}^{\triangleright} + t^{\triangleright(9)} D_{h[i}^{\triangleright} n_{j]} n_h\\
&\quad + t^{\triangleright(10)} n_{[i} D_{j]a}^{\triangleright} D_{ab}^{\triangleright} n_b + t^{\triangleright(11)} H_{h[i}^{\triangleright} n_{j]} n_h,\\
&\varpi_{ij}^{\triangleright} = \varepsilon_{ijk} n_k \varpi^{\triangleright(1)} + \varepsilon_{hb(j} D_{i)a}^{\triangleright} D_{ab}^{\triangleright} n_h \varpi^{\triangleright(2)} + n_{(i} \varepsilon_{j)ab} D_{ac}^{\triangleright} n_b n_c \varpi^{\triangleright(3)}\\
&\quad + n_l D_{h(i}^{\triangleright} \varepsilon_{j)lh} \varpi^{\triangleright(4)} + \tfrac{1}{2} \varepsilon_{ijk} D_{kl}^{\triangleright} n_l \left[\varpi^{\triangleright(3)} - \varpi^{\triangleright(4)}\right] - \tfrac{1}{2} \varepsilon_{ijk} D_{ka}^{\triangleright} D_{ab}^{\triangleright} n_b \varpi^{\triangleright(2)}.
\end{aligned}\right\} \tag{6.33}$$

such that

$$\begin{aligned}
&\kappa_{ij}^{\triangleright(b)} = \kappa^{\triangleright(1)} n_i n_j + \kappa^{\triangleright(3)} \delta_{ij}, \quad q_{ij}^{\triangleright(b)} = q^{\triangleright(1)} n_i n_j + q^{\triangleright(3)} \delta_{ij}, \quad \phi_{ij}^{\triangleright(b)} = \phi^{\triangleright(1)} n_i n_j + \phi^{\triangleright(3)} \delta_{ij},\\
&\xi_{ij}^{\triangleright(b)} = \xi^{\triangleright(1)} \left[n_i n_j - \delta_{ij}\right], \quad \varphi_{ij}^{\triangleright(b)} = \varphi^{\triangleright(1)} \left[n_i n_j - \delta_{ij}\right], \quad \gamma_{dij}^{\triangleright(b)} = \gamma_d^{\triangleright(1)} \left[n_i n_j - \delta_{ij}\right],
\end{aligned} \tag{6.34}$$

and the indexed quantities in (6.33) and (6.34), e.g. $(\cdot)^{(a)}$ $(a = 1, ..., 11)$, are functions of the scalar invariants

$$\mathfrak{X} := \left\{D, \varrho^{\triangleright}, \beta_a, T^{\triangleright}, \rho_d^{\triangleright}, D_{kk}^{\triangleright}, D_{ij}^{\triangleright} D_{ji}^{\triangleright}, n_i D_{ij}^{\triangleright} n_j, n_i D_{ij}^{\triangleright} D_{ja}^{\triangleright} n_a\right\}. \tag{6.35}$$

The results of the Representation Theorems are stated in (6.33-6.35). Now, we will explain how to build the representation of the orientational couple stress $\varpi_{ij}^{\triangleright}$; the other constitutive quantities are treated analogously. The orientational couple stress satisfies the property (4.67) and, following Table 6.2, is an axial tensor (with a symmetric and a skew-symmetric part), and it changes its sign under a change of the sign of n_j. Once one notes that the scalar invariant $n_j T^{\triangleright}$ belonging to the third column in Table 6.3 is linear and disregarding for a moment condition (4.67), the most general representation is given by the expression

$$\begin{aligned}
\varpi_{ij}^{\triangleright} \;=\; & \varpi^{\triangleright(1)} \varepsilon_{ijk} n_k + \varpi^{\triangleright(2)} \varepsilon_{hb(j} D_{i)a}^{\triangleright} D_{ab}^{\triangleright} n_h + \varpi^{\triangleright(3)} n_{(i} \varepsilon_{j)ab} D_{ac}^{\triangleright} n_b n_c\\
& + \varpi^{\triangleright(4)} n_l D_{h(i}^{\triangleright} \varepsilon_{j)lh} + \varpi^{\triangleright(5)} \varepsilon_{ab(i} n_{j)} H_{ab}^{\triangleright} + \varpi^{\triangleright(6)} \varepsilon_{ijk} D_{kl}^{\triangleright} n_l\\
& + \varpi^{\triangleright(7)} \varepsilon_{ijk} D_{ka}^{\triangleright} D_{ab}^{\triangleright} n_b + \varpi^{\triangleright(8)} \varepsilon_{ijk} H_{kl}^{\triangleright} n_l.
\end{aligned} \tag{6.36}$$

Let us expand the above symmetrizations and multiply (6.36) by n_j. On account of (4.67)

this yields

$$\begin{aligned} 0 \;=\; & \varpi^{\triangleright}_{ij} n_j = \tfrac{1}{2}\varpi^{\triangleright(2)}\varepsilon_{hbi} D^{\triangleright}_{ja} D^{\triangleright}_{ab} n_h n_j + \tfrac{1}{2}\varpi^{\triangleright(3)} n_j \varepsilon_{iab} D^{\triangleright}_{ac} n_b n_c n_j \\ & + \tfrac{1}{2}\varpi^{\triangleright(4)} n_l D^{\triangleright}_{hj} \varepsilon_{ilh} n_j + \varpi^{\triangleright(5)} \varepsilon_{ab(i} n_{j)} H^{\triangleright}_{ab} n_j + \varpi^{\triangleright(6)} \varepsilon_{ijk} D^{\triangleright}_{kl} n_l n_j \\ & + \varpi^{\triangleright(7)} \varepsilon_{ijk} D^{\triangleright}_{ka} D^{\triangleright}_{ab} n_b n_j + \varpi^{\triangleright(8)} \varepsilon_{ijk} H^{\triangleright}_{kl} n_l n_j . \end{aligned} \tag{6.37}$$

Collecting the terms with the same structure and accounting for the fact that in a general process each of them is independent, (6.37) leads to

$$\left.\begin{aligned} \tfrac{1}{2}\varpi^{\triangleright(2)} + \varpi^{\triangleright(7)} = 0, \quad \varpi^{\triangleright(5)} = 0, \\ \varpi^{\triangleright(6)} = \tfrac{1}{2}\left[\varpi^{\triangleright(3)} - \varpi^{\triangleright(4)}\right], \quad \varpi^{\triangleright(8)} = 0. \end{aligned}\right\} \tag{6.38}$$

Inserting (6.38) into (6.36) yields the result stated in the last expression of (6.33).

Further restrictions on the constitutive equations are dictated by the 2^{nd} Law of Thermodynamics and emerge when all above isotropic representations are combined with the Liu Equations (6.28-6.30).

6.6 Further Restrictions from the Liu Equations

In this section we refer to the Liu Equations in the form stated in (6.28-6.30), however, in a more readily accessible form of these equations, see their extended representation (7.2-7.6) given in the Appendix.

The representations (6.33) for the heat flux density $q^{\triangleright}_i$, the density of the non-convective entropy flux, $\phi^{\triangleright}_i$ and the relative Liu Equations stated in (6.29) when applied to $y = T^{\triangleright}_{,i}$ allow us to prove that entropy flux, $\phi^{\triangleright}_i$ and heat flux, $q^{\triangleright}_i$ are collinear, viz.,

$$\phi^{\triangleright}_i = \Lambda^{\triangleright e} q^{\triangleright}_i . \tag{6.39}$$

The same Liu Equations evaluated for the other y-variables, see $(6.30)_2$, the results (6.24) and (6.39), then yield

$$\Lambda^{\triangleright e} = \Lambda^{\triangleright e(1)}\left(T^{\triangleright}, D\right). \tag{6.40}$$

Müller [108] noted that for an ideal fluid $\Lambda^{\triangleright e}$ is only a function of the temperature, and its explicit form is given by

$$\Lambda^{\triangleright e} = \frac{1}{T^{\triangleright}}. \tag{6.41}$$

To achieve here the analogous result, let us formulate the jump conditions of energy and entropy across an *ideal wall* that is impermeable and at which the tangential components of the velocity vanish on either side of it. The formulas are given in (4.74), and may, because of (6.39), be combined to yield

$$\left[\left[\Lambda^{\triangleright e} q^{\triangleright}_i\right]\right] e^W_i = \left[\left[\Lambda^{\triangleright e}\right]\right] q^{\triangleright}_i e^W_i = 0, \qquad \Rightarrow \qquad \left[\left[\Lambda^{\triangleright e}\right]\right] = 0. \tag{6.42}$$

Let the ideal wall separate a general polycrystalline material from an ideal fluid. It then follows from $(6.42)_2$ that the function $\Lambda^{\triangleright e(1)}\left(T^{\triangleright}, D\right)$ in (6.40) should have the same value on either side of the wall. Together with the ideal fluid result (6.41), this yields

$$\Lambda^{\triangleright e(1)}\left(T^{\triangleright}, D\right) = \frac{1}{T^{\triangleright}}. \tag{6.43}$$

The first Liu Equation of the second line of (6.29) evaluated with $z = T^{\triangleright}_{,i}$, relation (6.43) and the general representation of the quantities that are involved there ($\varphi^{\triangleright}_j$, $\xi^{\triangleright}_j$ and $\gamma^{\triangleright}_{dj}$) imply the relationship

$$\varphi^{\triangleright}_j = \frac{1}{T^{\triangleright}}\xi^{\triangleright}_j + \Lambda^{\triangleright}_d \gamma^{\triangleright}_{dj} \tag{6.44}$$

If we take (6.44) into account, then the same Liu Equations evaluated for the other values of z, see $(6.30)_3$, imply the restrictions

$$\xi^{\triangleright}_j = (T^{\triangleright})^2 \frac{\partial \Lambda^{\triangleright}_d}{\partial T^{\triangleright}} \gamma^{\triangleright}_{dj}, \qquad \Lambda^{\triangleright}_d = \Lambda^{\triangleright}_d \left(D, \beta_a, T^{\triangleright}\right). \tag{6.45}$$

If we define the Helmholtz free energy $\psi^{\triangleright}$ by

$$\psi^{\triangleright} \equiv e^{\triangleright} - T^{\triangleright}\eta^{\triangleright}, \tag{6.46}$$

then the first Liu Equation of the first line of (6.29) evaluated in $x = \beta_a, D^{\triangleright}_{ij}, H^{\triangleright}_{ij}, T^{\triangleright}_{,i}$ gives a restriction on the functional dependence of $\psi^{\triangleright}$, i.e.,

$$\psi^{\triangleright} = \psi^{\triangleright}\left(D, \varrho^{\triangleright}, T^{\triangleright}, \rho^{\triangleright}_d\right). \tag{6.47}$$

When evaluated for $x = T^{\triangleright}$, the same Liu Equation implies that $\eta^{\triangleright}$ and $e^{\triangleright}$ can be easily derived from $\psi^{\triangleright}$,

$$\eta^{\triangleright} = -\frac{\partial \psi^{\triangleright}}{\partial T^{\triangleright}}, \qquad e^{\triangleright} = \psi^{\triangleright} - T^{\triangleright}\frac{\partial \psi^{\triangleright}}{\partial T^{\triangleright}}, \tag{6.48}$$

and when evaluated for $x = \varrho^{\triangleright}, \rho^{\triangleright}_d$, the interpretation of the Lagrange multipliers for the balances of mass and dislocation can be derived in the form

$$\Lambda^{\triangleright}_m = \Lambda^{\triangleright}_m\left(D, \varrho^{\triangleright}, T^{\triangleright}, \rho^{\triangleright}_d\right) = \varrho^{\triangleright}\left[\frac{\partial \eta^{\triangleright}}{\partial \varrho^{\triangleright}} - \Lambda^{\triangleright}_e \frac{\partial e^{\triangleright}}{\partial \varrho^{\triangleright}}\right] = -\frac{\varrho^{\triangleright}}{T^{\triangleright}}\frac{\partial \psi^{\triangleright}}{\partial \varrho^{\triangleright}}, \tag{6.49}$$

$$\Lambda^{\triangleright}_d = \Lambda^{\triangleright}_d\left(D, T^{\triangleright}\right) = \varrho^{\triangleright}\left[\frac{\partial \eta^{\triangleright}}{\partial \rho^{\triangleright}_d} - \Lambda^{\triangleright}_e \frac{\partial e^{\triangleright}}{\partial \rho^{\triangleright}_d}\right] = -\frac{\varrho^{\triangleright}}{T^{\triangleright}}\frac{\partial \psi^{\triangleright}}{\partial \rho^{\triangleright}_d}, \tag{6.50}$$

where condition $(6.45)_2$ is already taken into account.

Another important result can be deduced from the representation of the orientational couple stress $\varpi^{\triangleright}_{ij}$ in (6.33) and the Liu Equation stated in the second line of (6.28). Once one recognizes from (6.49) and (6.50) that the Lagrange multipliers $\Lambda^{\triangleright}_m$ and $\Lambda^{\triangleright}_d$ do not depend on the stretching tensor, we have that

$$\varpi^{\triangleright(2)} = \varpi^{\triangleright(3)} = 0, \tag{6.51}$$

and the orientational couple stress reduces to the following remarkable simple form, i.e.,

$$\varpi^{\triangleright}_{ij} = \varepsilon_{ijk} n_k p^{\triangleright}, \tag{6.52}$$

where

$$p^{\triangleright} = \varpi^{\triangleright(1)} = T^{\triangleright}\left(\Lambda^{\triangleright}_m \varrho^{\triangleright} + \Lambda^{\triangleright}_d \rho^{\triangleright}_d\right) = -\varrho^{\triangleright}\left(\varrho^{\triangleright}\frac{\partial \psi^{\triangleright}}{\partial \varrho^{\triangleright}} + \rho^{\triangleright}_d \frac{\partial \psi^{\triangleright}}{\partial \rho^{\triangleright}_d}\right). \tag{6.53}$$

This is a very important result. In fact, in Chapter 4 we claimed that the interpretation of polygonization within this Theory of Mixture with Continuous Diversity can be given

through the orientational couple stress. We now demonstrated that the representation of $\varpi_{ij}^{\triangleright}$ able to model polygonization is (6.52). To be accounted for it necessarily requires the free energy to depend on mass and/or dislocation density. By taking the definition (6.53) into account, the last Liu Equations (the second of the second line of (6.29)) can be written as

$$\left.\begin{aligned}
&T^{\triangleright}\frac{\partial n^{\triangleright}}{\partial \varrho^{\triangleright}}-\frac{\partial h^{\triangleright}}{\partial \varrho^{\triangleright}}-T^{\triangleright}\Lambda_d^{\triangleright}\frac{\partial \Delta_d^{\triangleright}}{\partial \varrho^{\triangleright}}-p^{\triangleright}\frac{\partial w^{\triangleright}}{\partial \varrho^{\triangleright}}=0,\\
&T^{\triangleright}\frac{\partial n^{\triangleright}}{\partial T^{\triangleright}}-\frac{\partial h^{\triangleright}}{\partial T^{\triangleright}}-T^{\triangleright}\Lambda_d^{\triangleright}\frac{\partial \Delta_d^{\triangleright}}{\partial T^{\triangleright}}-p^{\triangleright}\frac{\partial w^{\triangleright}}{\partial T^{\triangleright}}=0,\\
&T^{\triangleright}\frac{\partial n^{\triangleright}}{\partial D_{hk}^{\triangleright}}-\frac{\partial h^{\triangleright}}{\partial D_{hk}^{\triangleright}}-T^{\triangleright}\Lambda_d^{\triangleright}\frac{\partial \Delta_d^{\triangleright}}{\partial D_{hk}^{\triangleright}}-p^{\triangleright}\frac{\partial w^{\triangleright}}{\partial D_{hk}^{\triangleright}}=0,\\
&T^{\triangleright}\frac{\partial n^{\triangleright}}{\partial \rho_d^{\triangleright}}-\frac{\partial h^{\triangleright}}{\partial \rho_d^{\triangleright}}-T^{\triangleright}\Lambda_d^{\triangleright}\frac{\partial \Delta_d^{\triangleright}}{\partial \rho_d^{\triangleright}}-p^{\triangleright}\frac{\partial w^{\triangleright}}{\partial \rho_d^{\triangleright}}=0.
\end{aligned}\right\} \tag{6.54}$$

Restrictions (6.54) will be important to determine the functional dependence of the size transition rate, $w^{\triangleright}$.

If we now define

$$\begin{aligned}
F^{\triangleright} \;=\; & -\varrho^{\triangleright}\Gamma^{\triangleright}\psi^{\triangleright}+\frac{1}{2}\varrho^{\triangleright}\Gamma^{\triangleright}v_i^{\triangleright}v_i^{\triangleright}+\frac{1}{2}\varrho^{\triangleright}\Gamma^{\triangleright}\sigma_i^{\triangleright}s_i^{\triangleright}+T^{\triangleright}\Lambda_m^{\triangleright}\varrho^{\triangleright}\Gamma^{\triangleright}+\varrho^{\triangleright}\epsilon^{\triangleright}+T^{\triangleright}\Lambda_d^{\triangleright}\Pi^{\triangleright}\\
& -\varrho^{\triangleright}w^{\triangleright}\hat{\partial}_D\psi^{\triangleright}+T^{\triangleright}\hat{\partial}_D n^{\triangleright}-T^{\triangleright}\Lambda_d^{\triangleright}\hat{\partial}_D\Delta_d^{\triangleright}-\hat{\partial}_D h^{\triangleright},
\end{aligned} \tag{6.55}$$

then the residual entropy inequality reduces to

$$T^{\triangleright}\varsigma^{\triangleright P}=F^{\triangleright}-T^{\triangleright}\varrho^{\triangleright}\delta^{\triangleright}-\phi_i^{\triangleright}T_{,i}^{\triangleright}-H_{jk}^{\triangleright}t_{[jk]}^{\triangleright}+D_{\langle jk\rangle}^{\triangleright}t_{\langle jk\rangle}^{\triangleright}+\frac{1}{3}D_{aa}^{\triangleright}t_{bb}^{\triangleright}+p^{\triangleright}\left[\hat{\partial}_D w^{\triangleright}+D_{aa}^{\triangleright}\right]\geqslant 0. \tag{6.56}$$

In the next section, we complete the exploitation of the entropy inequality with the analysis of thermodynamic equilibrium.

6.7 Analysis of Thermodynamic Equilibrium

Thermodynamic equilibrium is defined here as the state where the body motion is rigid ($v_{i,j}^{\triangleright}=W_{ij}^{\triangleright}$, $H_{ij}^{\triangleright}=w^{\triangleright}=0$), the temperature is homogeneous ($T^{\triangleright}=$const.), the production terms $\delta^{\triangleright}$, $\kappa_i^{\triangleright}$, $\nu_i^{\triangleright}$, $\epsilon^{\triangleright}$, $\Gamma^{\triangleright}$ and $\Pi^{\triangleright}$ and the size-derivative of size-flux densities $\partial_D n^{\triangleright}$, $\partial_D h^{\triangleright}$, $\partial_D\Delta_d^{\triangleright}$ vanish, i.e., when the following conditions hold:

$$\left.\begin{aligned}
&v_{i,j}^{\triangleright}\big|_E\equiv W_{ij}^{\triangleright},\quad T^{\triangleright}\big|_E\equiv const.,\\
&\left[D_{ij}^{\triangleright},H_{ij}^{\triangleright},T_{,j}^{\triangleright},w^{\triangleright},\delta^{\triangleright},\kappa_i^{\triangleright},\nu_i^{\triangleright},\epsilon^{\triangleright},\Gamma^{\triangleright},\Pi^{\triangleright},\partial_D n^{\triangleright},\partial_D h^{\triangleright},\partial_D\Delta_d^{\triangleright}\right]_E\equiv 0,
\end{aligned}\right\} \tag{6.57}$$

where the subscript E denotes evaluation at equilibrium. A consequence of definition (6.57) is that, under such conditions and from (6.55) and (6.56), the function $\varsigma^{\triangleright P}$ vanishes

and assumes its minimum value. Thus, of necessity then,

$$\left.\begin{array}{l} \varsigma^{\triangleright P}\big|_E = 0, \\ \left.\dfrac{\partial T^{\triangleright}\varsigma^{\triangleright P}}{\partial x}\right|_E = 0, \qquad \text{where} \qquad x = \left\{D^{\triangleright}_{aa}, D^{\triangleright}_{\langle ab\rangle}, H^{\triangleright}_{ab}, T^{\triangleright}_{,i}\right\}, \\ \left.\dfrac{\partial^2 \left(T^{\triangleright}\varsigma^{\triangleright P}\right)}{\partial x \partial y}\right|_E \text{ is positive definitive, where } x, y = \left\{D^{\triangleright}_{aa}, D^{\triangleright}_{\langle ab\rangle}, H^{\triangleright}_{ab}, T^{\triangleright}_{,i}\right\} \end{array}\right\} \tag{6.58}$$

The requirements $(6.58)_{2,3}$ are the mathematical implication of this minimal condition. The analysis of $(6.58)_2$ is given in the Appendix and yields four important relations, namely

$$t^{\triangleright(1)}\big|_E + \tfrac{1}{3}\, t^{\triangleright(2)}\big|_E = -\left.\frac{\partial F^{\triangleright}}{\partial D^{\triangleright}_{aa}}\right|_E + T^{\triangleright}\varrho^{\triangleright}\left.\frac{\partial \delta^{\triangleright}}{\partial D^{\triangleright}_{aa}}\right|_E - p^{\triangleright}, \tag{6.59}$$

$$t^{\triangleright(2)}\big|_E \left(n_i n_j - \tfrac{1}{3}\delta_{ij}\right) = -\left.\frac{\partial F^{\triangleright}}{\partial D^{\triangleright}_{\langle ij\rangle}}\right|_E + T^{\triangleright}\varrho^{\triangleright}\left.\frac{\partial \delta^{\triangleright}}{\partial D^{\triangleright}_{\langle ij\rangle}}\right|_E, \tag{6.60}$$

$$\left.\frac{\partial \delta^{\triangleright}}{\partial H^{\triangleright}_{ab}}\right|_E = \left.\frac{\partial \delta^{\triangleright}}{\partial T^{\triangleright}_{,a}}\right|_E = 0. \tag{6.61}$$

Relations (6.59) and (6.60) are the restrictions of the equilibrium on the Cauchy stress tensor and (6.61) are further constraints.

6.8 Incompressible Polycrystalline Materials

In this section, we summarize the results of the present constitutive theory for incompressible polycrystalline materials. In this regards, we claim that the temperature and the velocity have no microstructural dependence, i.e.,

$$T^{\triangleright} = T, \quad \upsilon^{\triangleright}_i = \upsilon_i \quad \Longrightarrow \quad D^{\triangleright}_{ij} = D_{ij}. \tag{6.62}$$

The incompressibility condition can be implemented by restricting the stretching tensor to be traceless,

$$D_{aa} = 0, \tag{6.63}$$

and avoiding any functional dependence of the constitutive quantities from D_{aa}. We will also neglect all the interspecies fluxes of energy, entropy and dislocation,

$$\xi^{\triangleright}_j = \varphi^{\triangleright}_j = \gamma^{\triangleright}_{dj} = h^{\triangleright} = n^{\triangleright} = \Delta^{\triangleright}_d = 0. \tag{6.64}$$

Thus, the balance equations are

$$\acute{\varrho}^{\triangleright} + \varrho^{\triangleright}\partial_j u^{\triangleright}_j + \varrho^{\triangleright}\partial_D w^{\triangleright} = \varrho^{\triangleright}\Gamma^{\triangleright}, \tag{6.65}$$

$$\varrho^{\triangleright}\dot{\upsilon} = t^{\triangleright}_{ij,j} + \varrho^{\triangleright}\left(\kappa^{\triangleright}_i - \upsilon_i\Gamma^{\triangleright}\right), \tag{6.66}$$

$$\varepsilon_{ijk}\left[t^{\triangleright}_{[jk]} + n_{[k}\partial_{j]}p^{\triangleright}\right] + \varrho^{\triangleright}\nu^{\triangleright}_i = 0, \tag{6.67}$$

$$\varrho^{\triangleright}\acute{e} + q^{\triangleright}_{i,i} - p^{\triangleright}\partial_j u^{\triangleright}_j + H^{\triangleright}_{jk}t^{\triangleright}_{[jk]} - D^{\triangleright}_{jk}t^{\triangleright}_{\langle jk\rangle} - \tfrac{1}{2}\varrho^{\triangleright}\Gamma^{\triangleright}\upsilon_i\upsilon_i = \varrho^{\triangleright}\left(\epsilon^{\triangleright} - \Gamma^{\triangleright}e^{\triangleright}\right), \tag{6.68}$$

$$\acute{\rho}^{\triangleright}_d + \rho^{\triangleright}_d\partial_j u^{\triangleright}_j + \rho^{\triangleright}_d\partial_D w^{\triangleright} = \Pi^{\triangleright}, \tag{6.69}$$

where the constitutive quantities are prescribed as follows. Once the Helmholtz free energy (6.47) is prescribed, the specific entropy and internal energy are given by (6.48) and $p^{\triangleright}$ is given by (6.53). The size-transition rate is constrained by the combination of (6.54) and (6.64), i.e.,

$$w^{\triangleright} = w^{\triangleright}\left(D, \beta_a\right). \tag{6.70}$$

Equation (6.70) is of interest. It tells us that the size-transition rate can depend upon D and all global variables β_a and no others. In subsection 6.3.4 we remarked that the specialization of β_a with $\beta_2 = \varrho\left\langle D\right\rangle$ allows us to derive a correct expression for the grain growth term in the equation of the evolution of texture. On the other hand, experimental data tell us that $w^{\triangleright}$ depends upon temperature. In order to achieve the goal of this dependence, we can simply define β_4,

$$\beta_4\left(t, x_i\right) = \int\limits_{\mathcal{S}^2}\int\limits_{\mathcal{I}} \varrho^{\triangleright} T^{\triangleright} dD d^2n = T\left(t, x_i\right), \tag{6.71}$$

and claim that $w^{\triangleright}$ depends upon β_4.

The remainder of the entropy inequality is

$$F^{\triangleright} - T^{\triangleright}\varrho^{\triangleright}\delta^{\triangleright} - \phi_i^{\triangleright} T_{,i}^{\triangleright} - H_{jk}^{\triangleright} t_{[jk]}^{\triangleright} + D_{\langle jk\rangle}^{\triangleright} t_{\langle jk\rangle}^{\triangleright} + p^{\triangleright}\partial_D w^{\triangleright} \geqslant 0, \tag{6.72}$$

where

$$F^{\triangleright} = \varrho^{\triangleright}\Gamma^{\triangleright}\left(\tfrac{1}{2}\upsilon_i\upsilon_i - \psi^{\triangleright}\right) + \varrho^{\triangleright}\epsilon^{\triangleright} + \varrho^{\triangleright}\left(\frac{\partial\psi^{\triangleright}}{\partial\varrho^{\triangleright}}\varrho^{\triangleright}\Gamma^{\triangleright} + \frac{\partial\psi^{\triangleright}}{\partial\rho_d^{\triangleright}}\Pi^{\triangleright}\right). \tag{6.73}$$

Besides, we remark that the collinearity between the entropy and energy fluxes can be represented with (6.33),

$$q_i^{\triangleright} = T\phi_i^{\triangleright} = T\phi^{\triangleright(3)} T_{,i}, \tag{6.74}$$

if we neglect the terms $\phi^{\triangleright(1)}$ and $q^{\triangleright(1)}$. Moreover, the representation of the specific production terms of momenta are

$$\kappa_i^{\triangleright} = \kappa^{\triangleright(3)} T_{,i}, \quad \nu_i^{\triangleright} = \nu^{\triangleright(1)}\varepsilon_{ijk} H_{jk}^{\triangleright}, \tag{6.75}$$

where $\kappa^{\triangleright(1)}$ and $\nu^{\triangleright(2)}$ are assumed to be of no importance. If we neglect $t^{\triangleright(2)}$, claim that $t^{\triangleright(1)}\big|_{E} = t^{\triangleright(1)}$, neglect any generators of the Cauchy stress tensor quadratic in the stretching and take the constraint (6.59) into account, we have

$$t_{ij}^{\triangleright} = -p^{\triangleright}\,\delta_{ij} + t^{\triangleright(3)} D_{ij}^{\triangleright} + t^{\triangleright(5)} D_{h(i}^{\triangleright} n_{j)} n_h + t^{\triangleright(7)} H_{h(i}^{\triangleright} n_{j)} n_h + t^{\triangleright(8)} H_{ij}^{\triangleright} + t^{\triangleright(9)} D_{h[i}^{\triangleright} n_{j]} n_h + t^{\triangleright(11)} H_{h[i}^{\triangleright} n_{j]} n_h. \tag{6.76}$$

The general dependence of the scalar non-vanishing constitutive functions

$$C^{\triangleright} = \left\{\Gamma^{\triangleright}, t^{\triangleright(3)}, t^{\triangleright(5)}, t^{\triangleright(7)}, t^{\triangleright(8)}, t^{\triangleright(9)}, t^{\triangleright(11)}, \kappa^{\triangleright(3)}, \nu^{\triangleright(1)}, \phi^{\triangleright(3)}, \epsilon^{\triangleright}, \Pi^{\triangleright}\right\}, \tag{6.77}$$

remains that of equation (6.35), i.e.,

$$C^{\triangleright} = C^{\triangleright}\left(\mathfrak{X}\right). \tag{6.78}$$

It is important to remark that the dependence of $\Gamma^{\triangleright}$ upon β_1 (see eqn. (6.12)) guarantees that the results on recrystallization fabrics we achieved at the end of Chapter 5 are thermodynamically consistent. Moreover, the dependence of the same quantity, $\Gamma^{\triangleright}$, upon

β_2 and β_3 comprehend the expression for the polygonization term in the equation of the evolution of texture. Besides, we see that polygonization (represented by $p^{\triangleright}$) plays also a role in the microscopic Cauchy stress tensor. If we recall the homogenization rules, then the macroscopic Cauchy stress tensor t_{ij} can be derived from the microscopic stress tensor $t^{\triangleright}_{ij}$ by the following integration:

$$t_{ij} = \int\limits_{\mathcal{S}^2}\int\limits_{\mathcal{I}} t^{\triangleright}_{ij}\, dDd^2n. \tag{6.79}$$

The classical pressure, p, can be calculated by a similar integration, i.e.,

$$p = \int\limits_{\mathcal{S}^2}\int\limits_{\mathcal{I}} p^{\triangleright}\, dDd^2n. \tag{6.80}$$

Equation (6.80) is an important result. It establishes a relationship between polygonization and pressure.

The macroscopic deviatoric stress tensor S_{ij} is given by

$$S_{ij} = t_{\langle ij\rangle} = D_{ij}\int\limits_{\mathcal{S}^2}\int\limits_{\mathcal{I}} t^{\triangleright(3)} dDd^2n, \tag{6.81}$$

if we neglect $t^{\triangleright(5)}$ and $t^{\triangleright(7)}$. We remark that the functional dependence of $t^{\triangleright(3)}$ with respect to β_1 of equation (6.12) guarantees thermodynamic consistency of the results presented in Chapter 3.

The symmetry of the macroscopic Cauchy stress tensor on the other hand implies

$$\int\limits_{\mathcal{S}^2}\int\limits_{\mathcal{I}} \left[t^{\triangleright(8)} H^{\triangleright}_{ij} + t^{\triangleright(9)} D^{\triangleright}_{h[i} n_{j]} n_h + t^{\triangleright(11)} H^{\triangleright}_{h[i} n_{j]} n_h\right]\, dDd^2n = 0. \tag{6.82}$$

From the balance of angular momentum (6.67) and from the representation of its production term $(6.75)_2$, we have

$$t^{\triangleright}_{[ij]} + n_{[j}\partial_{i]} p^{\triangleright} + \varrho^{\triangleright}\nu^{\triangleright(1)} H^{\triangleright}_{ij} = 0. \tag{6.83}$$

Thus, the skew symmetric part of the microscopic Cauchy stress tensor is not constrained to vanish. Moreover, if we insert the representation of the skew symmetric part of microscopic Cauchy stress tensor into (6.83) and multiply the result by n_j, we obtain

$$t^{\triangleright(8)} H^{\triangleright}_{ij} n_j + t^{\triangleright(9)} D_{h[i} n_{j]} n_h n_j + \tfrac{1}{2} t^{\triangleright(11)} H^{\triangleright}_{ij} n_j - \tfrac{1}{2}\partial_i p^{\triangleright} + \varrho^{\triangleright}\nu^{\triangleright(1)} H^{\triangleright}_{ij} n_j = 0.$$

If we collect the terms involving the same factor and take $(4.54)_1$ into account, a general form for the orientation transition rate emerges; it reads

$$u^{\triangleright}_i = W^{\triangleright}_{ij} n_j - \frac{t^{\triangleright(9)}}{\left(\frac{1}{2} t^{\triangleright(11)} + t^{\triangleright(8)} + \varrho^{\triangleright}\nu^{\triangleright(1)}\right)} D_{h[i} n_{j]} n_h n_j + \frac{1}{2\left(\frac{1}{2} t^{\triangleright(11)} + t^{\triangleright(8)} + \varrho^{\triangleright}\nu^{\triangleright(1)}\right)}\partial_i p^{\triangleright}. \tag{6.84}$$

Thus, the constitutive equation (5.21) that we have assumed in Chapter 5 for the orientation transition rate can be obtained if we integrate (6.84) over the grain-size range, neglect rigid rotation ($W^{\triangleright}_{ij} = 0$) and polygonization ($p^{\triangleright} = 0$) and recall ι^* as follows,

$$\iota^* = \int\limits_{\mathcal{I}} \frac{-t^{\triangleright(9)}}{[t^{\triangleright(11)} + 2t^{\triangleright(8)} + 2\varrho\nu^{\triangleright(1)}]}\, dD.$$

6.9 Conclusion

In this chapter we have discussed the thermodynamical compatibility of the results stated in the earlier chapters. Such compatibility has been achieved through the formulation of an extended constitutive theory that was able to survive under the attack of the restrictions of the Second Principle of Thermodynamics and of the Analysis of Thermodynamic Equilibrium. The reason of this chapter is, therefore, to give a theretical framework for the presented theory. For some scientists, this framework must be achieved for the reason of beauty. On the other hand, a more acceptable point of view is that a theoretical framework is necessary to analyse further modifications in the case experiments will not be in accordance to our predictions. In fact, if all the postulates are explicit, then the modifications of the theory will be easier.

Chapter 7

Appendix

7.1 The Orientational Gradient Operator

The gradient operator in spherical coordinates and in the spherical frame of reference is

$$\bigtriangledown = \mathbf{e}_r \frac{\partial}{\partial r} + \mathbf{e}_\theta \frac{1}{r}\frac{\partial}{\partial \theta} + \mathbf{e}_\varphi \frac{1}{r\sin\theta}\frac{\partial}{\partial \varphi},$$

where $\mathbf{e}_r$, $\mathbf{e}_\theta$ and $\mathbf{e}_\varphi$ are the three othonormal vectors of the classical spherical coordinates. They can be represented in terms of the orthonormal vectors $\mathbf{e}_1$, $\mathbf{e}_2$ and $\mathbf{e}_3$ of the Cartesian system as follows,

$$\begin{aligned}
\mathbf{e}_r &= \sin\theta\cos\varphi\mathbf{e}_1 + \sin\theta\sin\varphi\mathbf{e}_2 + \cos\theta\mathbf{e}_3, \\
\mathbf{e}_\theta &= \cos\theta\cos\varphi\mathbf{e}_1 + \cos\theta\sin\varphi\mathbf{e}_2 - \sin\theta\mathbf{e}_3, \\
\mathbf{e}_\varphi &= -\sin\varphi\mathbf{e}_1 + \cos\varphi\mathbf{e}_2.
\end{aligned}$$

Therefore, the gradient operator in spherical coordinates

$$\begin{aligned}
\bigtriangledown &= \left[\sin\theta\cos\varphi\mathbf{e}_1 + \sin\theta\sin\varphi\mathbf{e}_2 + \cos\theta\mathbf{e}_3\right]\frac{\partial}{\partial r} \\
&\quad + \left[\cos\theta\cos\varphi\mathbf{e}_1 + \cos\theta\sin\varphi\mathbf{e}_2 - \sin\theta\mathbf{e}_3\right]\frac{1}{r}\frac{\partial}{\partial\theta} \\
&\quad + \left[-\sin\varphi\mathbf{e}_1 + \cos\varphi\mathbf{e}_2\right]\frac{1}{r\sin\theta}\frac{\partial}{\partial\varphi} \\
&= \left[\sin\theta\cos\varphi\frac{\partial}{\partial r} + \cos\theta\cos\varphi\frac{1}{r}\frac{\partial}{\partial\theta} - \sin\varphi\frac{1}{r\sin\theta}\frac{\partial}{\partial\varphi}\right]\mathbf{e}_1 \\
&\quad + \left[\sin\theta\sin\varphi\frac{\partial}{\partial r} + \cos\theta\sin\varphi\frac{1}{r}\frac{\partial}{\partial\theta} + \cos\varphi\frac{1}{r\sin\theta}\frac{\partial}{\partial\varphi}\right]\mathbf{e}_2 \\
&\quad + \left[\cos\theta\frac{\partial}{\partial r} - \sin\theta\frac{1}{r}\frac{\partial}{\partial\theta}\right]\mathbf{e}_3.
\end{aligned}$$

The orientational gradient can be obtained by setting the radius r equal to unity, i.e.,

$$\bigtriangledown = \left[\cos\theta\cos\varphi\frac{\partial}{\partial\theta} - \frac{\sin\varphi}{\sin\theta}\frac{\partial}{\partial\varphi}\right]\mathbf{e}_1 + \left[\cos\theta\sin\varphi\frac{\partial}{\partial\theta} + \frac{\cos\varphi}{\sin\theta}\frac{\partial}{\partial\varphi}\right]\mathbf{e}_2 - \sin\theta\frac{\partial}{\partial\theta}\mathbf{e}_3.$$

Thus, the explicit expression for the components of the orientational gradient in spherical coordinates is given by

$$\partial_1 = \cos\theta\cos\varphi\frac{\partial}{\partial\theta} - \frac{\sin\varphi}{\sin\theta}\frac{\partial}{\partial\varphi}, \quad \partial_2 = \cos\theta\sin\varphi\frac{\partial}{\partial\theta} + \frac{\cos\varphi}{\sin\theta}\frac{\partial}{\partial\varphi}, \quad \partial_3 = -\sin\theta\frac{\partial}{\partial\theta}. \quad (7.1)$$

7.2 The Derivation of the Liu Equations

7.2.1 Part I: The Expansion of the Inequality (6.23)

In this subsection we expand the entropy inequality (6.23). We substitute the balance equations (6.17-6.22) and perform all the derivative operations on the constitutive quantities that follow from applying the chain rule of differentiation. Because the emerging inequality is very lengthy, we divide it into three parts: the expansion of that part of (6.23) that relates to the entropy imbalance and the expansion of the parts pertaining to the balances of mass, momenta, dislocation and energy.

Expansion of the Contribution of the Entropy

The constitutive functions that we expand in this part are $\eta^{\triangleright}$, $\phi_i^{\triangleright}$, $\varphi_j^{\triangleright}$ and $n^{\triangleright}$. They are functions of the quantities $\mathcal{X}$ listed in (6.16); thus

$$\varrho^{\triangleright}[\frac{\partial\eta^{\triangleright}}{\partial\varrho^{\triangleright}}\frac{\partial\varrho^{\triangleright}}{\partial t} + \frac{\partial\eta^{\triangleright}}{\partial\beta_a}\frac{\partial\beta_a}{\partial t} + \frac{\partial\eta^{\triangleright}}{\partial D^{\triangleright}_{\langle ij\rangle}}\frac{\partial D^{\triangleright}_{\langle ij\rangle}}{\partial t} + \frac{\partial\eta^{\triangleright}}{\partial D^{\triangleright}_{kk}}\frac{\partial D^{\triangleright}_{kk}}{\partial t} + \frac{\partial\eta^{\triangleright}}{\partial H^{\triangleright}_{ij}}\frac{\partial H^{\triangleright}_{ij}}{\partial t} + \frac{\partial\eta^{\triangleright}}{\partial T^{\triangleright}}\frac{\partial T^{\triangleright}}{\partial t} + \frac{\partial\eta^{\triangleright}}{\partial T^{\triangleright}_{,i}}\frac{\partial T^{\triangleright}_{,i}}{\partial t}$$
$$+ \frac{\partial\eta^{\triangleright}}{\partial\rho_d^{\triangleright}}\frac{\partial\rho_d^{\triangleright}}{\partial t}]$$

$$+ \varrho^{\triangleright}[\frac{\partial\eta^{\triangleright}}{\partial\varrho^{\triangleright}}\varrho^{\triangleright}_{,i} + \frac{\partial\eta^{\triangleright}}{\partial\beta_a}\beta_{a,i} + \frac{\partial\eta^{\triangleright}}{\partial D^{\triangleright}_{\langle hk\rangle}}D^{\triangleright}_{\langle hk\rangle,i} + \frac{\partial\eta^{\triangleright}}{\partial D^{\triangleright}_{kk}}D^{\triangleright}_{kk,i} + \frac{\partial\eta^{\triangleright}}{\partial H^{\triangleright}_{hk}}H^{\triangleright}_{hk,i}\frac{\partial\eta^{\triangleright}}{\partial T^{\triangleright}}T^{\triangleright}_{,i} + \frac{\partial\eta^{\triangleright}}{\partial\rho_d^{\triangleright}}\rho^{\triangleright}_{d,i}]\upsilon_i^{\triangleright}$$
$$+ \varrho^{\triangleright}\frac{\partial\eta^{\triangleright}}{\partial T^{\triangleright}_{,(h}}T^{\triangleright}_{,hi}\upsilon^{\triangleright}_{i)}$$

$$+ \varrho^{\triangleright}[\frac{\partial\eta^{\triangleright}}{\partial\varrho^{\triangleright}}\partial_j\varrho^{\triangleright} + \frac{\partial\eta^{\triangleright}}{\partial D^{\triangleright}_{\langle hk\rangle}}\partial_j D^{\triangleright}_{\langle hk\rangle} + \frac{\partial\eta^{\triangleright}}{\partial D^{\triangleright}_{kk}}\partial_j D^{\triangleright}_{kk} + \frac{\partial\eta^{\triangleright}}{\partial H^{\triangleright}_{hk}}\partial_j H^{\triangleright}_{hk} + \frac{\partial\eta^{\triangleright}}{\partial T^{\triangleright}}\partial_j T^{\triangleright} + \frac{\partial\eta^{\triangleright}}{\partial T^{\triangleright}_{,i}}\partial_j T^{\triangleright}_{,i}$$
$$+ \frac{\partial\eta^{\triangleright}}{\partial\rho_d^{\triangleright}}\partial_j\rho_d^{\triangleright} + \hat{\partial}_i\eta^{\triangleright}]u_i^{\triangleright}$$

$$+ \varrho^{\triangleright}[\frac{\partial\eta^{\triangleright}}{\partial\varrho^{\triangleright}}\partial_D\varrho^{\triangleright} + \frac{\partial\eta^{\triangleright}}{\partial D^{\triangleright}_{\langle hk\rangle}}\partial_D D^{\triangleright}_{\langle hk\rangle} + \frac{\partial\eta^{\triangleright}}{\partial D^{\triangleright}_{kk}}\partial_D D^{\triangleright}_{kk} + \frac{\partial\eta^{\triangleright}}{\partial H^{\triangleright}_{hk}}\partial_D H^{\triangleright}_{hk} + \frac{\partial\eta^{\triangleright}}{\partial T^{\triangleright}}\partial_D T^{\triangleright} + \frac{\partial\eta^{\triangleright}}{\partial T^{\triangleright}_{,i}}\partial_D T^{\triangleright}_{,i}$$
$$+ \frac{\partial\eta^{\triangleright}}{\partial\rho_d^{\triangleright}}\partial_D\rho_d^{\triangleright} + \hat{\partial}_D\eta^{\triangleright}]w^{\triangleright}$$

$$+\frac{\partial\phi_i^{\triangleright}}{\partial\varrho^{\triangleright}}\varrho^{\triangleright}_{,i} + \frac{\partial\phi_i^{\triangleright}}{\partial\beta_a}\beta_{a,i} + \frac{\partial\phi_i^{\triangleright}}{\partial D^{\triangleright}_{\langle hk\rangle}}D^{\triangleright}_{\langle hk\rangle,i} + \frac{\partial\phi_i^{\triangleright}}{\partial D^{\triangleright}_{kk}}D^{\triangleright}_{kk,i} + \frac{\partial\phi_i^{\triangleright}}{\partial H^{\triangleright}_{hk}}H^{\triangleright}_{hk,i} + \frac{\partial\phi_i^{\triangleright}}{\partial T^{\triangleright}}T^{\triangleright}_{,i} + \frac{\partial\phi^{\triangleright}_{(i}}{\partial T^{\triangleright}_{,h)}}T^{\triangleright}_{,hi} + \frac{\partial\phi_i^{\triangleright}}{\partial\rho_d^{\triangleright}}\rho^{\triangleright}_{d,i}$$

$$+\frac{\partial\varphi_j^{\triangleright}}{\partial\varrho^{\triangleright}}\partial_j\varrho^{\triangleright}+\frac{\partial\varphi_j^{\triangleright}}{\partial D^{\triangleright}_{\langle hk\rangle}}\partial_j D^{\triangleright}_{\langle hk\rangle}+\frac{\partial\varphi_j^{\triangleright}}{\partial D^{\triangleright}_{kk}}\partial_j D^{\triangleright}_{kk}+\frac{\partial\varphi_j^{\triangleright}}{\partial H^{\triangleright}_{hk}}\partial_j H^{\triangleright}_{hk}+\frac{\partial\varphi_j^{\triangleright}}{\partial T^{\triangleright}}\partial_j T^{\triangleright}+\frac{\partial\varphi_j^{\triangleright}}{\partial T^{\triangleright}_{,i}}\partial_j T^{\triangleright}_{,i}+\frac{\partial\varphi_j^{\triangleright}}{\partial\rho_d^{\triangleright}}\partial_j\rho_d^{\triangleright}$$

$$+\frac{\partial n^{\triangleright}}{\partial\varrho^{\triangleright}}\partial_D\varrho^{\triangleright}+\frac{\partial n^{\triangleright}}{\partial D^{\triangleright}_{\langle hk\rangle}}\partial_D D^{\triangleright}_{\langle hk\rangle}+\frac{\partial n^{\triangleright}}{\partial D^{\triangleright}_{kk}}\partial_D D^{\triangleright}_{kk}+\frac{\partial n^{\triangleright}}{\partial H^{\triangleright}_{hk}}\partial_D H^{\triangleright}_{hk}+\frac{\partial n^{\triangleright}}{\partial T^{\triangleright}}\partial_D T^{\triangleright}+\frac{\partial n^{\triangleright}}{\partial T^{\triangleright}_{,i}}\partial_D T^{\triangleright}_{,i}$$
$$+\frac{\partial n^{\triangleright}}{\partial\rho_d^{\triangleright}}\partial_D\rho_d^{\triangleright}+\hat{\partial}_i\varphi_i^{\triangleright}+\hat{\partial}_D n^{\triangleright}-\varrho^{\triangleright}\delta^{\triangleright}+\varrho^{\triangleright}\Gamma^{\triangleright}\eta^{\triangleright}.$$

Contributions of Mass, Momenta and Dislocation

In this part we will not expand the constitutive quantities included in the balance of momenta. In fact, we remarked in the text that the Lagrange multipliers associated with the balances of momenta will be demonstrated to be equal to zero and so we do not need to work on their factors. Moreover, the expansions of $\partial_D w^{\triangleright}$ in the balances of mass and dislocation are collected at the end of this paragraph. The other constitutive quantities that are here expanded are the interspecies flux densities of dislocation $\gamma^{\triangleright}_{dj}$ and $\Delta^{\triangleright}_D$. Even in these cases the quantities to be expanded are functions of the quantities $\mathcal{X}$ listed in (6.16);

$$-\Lambda^{\triangleright}_m[\frac{\partial\varrho^{\triangleright}}{\partial t}+\varrho^{\triangleright}_{,i}v_i^{\triangleright}+\varrho^{\triangleright}v^{\triangleright}_{i,i}+(\partial_i\varrho^{\triangleright})\,u_i^{\triangleright}+\varrho^{\triangleright}\,(\partial_i H^{\triangleright}_{ik})\,n_k+\varrho^{\triangleright}\,(\partial_i W^{\triangleright}_{ik})\,n_k+(\partial_D\varrho^{\triangleright})\,w^{\triangleright}$$
$$-\varrho^{\triangleright}\Gamma^{\triangleright}]$$
$$-\Lambda^{\triangleright}_{li}[\varrho^{\triangleright}\frac{\partial v_i^{\triangleright}}{\partial t}+\varrho^{\triangleright}v^{\triangleright}_{i,j}v_j^{\triangleright}+\varrho^{\triangleright}\,(\partial_j v_i^{\triangleright})\,u_j^{\triangleright}+\varrho^{\triangleright}\,(\partial_D v_i^{\triangleright})\,w^{\triangleright}-t^{\triangleright}_{ij,j}-\partial_j\tau^{\triangleright}_{ij}-\partial_D F_i^{\triangleright}$$
$$-\varrho^{\triangleright}\,(\kappa_i^{\triangleright}-v_i^{\triangleright}\Gamma^{\triangleright})]$$
$$-\Lambda^{\triangleright}_{ai}[\varrho^{\triangleright}\frac{\partial\sigma_i^{\triangleright}}{\partial t}+\varrho^{\triangleright}\sigma^{\triangleright}_{i,j}v_j^{\triangleright}+\varrho^{\triangleright}\,(\partial_j\sigma_i^{\triangleright})\,u_j^{\triangleright}+\varrho^{\triangleright}\,(\partial_D\sigma_i^{\triangleright})\,w^{\triangleright}-\varepsilon_{ilk}t^{\triangleright}_{kl}-m^{\triangleright}_{il,l}-\partial_l\varpi^{\triangleright}_{il}-\partial_D a_i^{\triangleright}$$
$$-\varrho^{\triangleright}\,(\nu_i^{\triangleright}-\sigma_i^{\triangleright}\Gamma^{\triangleright})]$$
$$-\Lambda^{\triangleright}_d[\frac{\partial\rho_d^{\triangleright}}{\partial t}+\rho^{\triangleright}_{d,i}v_i^{\triangleright}+\rho_d^{\triangleright}v^{\triangleright}_{i,i}+(\partial_i\rho_d^{\triangleright})\,u_i^{\triangleright}+\rho_d^{\triangleright}\,(\partial_i H^{\triangleright}_{ik})\,n_k+\rho_d^{\triangleright}\,(\partial_i W^{\triangleright}_{ik})\,n_k+(\partial_D\rho_d^{\triangleright})\,w^{\triangleright}-\Pi^{\triangleright}]$$

$$-\Lambda^{\triangleright}_d[\frac{\partial\gamma^{\triangleright}_{dj}}{\partial\varrho^{\triangleright}}\partial_j\varrho^{\triangleright}+\frac{\partial\gamma^{\triangleright}_{dj}}{\partial D^{\triangleright}_{\langle hk\rangle}}\partial_j D^{\triangleright}_{\langle hk\rangle}+\frac{\partial\gamma^{\triangleright}_{dj}}{\partial D^{\triangleright}_{kk}}\partial_j D^{\triangleright}_{kk}+\frac{\partial\gamma^{\triangleright}_{dj}}{\partial H^{\triangleright}_{hk}}\partial_j H^{\triangleright}_{hk}+\frac{\partial\gamma^{\triangleright}_{dj}}{\partial T^{\triangleright}}\partial_j T^{\triangleright}+\frac{\partial\gamma^{\triangleright}_{dj}}{\partial T^{\triangleright}_{,i}}\partial_j T^{\triangleright}_{,i}$$
$$+\frac{\partial\gamma^{\triangleright}_{dj}}{\partial\rho_d^{\triangleright}}\partial_j\rho_d^{\triangleright}+\hat{\partial}_j\gamma^{\triangleright}_{dj}]$$
$$-\Lambda^{\triangleright}_d[\frac{\partial\Delta^{\triangleright}_d}{\partial\varrho^{\triangleright}}\partial_D\varrho^{\triangleright}+\frac{\partial\Delta^{\triangleright}_d}{\partial D^{\triangleright}_{\langle hk\rangle}}\partial_D D^{\triangleright}_{\langle hk\rangle}+\frac{\partial\Delta^{\triangleright}_d}{\partial D^{\triangleright}_{kk}}\partial_D D^{\triangleright}_{kk}+\frac{\partial\Delta^{\triangleright}_d}{\partial H^{\triangleright}_{hk}}\partial_D H^{\triangleright}_{hk}+\frac{\partial\Delta^{\triangleright}_d}{\partial T^{\triangleright}}\partial_D T^{\triangleright}+\frac{\partial\Delta^{\triangleright}_d}{\partial T^{\triangleright}_{,i}}\partial_D T^{\triangleright}_{,i}$$
$$+\frac{\partial\Delta^{\triangleright}_d}{\partial\rho_d^{\triangleright}}\partial_D\rho_d^{\triangleright}+\hat{\partial}_D\Delta^{\triangleright}_d]$$

$$-[\Lambda^{\triangleright}_d\rho_d^{\triangleright}+\Lambda^{\triangleright}_m\varrho^{\triangleright}]\,[\frac{\partial w^{\triangleright}}{\partial\varrho^{\triangleright}}\partial_D\varrho^{\triangleright}+\frac{\partial w^{\triangleright}}{\partial D^{\triangleright}_{\langle hk\rangle}}\partial_D D^{\triangleright}_{\langle hk\rangle}+\frac{\partial w^{\triangleright}}{\partial D^{\triangleright}_{kk}}\partial_D D^{\triangleright}_{kk}+\frac{\partial w^{\triangleright}}{\partial H^{\triangleright}_{hk}}\partial_D H^{\triangleright}_{hk}+\frac{\partial w^{\triangleright}}{\partial T^{\triangleright}}\partial_D T^{\triangleright}$$
$$+\frac{\partial w^{\triangleright}}{\partial T^{\triangleright}_{,i}}\partial_D T^{\triangleright}_{,i}+\frac{\partial w^{\triangleright}}{\partial\rho_d^{\triangleright}}\partial_D\rho_d^{\triangleright}+\hat{\partial}_D w^{\triangleright}].$$

Expansion of the Contribution of the Energy

The constitutive functions that we will expand in this part are $e^{\triangleright}$, $q_i^{\triangleright}$, $\xi_j^{\triangleright}$ and $h^{\triangleright}$. They vary with respect to the quantities $\mathcal{X}$ listed in (6.16). Thus the inequality continues and finishes its form as follows:

$$
\begin{aligned}
&- \Lambda_e^{\triangleright}\varrho^{\triangleright}[\frac{\partial e^{\triangleright}}{\partial \varrho^{\triangleright}}\frac{\partial \varrho^{\triangleright}}{\partial t} + \frac{\partial e^{\triangleright}}{\partial \beta_a}\frac{\partial \beta_a}{\partial t} + \frac{\partial e^{\triangleright}}{\partial D^{\triangleright}_{\langle ij\rangle}}\frac{\partial D^{\triangleright}_{\langle ij\rangle}}{\partial t} + \frac{\partial e^{\triangleright}}{\partial D^{\triangleright}_{kk}}\frac{\partial D^{\triangleright}_{kk}}{\partial t} + \frac{\partial e^{\triangleright}}{\partial H^{\triangleright}_{ij}}\frac{\partial H^{\triangleright}_{ij}}{\partial t} + \frac{\partial e^{\triangleright}}{\partial T^{\triangleright}}\frac{\partial T^{\triangleright}}{\partial t} \\
&+ \frac{\partial e^{\triangleright}}{\partial T^{\triangleright}_{,i}}\frac{\partial T^{\triangleright}_{,i}}{\partial t} + \frac{\partial e^{\triangleright}}{\partial \rho_d^{\triangleright}}\frac{\partial \rho_d^{\triangleright}}{\partial t}] \\
&\quad - \Lambda_e^{\triangleright}\varrho^{\triangleright}[\frac{\partial e^{\triangleright}}{\partial \varrho^{\triangleright}}\varrho^{\triangleright}_{,i} + \frac{\partial e^{\triangleright}}{\partial \beta_a}\beta_{a,i} + \frac{\partial e^{\triangleright}}{\partial D^{\triangleright}_{\langle hk\rangle}}D^{\triangleright}_{\langle hk\rangle,i} + \frac{\partial e^{\triangleright}}{\partial D^{\triangleright}_{kk}}D^{\triangleright}_{kk,i} + \frac{\partial e^{\triangleright}}{\partial H^{\triangleright}_{hk}}H^{\triangleright}_{hk,i} + \frac{\partial e^{\triangleright}}{\partial T^{\triangleright}}T^{\triangleright}_{,i} \\
&\quad + \frac{\partial e^{\triangleright}}{\partial \rho_d^{\triangleright}}\rho^{\triangleright}_{d,i}]\upsilon_i^{\triangleright} - \Lambda_e^{\triangleright}\varrho^{\triangleright}\frac{\partial e^{\triangleright}}{\partial T^{\triangleright}_{,(h}}\upsilon^{\triangleright}_{i)}T^{\triangleright}_{,hi} \\
&- \Lambda_e^{\triangleright}\varrho^{\triangleright}[\frac{\partial e^{\triangleright}}{\partial \varrho^{\triangleright}}\partial_j\varrho^{\triangleright} + \frac{\partial e^{\triangleright}}{\partial D^{\triangleright}_{\langle hk\rangle}}\partial_j D^{\triangleright}_{\langle hk\rangle} + \frac{\partial e^{\triangleright}}{\partial D^{\triangleright}_{kk}}\partial_j D^{\triangleright}_{kk} + \frac{\partial e^{\triangleright}}{\partial H^{\triangleright}_{hk}}\partial_j H^{\triangleright}_{hk} + \frac{\partial e^{\triangleright}}{\partial T^{\triangleright}}\partial_j T^{\triangleright} + \frac{\partial e^{\triangleright}}{\partial T^{\triangleright}_{,i}}\partial_j T^{\triangleright}_{,i} \\
&+ \frac{\partial e^{\triangleright}}{\partial \rho_d^{\triangleright}}\partial_j\rho_d^{\triangleright} + \hat{\partial}_i e^{\triangleright}]u_j^{\triangleright} \\
&\quad - \Lambda_e^{\triangleright}\varrho^{\triangleright}[\frac{\partial e^{\triangleright}}{\partial \varrho^{\triangleright}}\partial_D\varrho^{\triangleright} + \frac{\partial e^{\triangleright}}{\partial D^{\triangleright}_{\langle hk\rangle}}\partial_D D^{\triangleright}_{\langle hk\rangle} + \frac{\partial e^{\triangleright}}{\partial D^{\triangleright}_{kk}}\partial_D D^{\triangleright}_{kk} + \varrho^{\triangleright}\frac{\partial e^{\triangleright}}{\partial H^{\triangleright}_{hk}}\partial_D H^{\triangleright}_{hk} + \frac{\partial e^{\triangleright}}{\partial T^{\triangleright}}\partial_D T^{\triangleright} \\
&\quad + \frac{\partial e^{\triangleright}}{\partial T^{\triangleright}_{,i}}\partial_D T^{\triangleright}_{,i} + \frac{\partial e^{\triangleright}}{\partial \rho_d^{\triangleright}}\partial_D\rho_d^{\triangleright} + \hat{\partial}_D e^{\triangleright}]w^{\triangleright} \\
&- \Lambda_e^{\triangleright}[\frac{\partial q_i^{\triangleright}}{\partial \varrho^{\triangleright}}\varrho^{\triangleright}_{,i} + \frac{\partial q_i^{\triangleright}}{\partial \beta_a}\beta_{a,i} + \frac{\partial q_i^{\triangleright}}{\partial D^{\triangleright}_{\langle hk\rangle}}D^{\triangleright}_{\langle hk\rangle,i} + \frac{\partial q_i^{\triangleright}}{\partial D^{\triangleright}_{kk}}D^{\triangleright}_{kk,i} + \frac{\partial q_i^{\triangleright}}{\partial H^{\triangleright}_{hk}}H^{\triangleright}_{hk,i} + \frac{\partial q_i^{\triangleright}}{\partial T^{\triangleright}}T^{\triangleright}_{,i} + \frac{\partial q^{\triangleright}_{(i}}{\partial T^{\triangleright}_{,h)}}T^{\triangleright}_{,hi} \\
&+ \frac{\partial q_i^{\triangleright}}{\partial \rho_d^{\triangleright}}\rho^{\triangleright}_{d,i}] \\
&\quad + \tfrac{1}{2}\Lambda_e^{\triangleright}m^{\triangleright}_{ji}\varepsilon_{kjb}H^{\triangleright}_{kb,i} + \tfrac{1}{2}\Lambda_e^{\triangleright}m^{\triangleright}_{ji}\varepsilon_{kjb}W^{\triangleright}_{kb,i} + \tfrac{1}{2}\Lambda_e^{\triangleright}\varpi^{\triangleright}_{ji}\varepsilon_{kjb}\partial_i H^{\triangleright}_{kb} + \tfrac{1}{2}\Lambda_e^{\triangleright}\varpi^{\triangleright}_{ji}\varepsilon_{kjb}\partial_i W^{\triangleright}_{kb} \\
&- \Lambda_e^{\triangleright}[\frac{\partial \xi_j^{\triangleright}}{\partial \varrho^{\triangleright}}\partial_j\varrho^{\triangleright} + \frac{\partial \xi_j^{\triangleright}}{\partial D^{\triangleright}_{\langle hk\rangle}}\partial_j D^{\triangleright}_{\langle hk\rangle} + \frac{\partial \xi_j^{\triangleright}}{\partial D^{\triangleright}_{kk}}\partial_j D^{\triangleright}_{kk} + \frac{\partial \xi_j^{\triangleright}}{\partial H^{\triangleright}_{hk}}\partial_j H^{\triangleright}_{hk} + \frac{\partial \xi_j^{\triangleright}}{\partial T^{\triangleright}}\partial_j T^{\triangleright} + \frac{\partial \xi_j^{\triangleright}}{\partial T^{\triangleright}_{,i}}\partial_j T^{\triangleright}_{,i} \\
&+ \frac{\partial \xi_j^{\triangleright}}{\partial \rho_d^{\triangleright}}\partial_j\rho_d^{\triangleright} + \hat{\partial}_j\xi_j^{\triangleright}] \\
&-\Lambda_e^{\triangleright}H^{\triangleright}_{jk}t^{\triangleright}_{[jk]} + \Lambda_e^{\triangleright}D^{\triangleright}_{\langle jk\rangle}t^{\triangleright}_{(jk)} + \tfrac{1}{3}\Lambda_e^{\triangleright}\delta_{jk}D^{\triangleright}_{aa}t^{\triangleright}_{(jk)} + \Lambda_e^{\triangleright}\tau^{\triangleright}_{ji}\partial_i\upsilon_j^{\triangleright} + \tfrac{1}{2}\Lambda_e^{\triangleright}\varrho^{\triangleright}\Gamma^{\triangleright}\upsilon_i^{\triangleright}\upsilon_i^{\triangleright} + \tfrac{1}{2}\Lambda_e^{\triangleright}\varrho^{\triangleright}\Gamma^{\triangleright}\sigma_i^{\triangleright}s_i^{\triangleright} \\
&- \Lambda_e^{\triangleright}[\frac{\partial h^{\triangleright}}{\partial \varrho^{\triangleright}}\partial_D\varrho^{\triangleright} + \frac{\partial h^{\triangleright}}{\partial D^{\triangleright}_{\langle hk\rangle}}\partial_D D^{\triangleright}_{\langle hk\rangle} + \frac{\partial h^{\triangleright}}{\partial D^{\triangleright}_{kk}}\partial_D D^{\triangleright}_{kk} + \frac{\partial h^{\triangleright}}{\partial H^{\triangleright}_{hk}}\partial_D H^{\triangleright}_{hk} + \frac{\partial h^{\triangleright}}{\partial T^{\triangleright}}\partial_D T^{\triangleright} + \frac{\partial h^{\triangleright}}{\partial T^{\triangleright}_{,i}}\partial_D T^{\triangleright}_{,i} \\
&+ \frac{\partial h^{\triangleright}}{\partial \rho_d^{\triangleright}}\partial_D\rho_d^{\triangleright} + \hat{\partial}_D h^{\triangleright}] + \Lambda_e^{\triangleright}F_j^{\triangleright}\partial_D\upsilon_j^{\triangleright} + \Lambda_e^{\triangleright}a_j^{\triangleright}\partial_D s_j^{\triangleright} + \Lambda_e^{\triangleright}\varrho^{\triangleright}\epsilon^{\triangleright} - \Lambda_e^{\triangleright}\varrho^{\triangleright}\Gamma^{\triangleright}e^{\triangleright} \geq 0.
\end{aligned}
$$

Thus, we have rewritten (6.23) as a very long expression. It is therefore convenient to rearrange the terms, as we will do now in the second part.t

7.2.2 Part II: Rearranging Terms

In order to transform the preceding inequality into the form (6.26), we simply rearrange and order the terms in such a way that the parts $a_i\mathcal{Y}_i$ and Ω come one after the other. The rearrangement of the terms does not diminish the length of the expression, that will be separated into five parts: the sum of the first four parts will comprise the whole expression $a_i\mathcal{Y}_i$; the fifth part will be the remainder of the inequality, $\Omega \geq 0$. The four parts of the expression $a_i\mathcal{Y}_i$ are divided in such a way that they involve the first, the second, the third and the fourth line of the representation $\mathcal{Y}_i$ in (6.27), respectively. We will also take the definition (6.53) into account.

The First Part of the Linear Terms $a_i\mathcal{Y}_i$

$$
\begin{aligned}
&\frac{\partial \varrho^{\triangleright}}{\partial t}\left[\varrho^{\triangleright}\frac{\partial \eta^{\triangleright}}{\partial \varrho^{\triangleright}} - \Lambda_m^{\triangleright} - \Lambda_e^{\triangleright}\varrho^{\triangleright}\frac{\partial e^{\triangleright}}{\partial \varrho^{\triangleright}}\right] + \frac{\partial \beta_a}{\partial t}\varrho^{\triangleright}\left(\frac{\partial \eta^{\triangleright}}{\partial \beta_a} - \Lambda_e^{\triangleright}\frac{\partial e^{\triangleright}}{\partial \beta_a}\right) - \frac{\partial v_i^{\triangleright}}{\partial t}\varrho^{\triangleright}\Lambda_{li}^{\triangleright}\\
&+\frac{\partial D^{\triangleright}_{\langle ij\rangle}}{\partial t}\varrho^{\triangleright}\left(\frac{\partial \eta^{\triangleright}}{\partial D^{\triangleright}_{\langle ij\rangle}} - \Lambda_e^{\triangleright}\frac{\partial e^{\triangleright}}{\partial D^{\triangleright}_{\langle ij\rangle}}\right) + \frac{\partial D^{\triangleright}_{kk}}{\partial t}\varrho^{\triangleright}\left(\frac{\partial \eta^{\triangleright}}{\partial D^{\triangleright}_{kk}} - \Lambda_e^{\triangleright}\frac{\partial e^{\triangleright}}{\partial D^{\triangleright}_{kk}}\right)\\
&+\frac{\partial H^{\triangleright}_{ij}}{\partial t}\varrho^{\triangleright}\left(\frac{\partial \eta^{\triangleright}}{\partial H^{\triangleright}_{ij}} - \Lambda_e^{\triangleright}\frac{\partial e^{\triangleright}}{\partial H^{\triangleright}_{ij}}\right) - \frac{\partial \sigma_i^{\triangleright}}{\partial t}\varrho^{\triangleright}\Lambda_{a\,i}^{\triangleright} + \frac{\partial T^{\triangleright}}{\partial t}\varrho^{\triangleright}\left(\frac{\partial \eta^{\triangleright}}{\partial T^{\triangleright}} - \Lambda_e^{\triangleright}\frac{\partial e^{\triangleright}}{\partial T^{\triangleright}}\right)\\
&+\frac{\partial T^{\triangleright}_{,i}}{\partial t}\varrho^{\triangleright}\left(\frac{\partial \eta^{\triangleright}}{\partial T^{\triangleright}_{,i}} - \Lambda_e^{\triangleright}\frac{\partial e^{\triangleright}}{\partial T^{\triangleright}_{,i}}\right) + \frac{\partial \rho_d^{\triangleright}}{\partial t}\left[\varrho^{\triangleright}\frac{\partial \eta^{\triangleright}}{\partial \rho_d^{\triangleright}} - \Lambda_e^{\triangleright}\varrho^{\triangleright}\frac{\partial e^{\triangleright}}{\partial \rho_d^{\triangleright}} - \Lambda_d^{\triangleright}\right]
\end{aligned}
$$

The Second Part of the Linear Terms $a_i\mathcal{Y}_i$

$$
\begin{aligned}
&+\varrho^{\triangleright}_{,i}\left[\left(\varrho^{\triangleright}\frac{\partial \eta^{\triangleright}}{\partial \varrho^{\triangleright}} - \Lambda_m^{\triangleright} - \Lambda_e^{\triangleright}\varrho^{\triangleright}\frac{\partial e^{\triangleright}}{\partial \varrho^{\triangleright}}\right)v_i^{\triangleright} + \frac{\partial \phi_i^{\triangleright}}{\partial \varrho^{\triangleright}} - \Lambda_e^{\triangleright}\frac{\partial q_i^{\triangleright}}{\partial \varrho^{\triangleright}}\right]\\
&+\beta_{a,i}\left[\varrho^{\triangleright}\left(\frac{\partial \eta^{\triangleright}}{\partial \beta_a} - \Lambda_e^{\triangleright}\frac{\partial e^{\triangleright}}{\partial \beta_a}\right)v_i^{\triangleright} + \frac{\partial \phi_i^{\triangleright}}{\partial \beta_a} - \Lambda_e^{\triangleright}\frac{\partial q_i^{\triangleright}}{\partial \beta_a}\right]\\
&+D^{\triangleright}_{\langle hk\rangle,i}\left[\varrho^{\triangleright}\left(\frac{\partial \eta^{\triangleright}}{\partial D^{\triangleright}_{\langle hk\rangle}} - \Lambda_e^{\triangleright}\frac{\partial e^{\triangleright}}{\partial D^{\triangleright}_{\langle ij\rangle}}\right)v_i^{\triangleright} + \frac{\partial \phi_i^{\triangleright}}{\partial D^{\triangleright}_{\langle hk\rangle}} - \Lambda_e^{\triangleright}\frac{\partial q_i^{\triangleright}}{\partial D^{\triangleright}_{\langle hk\rangle}}\right]\\
&+D^{\triangleright}_{kk,i}\left[\varrho^{\triangleright}\left(\frac{\partial \eta^{\triangleright}}{\partial D^{\triangleright}_{kk}} - \Lambda_e^{\triangleright}\frac{\partial e^{\triangleright}}{\partial D^{\triangleright}_{kk}}\right)v_i^{\triangleright} + \frac{\partial \phi_i^{\triangleright}}{\partial D^{\triangleright}_{kk}} - \Lambda_e^{\triangleright}\frac{\partial q_i^{\triangleright}}{\partial D^{\triangleright}_{kk}}\right]\\
&+W^{\triangleright}_{kb,i}\left[\frac{1}{2}\Lambda_e^{\triangleright}m^{\triangleright}_{ji}\varepsilon_{kjb}\right]\\
&+H^{\triangleright}_{kb,i}\left[\varrho^{\triangleright}\left(\frac{\partial \eta^{\triangleright}}{\partial H^{\triangleright}_{kb}} - \Lambda_e^{\triangleright}\frac{\partial e^{\triangleright}}{\partial H^{\triangleright}_{kb}}\right)v_i^{\triangleright} + \frac{1}{2}\Lambda_e^{\triangleright}m^{\triangleright}_{ji}\varepsilon_{kjb} + \frac{\partial \phi_i^{\triangleright}}{\partial H^{\triangleright}_{kb}} - \Lambda_e^{\triangleright}\frac{\partial q_i^{\triangleright}}{\partial H^{\triangleright}_{kb}}\right]\\
&+T^{\triangleright}_{,hi}\left[+\varrho^{\triangleright}\left(\frac{\partial \eta^{\triangleright}}{\partial T^{\triangleright}_{,(h}} - \Lambda_e^{\triangleright}\frac{\partial e^{\triangleright}}{\partial T^{\triangleright}_{,(h}}\right)v^{\triangleright}_{i)} + \frac{\partial \phi^{\triangleright}_{(i}}{\partial T^{\triangleright}_{,h)}} - \Lambda_e^{\triangleright}\frac{\partial q^{\triangleright}_{(i}}{\partial T^{\triangleright}_{,h)}}\right]\\
&+\rho^{\triangleright}_{d,i}\left[\left(\varrho^{\triangleright}\frac{\partial \eta^{\triangleright}}{\partial \rho_d^{\triangleright}} - \Lambda_e^{\triangleright}\varrho^{\triangleright}\frac{\partial e^{\triangleright}}{\partial \rho_d^{\triangleright}} - \Lambda_d^{\triangleright}\right)v_i^{\triangleright} + \frac{\partial \phi_i^{\triangleright}}{\partial \rho_d^{\triangleright}} - \Lambda_e^{\triangleright}\frac{\partial q_i^{\triangleright}}{\partial \rho_d^{\triangleright}}\right]
\end{aligned}
$$

The Third Part of the Linear Terms $a_i\mathcal{Y}_i$

$$+\left(\partial_j \varrho^{\triangleright}\right)\left[\left(\varrho^{\triangleright}\frac{\partial \eta^{\triangleright}}{\partial \varrho^{\triangleright}}-\Lambda_m^{\triangleright}-\Lambda_e^{\triangleright}\varrho^{\triangleright}\frac{\partial e^{\triangleright}}{\partial \varrho^{\triangleright}}\right)u_j^{\triangleright}+\frac{\partial \varphi_j^{\triangleright}}{\partial \varrho^{\triangleright}}-\Lambda_e^{\triangleright}\frac{\partial \xi_j^{\triangleright}}{\partial \varrho^{\triangleright}}-\Lambda_d^{\triangleright}\frac{\partial \gamma_{dj}^{\triangleright}}{\partial \varrho^{\triangleright}}\right]$$
$$+\left(\partial_i v_j^{\triangleright}\right)\left[\Lambda_e^{\triangleright}\tau_{ji}^{\triangleright}\right]$$

$$+\left(\partial_j D_{\langle hk\rangle}^{\triangleright}\right)\left[\varrho^{\triangleright}\left(\frac{\partial \eta^{\triangleright}}{\partial D_{\langle hk\rangle}^{\triangleright}}-\Lambda_e^{\triangleright}\frac{\partial e^{\triangleright}}{\partial D_{\langle hk\rangle}^{\triangleright}}\right)u_j^{\triangleright}+\frac{\partial \varphi_j^{\triangleright}}{\partial D_{\langle hk\rangle}^{\triangleright}}-\Lambda_e^{\triangleright}\frac{\partial \xi_j^{\triangleright}}{\partial D_{\langle hk\rangle}^{\triangleright}}-\Lambda_d^{\triangleright}\frac{\partial \gamma_{dj}^{\triangleright}}{\partial D_{\langle hk\rangle}^{\triangleright}}\right]$$
$$+\left(\partial_j D_{kk}^{\triangleright}\right)\left[\varrho^{\triangleright}\left(\frac{\partial \eta^{\triangleright}}{\partial D_{kk}^{\triangleright}}-\Lambda_e^{\triangleright}\frac{\partial e^{\triangleright}}{\partial D_{kk}^{\triangleright}}\right)u_j^{\triangleright}+\frac{\partial \varphi_j^{\triangleright}}{\partial D_{kk}^{\triangleright}}-\Lambda_e^{\triangleright}\frac{\partial \xi_j^{\triangleright}}{\partial D_{kk}^{\triangleright}}-\Lambda_d^{\triangleright}\frac{\partial \gamma_{dj}^{\triangleright}}{\partial D_{kk}^{\triangleright}}\right]$$
$$+\left(\partial_j W_{hk}^{\triangleright}\right)\left[-\left(\Lambda_m^{\triangleright}\varrho^{\triangleright}+\Lambda_d^{\triangleright}\rho_d^{\triangleright}\right)\delta_{j[h}n_{k]}+\frac{1}{2}\Lambda_e^{\triangleright}\varpi_{aj}^{\triangleright}\varepsilon_{hak}\right]$$

$$+\left(\partial_j H_{hk}^{\triangleright}\right)\left[\varrho^{\triangleright}\left(\frac{\partial \eta^{\triangleright}}{\partial H_{hk}^{\triangleright}}-\Lambda_e^{\triangleright}\frac{\partial e^{\triangleright}}{\partial H_{hk}^{\triangleright}}\right)u_j^{\triangleright}+\frac{\partial \varphi_j^{\triangleright}}{\partial H_{hk}^{\triangleright}}-\Lambda_e^{\triangleright}\frac{\partial \xi_j^{\triangleright}}{\partial H_{hk}^{\triangleright}}-\Lambda_d^{\triangleright}\frac{\partial \gamma_{dj}^{\triangleright}}{\partial H_{hk}^{\triangleright}}\right.$$
$$\left.-\left(\Lambda_m^{\triangleright}\varrho^{\triangleright}+\Lambda_d^{\triangleright}\rho_d^{\triangleright}\right)\delta_{j[h}n_{k]}+\frac{1}{2}\Lambda_e^{\triangleright}\varpi_{aj}^{\triangleright}\varepsilon_{hak}\right]$$

$$+\left(\partial_j T^{\triangleright}\right)\left[\varrho^{\triangleright}\left(\frac{\partial \eta^{\triangleright}}{\partial T^{\triangleright}}-\Lambda_e^{\triangleright}\frac{\partial e^{\triangleright}}{\partial T^{\triangleright}}\right)u_j^{\triangleright}+\frac{\partial \varphi_j^{\triangleright}}{\partial T^{\triangleright}}-\Lambda_e^{\triangleright}\frac{\partial \xi_j^{\triangleright}}{\partial T^{\triangleright}}-\Lambda_d^{\triangleright}\frac{\partial \gamma_{dj}^{\triangleright}}{\partial T^{\triangleright}}\right]$$
$$+\left(\partial_j T_{,i}^{\triangleright}\right)\left[\varrho^{\triangleright}\left(\frac{\partial \eta^{\triangleright}}{\partial T_{,i}^{\triangleright}}-\Lambda_e^{\triangleright}\frac{\partial e^{\triangleright}}{\partial T_{,i}^{\triangleright}}\right)u_j^{\triangleright}+\frac{\partial \varphi_j^{\triangleright}}{\partial T_{,i}^{\triangleright}}-\Lambda_e^{\triangleright}\frac{\partial \xi_j^{\triangleright}}{\partial T_{,i}^{\triangleright}}-\Lambda_d^{\triangleright}\frac{\partial \gamma_{dj}^{\triangleright}}{\partial T_{,i}^{\triangleright}}\right]$$
$$+\left(\partial_j \rho_d^{\triangleright}\right)\left[\left(\varrho^{\triangleright}\frac{\partial \eta^{\triangleright}}{\partial \rho_d^{\triangleright}}-\Lambda_e^{\triangleright}\varrho^{\triangleright}\frac{\partial e^{\triangleright}}{\partial \rho_d^{\triangleright}}-\Lambda_d^{\triangleright}\right)u_j^{\triangleright}+\frac{\partial \varphi_j^{\triangleright}}{\partial \rho_d^{\triangleright}}-\Lambda_e^{\triangleright}\frac{\partial \xi_j^{\triangleright}}{\partial \rho_d^{\triangleright}}-\Lambda_d^{\triangleright}\frac{\partial \gamma_{dj}^{\triangleright}}{\partial \rho_d^{\triangleright}}\right]$$

The Fourth Part of the Linear Terms $a_i\mathcal{Y}_i$

$$+\left(\partial_D \varrho^{\triangleright}\right)\left[\left(\varrho^{\triangleright}\frac{\partial \eta^{\triangleright}}{\partial \varrho^{\triangleright}}-\Lambda_m^{\triangleright}-\Lambda_e^{\triangleright}\varrho^{\triangleright}\frac{\partial e^{\triangleright}}{\partial \varrho^{\triangleright}}\right)w^{\triangleright}+\frac{\partial n^{\triangleright}}{\partial \varrho^{\triangleright}}-\Lambda_e^{\triangleright}\frac{\partial h^{\triangleright}}{\partial \varrho^{\triangleright}}-\Lambda_d^{\triangleright}\frac{\partial \Delta_d^{\triangleright}}{\partial \varrho^{\triangleright}}-p^{\triangleright}\frac{\partial w^{\triangleright}}{\partial \varrho^{\triangleright}}\right]$$
$$+\left(\partial_D v_j^{\triangleright}\right)\left[\Lambda_e^{\triangleright}F_j^{\triangleright}\right]+\left(\partial_D s_j^{\triangleright}\right)\left[\Lambda_e^{\triangleright}a_j^{\triangleright}\right]$$

$$+\left(\partial_D D_{\langle hk\rangle}^{\triangleright}\right)\left[\varrho^{\triangleright}\left(\frac{\partial \eta^{\triangleright}}{\partial D_{\langle hk\rangle}^{\triangleright}}-\Lambda_e^{\triangleright}\frac{\partial e^{\triangleright}}{\partial D_{\langle hk\rangle}^{\triangleright}}\right)w^{\triangleright}+\frac{\partial n^{\triangleright}}{\partial D_{\langle hk\rangle}^{\triangleright}}-\Lambda_e^{\triangleright}\frac{\partial h^{\triangleright}}{\partial D_{\langle hk\rangle}^{\triangleright}}-\Lambda_d^{\triangleright}\frac{\partial \Delta_d^{\triangleright}}{\partial D_{\langle hk\rangle}^{\triangleright}}\right.$$
$$\left.-p^{\triangleright}\frac{\partial w^{\triangleright}}{\partial D_{\langle hk\rangle}^{\triangleright}}\right]$$

$$+\left(\partial_D D_{kk}^{\triangleright}\right)\left[\varrho^{\triangleright}\left(\frac{\partial \eta^{\triangleright}}{\partial D_{kk}^{\triangleright}}-\Lambda_e^{\triangleright}\frac{\partial e^{\triangleright}}{\partial D_{kk}^{\triangleright}}\right)w^{\triangleright}+\frac{\partial n^{\triangleright}}{\partial D_{kk}^{\triangleright}}-\Lambda_e^{\triangleright}\frac{\partial h^{\triangleright}}{\partial D_{kk}^{\triangleright}}-\Lambda_d^{\triangleright}\frac{\partial \Delta_d^{\triangleright}}{\partial D_{kk}^{\triangleright}}-p^{\triangleright}\frac{\partial w^{\triangleright}}{\partial D_{kk}^{\triangleright}}\right]$$
$$+\left(\partial_D H_{hk}^{\triangleright}\right)\left[\varrho^{\triangleright}\left(\frac{\partial \eta^{\triangleright}}{\partial H_{hk}^{\triangleright}}-\Lambda_e^{\triangleright}\frac{\partial e^{\triangleright}}{\partial H_{hk}^{\triangleright}}\right)w^{\triangleright}+\frac{\partial n^{\triangleright}}{\partial H_{hk}^{\triangleright}}-\Lambda_e^{\triangleright}\frac{\partial h^{\triangleright}}{\partial H_{hk}^{\triangleright}}-\Lambda_d^{\triangleright}\frac{\partial \Delta_d^{\triangleright}}{\partial H_{hk}^{\triangleright}}-p^{\triangleright}\frac{\partial w^{\triangleright}}{\partial H_{hk}^{\triangleright}}\right]$$

$$+\left(\partial_{D}T^{\triangleright}\right)\left[\varrho^{\triangleright}\left(\frac{\partial\eta^{\triangleright}}{\partial T^{\triangleright}}-\Lambda_{e}^{\triangleright}\frac{\partial e^{\triangleright}}{\partial T^{\triangleright}}\right)w^{\triangleright}+\frac{\partial n^{\triangleright}}{\partial T^{\triangleright}}-\Lambda_{e}^{\triangleright}\frac{\partial h^{\triangleright}}{\partial T^{\triangleright}}-\Lambda_{d}^{\triangleright}\frac{\partial\Delta_{d}^{\triangleright}}{\partial T^{\triangleright}}-p^{\triangleright}\frac{\partial w^{\triangleright}}{\partial T^{\triangleright}}\right]$$
$$+\left(\partial_{D}T_{,i}^{\triangleright}\right)\left[\varrho^{\triangleright}\left(\frac{\partial\eta^{\triangleright}}{\partial T_{,i}^{\triangleright}}-\Lambda_{e}^{\triangleright}\frac{\partial e^{\triangleright}}{\partial T_{,i}^{\triangleright}}\right)w^{\triangleright}+\frac{\partial n^{\triangleright}}{\partial T_{,i}^{\triangleright}}-\Lambda_{e}^{\triangleright}\frac{\partial h^{\triangleright}}{\partial T_{,i}^{\triangleright}}-\Lambda_{d}^{\triangleright}\frac{\partial\Delta_{d}^{\triangleright}}{\partial T_{,i}^{\triangleright}}-p^{\triangleright}\frac{\partial w^{\triangleright}}{\partial T_{,i}^{\triangleright}}\right]$$
$$+\left(\partial_{D}\rho_{d}^{\triangleright}\right)\left[\left(\varrho^{\triangleright}\frac{\partial\eta^{\triangleright}}{\partial\rho_{d}^{\triangleright}}-\Lambda_{d}^{\triangleright}-\Lambda_{e}^{\triangleright}\varrho^{\triangleright}\frac{\partial e^{\triangleright}}{\partial\rho_{d}^{\triangleright}}\right)w^{\triangleright}+\frac{\partial n^{\triangleright}}{\partial\rho_{d}^{\triangleright}}-\Lambda_{e}^{\triangleright}\frac{\partial h^{\triangleright}}{\partial\rho_{d}^{\triangleright}}-\Lambda_{d}^{\triangleright}\frac{\partial\Delta_{d}^{\triangleright}}{\partial\rho_{d}^{\triangleright}}-p^{\triangleright}\frac{\partial w^{\triangleright}}{\partial\rho_{d}^{\triangleright}}\right]$$

The Remainder of the Inequality $\Omega\geq 0$

$$+\upsilon_{i}^{\triangleright}\varrho^{\triangleright}\left(\frac{\partial\eta^{\triangleright}}{\partial T^{\triangleright}}-\Lambda_{e}^{\triangleright}\frac{\partial e^{\triangleright}}{\partial T^{\triangleright}}\right)T_{,i}^{\triangleright}+\left[\frac{\partial\phi_{i}^{\triangleright}}{\partial T^{\triangleright}}-\Lambda_{e}^{\triangleright}\frac{\partial q_{i}^{\triangleright}}{\partial T^{\triangleright}}\right]T_{,i}^{\triangleright}-p^{\triangleright}\left(\hat{\partial}_{D}w^{\triangleright}+D_{aa}^{\triangleright}\right)$$

$$-\varrho^{\triangleright}\delta^{\triangleright}+\varrho^{\triangleright}\Gamma^{\triangleright}\eta^{\triangleright}+\Lambda_{m}^{\triangleright}\varrho^{\triangleright}\Gamma^{\triangleright}-\Lambda_{e}^{\triangleright}H_{jk}^{\triangleright}t_{[jk]}^{\triangleright}+\Lambda_{e}^{\triangleright}D_{\langle jk\rangle}^{\triangleright}t_{\langle jk\rangle}^{\triangleright}+\tfrac{1}{3}\Lambda_{e}^{\triangleright}D_{aa}^{\triangleright}t_{(bb)}^{\triangleright}+\Lambda_{e}^{\triangleright}\varrho^{\triangleright}\epsilon^{\triangleright}$$
$$-\Lambda_{e}^{\triangleright}\varrho^{\triangleright}\Gamma^{\triangleright}e^{\triangleright}+\Lambda_{e}^{\triangleright}\tfrac{1}{2}\varrho^{\triangleright}\Gamma^{\triangleright}\upsilon_{i}^{\triangleright}\upsilon_{i}^{\triangleright}+\Lambda_{e}^{\triangleright}\tfrac{1}{2}\varrho^{\triangleright}\Gamma^{\triangleright}\sigma_{i}^{\triangleright}s_{i}^{\triangleright}+\Lambda_{d}^{\triangleright}\Pi^{\triangleright}$$

$$+\varrho^{\triangleright}\left[\hat{\partial}_{j}\eta^{\triangleright}-\Lambda_{e}^{\triangleright}\hat{\partial}_{j}e^{\triangleright}\right]u_{j}^{\triangleright}+\varrho^{\triangleright}\left[\hat{\partial}_{D}\eta^{\triangleright}-\Lambda_{e}^{\triangleright}\hat{\partial}_{D}e^{\triangleright}\right]w^{\triangleright}+\hat{\partial}_{i}\varphi_{i}^{\triangleright}-\Lambda_{d}^{\triangleright}\hat{\partial}_{j}\gamma_{dj}^{\triangleright}-\Lambda_{e}^{\triangleright}\hat{\partial}_{j}\xi_{j}^{\triangleright}$$
$$-\Lambda_{d}^{\triangleright}\hat{\partial}_{D}\Delta_{d}^{\triangleright}+\hat{\partial}_{D}n^{\triangleright}-\Lambda_{e}^{\triangleright}\hat{\partial}_{D}h^{\triangleright}$$

$$-\Lambda_{li}^{\triangleright}\left[\varrho^{\triangleright}\upsilon_{i,j}^{\triangleright}\upsilon_{j}^{\triangleright}+\varrho^{\triangleright}\left(\partial_{j}\upsilon_{i}^{\triangleright}\right)u_{j}^{\triangleright}+\varrho^{\triangleright}\left(\partial_{D}\upsilon_{i}^{\triangleright}\right)w^{\triangleright}-t_{ij,j}^{\triangleright}-\partial_{j}\tau_{ij}^{\triangleright}-\partial_{D}F_{i}^{\triangleright}-\varrho^{\triangleright}\left(\kappa_{i}^{\triangleright}-\upsilon_{i}^{\triangleright}\Gamma^{\triangleright}\right)\right]$$
$$-\Lambda_{ai}^{\triangleright}[\varrho^{\triangleright}\sigma_{i,j}^{\triangleright}\upsilon_{j}^{\triangleright}+\varrho^{\triangleright}\left(\partial_{j}\sigma_{i}^{\triangleright}\right)u_{j}^{\triangleright}+\varrho^{\triangleright}\left(\partial_{D}\sigma_{i}^{\triangleright}\right)w^{\triangleright}-\varepsilon_{ilk}t_{kl}^{\triangleright}-m_{il,l}^{\triangleright}-\partial_{l}\varpi_{il}^{\triangleright}-\partial_{D}a_{i}^{\triangleright}$$
$$-\varrho^{\triangleright}\nu_{i}^{\triangleright}+\varrho^{\triangleright}\Gamma^{\triangleright}\sigma_{i}^{\triangleright}]\geq 0.$$

We repeat that in the previous part we have not expanded the constitutive quantities involved in the balances of momenta, and here they are located at the end of the remainder of the inequality regardless of the formal representation of (6.26). This is so because we will prove that Lagrange Multipliers associated with the balances of momenta vanish immediately once one considers the linearity of the inequality with respect to $\partial\upsilon_{i}^{\triangleright}/\partial t$ and $\partial\sigma_{i}^{\triangleright}/\partial t$.

7.2.3 Part III: The Explicit Form of the Liu Equations

Because of the arbitrariness of the linear terms $\mathcal{Y}_{i}$ represented in (6.27) of inequality (6.26) we may now identify the following Liu Equations by setting $a_{i}=0$:

$$\left.\begin{aligned}&\Lambda_{li}^{\triangleright}=0,\quad\Lambda_{ai}^{\triangleright}=0,\quad m_{ji}^{\triangleright}=0,\quad\tau_{ji}^{\triangleright}=0,\quad F_{j}^{\triangleright}=0,\quad a_{j}^{\triangleright}=0,\\&-\left(\Lambda_{m}^{\triangleright}\varrho^{\triangleright}+\Lambda_{d}^{\triangleright}\rho_{d}^{\triangleright}\right)\delta_{j[h}n_{k]}+\tfrac{1}{2}\Lambda_{e}^{\triangleright}\varpi_{aj}^{\triangleright}\varepsilon_{hak}=0,\end{aligned}\right\}\tag{7.2}$$

$$\left.\begin{aligned}&\frac{\partial\eta^{\triangleright}}{\partial\varrho^{\triangleright}}-\Lambda_{e}^{\triangleright}\frac{\partial e^{\triangleright}}{\partial\varrho^{\triangleright}}=\frac{\Lambda_{m}^{\triangleright}}{\varrho^{\triangleright}},\quad\frac{\partial\eta^{\triangleright}}{\partial\beta_{a}}-\Lambda_{e}^{\triangleright}\frac{\partial e^{\triangleright}}{\partial\beta_{a}}=0,\\&\frac{\partial\eta^{\triangleright}}{\partial D_{hk}^{\triangleright}}-\Lambda_{e}^{\triangleright}\frac{\partial e^{\triangleright}}{\partial D_{hk}^{\triangleright}}=0,\quad\frac{\partial\eta^{\triangleright}}{\partial H_{ij}^{\triangleright}}-\Lambda_{e}^{\triangleright}\frac{\partial e^{\triangleright}}{\partial H_{ij}^{\triangleright}}=0,\quad\frac{\partial\eta^{\triangleright}}{\partial T^{\triangleright}}-\Lambda_{e}^{\triangleright}\frac{\partial e^{\triangleright}}{\partial T^{\triangleright}}=0,\\&\frac{\partial\eta^{\triangleright}}{\partial T_{,i}^{\triangleright}}-\Lambda_{e}^{\triangleright}\frac{\partial e^{\triangleright}}{\partial T_{,i}^{\triangleright}}=0,\quad\frac{\partial\eta^{\triangleright}}{\partial\rho_{d}^{\triangleright}}-\Lambda_{e}^{\triangleright}\frac{\partial e^{\triangleright}}{\partial\rho_{d}^{\triangleright}}=\frac{\Lambda_{d}^{\triangleright}}{\varrho^{\triangleright}},\end{aligned}\right\}\tag{7.3}$$

$$\left.\begin{array}{lll} \dfrac{\partial\phi_i^{\triangleright}}{\partial\varrho^{\triangleright}} - \Lambda_e^{\triangleright}\dfrac{\partial q_i^{\triangleright}}{\partial\varrho^{\triangleright}} = 0, & \dfrac{\partial\phi_i^{\triangleright}}{\partial\beta_a} - \Lambda_e^{\triangleright}\dfrac{\partial q_i^{\triangleright}}{\partial\beta_a} = 0, & \dfrac{\partial\phi_i^{\triangleright}}{\partial D_{hk}^{\triangleright}} - \Lambda_e^{\triangleright}\dfrac{\partial q_i^{\triangleright}}{\partial D_{hk}^{\triangleright}} = 0, \\ \dfrac{\partial\phi_i^{\triangleright}}{\partial H_{kb}^{\triangleright}} - \Lambda_e^{\triangleright}\dfrac{\partial q_i^{\triangleright}}{\partial H_{kb}^{\triangleright}} = 0, & \dfrac{\partial\phi_{(i}^{\triangleright}}{\partial T_{,h)}^{\triangleright}} - \Lambda_e^{\triangleright}\dfrac{\partial q_{(i}^{\triangleright}}{\partial T_{,h)}^{\triangleright}} = 0, & \dfrac{\partial\phi_i^{\triangleright}}{\partial\rho_d^{\triangleright}} - \Lambda_e^{\triangleright}\dfrac{\partial q_i^{\triangleright}}{\partial\rho_d^{\triangleright}} = 0, \end{array}\right\} \tag{7.4}$$

$$\left.\begin{array}{lll} \dfrac{\partial\varphi_j^{\triangleright}}{\partial\varrho^{\triangleright}} - \Lambda_e^{\triangleright}\dfrac{\partial\xi_j^{\triangleright}}{\partial\varrho^{\triangleright}} - \Lambda_d^{\triangleright}\dfrac{\partial\gamma_j^{\triangleright}}{\partial\varrho^{\triangleright}} = 0, & \dfrac{\partial\varphi_j^{\triangleright}}{\partial D_{hk}^{\triangleright}} - \Lambda_e^{\triangleright}\dfrac{\partial\xi_j^{\triangleright}}{\partial D_{hk}^{\triangleright}} - \Lambda_d^{\triangleright}\dfrac{\partial\gamma_j^{\triangleright}}{\partial D_{hk}^{\triangleright}} = 0, \\ \dfrac{\partial\varphi_j^{\triangleright}}{\partial H_{hk}^{\triangleright}} - \Lambda_e^{\triangleright}\dfrac{\partial\xi_j^{\triangleright}}{\partial H_{hk}^{\triangleright}} - \Lambda_d^{\triangleright}\dfrac{\partial\gamma_j^{\triangleright}}{\partial H_{hk}^{\triangleright}} = 0, & \dfrac{\partial\varphi_j^{\triangleright}}{\partial T^{\triangleright}} - \Lambda_e^{\triangleright}\dfrac{\partial\xi_j^{\triangleright}}{\partial T^{\triangleright}} - \Lambda_d^{\triangleright}\dfrac{\partial\gamma_j^{\triangleright}}{\partial T^{\triangleright}} = 0, \\ \dfrac{\partial\varphi_j^{\triangleright}}{\partial T_{,i}^{\triangleright}} - \Lambda_e^{\triangleright}\dfrac{\partial\xi_j^{\triangleright}}{\partial T_{,i}^{\triangleright}} - \Lambda_d^{\triangleright}\dfrac{\partial\gamma_j^{\triangleright}}{\partial T_{,i}^{\triangleright}} = 0, & \dfrac{\partial\varphi_j^{\triangleright}}{\partial\rho_d^{\triangleright}} - \Lambda_e^{\triangleright}\dfrac{\partial\xi_j^{\triangleright}}{\partial\rho_d^{\triangleright}} - \Lambda_d^{\triangleright}\dfrac{\partial\gamma_j^{\triangleright}}{\partial\rho_d^{\triangleright}} = 0, \end{array}\right\} \tag{7.5}$$

$$\left.\begin{array}{lll} \dfrac{\partial n^{\triangleright}}{\partial\varrho^{\triangleright}} - \Lambda_e^{\triangleright}\dfrac{\partial h^{\triangleright}}{\partial\varrho^{\triangleright}} - \Lambda_d^{\triangleright}\dfrac{\partial\Delta_d^{\triangleright}}{\partial\varrho^{\triangleright}} - p^{\triangleright}\dfrac{\partial w^{\triangleright}}{\partial\varrho^{\triangleright}} = 0, & \dfrac{\partial n^{\triangleright}}{\partial D_{hk}^{\triangleright}} - \Lambda_e^{\triangleright}\dfrac{\partial h^{\triangleright}}{\partial D_{hk}^{\triangleright}} - \Lambda_d^{\triangleright}\dfrac{\partial\Delta_d^{\triangleright}}{\partial D_{hk}^{\triangleright}} - p^{\triangleright}\dfrac{\partial w^{\triangleright}}{\partial D_{hk}^{\triangleright}} = 0, \\ \dfrac{\partial n^{\triangleright}}{\partial H_{hk}^{\triangleright}} - \Lambda_e^{\triangleright}\dfrac{\partial h^{\triangleright}}{\partial H_{hk}^{\triangleright}} - \Lambda_d^{\triangleright}\dfrac{\partial\Delta_d^{\triangleright}}{\partial H_{hk}^{\triangleright}} - p^{\triangleright}\dfrac{\partial w^{\triangleright}}{\partial H_{hk}^{\triangleright}} = 0, & \dfrac{\partial n^{\triangleright}}{\partial T^{\triangleright}} - \Lambda_e^{\triangleright}\dfrac{\partial h^{\triangleright}}{\partial T^{\triangleright}} - \Lambda_d^{\triangleright}\dfrac{\partial\Delta_d^{\triangleright}}{\partial T^{\triangleright}} - p^{\triangleright}\dfrac{\partial w^{\triangleright}}{\partial T^{\triangleright}} = 0, \\ \dfrac{\partial n^{\triangleright}}{\partial T_{,i}^{\triangleright}} - \Lambda_e^{\triangleright}\dfrac{\partial h^{\triangleright}}{\partial T_{,i}^{\triangleright}} - \Lambda_d^{\triangleright}\dfrac{\partial\Delta_d^{\triangleright}}{\partial T_{,i}^{\triangleright}} - p^{\triangleright}\dfrac{\partial w^{\triangleright}}{\partial T_{,i}^{\triangleright}} = 0, & \dfrac{\partial n^{\triangleright}}{\partial\rho_d^{\triangleright}} - \Lambda_e^{\triangleright}\dfrac{\partial h^{\triangleright}}{\partial\rho_d^{\triangleright}} - \Lambda_d^{\triangleright}\dfrac{\partial\Delta_d^{\triangleright}}{\partial\rho_d^{\triangleright}} - p^{\triangleright}\dfrac{\partial w^{\triangleright}}{\partial\rho_d^{\triangleright}} = 0. \end{array}\right\} \tag{7.6}$$

The residual entropy inequality is stated in (6.55) and (6.56). Let us further remark that (6.28-6.30) are simply the compact form of these equations (7.2-7.6).

7.3 The Analysis of Thermodynamic Equilibrium

The analysis of thermostatic equilibrium is considered only through the exploitation of the four derivatives prescribed by equations $(6.58)_2$. The evaluation of these derivatives is straightforward and comes from the natural consideration that only the constitutive

quantities (6.6) have a dependence on $D^{\triangleright}_{ij}$, $H^{\triangleright}_{ij}$ and $T^{\triangleright}_{,i}$. Thus,

$$\begin{aligned}
\frac{\partial T^{\triangleright}\varsigma^{\triangleright P}}{\partial D^{\triangleright}_{aa}} &= \frac{\partial F^{\triangleright}}{\partial D^{\triangleright}_{aa}} - T^{\triangleright}\varrho^{\triangleright}\frac{\partial \delta^{\triangleright}}{\partial D^{\triangleright}_{aa}} - \frac{\partial \phi^{\triangleright}_{i}}{\partial D^{\triangleright}_{aa}}T^{\triangleright}_{,i} - H^{\triangleright}_{jk}\frac{\partial t^{\triangleright}_{[jk]}}{\partial D^{\triangleright}_{aa}} + D^{\triangleright}_{\langle jk\rangle}\frac{\partial t^{\triangleright}_{\langle jk\rangle}}{\partial D^{\triangleright}_{aa}} + \tfrac{1}{3}t^{\triangleright}_{bb} + \tfrac{1}{3}D^{\triangleright}_{aa}\frac{\partial t^{\triangleright}_{cc}}{\partial D^{\triangleright}_{bb}} \\
&\quad + p^{\triangleright}\frac{\partial}{\partial D^{\triangleright}_{aa}}\left[\hat{\partial}_{D}w^{\triangleright}\right] + p^{\triangleright} \\
\frac{\partial T^{\triangleright}\varsigma^{\triangleright P}}{\partial D^{\triangleright}_{\langle ab\rangle}} &= \frac{\partial F^{\triangleright}}{\partial D^{\triangleright}_{\langle ab\rangle}} - T^{\triangleright}\varrho^{\triangleright}\frac{\partial \delta^{\triangleright}}{\partial D^{\triangleright}_{\langle ab\rangle}} - \frac{\partial \phi^{\triangleright}_{i}}{\partial D^{\triangleright}_{\langle ab\rangle}}T^{\triangleright}_{,i} - H^{\triangleright}_{jk}\frac{\partial t^{\triangleright}_{[jk]}}{\partial D^{\triangleright}_{\langle ab\rangle}} + t^{\triangleright}_{(ab)} + D^{\triangleright}_{\langle jk\rangle}\frac{\partial t^{\triangleright}_{\langle jk\rangle}}{\partial D^{\triangleright}_{\langle ab\rangle}} \\
&\quad + \tfrac{1}{3}D^{\triangleright}_{cc}\frac{\partial t^{\triangleright}_{bb}}{\partial D^{\triangleright}_{\langle ab\rangle}} + p^{\triangleright}\frac{\partial}{\partial D^{\triangleright}_{ab}}\hat{\partial}_{D}w^{\triangleright} \\
\frac{\partial T^{\triangleright}\varsigma^{\triangleright P}}{\partial H^{\triangleright}_{ab}} &= -T^{\triangleright}\varrho^{\triangleright}\frac{\partial \delta^{\triangleright}}{\partial H^{\triangleright}_{ab}} - t^{\triangleright}_{[ab]} - H^{\triangleright}_{jk}\frac{\partial t^{\triangleright}_{[jk]}}{\partial H^{\triangleright}_{ab}} + D^{\triangleright}_{\langle jk\rangle}\frac{\partial t^{\triangleright}_{\langle jk\rangle}}{\partial H^{\triangleright}_{ab}} + \tfrac{1}{3}D^{\triangleright}_{aa}\frac{\partial t^{\triangleright}_{bb}}{\partial H^{\triangleright}_{ab}} + p^{\triangleright}\frac{\partial}{\partial H^{\triangleright}_{ab}}\hat{\partial}_{D}w^{\triangleright}, \\
\frac{\partial T^{\triangleright}\varsigma^{\triangleright P}}{\partial T^{\triangleright}_{,a}} &= -T^{\triangleright}\varrho^{\triangleright}\frac{\partial \delta^{\triangleright}}{\partial T^{\triangleright}_{,a}} - 2\phi^{\triangleright}_{a} - H^{\triangleright}_{jk}\frac{\partial t^{\triangleright}_{[jk]}}{\partial T^{\triangleright}_{,a}} + D^{\triangleright}_{\langle jk\rangle}\frac{\partial t^{\triangleright}_{\langle jk\rangle}}{\partial T^{\triangleright}_{,a}} + \tfrac{1}{3}D^{\triangleright}_{aa}\frac{\partial t^{\triangleright}_{bb}}{\partial T^{\triangleright}_{,a}} + p^{\triangleright}\frac{\partial}{\partial T^{\triangleright}_{,a}}\hat{\partial}_{D}w^{\triangleright}.
\end{aligned}$$

The definition of the Equilibrium is stated in the text. Therefore, the above four derivatives are simplified as follows,

$$\begin{aligned}
0 &= \left.\frac{\partial F^{\triangleright}}{\partial D^{\triangleright}_{aa}}\right|_{E} - T^{\triangleright}\varrho^{\triangleright}\left.\frac{\partial \delta^{\triangleright}}{\partial D^{\triangleright}_{aa}}\right|_{E} + \frac{1}{3}\left.t^{\triangleright}_{bb}\right|_{E} + p^{\triangleright}, \\
0 &= \left.\frac{\partial F^{\triangleright}}{\partial D^{\triangleright}_{\langle jk\rangle}}\right|_{E} - T^{\triangleright}\varrho^{\triangleright}\left.\frac{\partial \delta^{\triangleright}}{\partial D^{\triangleright}_{\langle jk\rangle}}\right|_{E} + \left.t^{\triangleright}_{\langle jk\rangle}\right|_{E}, \\
0 &= -T^{\triangleright}\varrho^{\triangleright}\left.\frac{\partial \delta^{\triangleright}}{\partial H^{\triangleright}_{ab}}\right|_{E} - \left.t^{\triangleright}_{[ab]}\right|_{E}, \\
0 &= -T^{\triangleright}\varrho^{\triangleright}\left.\frac{\partial \delta^{\triangleright}}{\partial T^{\triangleright}_{,a}}\right|_{E}.
\end{aligned}$$

where the evaluation of the Cauchy stress tensor, at the equilibrium, gives the following results

$$\begin{aligned}
\left.t^{\triangleright}_{bb}\right|_{E} &= 3\left.t^{\triangleright(1)}\right|_{E} + \left.t^{\triangleright(2)}\right|_{E}, \\
\left.t^{\triangleright}_{\langle jk\rangle}\right|_{E} &= \left.t^{\triangleright(2)}\right|_{E}\left(n_i n_j - \tfrac{1}{3}\delta_{ij}\right), \\
\left.t^{\triangleright}_{[ab]}\right|_{E} &= 0.
\end{aligned}$$

Bibliography

[1] Alley, R.B.: Fabrics in polar ice sheets: development and prediction. *Science* **240**: 493 - 495 (1988)

[2] Alley, R.B.: Flow-law hypotheses for ice-sheet modelling. *J. Glaciol.* **38**: 245 - 256 (1992)

[3] Armienti, P.; Tarquini, S.: Power law olivine crystal size distributions in lithispheric mantle xenoliths. *Lithos* **65**: 273 - 285 (2002)

[4] Asaro, R.J.: Micromechanics of crystals and polycrystals. *Adv. Appl. Mech.* **23**: 1 - 115 (1983)

[5] Ashby, M.F.: Mechanisms of deformation and fracture *Adv. Appl. Mech.* **23**: 117 - 177 (1983)

[6] Atkinson, H.V.: Theories of normal grain growth in pure single phase system *Acta Metall.* **36**: 469 - 491 (1988)

[7] Azuma, N.: A flow law for anisotropic ice and its application to ice sheets. *Earth Planet. Sci. Lett.* **128**: 601 - 614 (1994)

[8] Azuma, N.; Goto-Azuma, K.: An anisotropic flow law for ice-sheet ice and its implications. *Ann. Glaciol.* **23**: 202 - 208 (1996)

[9] Azuma, N.; Higashi, A.: Formation processes of ice fabric patterns in ice sheets. *Ann. Glaciol.* **6**: 130 - 134 (1985)

[10] Baker, I.; Liu, F.; Jia, K.; Hu, X.; Dudley, M.: Dynamic observations of dislocation/grain-boundary interactions in ice. *Annals of Glaciology* **31**: 236 - 240 (2000)

[11] Baker, R.W.: Is the creep of ice really independent of the third deviatoric stress invariant? *International association of Scientific Hydrolegy(IAHS)* **170**: 7 - 16 (1987)

[12] Barnes, P.; Tabor, D.; Walker, J.C.F.: The friction and creep of polycrystalline ice. *Proc. Roy. Soc. London A* **324**: 127 - 155 (1971)

[13] Boehler, J.P.: *Applications of tensor functions in solid mechanics.* New York: Springer-Verlag (1987)

[14] Bowen, R.M.: Incompressible porous media models by use of the theory of mixtures. *Int. J. Engng. Sci.* **18**: 1129 - 1148 (1980)

[15] Budd, W.F.; Jacka, T.H.: A review of ice rheology for ice sheet modelling. *Cold Reg. Sci. Technol.* **16**: 107 - 144 (1989)

[16] Castelnau, O.; Canova, G.R.; Lebensohn, R.A.; Duval, P.: Modelling viscoplastic behaviour of anisotropic polycrystalline ice with a self-consistent approach. *Acta Mater.* **45**: 4823 - 4834 (1997)

[17] Castelnau, O.; Duval, P.: Simulations of anisotropy and fabric development in polar ices. *Ann. Glaciol.* **20**: 277 - 282 (1995)

[18] Castelnau, O.; Duval, P.; Lebensohn, R.A.; Canova, G.R.: Viscoplastic modelling of texture development in polycrystalline ice with a self-consistent approach: comparison with bound estimates. *J. Geophys. Res.* **101**: 13851 - 13868 (1996)

[19] Castelnau, O.; Shoji, H.; Milsch, H.; Mangeney, A.; Duval, P.; Miyamoto, A.; Kawada, K.; Watanabe, O.: Anisotropic behaviour of GRIP ices and flow in Central Greenland. *Earth Planet. Sci. Lett.* **154**: 307 - 322 (1998)

[20] Castelnau, O.; Thorsteinsson, T.; Kipfstuhl, J.; Duval, P.; Canova, G.R.: Modelling fabric development along the GRIP ice core, central Greenland. *Ann. Glaciol.* **23**: 194 - 201 (1996)

[21] Colbeck, S.C.; Evans, A.: A flow law for temperate glaciers. *J. Glaciology* **12**: 71 - 86 (1973)

[22] Cuffey, K.M.; Conway, H.; Gades, A.; Hallet, B.; Raymond, C.F.; Withlow, S.: Deformation properties of subfreezing glacier ice: Role of crystal size, chemical impurities, and rock particles inferred from in situ measuraments. *J. of Geophysical Research* **105**: 27895 - 27915 (2000)

[23] Cuffey, K.M.; Thorsteinsson, T.; Waddinghton, E.D.: A renewed argument for crystal size control of ice sheet strain rates. *J. of Geophysical Research* **105**: 27889 - 27894 (2000)

[24] de Gennes, P.G.; Prost, J.: *The Physics of Liquid Crystals,* 2nd Edn. Oxford: Clarendon Press (1993)

[25] de la Chapelle, S.; Castelnau, O.; Lipenkov, V.; Duval, P.: Dynamic recrystallization and texture development in ice as revealed by the study of deep ice cores in Antarctica and Greenland. *J. Geophys. Res.* **103**: 5091 - 5105 (1998)

[26] de la Chapelle, S.; Duval, P.; Baudelet, B.: Compressive creep of polycrystyalline ice conteining a liquid phase. *Scripta Metallurgica et Materialia* **33** 447-450 (1995)

[27] Dafalias, Y.F.: Orientation distribution function in non-affine rotations. *Journal of the Mechanics and Physics of Solids* **49** 2493 - 2516 (2001)

[28] Derby, B.: Dynamic recrystallization: The steady state grain size. *Scripta Metallurgica et Materialia* **27** 1581-1586 (1992)

[29] Dillamore, I.L.; Morris, P.L.; Smith, C.J.E.; Hutchinson, W.B.: Transition bands and recrystallization in metals. *Proc. Roy. Soc. London A* **329**: 405 - 420 (1972)

[30] durham kirby stern. Creep of water aces at planetary conditions: A compilation. (1997)

[31] Duval, P.; Arnaud, L.; Brissaud, O.; Montagnat, M.; de La Chapelle , S.: Deformation and recrystallization processes of ice from polar ice sheets. *Ann. Glaciol.* **30**: 83 - 87 (2000)

[32] Duval, P.; Ashby, M.F.; Anderman, I.: Rate-controlling processes in the creep of polycrystalline ice. *J. Phys. Chem.* **87**: 4066 - 4074 (1983)

[33] Duval, P.; Castelnau, O.: Dynamic recrystallization of ice in polar ice sheets. *J. Phys. IV (Paris), colloq. C3* **5**: 197 - 205 (1995)

[34] Duval, P.; Montagnat, M.: Comment on *Superplastic deformation of ice: Experimental observations.* by D.L. Goldsby and D.L. Kohlstedt. *Journal of Geophysical Research* **107**: No B4 (2002)

[35] Eicken, H.; Oerter, H.; Miller, H., Graf, W.; Kipfstuhl, J. Textural characteristics and impurity content of meteoric and marine ice in the Ronne Ice Shelf, Antarctica. *Journal of Glaciology* **40**(135): 386 - 398 (1994)

[36] Faria, S. H.: Mixtures with continuous diversity: general theory and application to polymer solutions. *Continuum Mech. Thermodyn.* **13**: 91 - 120 (2001)

[37] Faria, S. H.; Hutter, K.: A systematic approach to the thermodynamics of single and mixed flowing media with microstructure. Part I: balance equations and jump conditions. *Continuum Mech. Thermodyn.* **14** (5): 459 - 481 (2002)

[38] Faria S.H.; Hutter, K.: The challenge of polycrystalline ice dynamics. In Kim,S. and D.Jung, (Eds.): *Advances in Thermal Engineering and Sciences for Cold Regions*, pp. 3 - 31. Seoul: Society of Air-Conditioning and Refrigerating Engineers of Korea – SAREK (2001)

[39] Faria, S.H.; Kipfstuhl, J.: Preferred slip band orientations and bending observed in the Dome Concordia ice core. *Annals of Glaciology* **39**: (in press)(2004)

[40] Faria,S.H.; Kremer,G.M.; Hutter,K.: On the inclusion of recrystallization processes in the modeling of induced anisotropy in ice sheets: a thermodynamicist's point of view. *Annals of Glaciology* **37**: 29-34 (2003)

[41] Faria,S.H.; Ktitarev,D.; Hutter,K.: Modelling evolution of anisotropy in fabric and texture of polar ice. *Annals of Glaciology* **35**: 545-551 (2002)

[42] Frenkel, J.: *Z. Physik* **37**: 572 (1926)

[43] Fujita, S.; Nakawo, M.; Mae, S.: Orientation of the 700 m Mizuho core and its strain story. *Proc. NIPR Symp. Polar Meteo. Glaciol.* **1**: 122 - 131 (1987)

[44] Gagliardini, O.; Meyssonnier, J.: Plane flow of an ice sheet exhibiting strain-induced anisotropy. In K. Hutter; Y. Wang; H. Beer (Eds.): *Advances in cold-region thermal engineering and sciences*, pp. 171 - 182. Berlin: Springer (1999)

[45] Gagliardini, O.; Meyssonnier, J.: Simulation of anisotropic ice flow and fabric evolution along the GRIP-GISP2 flow line, central Greenland. *Ann. Glaciol.* **30**: 217 - 223 (2000)

[46] Garofalo, F.: An empirical relation defining the stress dependence of minimum creep rate in metals. *Trans. Metall. Soc. AIME* **227**: 351 - 355 (1963)

[47] Glen, J.W.: The creep of polycrystalline ice. *Proc. Roy. Soc. London A* **228**: 519 - 538 (1955)

[48] Glen, J.W.: The flow law of ice: A discussion of the assumptions made in glacier theory, their experimental foundations and consequences. *IASH* **47**: 171 - 183 (1958)

[49] Glen, J.W.: The mechanics of ice. *Cold regions science and engineering monograph II-C2b.* Hanover: U.S. Army CRREL (1975)

[50] Glen, J.W.: The physics of ice. *Cold regions science and engineering monograph II-C2a.* Hanover: U.S. Army CRREL (1974)

[51] Gödert, G.: A meso-macro model for the description of induced anisotropy of natural ice, including grain interaction. In K. Hutter; Y. Wang; H. Beer (Eds.): *Advances in cold-region thermal engineering and sciences*, pp. 183 - 196. Berlin: Springer (1999)

[52] Gödert, G.; Hutter, K.: Induced anisotropy in large ice shields: theory and its homogenization. *Continuum Mech. Thermodyn.* **10**: 293 - 318 (1998)

[53] Gödert, G.; Hutter, K.: Material update procedure for planar transient flow of ice with evolving anisotropy. *Ann. Glaciol.* **30**: 107 - 114 (2000)

[54] Goldsby, D.L.; Kohlstedt, D.L.: Grain boundary sliding in fine-grained ice I. *Scripta Mater.* **37**: 1399 - 1406 (1997)

[55] Goldsby, D.L.; Kohlstedt, D.L.: Reply to comment by P. Duval and M. Montagnat on *Superplastic deformation of ice: Experimental observations.* (2002) *Journal of Geophysical Research* **107**: No B11 (2002)

[56] Goldsby, D.L.; Kohlstedt, D.L.: Superplastic deformation of ice: Experimental observations. *J. of Geophysical Research* **106**: 11017 - 11030 (2001)

[57] Goodman, D.J.; Frost, H.J.; Ashby, M.F.: The plasticity of polycrystalline ice. *Philos. Mag.* **43**: 665 - 695 (1981)

[58] Gow, A. J.: On the rates of growth of grains and crystals in south polar firns. *Journal of Glaciology* **8**: 241-252 (1969)

[59] Gow, A.J.; Meese, D.A.; Alley, R.B.; Fitzpatrick, J.J.; Anandakrishnan, S.; Woods, G.A.; Elder, B.C.: Physical and structural properties of the Greenland ice sheet project 2 ice core: a review. *J. Geophys. Res.* **102**: 26559 - 26575 (1997)

[60] Gow, A.J.; Williamson, T.: Rheological implications of the structure and crystal fabrics of the West Antarctic ice sheet as revealed by deep core drilling at Byrd Station. *Geological Society of America Bulletin* **87**: 1665 - 1677 (1976)

[61] Greve, R.: A continuum-mechanical formulation for shallow poly-thermal ice sheets. *Phil. Trans. R. Soc. London* A**35**: 921 - 974 (1997)

[62] Hansen, N.: Deformation microstructures. *Scr. Metall. Mater.* **27**: 1447 - 1452 (1992)

[63] Harren, S.V.; Asaro, R.J.: Nonuniform deformations in polycrystals and aspects of the validity of the Taylor model. *J. Mech. Phys. Solids* **37**: 191 - 232 (1989)

[64] Hobbs, P.V.: *Ice physics.* Oxford: Clarendon (1974)

[65] Hondoh, T.: Nature and behaviour of dislocations in ice. In T. Hondoh (Ed.): *Physics of ice core records*, pp. 3 - 24. Sapporo: Hokkaido Univ. Press (2000)

[66] Huang, K.: *Statistical Mechanics*, 2nd Edn. John Wiley & Sons, Inc. (1987)

[67] Hutchinson, J.W.: Bounds and self-consistent estimates for creep of polycrystalline materials. *Proc. R. Soc. Lond. A* **348**: 101 - 127 (1976)

[68] Humphreys, F.J.; Hatherly, M.: *Recrystallization and related annealing phenomena.* Oxford: Pergamon (1996)

[69] Hutter, K.: Schnee- und Gletscherrheologie Snow and Glacier Rheology. *Applied Rheology* **7**: 266 - 276 (1997)

[70] Hutter, K.: *Theoretical glaciology* Dordrecht: Reidel (1983)

[71] Hutter, K.; Legerer, F.; Spring, U.: First order stresses and deformations in glaciers and ice sheets. *J. Glaciology* **27**: 227 - 270 (1981)

[72] Hutter, K.; Vulliet, L.: Gravity driven slow creeping flow of a thermoviscous body at elevated temperature. *J. Thermal Stresses* **8**: 99 - 138 (1985)

[73] Jacka, T.H.: Laboratory studies on relationships between ice crystal size and flow rate. *Cold Reg. Sci. Technol.* **10**: 31 - 42 (1984)

[74] Jacka, T.H.; Budd, W.F.: Isotropic and anisotropic flow relations for ice dynamics. *Annals of Glaciology* **12**: 81 - 84 (1989)

[75] Jacka, T.H.; Jun, L.: The steady-state crystal size of deforming ice. *Annals of Glaciology* **20**: 13 - 18 (1994)

[76] Jensen, D.J.: Effects of orientation on growth during recrystallization. In Hansen, N.; Jensen, D.J.; Liu, Y.L.; Ralph, B. (Eds.): *Microstructure and Crystallographic Aspects of Recrystallization.* pp. 119 - 137. Riso National Laboratory, Roskilde, Denmark: Proceedings of the 16th Riso International Symposium on Material Science (1972)

[77] Jun, L.; Jacka, T.H.: Isotropic ice flow rates derived from deformation tests in simultaneous shear and compression. Proceedings of the 13^{th} International Symposium on Ice. Volume III. pp. 937 - 947 (1996)

[78] Jun, L.; Jacka, T.H.; Budd, W.F.: Deformation rates in combined compression and shear for ice which is initially isotropic and after the development of strong anisotropy. *Ann. Glaciol.* **23**: 247 - 252 (1996)

[79] Jun, L.; Jacka, T.H.; Budd, W.F.: Strong single-maximum crystal fabrics developed in ice undergoing shear with unconstrained normal deformation. *Ann. Glaciol.* **30**: 88 - 92 (2000)

[80] Kamb, B.: Experimental Recrystallization of Ice Under Stress. In Heard, H.C.; Borg, I.Y.; Carter, N.L. Raileigh, C.B. (Eds.): *Flow and Fracture of Rocks.*, pp. 211 - 241. Washington DC: American Geophysical Union **16** (1972)

[81] Kittel, C.: *Introduction to Solid State Physics.* New York: John Wiley Sons (1966)

[82] Kocks, U.F.; Tomé, C.N.; Wenk, H.-R.: *Texture and anisotropy.* Cambridge: Cambridge Univ. Press (1998)

[83] Ktitarev, D.; Gödert, G.; Hutter, K.: Cellular automaton model for recrystallization, fabric and texture development in polar ice. *J. Geophys. Res.* **107**NO. B8.10.1029/2001JB000621 (2002)

[84] Langdon, T.G.: Regimes of Plastic Deformation. In *Preferred orientation in deformed metals and rocks: an introduction to modern texture analysis.* Preferred Orientation in Deformed Metals and Rocks: An Introduction to Modern Texture Analysis. pp. 219 - 232. (1985)

[85] Larson, R.G.: *Constitutive equations for polymer melts and solutions.* Boston: Butterworths (1988)

[86] Lebensohn, R.A..; Tomé, C.N.: A self-consistent anisotropic approach for the simulation of plastic deformation and texture development of polycrystals: application to zirconium alloys. *Acta Metall.* **41**: 2611 - 2624 (1993)

[87] Lipenkov, V.Y.; Barkov, N.I.; Duval, P.; Pimienta, P.: Crystalline texture of the 2083 m ice core at Vostok Station, Antarctica. *J. Glaciol.* **35**: 392 - 398 (1989)

[88] Liu, I.S.: Method of Lagrange Multipliers for Exploitation of the Entropy Principle. *Arch. Rat. Mech. Anal.* **46**: 131 - 148 (1972)

[89] Liu, I.S.: Continuum Mechanic. Springer. Berlin (2002)

[90] Lliboutry, L.A.: The dynamics of temperate glaciers from the deteiled viewpoint. *J. Glaciology* **8**: 185 - 205 (1969)

[91] Lliboutry, L.A.: *Very slow flows of solids.* Dordrecht: Kluwer (1987)

[92] Lliboutry, L.A.: Anisotropic, transversely isotropic nonlinear viscosity of rock ice and rheological parameters inferred from homogenization. *J. Plast.* **9**: 619 - 632 (1993)

[93] Lliboutry, L.A.; Duval, P.: Various isotropic and anisotropic ices found in glaciers and polar ice caps and their corresponding rheologies. *Ann. Geophysicae* **3**: 207 - 224 (1985)

[94] Mangeney, A; Califano, F; Hutter, K.: A numerical study of anisotropic, low Reynolds numbers, free surface flows for ice sheet modeling. *Journal of Geophysical Research* **102** (No B10) 22749 - 64 (1997)

[95] Mansuy, P.; Meyssonnier, J.; Philip, A.: Modelling the ice single-crystal Viscoplastic Behaviour. In K. Hutter; Y. Wang; H. Beer (Eds.): *Advances in cold-region thermal engineering and sciences*, pp. 183 - 196. Berlin: Springer (1999)

[96] Mansuy, P.; Philip, A.; Meyssonnier, J.: Identification of strain heterogeneities arising during deformation of ice. *Ann. Glaciol.* **30**: 121 - 126 (2000)

[97] Marsh, B.D.: Crystal size distribution (CSD) in rocks and the kinetics and dynamics of crystallization *Contrib. Mineral Petrol.* **99**: 277 - 291 (1988)

[98] Mason, B.J.; Bryant, G.W.; van den Heuvel, A.P.: The growth habits and surface structure of ice crystals. *Philos. Mag.* **8**: 505 - 526 (1963)

[99] McConnel, J.C.: On the plasticity of an ice crystal. *Proc. Roy. Soc. London* **49**: 323 - 343 (1891)

[100] McDowell, R.C.; Bolton, M.D.: Effect of particle distribution on pile tip resistance in calareous sand in the geotechnical centrifuge. *Granular Matter* **2**: 179 - 187 (2000)

[101] McElroy, R.J.; Szkopiak, Z.C. *Int. Met. Reviews.* **17**: 175

[102] Mellor, M.; Testa, R.: Effect of temperature on the creep of ice. *J. Glaciology* **8**: 131 - 145 (1969)

[103] Meyssonnier, J.; Philip, A.: A model for the tangent viscous behaviour of anisotropic polar ice. *Ann. Glaciol.* **23**: 253 - 261 (1996)

[104] Meyssonnier, J.; Philip, A.: Comparison of finite-element and homogenization methods for modelling the viscoplastic behaviour of a S2-columnar-ice polycrystal. *Ann. Glaciol.* **30**: 115 - 120 (2000)

[105] Montagnat, M.; Duval, P.: Rate controlling processes in the creep of polar ice, influence of grain boundary migration associated with recrystallization. *Earth Planet. Sci. Lett.* **183**: 179 - 186 (2000)

[106] Morland L. W. : Influence of lattice distortion on fabric evolution in polar ice *Continuum Mech. Thermodyn.* **14** (1): 9 - 24 (2002)

[107] Morland, L.W.; Staroszczyk, R.: Viscous response of polar ice with evolving fabric. *Continuum Mech. Thermodyn.* **10**: 135 - 152 (1998)

[108] Müller, I. Thermodynamics. Pitman Advanced Publishing Program. Boston (1985)

[109] Nye, J.F.: The flow law of glaciers and ace sheets as a problem in plasticity. *Proc. Roy. Soc. London A* **213**: 546 - 558 (1951)

[110] Paterson, W.S.B.: *The physics of glaciers*, 3rd Edn. Oxford: Pergamon (1994)

[111] Peltier, W.R.; Goldsby, D.L.; Kohlstedt, D.L.; Tarasov, L.: Ice-age ice-sheet rheology: constraints from the Last Glacial Maximum form of the Laurentide ice sheet. *Ann. Glaciol.* **30**: 163 - 176 (2000)

[112] Petit, J.R.; Duval, P.; Lorius, C.: Long-term climatic changes indicated by crystal growth in polar ice. *Nature* **326**: 62 - 64 (1999)

[113] Pineda, E.; Pradell, T.; Crespo, D.: On the equations describing the grain size distribution change for KJMA kinetics. *Journal of Non-Crystalline Solids* **287**: 88 - 91 (2001)

[114] Placidi, L.; Faria, S.H.; Hutter, K.: Advances in Constitutive Modelling of Anisotropic Ice in polar Ice Sheets. In: Milestones in Physical Glaciology. From the Pioneers to a Modern Science. *Versuchsanstalt für Wasserbau Hydrologie und Glaziologie an der Eidgenössischen Technischen Hochschule Zürich* **180**: 55 - 72 (2003)

[115] Placidi, L.; Faria, S.H.; Hutter, K.: On the role of grain growth, recrystallization and polygonization in a continuum theory for anisotropic ice sheets. *Annals of Glaciology* **39**: in press (2004)

[116] Poirier, J.-P.: *Creep of crystals.* Cambridge: Cambridge Univ. Press (1985)

[117] Rashid, M.M.: Texture evolution and plastic response of two-dimensional polycrystals. *J. Mech. Phys. Solids* **40**: 1009 - 1029 (1992)

[118] Readings, C.J.; Bartlett, J.T.: Slip in single crystals of ice. *J. Glaciol.* **7**: 479 - 491 (1968)

[119] Reuss, A.: Berechnung der Fließgrenze von Mischkristallen auf Grund der Plastizitätsbedingung für Einkristalle. *Z. Angew. Math. Mech.* **9**: 49 - 58 (1929)

[120] Sachs, G.: Zur Ableitung einer Fließbedingung. *Z. Ver. Deutscher Ing.* **72**: 734 - 736 (1928)

[121] Shimizu, I.: A stochastic model of grain size distribution during dynamic recrystallization. *Philosophical Magazzine A* **79** (5): 1217 - 1231 (1999)

[122] Shimizu, I.; Takahashi, K.; Nomura, T.: Effect of baffle geometries on crystal size distribution of alluminum potassium sulfate in a seeded batch crystallizer. *Journal of Crystal Growth* **197**: 921 - 926 (1999)

[123] Schmid, E.; Boas, W.: *Kristallplastizität.* Berlin: Springer (1935)

[124] Smith, C.S.: Grains, phases, and interfaces: an interpretation of microstructure. *Transaction of the Metallurgical sciety of AIME* **230 No.5**: 1134-1137 (1948)

[125] Staroszczyk, R.; Morland, L.W.: Orthotropic viscous model for ice. In K. Hutter; Y. Wang; H. Beer (Eds.): *Advances in cold-region thermal engineering and sciences*, pp. 249 - 258. Berlin: Springer (1999)

[126] Staroszczyk, R.; Morland, L.W.: Plane ice-sheet flow with evolving orthotropic fabric. *Ann. Glaciol.* **30**: 93 - 101 (2000)

[127] Staroszczyk, R.; Morland, L.W.: Orthotropic viscous response of polar ice. *J. Engng. Math.* **37**: 191 - 209 (2000)

[128] Staroszczyk, R.; Morland, L.W.: Strengthening and weakening of induced anisotropy in polar ice. *Proc. Roy. Soc. London A* **457 (2014)**: 2419-2440 (2001)

[129] Steinemann, S.: *Experimentelle Untersuchungen zur Plastizität von Eis.* Ph.D. Thesis, Eidgenössischen Technischen Hochschule (ETH), Zürich (1958)

[130] Svendsen, B.; Hutter, K.: A continuum approach for modelling induced anisotropy in glaciers and ice sheets. *Ann. Glaciol.* **23**: 262 - 269 (1996)

[131] Taylor, G.I.: Plastic strain in metals. *J. Inst. Metals* **62**: 307 - 324 (1938)

[132] Thorsteinsson, T.: Textures and fabrics in the GRIP ice core, in relation to climate history and ice deformation. *Ber. Polarforsch.* **205**: 1 - 146 (1996)

[133] Thorsteinsson, T.; Kipfstuhl, J.; Eicken, H.; Johnsen, S. J.; Fuhrer, K.: Crystal size variations in Eemian-age ice from the GRIP ice core, Central Greenland. *Earth and Planet Science Letters* **131**: 381 - 394 (1995)

[134] Thorsteinsson, T.; Kipfstuhl, J.; Miller, H.: Textures and fabrics in the GRIP ice core. *J. Geophys. Res.* **102**: 26583 - 26599 (1997)

[135] Thorsteinsson, T.; Waddington, E.D.; Taylor, K.C.; Alley, R.B.; Blankenship, D.D.: Strain-rate enhancement at Dye 3, Greenland. *J. Glaciol.* **45**: 338 - 345 (1999)

[136] Trickett, Y.L.; Baker, I.; Pradhan, P.M.S.: The orientation dependence of the strenght of ice single crystals. *Journal of Glaciology* **46** (152): 41 -44 (2000)

[137] Truesdell, C.; Toupin, R.: The classical field theories. In S. Flügge (Ed.): *Handbuch der Physik, III/3*, pp. 226-793. Berlin: Springer (1960)

[138] Truesdell, C.; Noll, W.: The nonlinear field theories of mechanics. In S. Flügge (Ed.): *Handbuch der Physik, III/3.* Berlin: Springer (1965)

[139] Van der Veen, C.J.: *Fundamentals of glacier dynamics.* Rotterdam: Balkema (1999)

[140] Van der Veen, C.J.; Whillans, I.M.: Flow laws for glacier ice: comparison of numerical predictions and field measurements. *J. Glaciol.* **36**: 324 - 339 (1990)

[141] Van der Veen, C.J.; Whillans, I.M.: Development of fabric in ice. *Cold Reg. Sci. Technol.* **22**: 171 - 195 (1994)

[142] Van Houtte, P.: On the equivalence of the relaxed Taylor theory and the Bishop and Hill theory for partially constrained plastic deformation of crystals. *J. Mater. Sci. Engng.* **55**: 69 - 77 (1982)

[143] Von Mises, R.: Mechanik der plastischen Formänderung von Kristallen. *Z. Angew. Math. Mech.* **8**: 161 - 185 (1928)

[144] Weertman, J.: Creep deformation of ice. *Ann. Rev. Earth Planet. Sci.* **11**: 215 - 240 (1983)

[145] Weertman, J.: Creep of ice. In: S.J.Jones and L.W.Gold (Ed.): *Physics and Chemistry of Ice, Royal Society of Canada* Ottawa , pp. 320-337.(1973)

[146] Whitworth, R.W.: The influence of the choice of glide plane on the theory of the velocity of dislocations in ice. *Philos. Mag.* **41**: 521 - 528 (1980)

[147] Wilson, C.J.L.; Zhang, Y.: Development of microstructure in the high-temperature deformation of ice. *Ann. Glaciol.* **23**: 293 - 302 (1996)